frontiers | Research Topics

Community series in resident memory T cells: Guardians of the balance of local immunity and pathology, volume II

Edited by
Nick P. Goplen, Shiki Takamura and Chaofan Li

Published in
Frontiers in Immunology

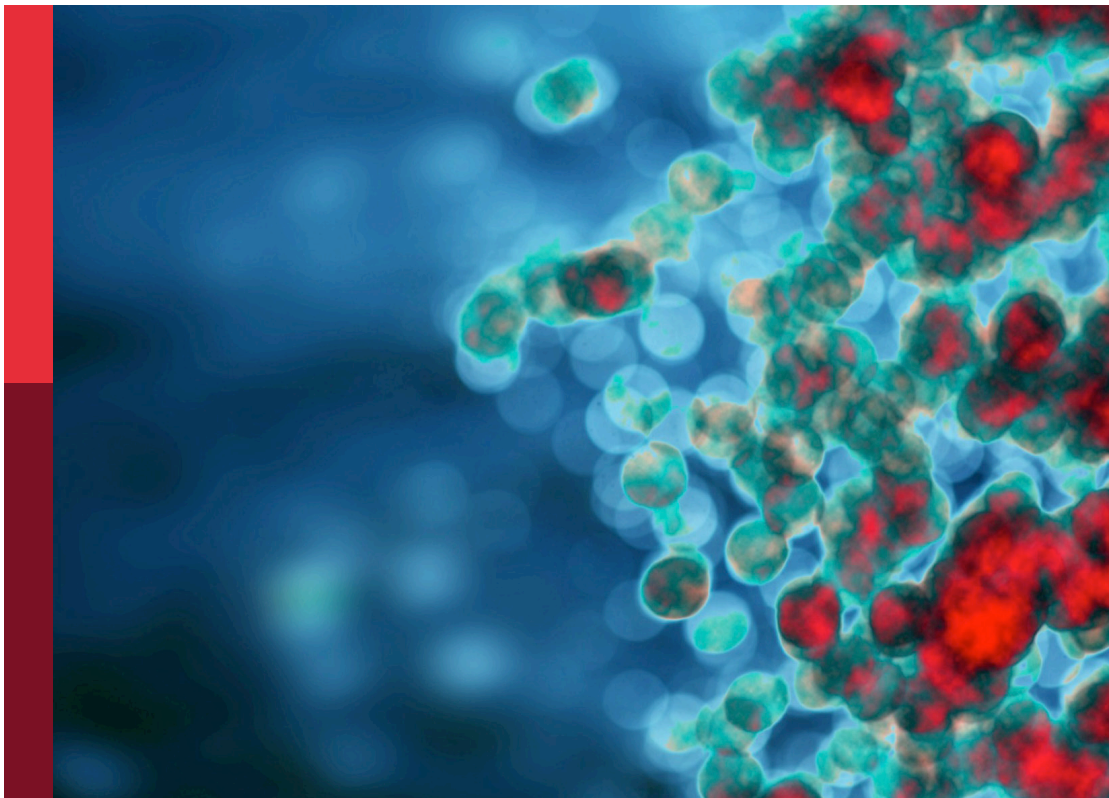

ISSN 1664-8714
ISBN 978-2-8325-5052-6
DOI 10.3389/978-2-8325-5052-6

About Frontiers

Frontiers is more than just an open access publisher of scholarly articles: it is a pioneering approach to the world of academia, radically improving the way scholarly research is managed. The grand vision of Frontiers is a world where all people have an equal opportunity to seek, share and generate knowledge. Frontiers provides immediate and permanent online open access to all its publications, but this alone is not enough to realize our grand goals.

Frontiers journal series

The Frontiers journal series is a multi-tier and interdisciplinary set of open-access, online journals, promising a paradigm shift from the current review, selection and dissemination processes in academic publishing. All Frontiers journals are driven by researchers for researchers; therefore, they constitute a service to the scholarly community. At the same time, the *Frontiers journal series* operates on a revolutionary invention, the tiered publishing system, initially addressing specific communities of scholars, and gradually climbing up to broader public understanding, thus serving the interests of the lay society, too.

Dedication to quality

Each Frontiers article is a landmark of the highest quality, thanks to genuinely collaborative interactions between authors and review editors, who include some of the world's best academicians. Research must be certified by peers before entering a stream of knowledge that may eventually reach the public - and shape society; therefore, Frontiers only applies the most rigorous and unbiased reviews. Frontiers revolutionizes research publishing by freely delivering the most outstanding research, evaluated with no bias from both the academic and social point of view. By applying the most advanced information technologies, Frontiers is catapulting scholarly publishing into a new generation.

What are Frontiers Research Topics?

Frontiers Research Topics are very popular trademarks of the *Frontiers journals series*: they are collections of at least ten articles, all centered on a particular subject. With their unique mix of varied contributions from Original Research to Review Articles, Frontiers Research Topics unify the most influential researchers, the latest key findings and historical advances in a hot research area.

Find out more on how to host your own Frontiers Research Topic or contribute to one as an author by contacting the Frontiers editorial office: frontiersin.org/about/contact

Community series in resident memory T cells: Guardians of the balance of local immunity and pathology, volume II

Topic editors

Nick P. Goplen — Mayo Clinic, United States
Shiki Takamura — RIKEN Yokohama, Japan
Chaofan Li — University of Virginia, United States

Citation

Goplen, N. P., Takamura, S., Li, C., eds. (2024). *Community series in resident memory T cells: Guardians of the balance of local immunity and pathology, volume II*. Lausanne: Frontiers Media SA. doi: 10.3389/978-2-8325-5052-6

Table of contents

frontiers | Frontiers in Immunology

TYPE Editorial
PUBLISHED 10 June 2024
DOI 10.3389/fimmu.2024.1401196

OPEN ACCESS

EDITED AND REVIEWED BY
Scott N. Mueller,
The University of Melbourne, Australia

*CORRESPONDENCE
Nicholas P. Goplen
goplen.nicholas@mayo.edu

RECEIVED 14 March 2024
ACCEPTED 20 March 2024
PUBLISHED 10 June 2024

CITATION
Goplen NP, Li C and Takamura S (2024) Editorial: Community series in resident memory T cells: guardians of the balance of local immunity and pathology, volume II. *Front. Immunol.* 15:1401196. doi: 10.3389/fimmu.2024.1401196

Editorial: Community series in resident memory T cells: guardians of the balance of local immunity and pathology, volume II

Nicholas P. Goplen[1*], Chaofan Li[2] and Shiki Takamura[3]

[1]Department of Physiology and Biomedical Engineering, Mayo Clinic, Rochester, MN, United States, [2]Division of Infectious Disease and International Health, Department of Medicine, University of Virginia, Charlottesville, VA, United States, [3]Department of Immunology, Faculty of Medicine, Kindai University, Osaka, Japan

KEYWORDS

memory T cell, cancer, infection, vaccine, immunotherapy

Editorial on the Research Topic
Community series in resident memory T cells: guardians of the balance of local immunity and pathology, volume II

What happens between the time a T cell loses its naivety, expands thousands-fold, and all its clonal progeny die can impact T cell sentinel functions in tissues. Holistically understanding the dynamic control that imparts heterogeneous functional responses of tissue-resident memory T cells (T_{RM}) could clinically aid in balancing health and disease at the level of local immunity. Notably, surrogate measurements of the functional quality of T_{RM} are quickly becoming a favored prognostic tool in the fight against cancer, with signs of the same on the horizon for local infections, allergies, and autoimmune diseases. If you are interested in how T cells in yourself, others, or model organisms, act, or how human T cells in mice act the way they do, we have some recommended reading for you exploring origin stories and fate decisions that influence "The Guardians of The Tissue".

Did somebody have the gall to tell you your work needs more clinical relevance and you now find yourself looking for a road map of how to establish it, to validate your existence and appease the grant gods at the same time? Look no further, as Fujiki et al. have paved the way. This one did not even use the word *resident* once, but we could not put it down. Vitamin A metabolite signaling promotes $CD4^+$ and $CD8^+$ T cell effector function after productive T Cell Receptor (TCR) signaling. Fujiki et al. discovered that T cells do the metabolizing themselves. But not in a way that makes them full-fledged terminal effectors; the good stuff (retinoic acid) that encourages that commitment comes from exogenous sources such as tumor microenvironments. However, when the goal is memory generation, too much of the good stuff is a bad thing, or perhaps, just cancers' nefarious way of making sure no memories remain. To learn more on the epigenetic modifications of this intrinsic pathway that controls T cell fate, tune in to this riveting article with classic competition experiments, tertiary memory generation, and xenografts. We recommend you get your lab

some LE540 yesterday; this paper could cause a supply crunch driven by T cell fate enthusiasts!

The right and the left colon differ in terms of their embryonic origin, vascularization, innervation, and gut flora. Talhouni et al. make it obvious from the get-go that, since left- and right-sided colorectal cancers (CRC) develop in different environments, the approach to understand and treat them should not be "one side fits all". Since high numbers of T cells inside tumors (tumor hotness) is a better prognostic indicator than the stage of the tumor itself, what if you could find out something unique about those T cells in tumors that improved our ability to monitor disease progression and dynamically guide treatment decisions? Many independent studies of cancers throughout the body have done just that. This massive undertaking, where over 900 patients with CRC contributed to findings that are going to improve clinical assessment and treatment of left- and right-sided CRC, is the largest imaging study of T_{RM} in tumor microenvironments. Machine learning trained on unique combinations of three immunofluorescent markers (CD8α, CD103, and CD39) on tissue microarray biopsies aided quantitation of cellular densities in right- and left-sided hot and cold tumors. They speculate on why their CRC findings are not "one side fits all" in the context of recent understandings of checkpoint blockade mechanisms of action and what they know of colon sidedness, with a discussion as captivating as the article was throughout.

Presumably, there is prognostic value of absolute counts of lymphocyte subsets in the circulation over measuring frequency of the same; an easy adjustment to make for flow cytometry based clinical measurements. Zhang et al. test this principle with transparent methods to predict progression-free survival and immune therapy efficacy for patients with advanced non-small cell lung cancer. They suggest studies unwittingly including T memory stem cells without separating them from their corresponding naïve pools can misguide study conclusions. These blood screening methods could guide patient specific monitoring and treatment and could find relevance in many T cell-mediated diseases.

When you hear IL-7 mentioned in everyday conversation, do you ever just think about how its receptor mediates STAT-5 dependent survival in T cells during early stages of development and naïve existence? Do you then try and recall which cytokine receptors all share the common gamma chain? Or does it hit deeper and conjure up vivid pictures of tonic TCR signaling in survival and homeostatic proliferation leading to memory differentiation in lymphopenic conditions described in landmark papers from Charlie Surh's group circa 2000 that quickly evolved into Kaech et al. discovering IL-7Rα could selectively predict T cell fates early in a response demonstrating its functional importance for $CD8^+$ T cell memory generation? This thorough and well-organized review of the role of IL-7 in T cell biology by Zhao et al. covers this and so much more. It turns out survival is somewhat key to generating long-lasting memory T cells, an indisputable goal in cancer immunotherapy regimens. Efforts to add IL-7 to immunotherapies in preclinical and clinical trials. Improvements on IL-7 adjuvant are discussed including altering formulations, chaperones, and candidate adjuvants for IL-7 adjuvants.

We are often left with the same somber impression as these authors that the only good measure of a T cell response in therapeutic development pipelines is clinical success or failure. Nerves are immediately hit, reminding us of our repressed thoughts: *vaccines are optimized for their antibody production; those that induce cellular immunity do so because of happy accidents, not design.* Imagine how much good we could do for so many more diseases if measuring resting antigen-specific memory T cells was as convenient (or more) as antibody titers from serum. The goal is simple, noble, and rightfully reverent of T cell memory, namely, to develop a measure of anti-tumor CD4 and CD8 memory T cell responses that can be "easily standardized". Gao and Bergman apply bulk TCRseq clonal analysis in a model of curative viral onco-immunotherapy. Although clonal expansion is 10 times greater in the peritoneum upon tumor rechallenge, ~70% of the high-responding memory T cell clonotypes were also high responders in the spleen. This is encouraging, indicating the plausibility of blood monitoring. The importance of such a patient-specific method in tumor vaccine models is demonstrated as each mouse mostly had unique clones (compared within group) that were high responders to the same antigen (private TCR repertoire). While the conclusions indicate responsive anti-tumor memory T cell clones cannot currently be predicted/measured at resting state alone, the method can certainly aid discovery and hypothesis testing in preclinical models after antigen rechallenge.

Select serine-proteases from the granzyme family are traditionally recognized for their intracellular roles (*in trans*) in perforin-dependent immune-targeted cell death, a major mechanism of both innate and adaptive immunity. Non-canonical functions of these proteases include tunneling through tissues, cleavage of viral proteins that mediate infection, production of autoantigens, collagen degradation, fibroblast activation, wound repair, and biological aging. Thus, as both a family and individual molecules, granzymes are functionally diverse. Very little is known about granzyme C (human ortholog(ue), granzyme H). In a venture into the unknown, Lujan et al. looked at the usual [granzyme] suspects - innate and adaptive T cell subsets in the skin of mice at steady-state. About ¼ of dendritic epidermal [γδ] T cells expressed granzyme C, often in the dendritic extensions between keratinocytes which could be functionally suggestive. These cells acutely increased granzyme C expression in response to cutaneous poxvirus infection. 30 days later ~15% of steady-state dermal and epidermal $CD8^+$ T_{RM} also expressed granzyme C. Secondary exposure to virus with or without cognate antigen, cognate antigen alone, or IL-15 alone augmented granzyme C expression to various degrees in T_{RM}. We and the authors await conditional knockouts of granzyme C to assess cell-specific bystander and antigen-specific functions in the skin.

This Research Topic includes a perspective with a data-tease that supports the hypothesis that lung pathogens should enter the lung to induce a "quality" $CD8^+$ T_{RM} cell response (increased quantity and diversity of functionality, in our opinion). Viruses with lung tropism might be "better" at T_{RM} differentiation in general, versus viruses with no affection for the lung that were forced to abide there through the machinations of Macedo et al.

While ostensibly they anthropomorphize pathogens to help us understand the big questions we should all ponder, are the authors really just ascribing that voice to CD8 T cell antigens and local microenvironments in which memories are made? You decide. Regardless, *we and they* think this may also have implications for mRNA vaccinations, which supports their subtle message of getting quality TCR-pMHC interactions to where you want the sensitive, rapidly responding memories while also keeping a less zealous polyclonal backup pool to guard against mutating pathogens.

Zhou et al. raise the bar for establishing vaccine efficacy for communicable diseases. In short, they provide a missing proof of principle demonstrating the value of both systemic, but especially respiratory tract, immunization to the population writ large. They demonstrate substantial and stable $CD8^+$ T_{RM} establishment in airways and lung parenchyma after intranasal vaccination with Sendai virus nucleoprotein. After infecting with transmittable murine parainfluenza virus (Sendai) that encodes luciferase, parainfluenza replication was well contained in vaccinated hosts - longitudinally measured with bioluminescence as a demonstrated surrogate for viral titers. Those that received intranasal vaccine allowed very little, if any, viral replication with all other groups reaching 10,000-fold initial fluorescent intensity in the first three days of infection. This sterilizing immunity was dependent on CD8 T cells, IFNγ, IFNγR, and, to a lesser extent, perforin. Cohousing of a mouse infected 150 days after intranasal vaccination produced no new infections among the naïve cohoused population compared to sham nucleoprotein and unvaccinated mice spreading infection to 100% of cohabitants. While subcutaneous vaccinations led to viral spread, the secondary contacts exhibited well-controlled infections compared to sham and unvaccinated mice. These studies suggest that vaccinations that establish T_{RM} are paramount for herd immunity to communicable respiratory viruses. Optimizing respiratory vaccines based on limiting transmission in preclinical models may substantially improve vaccine efficacy and benefit humanity.

Most adults worldwide have been infected with the herpesvirus human cytomegalovirus (CMV). In case of immune dysregulation, reactivation of latent CMV carries a severe or even fatal risk in immunocompromised individuals. This reactivation is kept in check by CD8 T cells but the location and nature of those CD8 T cells in humans is poorly understood. White adipose tissue (WAT) has been considered an endocrine organ for decades and, more recently, an immune organ that sponsors fat-associated lymphoid clusters (FALCs). FALCs are highly enriched in resident memory CD8 T cells (T_{RM}) against chronic and/or latent viruses with WAT and non-WAT tropisms. Redruello-Romero et al. used high-throughput sequencing analyses of the TCR locus in subcutaneous sWAT, lesser studied omental oWAT, and liver samples from 11 obese donors. Hyperexpanded clones from the whole repertoire were particularly enriched in each of these tissues relative to blood, consistent with their findings that most were tissue-resident memory phenotypes. The oWAT contained the most cells predicted, and confirmed, to react to CMV epitopes. This work highlights omental WAT depots in humans as a site where latency of CMV may be kept in check over the lifespan by resident memory CD8 T cells that preferentially reside there.

We hope this volume leaves you in awe at the quality and ingenuity of tools being used to explore cutting edge questions and has you pondering the future of T cell responses throughout the body.

Author contributions

NG: Conceptualization, Supervision, Writing – original draft, Writing – review & editing. CL: Supervision, Writing – review & editing. ST: Supervision, Writing – original draft, Writing – review & editing.

In memoriam of Toshinori Nakayama

We thank all the authors, reviewers, readership, and, in particular, Dr. Toshinori Nakayama, *in memoriam*, for his contributions to humankind. We regret to announce our co-guest editor on this Research Topic passed away on November 2, 2023. It goes without saying that he made enormous contributions to the field of immunology. In his later years, he especially devoted himself to the training of the next generation of researchers. He never told anyone of his illness and continued his research until the end of his life, fulfilling the words he left his members at the Annual Meeting of the Japanese Society for Immunology in January 2024, where he was supposed to host, touching the hearts of all attendees in a video message that began: “Keep running as best you can 全力で走れ.”

Conflict of interest

The authors declare that the research was conducted in the absence of any commercial or financial relationships that could be construed as a potential conflict of interest.

Publisher’s note

frontiers | Frontiers in Immunology

ORIGINAL RESEARCH
published: 30 June 2022
doi: 10.3389/fimmu.2022.935465

T Cell-Intrinsic Vitamin A Metabolism and Its Signaling Are Targets for Memory T Cell-Based Cancer Immunotherapy

Fumihiro Fujiki[1], Soyoko Morimoto[2], Akiko Katsuhara[3], Akane Okuda[3], Saeka Ogawa[3], Eriko Ueda[3], Maki Miyazaki[3], Ayako Isotani[4,5], Masahito Ikawa[4], Sumiyuki Nishida[6], Hiroko Nakajima[1], Akihiro Tsuboi[7], Yoshihiro Oka[2,6,8], Jun Nakata[9], Naoki Hosen[2,10], Atsushi Kumanogoh[6,8], Yusuke Oji[9] and Haruo Sugiyama[1]**

[1] Department of Cancer Immunology, Graduate School of Medicine, Osaka University, Suita, Japan, [2] Department of Cancer Stem Cell Biology, Graduate School of Medicine, Osaka University, Suita, Japan, [3] Department of Functional Diagnostic Science, Graduate School of Medicine, Osaka University, Suita, Japan, [4] Department of Experimental Genome Research, Research Institute for Microbial Diseases, Osaka University, Suita, Japan, [5] Graduate School of Science and Technology, Nara Institute of Science and Technology, Ikoma, Japan, [6] Department of Respiratory Medicine and Clinical Immunology, Graduate School of Medicine, Osaka University, Suita, Japan, [7] Department of Cancer Immunotherapy, Graduate School of Medicine, Osaka University, Suita, Japan, [8] Department of Immunopathology, WPI Immunology Frontier Research Center, Osaka University, Suita, Japan, [9] Department of Clinical Laboratory and Biomedical Sciences, Graduate School of Medicine, Osaka University, Suita, Japan, [10] Department of Hematology and Oncology, Graduate School of Medicine, Osaka University, Suita, Japan

Memory T cells play an essential role in infectious and tumor immunity. Vitamin A metabolites such as retinoic acid are immune modulators, but the role of vitamin A metabolism in memory T-cell differentiation is unclear. In this study, we identified retinol dehydrogenase 10 (Rdh10), which metabolizes vitamin A to retinal (RAL), as a key molecule for regulating T cell differentiation. T cell-specific Rdh10 deficiency enhanced memory T-cell formation through blocking RAL production in infection model. Epigenetic profiling revealed that retinoic acid receptor (RAR) signaling activated by vitamin A metabolites induced comprehensive epigenetic repression of memory T cell-associated genes, including TCF7, thereby promoting effector T-cell differentiation. Importantly, memory T cells generated by Rdh deficiency and blocking RAR signaling elicited potent anti-tumor responses in adoptive T-cell transfer setting. Thus, T cell differentiation is regulated by vitamin A metabolism and its signaling, which should be novel targets for memory T cell-based cancer immunotherapy.

Keywords: vitamin A, RDH10, memory T cell, retinoic acid, cancer immunotherapy, vitamin A metabolism, effector T cell

OPEN ACCESS

Edited by:
Chih-Hao Chang,
Jackson Laboratory, United States

Reviewed by:
Colby Zaph
Monash University, Australia
Leonid A. Pobezinsky,
University of Massachusetts Amherst, United States

****Correspondence:***
Fumihiro Fujiki,
fu-fuji@sahs.med.osaka-u.ac.jp
Haruo Sugiyama,
sugiyama@sahs.med.osaka-u.ac.jp

Specialty section:
This article was submitted to Cancer Immunity and Immunotherapy, a section of the journal Frontiers in Immunology

Received: *04 May 2022*
Accepted: *03 June 2022*
Published: *30 June 2022*

Citation:
Fujiki F, Morimoto S, Katsuhara A, Okuda A, Ogawa S, Ueda E, Miyazaki M, Isotani A, Ikawa M, Nishida S, Nakajima H, Tsuboi A, Oka Y, Nakata J, Hosen N, Kumanogoh A, Oji Y and Sugiyama H (2022) T Cell-Intrinsic Vitamin A Metabolism and Its Signaling Are Targets for Memory T Cell-Based Cancer Immunotherapy. Front. Immunol. 13:935465. doi: 10.3389/fimmu.2022.935465

INTRODUCTION

The efficient generation of memory T cells is critical to develop effective cancer immunotherapy and robust protective immunity against infectious diseases. Accumulating evidence demonstrates that nutrient metabolism plays a critical role in T cell differentiation; glycolysis and fatty acid oxidation accelerate effector and memory T cell differentiation, respectively (1–4). Thus, it may be possible to guide T cells in a favorable direction by manipulating nutrient metabolism (4).

Vitamin A is an essential nutrient for reproduction, development, cell differentiation, and vision (5–9). Vitamin A (retinol, ROL) is metabolized into retinoic acid (RA) *via* retinaldehyde (also known as retinal, RAL) by two oxidation steps that are strictly regulated by retinol dehydrogenases (RDHs) and retinaldehyde dehydrogenases (RALDHs) (9). Vitamin A and its metabolites are multifunctional and can positively or negatively regulate the acquired immune response. RA, the most active form of these metabolites, enhances the extra-thymic induction of regulatory T (Treg) cells (10, 11) and is required for the proper function of effector $CD8^+$ T cells (12) as well as the development of both Th1 and Th17 cells (13). Thus, vitamin A metabolites can influence T cell function and differentiation. However, it remains unsolved whether T cell itself can metabolize vitamin A, and how the metabolites regulate the T cell differentiation.

In this study, we describe that T cell itself can metabolize vitamin A into RAL by RDH10, a rate-limiting enzyme for RA biosynthesis, and that lack of the vitamin A metabolism by T-cell-specific Rdh10 knockout enhances the induction of memory, especially, central memory T cells (T_{CM}) in Listeria infection model, indicating that vitamin A metabolites such as RAL and RA regulate T cell differentiation. Furthermore, we describe that RA comprehensively induces repressive chromatin states and deletes the memory T cell profile through retinoic acid receptor (RAR), thereby promoting effector T-cell differentiation. Conversely, blockage of RAR signaling suppresses terminal T cell differentiation and efficiently increases T_{CM} with a potent anti-tumor immunity. Thus, vitamin A metabolism and RAR signaling are novel targets to enhance anti-cancer immunity.

MATERIALS AND METHODS

Mice

C57BL/6J mice were purchased from Clea Japan, Inc. (Tokyo, Japan). C57BL/6 mice congenic for the CD45 locus (B6-CD45.1) were purchased from Sankyo Lab Service (Tsukuba, Japan). *Cd4Cre*, *Rag1*$^{-/-}$, OT-I, and OT-II mice were purchased from Taconic (Albany, NY, USA). NOD/shi-scid/γc^{null} (NOG) mice were obtained from the Central Institute for Experimental Animals (Kawasaki, Kanagawa, Japan). To generate Rdh10 conditional knock-out and Rdh10-lacZ knock-in mice, an *Rdh10* gene targeting vector (PRPGS00072_B_F12) purchased from the International Knockout Mouse Consortium (IKMC) was electroporated into C57BL/6 background embryonic stem cells (EGR-G101). After G418 selection, clones in which homologous recombination correctly occurred were identified by PCR with the following primers: 5′-CAC TAA CTT CTT ACC TTA GTT CAT CCG TC-3′ (GF3) and 5′-CAC AAC GGG TTC TTC TGT TAG TCC-3′ (LAR3) for the 5′ end and 5′-TCT ATA GTC GCA GTA GGC GG-3′ (R2R) and 5′-GCC GGC CGG TCC TGC AAT GGA CTG-3′ (GR3) for the 3′ end. The gene-targeted EGR-G101 was injected into 8-cell stage ICR embryos to obtain chimeric mice. The chimeric males were crossed with C57BL/6J females and germ-line transmission was confirmed by PCR with the following primers: 5′-GCA TTT GTG CTC CCT ACC CAA TCT T-3′ (Rdh5′F) and 5′-CCA ACT GAC CTT GGG CAA GAA CAT-3′ (Common en2R). F1 mice were crossed with CAG-Flpe or CAG-Cre mice to generate Rdh10 floxed (*Rdh10* ^{f}) or lacZ knock-in reporter (*Rdh10* ^{lacZ}) alleles, respectively (see **Supplementary Figure 2A**). Cre recombinase-mediated deletion of the floxed site was confirmed by PCR with the following primers: 5′-TTC ATA AGG CGC ATA ACG ATA CCA C-3′ (P1), 5′-GAA CTG ATC TCA GCC CAG AGA ATA-3′ (P2) and 5′-CCA CCA CCT GAA CAG TGT GGA T-3′ (P3). The *Rdh10*^{lacZ} allele was identified by PCR with 5′-CAC ACC TCC CCC TGA ACC TGA AAC-3′ (RAF5) and P3. All the transgenic and gene-modified mice had C57BL/6 background except for NOG mice. All animals were maintained under specific pathogen-free (SPF) conditions and all animal experiments were approved by the Institutional Animal Care and Use Committee of Osaka University Graduate School of Medicine (approval number 27-009-001). For phenotype analysis of Rdh10-deficient T cells, sex-matched and littermate mice raised in the same cage were used.

LM-OVA and Infection

LM-OVA (14) was kindly provided by Dr. H. Shen (University of Pennsylvania, Philadelphia, PA, USA). LM-OVA was prepared as described previously (14, 15) and injected into the tail vein. Unless otherwise stated, mice were infected with 2×10^4 colony-forming units (CFU) of LM-OVA on the day after adoptive transfer.

Adoptive Transfer and Isolation of Lymphocytes

For the adoptive transfer of naïve T cells, $CD8^+$ T cells (OT-I cells) were isolated from the spleen of naive *Rdh10*$^{f/f}$ *Cd4Cre* *Rag1*$^{-/-}$ OT-I $CD45.1^+$ $CD45.2^+$ (Rdh10CKO) or *Rdh10*$^{f/f}$ *Rag1*$^{-/-}$ OT-I $CD45.1^+$ (control) mice using the Pan T Cell Isolation Kit II (Miltenyi Biotec, Bergisch Gladbach, Germany). For the adoptive transfer of memory T cells, $CD45.1^+$ OT-I cells were isolated from pooled cells of the spleen and lymph nodes from several mice >30 days post-infection by magnetic selection using biotin-conjugated anti-CD45.1 mAb and streptavidin beads. The isolated cells were stained with anti-CD45.2-PE mAb and Rdh10CKO ($CD45.1^+$ $CD45.2^+$) and control ($CD45.1^+$) memory OT-I cells were separately sorted by FACSAria. The

isolated Rdh10CKO and control OT-I cells were mixed at a ratio of 1:1 (0.5–1 × 10^4 each) and then transferred into sex-matched C57BL/6J (CD45.2$^+$) mice after the confirmation of the ratio by flow cytometry.

Adoptive T-Cell Therapy Using Rdh10CKO Memory T Cells

For assessment of anti-tumor activity of Rdh10CKO and control memory OT-I cells that were generated in LM-OVA infection model as described above, six-week-old B6 mice were irradiated (3 Gy) and then subcutaneously injected on the left side of abdomen with 2.0 × 10^6 OVA-expressing EL-4 (EG-7) cells, immediately followed by i.v. injection with 1.5 × 10^5 memory OT-I cells. In this experiment, we set a humane endpoint; mice were sacrificed when tumor volume reached 15 mm in length. For measurement of tumor volume, blinding was not performed but there were two measurers to obtain accurate data.

Reagents, Antibodies, and Flow Cytometry

All recombinant interleukins (ILs) were purchased from PeproTec (London, UK), except for human IL-2 (Shionogi, Osaka, Japan). All retinoids (all-trans form), LE540, and UVI3003 were purchased from Sigma-Aldrich (St. Louis, MO, USA), Wako (Osaka, Japan), and Tocris Bioscience (Ellisville, MO, USA), respectively. All antibodies used in this study are listed in **Supplementary Table 4**. Cells were incubated with FcR blocking Reagent (Miltenyi Biotec) and then stained with the appropriate combinations of mAbs and fluorochrome-conjugated streptavidin. For intracellular cytokine staining, cells were incubated with or without SIINFEKL peptide (1 μM) or PMA + ionomycin in the presence of brefeldin A for 4 h and stained using the Cytofix/Cytoperm Kit (BD Bioscience, Franklin Lakes, NJ, USA). Foxp3-positive cells and apoptotic cells were detected using the BD Foxp3 Staining Kit (BD Bioscience) and Apoptosis Detection Kit (BD Bioscience), respectively. For cell surface-stained samples, 7-aminoactinomycin D (7AAD; eBioscience) was added just before the flow cytometric analysis to exclude dead cells. Flow cytometry was performed using FACSAria. The data were analyzed using FlowJo software (TreeStar, San Carlos, CA, USA).

Homing Assay

T cells were isolated from splenocytes of *Rdh10*$^{f/f}$ *Cd4Cre* and *Rdh10*$^{f/f}$ mice and labeled with either CFSE or CellTrace Violet (CTV). Both labeled cells were mixed at a ratio of 1:1 (4 × 10^6 per each) and transferred into sex-matched 5–7-week-old B6 mice after the actual ratio was determined by flow cytometry. Sixteen hours later, the ratio of transferred cells from the spleen and lymph nodes was determined by flow cytometry.

Culture of Human Cells and Assessment of Their Functions

CD4$^+$CD45RO$^+$ T cells were freshly isolated from PBMCs of healthy donors using the BD IMag Cell Separation System, stimulated with plate-bound anti-CD3 and soluble anti-CD28 mAbs, and cultured in the presence of IL-2 (20 IU/ml) and RA (1 μM), LE540 (10 μM), or dimethyl sulfoxide (DMSO). Seven days later, the cells were harvested, washed twice, and cultured in an IL-2-free medium overnight. On the next day, the cell phenotypes and functions were evaluated, as described below. To induce apoptosis, the cells were incubated with anti-Fas Ab (100 ng/ml) for 4 h. To assess their proliferation and reconstitution capacity *in vitro*, the cells were labeled with CellTrace Violet (CTV; Thermo Fisher Scientific) and then cultured in the presence of IL-7 (5 ng/ml) or anti-CD3/CD28 mAbs. For reconstitution in NOG mice, the cells (1 × 10^6) were co-transferred with CD3$^+$ cell-depleted autologous PBMCs (2 × 10^6) isolated using CD3 Microbeads and the LD Column (Miltenyi Biotec) into 5- to 7-week-old female mice. Four weeks later, splenocytes were prepared from the mice and the reconstituted T cells were evaluated by flow cytometry. For assessment of T cell differentiation in RDH10-overexpressed and -silenced T cells, CD4$^+$CD45RO$^+$ T cells infected with lentivirus vector were purified by sorting and stimulated with anti-CD3/CD28 mAbs in serum-free medium supplemented with the indicated concentration of all-trans ROL and IL-2. Jurkat cells were cultured in the presence of Retinoid (1 μM) or DMSO for 4 days. In treated Jurkat cells, the expression of CD62L was measured at the protein and mRNA levels by flow cytometry and real-time PCR, respectively. All experiments were performed in duplicate or triplicate.

Anti-Tumor Activity and Persistency of Tumor Antigen-Specific Human T Cells in NOG Mice

B10-T cells were stimulated with plate-bound anti-CD3 (2 μg/ml) and soluble anti-CD28 (2 μg/ml) mAbs, and cultured in the presence of IL-2 (40 IU/ml) and RA (1 μM), LE540 (10 μM), or dimethyl sulfoxide (DMSO). Three days later, the cells were harvested, washed twice, and further cultured for 4 days in 40 IU/ml of IL-2-supplemented medium. For assessment of anti-tumor activity, NOG mice were subcutaneously injected with HLA-A*24:02- and Luciferase gene-expressing K562 leukemia cell line (K562-A24-Luc, 3 × 10^5 cells). After confirmation of engraftment by *In Vivo* Imaging System IVIS (Xenogen, Alameda, CA) on day 3, mice were irradiated (2 Gy) and then transferred with LE540- or DMSO-treated B10-T cells (1 × 10^7 cells) and modified $WT1_{235}$ peptide-pulsed CD3-depleted autologous PBMCs (5 × 10^6 cells), followed by ip injection of recombinant human IL-2 (500 IU) on day 4. Mice were allocated into groups of equal average base line tumor burden prior to treatments. Tumor volumes were evaluated with IVIS imaging system. In some experiments, blood was collected from tail vein at the same time as that of measurement of tumor volumes and examined for frequency of the transferred GFP$^+$ CD8$^+$ T cells by using flow cytometry. Cell number of transferred GFP$^+$ CD8$^+$ T cells in 1 × 10^6 living cells were estimated with both frequency of transferred T cells (hCD45$^+$ hCD3$^+$ cells) and frequency of GFP$^+$ hCD8$^+$ cells in the transferred T cells.

Preparation and Transfection of the Viral Vector

Human *RDH10* (NM_172037.4) and mouse *Rdh10* (NM_133832.3) cDNA were isolated from PBMCs and splenocytes, respectively. The RARα open reading frame (NP_000955) was sub-cloned from the original plasmid (pFN21AE1591, Promega KK, Tokyo, Japan) into the pFC14K plasmid (Promega). Lentivirus vectors encoding full-length RARα, RARα Δ81-153 (RARα-dDBD), or RARα403 (RARα-dAF2) (16) with a C-terminal Halo-tag were generated using the In-Fusion Cloning Kit (TaKaRa Bio Inc, Shiga, Japan). Lentiviruses were generated using CSII-EF-MCS-IRES2-Venus (for overexpression), CS-RfA-EG (for shRNA expression), pCAG-HIVgp, and pCMV-VSVG-RSV-Rev by a standard method. Target sequences for shRNAs are listed in **Supplementary Table 5**. Retroviruses were generated from the plat-E packaging cell line by the transduction of MSCV-IRES-GFP encoding Rdh10 or from plat-gp packaging cell line by the transduction of MSCV-IRES-GFP encoding B10-TCR and pCMV-VSVG-RSV-Rev. For transfection with the lentivirus, $CD4^+$ $CD45RO^+$ T cells were stimulated for 3 days as described above and then spin-infected in the presence of polybrene on a RetroNectin-coated plate. Three days later, the cells were maintained in IL-2-free medium overnight, analyzed for their surface phenotype by flow cytometry, and then transfected cells ($Venus^+$ cells) were sorted for various experiments, as described above. Lentivirus-transfected Jurkat cells were also generated by a spin-infection method, purified by sorting $Venus^+$ or GFP^+ cells, and then used for experiments. For a generation of B10-T cells, T cells were activated with anti-CD3/CD28 mAbs in the presence of IL-2 for 2-3 days and then spin-infected with B10-TCR-encoding retrovirus as described above. Six hours later, retrovirus infection was repeated. B10-T cells were further cultured for 5-4 days and then treated with RAR agonist/antagonist as described above.

High-Performance Liquid Chromatography (HPLC)

Naïve and activated T cells ($0.5–1.0 \times 10^7$ cells) were plated in 3 ml of complete medium supplemented with IL-2 (20 IU/ml) and incubated with 1 μl of ^{3}H-labeled ROL (PerkinElmer, Boston, MA, USA) for 4 h. Cells were harvested and washed three times with PBS and intracellular retinoids were extracted as described previously (17). The extracted retinoids and non-labeled standard all-trans ROL, RAL, and RA were mixed and then fractionated using the HPLC system (Shimadzu, Kyoto, Japan). Separation was performed using the Synergi 4 μm Hydro-RP 80A Column (Phenomenex, Torrance, CA, USA) and an isocratic elution by the solvent composed of 75% acetonitrile and 25% 50 mM ammonium acetate (pH 7) at a flow rate of 1.5 ml/min. Retinoid standards were detected by measuring ultraviolet absorption at 350 nm.

To evaluate the relationship between CD62L expression and plasma ROL, heparinized blood collected from 6- to 7-week-old female mice was used to measure CD62L expression and the concentration of plasma ROL, as described previously (18). To investigate the effect of a high vitamin A (HVA) diet on CD62L expression, all 6- to 7-week-old female mice were fed an AIN93G-based control (vitamin A, 4 IU/g) diet for 1 week prior to feeding AIN93G-based HVA (250 IU/g). These diets were purchased from Clea Japan, Inc. Extracted retinoids were dissolved in acetonitrile and then analyzed by HPLC as described above. To determine the concentration of ROL, a standard curve was obtained using serial dilutions of all-trans ROL.

Chromatin Immunoprecipitation (ChIP) Assay

ChIP assays were performed using a SimpleChIP Plus Enzymatic Chromatin IP Kit (Cell Signaling Technology, Danvers, MA, USA) according to the manufacturer's instructions.

Quantitative Real-Time PCR

mRNAs were extracted using TRIzol reagent (Thermo Scientific) and reverse-transcribed into cDNA using SuperScript VILO (Thermo Scientific). Quantitative real-time PCR was performed using Power SYBR Green Master Mix (Thermo Scientific) following a standard protocol. Primers are listed in **Supplementary Table 6**. Data were analyzed by a comparative quantification method.

ChIP-Seq Analysis

A ChIP-seq and bio-informatics analysis were performed by the TaKaRa Bio Dragon Genomics Center (Yokkaichi, Mie, Japan) using the Illumina HiSeq2500 system. Data quality was checked using FastQC software and all data were found to be of good quality. Reads were aligned to the hg19 human genome using bowtie2 version 2.2.5. Duplicate reads were removed before peak calling using MACS version 1.4.2. Peaks were assigned to genomic regions using BEDTools. According to RefSeq, genes located within 10 kb upstream or downstream of peaks were identified and extracted.

Statistical Analysis

Data were analyzed using Prism 6, 8, or 9. Normally and non-normally distributed data were analyzed by parametric (unpaired *t*-test) and nonparametric (Mann–Whitney test and Wilcoxon test) tests, respectively. For multiple comparisons, ANOVA with *post-hoc* Dunnett's test was used. In the case that the objective cell number was less than 10, the samples were excluded from statistical analysis due to unreliable data (**Figure 3F** left and **Supplementary Figure 5D**).

RESULTS

Vitamin A Metabolism Promotes Human T Cell Differentiation

Wilms' tumor gene 1 (WT1) -specific $CD4^+$ T cell clone differentiated during culture into four subsets, $CD62L^+CD127^+$ (P1), $CD62L^-CD127^+$ (P2), $CD62L^+CD127^-$ (P3), and $CD62L^-CD127^-$ (P4) cells, which were considered as central memory (T_{CM}), effector memory, effector, and terminal effector T (T_{EFF}) cells, respectively, according to cytokine production,

proliferation and self-renewal capacity, and pluripotency (**Supplementary Figures 1A–D**). Differential gene expression among P1, P2, and P4 was examined using a microarray approach, followed by quantitative PCR. *RDH10* expression increased as a function of the differentiation stage (**Supplementary Table 1** and **Supplementary Figure 1E**). This was also observed in freshly isolated $CD4^+$ and $CD8^+$ T cell subsets (**Supplementary Figure 1F**). Furthermore, *RDH10* mRNA expression levels in $CD4^+$ and $CD8^+$ T cells increased sharply and then decreased following T cell receptor (TCR) stimulation (**Supplementary Figure 1G**). RDH10 catalyzes the oxidation of ROL to RAL, which is the rate-limiting step in RA biosynthesis (19, 20). To investigate whether human T cells themselves can metabolize vitamin A *via* RDH10, RDH10-knocked down and -overexpressed $CD4^+$ T cells were generated and examined for RAL and RA production from tritium (^3H) -labeled ROL. Knockdown (**Figures 1A, B**) and overexpression (**Figures 1C, D**) of RDH10 decreased and increased the production of the RAL metabolite from ROL, respectively. Importantly, RA, the most active form of vitamin A, was not detected in the activated T cells (**Figures 1B, D**).

Next, to examine the effect of vitamin A metabolism on T cell differentiation, RDH10-knocked down and -overexpressed $CD4^+$ T cells were activated with TCR stimulation and cultured in serum-free medium supplemented with IL-2 and various concentrations of ROL. Seven days later, the cell expansion and phenotypes (CD62L expression and cytokine production capacity) were analyzed. When RDH10 was knocked down, both T cell expansion and IFN-γ-positive T cells decreased, while both IL-2-single positive T cells and CD62L-positive memory phenotype T cells increased, suggesting the blockage of T cell differentiation to terminal stages (**Figure 1E**). In contrast, the overexpression of RDH10 resulted in increases in both T cell expansion and IFN-γ-positive T cells, but a decrease in CD62L-positive memory phenotype T cells, suggesting the promoted T cell differentiation (**Figure 1F**). The blockage and promotion of T cell differentiation were dependent on the concentration of ROL in serum-free medium without contamination of vitamin A. These results indicate that human T cells themselves metabolize vitamin A, the metabolites of which regulate T cell differentiation, *via* RDH10.

Rdh10 and Vitamin A Regulate CD62L Expression *In Vivo*

To examine the roles of Rdh10 in T cell differentiation, T cell-specific Rdh10 conditional knockout (Rdh10CKO) mice were

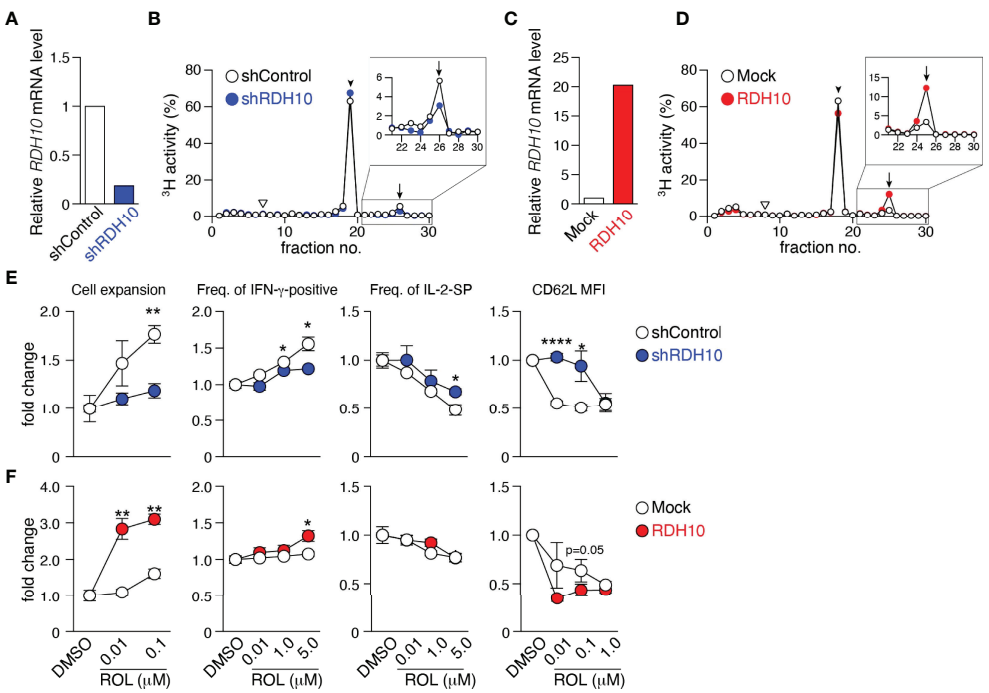

FIGURE 1 | RDH10 metabolizes vitamin A and regulates T cell differentiation. RDH10 in human $CD4^+$ T cells was lentivirally knocked down **(A, B, E)** or overexpressed **(C, D, F)**. **(A, C)** RDH10 mRNA expression level. **(B, D)** shRDH10- **(B)** or RDH10 **(D)**-transduced T cells were cultured in the presence of [^{3}H]-all-trans ROL for 4 h. Then, cell extracts were fractionated by HPLC and the radioactivity of each fraction was measured. Arrowhead, arrow, and inverted triangle indicate the peak fraction of standard all-trans ROL, RAL, and RA, respectively. Representative results from two independent experiments are shown. **(E, F)** shRDH10- **(E)** or RDH10 **(F)** -transduced T cells were cultured in the presence of anti-CD3/28 mAbs, IL-2, and all-trans ROL (or DMSO) for 7 days, and then the cell number, cytokine-producing capacity in response to PMA/Ionomycin, and expression level of CD62L were measured. Data from three (cell number and cytokine-producing capacity) or five (CD62L expression) independent experiments were analyzed by unpaired t-tests. Error bars show s.e.m. *$p < 0.05$; **$p < 0.01$; ****$p < 0.0001$.

established (**Supplementary Figure 2A**). A deficiency of Rdh10 was confirmed by PCR and the loss of RAL production from ROL in T cells (**Supplementary Figures 2B, C**). Rdh10-deficient thymocytes exhibited CD4, CD8, CD24, and TCR-β expression levels comparable to those of control mice (**Supplementary Figure 3A**). In addition, the frequencies of Foxp3$^+$ regulatory and α4β7 integrin-expressing T cells, which are induced by RA (10, 11, 17), were not different between Rdh10-deficient and control mice (**Supplementary Figures 3B, C**). CD4$^+$ and CD8$^+$ T cells in lymphoid organs expressed CD62L at higher levels in Rdh10-deficient mice than in control mice (**Figures 2A–C**). Enhanced CD62L expression was observed at as early as the double-positive stage when the expression of Cre recombinase was initiated during T cell development in the thymus (**Figure 2D**). It is well known that CD62L expression is enhanced in non-activated T cells. However, no difference in the expression of CD44, an activation marker of T cells, between Rdh10-deficient and control mice (**Supplementary Figure 3D**) suggested that the enhanced CD62L expression was not due to the change in T cell activation, but was caused by altered vitamin A metabolism. This was consistent with the observation that an Rdh10 deficiency also enhanced CD62L expression in OT-II cells (21) that are unresponsive to environmental and self-derived antigens in a Rag1-/- background (**Figure 2E**).

Next, the functional effect of enhanced CD62L expression on T cell homing *in vivo* was examined. The mixtures of Rdh10-deficient and control T cells in the ratio of 1:1 were intravenously injected into B6 mice, and the ratio was investigated in secondary lymphoid organs 16 h later. Consistent with the enhanced expression of CD62L, which was a receptor for T cell migration into lymph nodes, the ratio of Rdh10-deficient T cells to control T cells significantly increased in the lymph nodes (**Figure 2F**). These results demonstrated that the ability of Rdh10-deficient T cells to migrate into lymph nodes was potentiated compared to that of control T cells. Thus, these results indicate that Rdh10 regulates the homing capacity of T cells to lymph nodes by the regulation of CD62L expression.

ROL down-regulated CD62L expression in both dose- and Rdh10-dependent manners even in OT-I cells (mouse CD8$^+$ T cells) (**Supplementary Figure 4A**). Furthermore, RAL and RA, which are ROL metabolites downstream of Rdh10, decreased CD62L expression in OT-I cells independently of Rdh10 (**Supplementary Figure 4B**). These results show that ROL metabolism regulates CD62L expression, suggesting that ROL

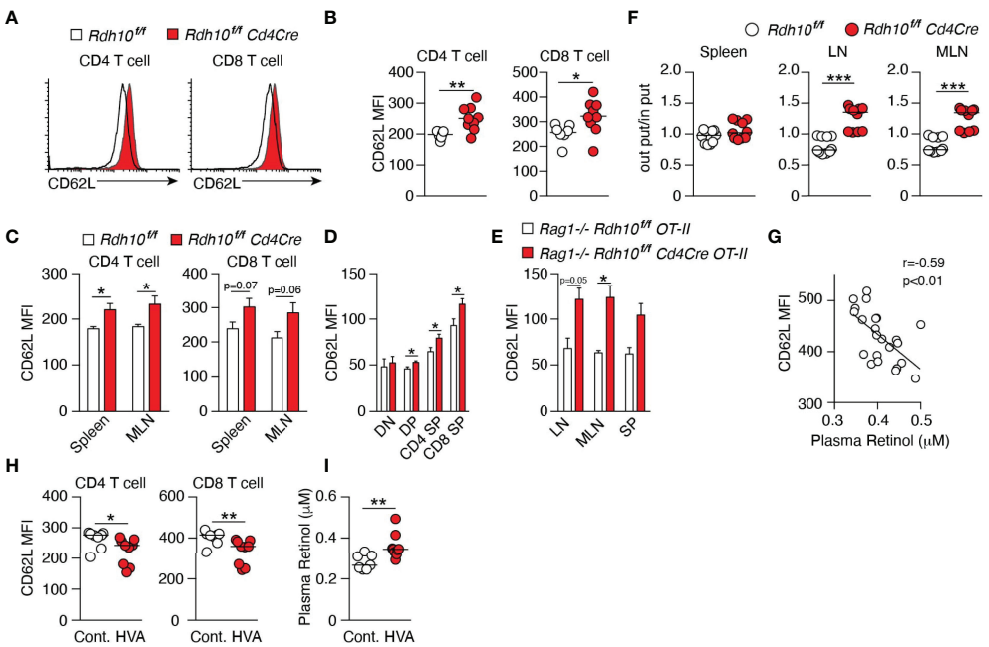

FIGURE 2 | Vitamin A metabolism mediated by Rdh10 physiologically regulates CD62L expression in T cells. **(A–C)** CD62L expression in CD4$^+$ and CD8$^+$ T cells isolated from the lymph node (LN) **(A, B)**, spleen, and mesenteric lymph node (MLN) **(C)** of 6- to 8-week-old mice. Data represent n = 7 littermate control and n = 9 Cd4Cre mice. **(D)** CD62L expression in CD4$^-$ CD8$^-$ double-negative (DN), CD4$^+$ CD8$^+$ double-positive (DP), CD4 single-positive (SP), and CD8 SP thymocytes of 5-week-old mice. Data represent n = 8 littermate control and n = 10 Cd4Cre mice. **(E)** CD62L expression in OT-II cells isolated from the LN, MLN, and spleen (SP) of 6- to 8-week-old mice. Data represent n = 2 littermate control and n = 4 Cd4Cre mice. **(F)** T cells purified from splenocytes of littermate control and Cd4Cre mice were labeled with either CFSE or CTV, mixed at a ratio of 1:1 and injected into B6 mice (8 × 10^6 cells per mouse). Donor cells were analyzed in the spleen, LN, and MLN 16 h later. Each symbol indicates one host mouse (n = 10). Data from two independent experiments are shown. **(G–I)** B6 mice were fed a high vitamin A (HVA) or control diet for 1 week. Peripheral blood was collected pre- **(G)** and post-feeding **(H, I)**, and CD62L expression levels in T cells and the plasma retinol concentration were measured. Data represent CD62L expression levels pre-feeding (n = 23) **(G)** and in control diet-fed (n = 8) and HVA diet-fed (n = 9) mice **(H, I)**. Data were analyzed by unpaired t-tests **(B–F, I)**, Pearson's correlation coefficients **(G)**, or Mann–Whitney tests **(H)**. Error bars show s.e.m. *p < 0.05; **p < 0.01; ***p < 0.001.

concentration in blood closely links to CD62L expression level on T cells. Indeed, an inverse correlation was observed between plasma ROL concentration and CD62L expression in T cells in wild-type mice (**Figure 2G**). These results indicated that food-derived vitamin A can regulate CD62L expression level in T cells. To confirm them, female B6 mice were fed with control diet (4 IU/g) for one week and then with either a high-vitamin A (HVA) (vitamin A, 250 IU/g) or control diet for the next 1 week. As expected, HVA diet reduced CD62L expression in both $CD8^+$ and $CD4^+$ T cells, with a concomitant increase in ROL concentration in plasma (**Figures 2H, I**). Taken together, these results demonstrate that vitamin A (ROL) and its metabolites are physiologically involved in the regulation of CD62L expression in T cells.

Rdh10 Deficiency Promotes Memory T Cell Differentiation

The immune response of Rdh10-deficient $CD8^+$ T cells was investigated in an ovalbumin-expressing *Listeria monocytogenes* (LM-OVA) infection model (14, 22). B6 recipient mice ($CD45.2^+$) were transferred with a 1:1 mixture of naïve Rdh10CKO ($CD45.1^+CD45.2^+$) and control ($CD45.1^+CD45.2^-$) OT-I cells, followed by LM-OVA infection. This experimental model made it possible to discriminate the differentiation of Rdh10CKO ($CD45.1^+CD45.2^+$) OT-I cells from that of controls under the same environmental conditions. Upon LM-OVA infection, the proportions of Rdh10CKO OT-I cells were lower at both the effector phase on day 7 and the early contraction phase on day 10 than those of control OT-I cells (**Figures 3A, B**). IFN-γ production was lower in Rdh10CKO OT-I cells than in control OT-I cells on day 7 (**Supplementary Figure 5A**). Furthermore, short-lived effector cells (SLECs: $CD127^{lo}KLRG1^{hi}$) (23), which are destined to die at the contraction phase, existed at a low frequency in Rdh10CKO OT-I cells on day 10, whereas memory-precursor effector cells (MPECs: $CD127^{hi}KLRG1^{lo}$) (23) that would differentiate into long-lived memory T cells were at a high frequency in the OT-I cells (**Supplementary Figures 5B, C**). Consequently, the proportion of Rdh10CKO OT-I cells dramatically increased in the memory phase on days 36 and 86, and the proportion of Rdh10CKO OT-I cells became dominant compared to that of control OT-I cells (**Figures 3A–C**). Similar kinetics were also observed in the number of transferred OT-I cells (**Figure 3D**). These results indicated that an Rdh10 deficiency in OT-I cells induced differentiation toward memory T cells.

Next, Rdh10CKO OT-I cells in the memory phase were characterized in more detail. Rdh10CKO OT-I cells expressed CD62L at higher levels and contained T_{CM} ($CD62L^+CD127^+$) cells at a higher frequency in both the spleen (**Figures 3E, F**) and lymph nodes (**Supplementary Figures 5D, E**), compared to control OT-I cells. The T_{CM} marker CD127, but not the T_{EFF} marker KLRG1, was also expressed at higher levels in Rdh10CKO OT-I cells than in control OT-I cells (**Supplementary Figures 5F, G**). To confirm that Rdh10CKO OT-I cells were potential memory T cells, the recall responses of these memory T cells were examined after LM-OVA re-challenge because a strong recall response is a hallmark of T_{CM}. A large number of Rdh10CKO OT-I cells were observed in the spleen and liver on day 5 after re-challenge (**Figure 3G**). Importantly, these Rdh10CKO OT-I cells were resistant to the attenuation of T_{CM} generation induced by repetitive antigen exposure (24) with a higher frequency and a greater absolute T_{CM} count, compared to control OT-I cells (**Figures 3H, I**). Thus, these results indicate that Rdh10 deficiency not only enhances memory T cell generation, but also improves the potential for the memory T cells to rapidly expand after re-challenge and to re-generate the T_{CM} pool. The properties of Rdh10-deficient memory T cells suggest Rdh10 as a potential target to improve an effect of cancer immunotherapy because T_{CM} has been shown to have a great anti-tumor activity (25). To confirm this concept, Rdh10-deficient memory OT-I cells were investigated for anti-tumor activity against OVA-expressing EL-4 tumor cell line (EG-7) in an adoptive T cell therapy model. As expected, Rdh10-deficient memory OT-I cells suppressed the tumor growth greater than control memory OT-I cells, resulting in prolonged survival (**Figures 3J, K**).

In Rdh10 (+/-)-lacZ knock-in reporter mice (**Supplementary Figure 2A**), Rdh10 expression was transiently enhanced in OT-I cells after LM-OVA infection (**Supplementary Figure 6A**), which was consistent with the transient production of RAL in activated T cells (**Supplementary Figures 6B–D**). These findings raised the possibility that RAL produced by Rdh10 in the effector phase could promote the differentiation of T cells into effector T cells. Therefore, the recall response was compared between $Rdh10^{hi}$ and $Rdh10^{lo}$ T cells isolated from Rdh10-lacZ knock-in reporter mice in the effector phase (**Supplementary Figure 7A**). $Rdh10^{lo}$ T cells showed a greater recall response than $Rdh10^{hi}$ T cells (**Supplementary Figures 7B, C**), indicating that low Rdh10 expression in the effector phase strengthened the recall response as a result of the increase in T_{CM} cells. This was also confirmed by the lower proliferative capacity and lower T_{CM} generation in the recall response in Rdh10-overexpressing T cells (**Supplementary Figures 7D, E**). Thus, these results demonstrate that Rdh10 regulates T cell differentiation in the effector phase *via* RAL.

RA Receptor Signaling Regulates Human T Cell Differentiation

Not only RA but also RAL binds to retinoic acid receptor (RAR) and the ligand-RAR complex regulates the expression of various genes (26). To examine the effect of RAR signaling downstream of RDH10 on human T cell differentiation, $CD45RO^+CD4^+$ T cells were stimulated with anti-CD3 and -CD28 mAbs in the presence of RA or LE540 (an RAR antagonist) (27), and the expression levels of T cell differentiation markers (CD62L, CD127, CCR7, and CD27) (28–30) were examined after 8 days (**Figures 4A, B**, and **Supplementary Figure 8A**). RAR signaling promoted by RA decreased T_{CM} phenotype T cells, such as $CD62L^+CD127^+$ and $CD62L^+CD27^+$ T cells, whereas the blockage of RAR signaling by LE540 decreased T_{EFF} phenotype T cells, such as $CD62L^-CD127^-$, $CD62L^-CCR7^-$, and $CD62L^-CD27^-$ T cells. These

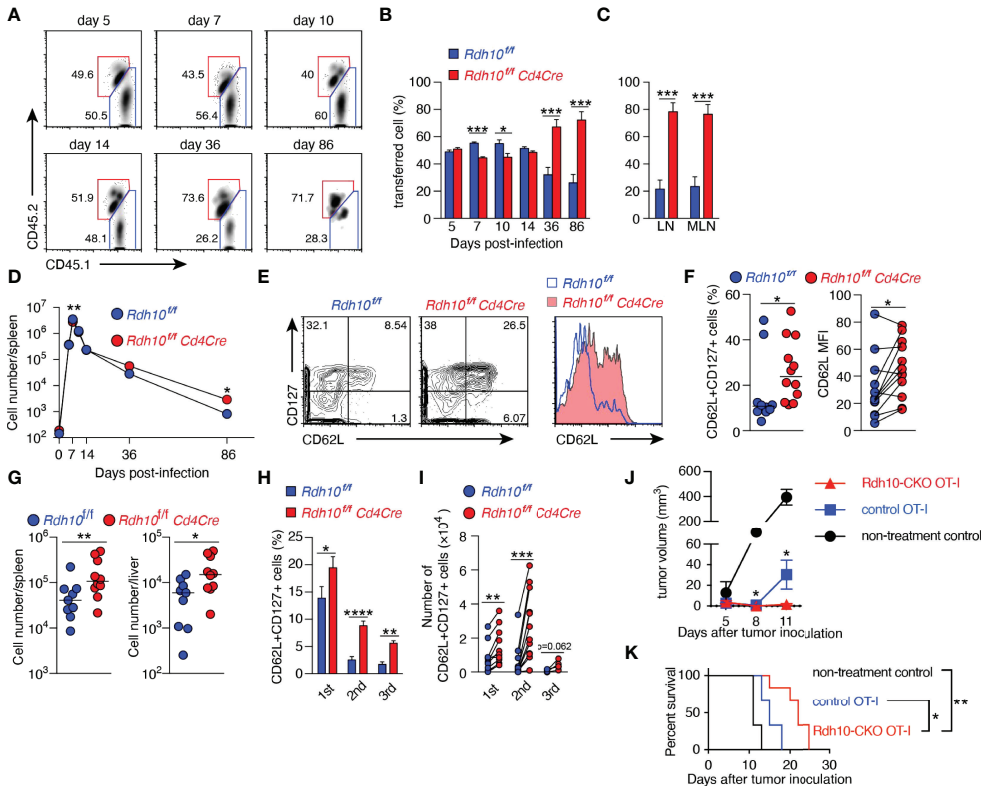

FIGURE 3 | Rdh10 deficiency enhances the generation of central memory T cells. **(A–F)** OT-I cells were isolated from Rdh10CKO (CD45.1$^+$CD45.2$^+$) and control (CD45.1$^+$) mice, mixed at a ratio of 1:1, and then intravenously transferred into the B6 host (CD45.2$^+$). On the next day, the mice were intravenously infected with LM-OVA. **(A)** Representative dot plots showing the frequency of transferred OT-I cells in the spleen on the indicated days post-infection (pi). **(B, C)** Frequencies of the indicated OT-I cells among total transferred OT-I cells from the spleen **(B)** and lymph nodes (**C**, 86 days pi). **(D)** Kinetics of OT-I cell number in the spleen. Symbols show median values. Data represent n = 5 (day 0), n = 8 (day 5, 7, 10, and 14), and n = 12 (day 36 and 86) mice from two independent experiments **(B–D)**. **(E, F)** Frequency of CD62L$^+$CD127$^+$ T_{CM} (left) and the level of CD62L expression (right) in OT-I cells from the spleen in the memory phase (>30 days pi). Representative dot plots and histogram **(E)**. Data represent n = 10 (left) or n = 12 (right) control OT-I cells and n = 12 Rdh10CKO OT-I cells **(F)**. **(G)** Memory OT-I cells were transferred into B6 mice, and OT-I cells were counted in the spleen and liver on day 5 after LM-OVA re-challenge (1×10^6 CFU/mouse). **(H, I)** Serial transfer of primary (1st) memory OT-I cells and LM-OVA infection were performed. The resultant secondary (2nd) and tertiary (3rd) memory OT-I cells were obtained from the spleen and were measured for the frequency **(H)** and absolute number **(I)** of T_{CM}. Data represent n = 12 (1st and 2nd) and n = 6 (3rd) mice from two independent experiments. **(J, K)** Rdh10CKO or control memory OT-I cells were intravenously transferred immediately after subcutaneous inoculation of EG-7 tumor cells into 3 Gy-irradiated B6 mice. Tumor volumes **(J)** and survival rates **(K)** were evaluated. Data represent n = 3 (non-treatment control and control OT-I) and n = 6 (Rdh10CKO OT-I). Data were analyzed by unpaired t-tests **(B, C, H, J)**, Mann–Whitney test (**D**, **F**-left and **G**), Wilcoxon test (**F**-right and **I**), or Log-rank test **(K)**. Error bars show s.e.m. *p < 0.05; **p < 0.01; ***p < 0.001; ****p < 0.0001.

results show that the up- and down-regulation of RAR signaling respectively suppress and promote the expression of CD62L indicating that RAR signaling is a key pathway for the regulation of CD62L expression.

Next, it was examined whether these RA- and LE540-treated T cells (named as T_{RA} and T_{LE} cells, respectively) exhibited the functional characteristics of T_{EFF} and T_{CM}, respectively. DMSO-treated T cells (T_{DM}) were used as a control. It is generally known that T_{EFF} is lower in resistance to apoptosis, proliferative capacity, T_{CM} production after cell division, and *in vivo* expansion capacity, compared to T_{CM}. Consistent with these findings, T_{RA} cells showed high frequencies of apoptosis regardless of the presence or absence of anti-Fas mAb (**Figure 4C**), and showed decreases in both the proliferative capacity (**Figure 4D** and **Supplementary Figure 8B**) and the frequency of T_{CM} (CD62L$^+$CD127$^+$) under two different stimulatory conditions (**Figure 4E** and **Supplementary Figure 8C**). Furthermore, the number of the transferred T_{RA} cells in NOG mice was lower compared to that of T_{DM} cells 4 weeks after T cell transfer (**Figure 4F**). On the other hand, the down-regulation of RAR signaling induced by LE540 had the opposite effect on T cells. Thus, these results demonstrate that RAR signaling promotes T cell differentiation into T_{EFF}. It should be noted that the effect of RA on T cell differentiation required TCR signaling (**Supplementary Figure 8D**), and that UVI3003 (31), an antagonist of retinoid X receptor (RXR) whose heterodimer with RAR acts as a transcription factor (32, 33) could not induce T_{CM} (**Supplementary Figure 8E**). In addition, RAL down-regulated CD62L expression and decreased T_{CM} generation although these functions of RAL

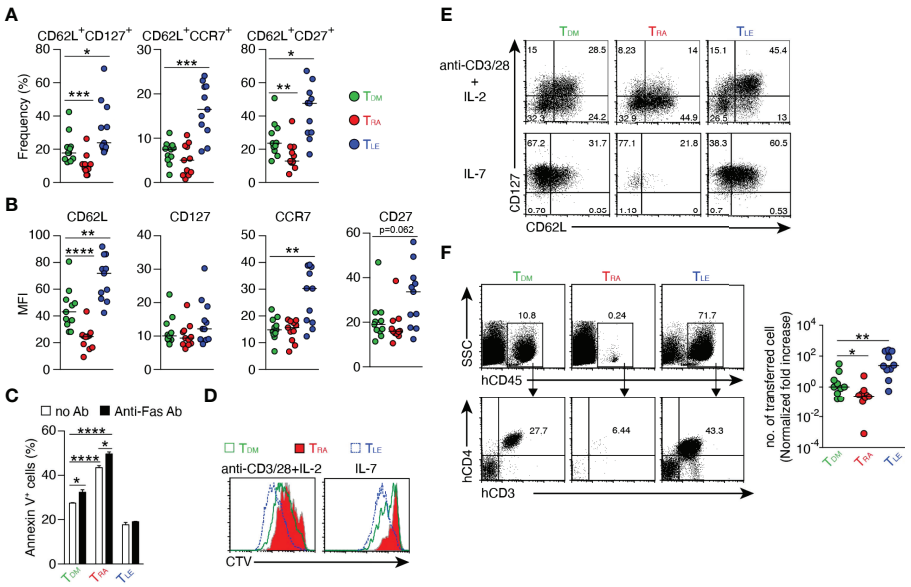

FIGURE 4 | Regulation of T cell differentiation by RAR signaling. Human $CD4^+$ $CD45RO^+$ T cells were stimulated with anti-CD3/CD28 mAbs in the presence of DMSO, RA (1 μM), or LE540 (10 μM). Seven days later, the T cells were rested in IL-2-free medium overnight and then used for subsequent experiments. **(A, B)** Surface phenotypes of T_{DM}, T_{RA}, and T_{LE} cells. Each symbol indicates the results (n = 11) obtained from six independent experiments. **(C)** Frequency of apoptotic cells for T_{DM}, T_{RA}, and T_{LE} cells after 4 h of incubation with or without anti-Fas Ab (n = 3). **(D, E)** T_{DM}, T_{RA}, and T_{LE} cells were labeled with CTV and stimulated with the indicated agents. **(D)** Analysis of cell proliferation using CTV dilution after 4 days of stimulation. **(E)** The T cells were harvested after 5 days of the stimulation, rested in a cytokine-free medium overnight, and analyzed for their surface phenotypes. Representative data from three independent experiments are shown **(C-E)**. **(F)** T_{DM}, T_{RA}, and T_{LE} cells were co-transferred with $CD3^+$ T cell-depleted autologous PBMCs into NOG mice. Four weeks later, a flow cytometric analysis was performed to evaluate transferred cells in the spleen. Representative dot plots (Left) and normalized fold increases in the cell number (Right) are shown. The normalized fold increase was calculated by dividing each value by a median value of the corresponding control (i.e., T_{DM}) group. Data from three independent experiments are shown. Each symbol indicates results from a single mouse (n = 10). Data were analyzed by Mann–Whitney tests **(A, F)** or unpaired t-tests **(C)**. Error bars show s.e.m. *p < 0.05; **p < 0.01; ***p < 0.001; ****p<0.0001.

were weaker than those of RA (**Supplementary Figure 8F**). Importantly, even in human $CD8^+$ T cells, RAR signaling promoted T_{EFF} differentiation as evidenced by low expression of CD62L and weak proliferative capacity in response to IL-7- or TCR-stimulation in RA-treated $CD8^+$ T cells (**Supplementary Figure 9**).

Blocking of RAR Signaling Confers a Strong Anti-Tumor Activity on T Cells

Anti-tumor activity of T_{LE} cells was examined by using an adoptive T cell therapy model. T cells were transduced with B10-TCR (34, 35) which recognized a WT1-derived CTL epitope, $WT1_{235}$ in an HLA-A*24:02-restricted manner, and the T cells were treated with DMSO or LE540. The LE540-treated B10-TCR-transduced T cells (B10-T_{LE} cells) expressed more highly memory or undifferentiated T cell markers such as CD62L, CCR7, and CD45RA, compared to B10-T_{DM} cells (**Supplementary Figure 10**). B10-T_{DM} cells or B10-T_{LE} cells were intravenously transferred into K562-A24-luc tumor-bearing NOG mice. In addition, autologous $WT1_{235}$-pulsed, $CD3^+$ T cell-depleted PBMCs were co-transferred as antigen-presenting cells into the NOG mouse (**Figure 5A**). B10-T_{LE} cells began to suppress tumor growth at day 11 (7 days after T cell transfer) and let the tumor decrease on day 28 (24 days after T cell transfer) whereas statistically significant anti-tumor effect of B10-T_{DM} cells was not observed (**Figures 5B–D**). Importantly, B10-TCR^+ (GFP^+) $CD8^+$ T cells in B10-T_{LE} cells reached a peak on day 18 and were maintained whereas those in B10-T_{DM} cells once reached a peak on day 18 but then remarkably decreased (**Figure 5E**). Persistence of tumor-specific $CD8^+$ T cells has been shown to be a major factor for eliciting an anti-tumor response in adoptive T-cell therapy (36, 37). Therefore, the strong anti-tumor responses of B10-T_{LE} cells likely resulted from the persistence of GFP^+ $CD8^+$ T cells. Thus, these results show that blocking RAR signaling by LE540 confers a potent anti-tumor activity through the increase in memory $CD8^+$ T cells that play a central role in anti-tumor immunity.

Epigenetic Regulation of CD62L Expression by RAR Signaling

CD62L expression in memory T cells is critical for the elimination of tumor cells (25, 38) and viral infection (39), and the results described above clearly demonstrate that vitamin A metabolism and RAR signaling regulate CD62L expression. Therefore, the mechanism underlying the regulation of CD62L expression was investigated. Enforced expression of RARα decreased CD62L expression at both the protein and mRNA

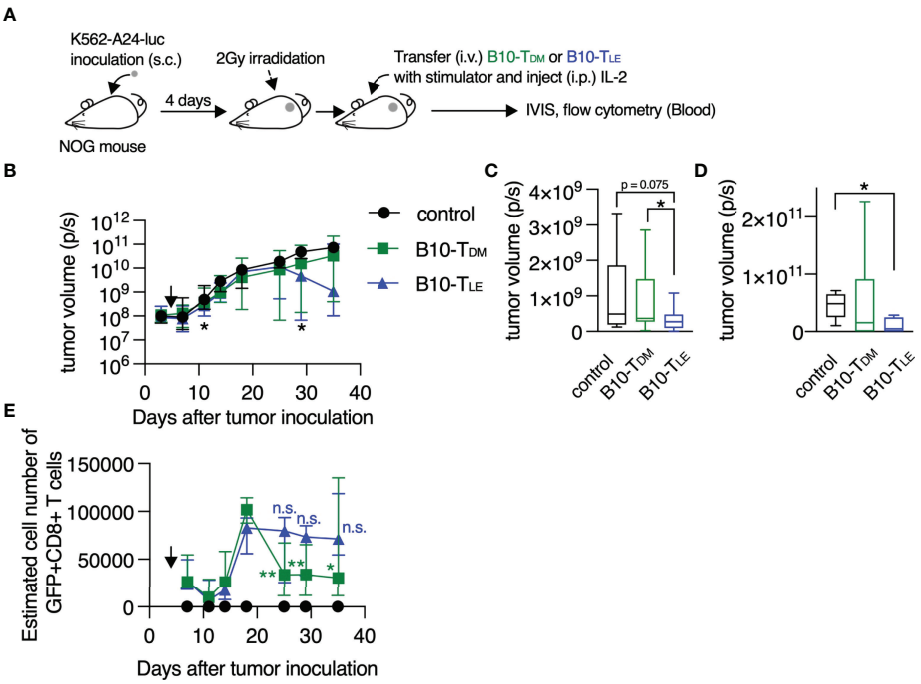

FIGURE 5 | RAR signal blockade confers a strong anti-tumor activity on human T cells. **(A)** Experimental schematic. B10-T_{DM} or B10-T_{LE} cells were intravenously co-transferred with WT1 peptide-pulsed autologous $CD3^+$ cell-depleted PBMCs into K562-A24-luc tumor-bearing NOG mice. Control mice were treated in the same procedure without T-cell transfer. **(B)** Kinetics of tumor growth. Significant differences were observed in the three groups on days 11 and 29 after tumor inoculation, as marked with asterisk (*). Symbols show median with interquartile range. **(C)** Tumor volume on day 11 after tumor inoculation (control, n = 11; B10-T_{DM} and B10-T_{LE}, n = 17). **(D)** Tumor volume on day 29 after tumor inoculation (control and B10-T_{LE}, n = 5; B10-T_{DM}, n = 6). **(E)** Kinetics of persistence of GFP^+ $CD8^+$ T cells. GFP^+ $CD8^+$ T cells in B10-T_{DM} significantly decreased from a peak (day 18), whereas those in B10-T_{LE} persisted. Symbols show median (with interquartile range) of estimated number of cells (each group, n = 6). The estimated number of cells were calculated from frequencies of GFP^+ $CD8^+$ cells in blood. Data from six **(B, C)** or two **(D, E)** independent experiments were analyzed by Mann-Whitney test **(C, D)** or paired t-test (**E**; day 18 vs. day 25, 29, and 35). *p < 0.05; **p < 0.01. n.s., not significant.

levels in Jurkat cells in the presence of RAL or RA (**Figures 6A, B**), indicating that shedding of CD62L from the cell surface (40) was not the cause of the down-regulation of surface CD62L expression. KLF2, a key transcription factor that induces CD62L expression (40–42), increased regardless of the decrease in CD62L expression by RA treatment (**Figure 6C**), suggesting the existence of a novel regulatory mechanism of CD62L expression. RARα directly binds to DNA, recruits co-repressors, and suppresses the transcription of target genes. Both the DNA-binding domain (DBD) and activation function 2 (AF2) domain are critical for regulating target gene transcription (16, 43). Neither DBD- nor AF2 domain-deficient RARα proteins down-regulated CD62L expression, regardless of the presence of RA (**Figure 6D**). Furthermore, two co-repressor proteins, i.e., nuclear receptor co-repressor (NCoR) (44) and silencing mediator for retinoid/thyroid hormone receptor (SMRT) (45), were needed for RAR signaling-dependent CD62L repression, as evidenced by significant restoration of CD62L expression after the knockdown of both co-repressors (**Figure 6E**). Since these co-repressors recruit histone deacetylases (HDACs) and confer a deacetylated status on histones, the role of histone deacetylation at the *CD62L* locus in the downregulation of CD62L expression was investigated. RA treatment decreased histone acetylation (H3K9/14ac) at the *CD62L* promoter region (**Figures 6F, G** and **Supplementary Figure 11**). On the other hand, LE540-treatment increased H3K9/14ac (**Supplementary Figure 11**). Furthermore, Trichostatin A (TSA), an HDAC inhibitor, could abrogate the RA-induced CD62L downregulation (**Figure 6H**). Thus, these results demonstrate that RAR signaling induced by RAL or RA represses CD62L expression *via* the deacetylation of H3K9/14 at the *CD62L* promoter region.

RA Signaling Induces Comprehensive Epigenetic Repression of Memory T Cell-Associated Genes

In addition to the down-regulation of CD62L, RA signaling also induced various effector T cell properties, as described in **Figure 4**, suggesting that the epigenetic regulation of multiple genes was associated with T cell differentiation. To examine broad-scale epigenetic regulatory effects, a ChIP-seq analysis was performed for T_{DM}, T_{RA}, and T_{LE} cells with antibodies specific for H3K9/14ac and H3K27me3, which are markers for "opened" and "closed" chromatin structures, respectively (46, 47). The

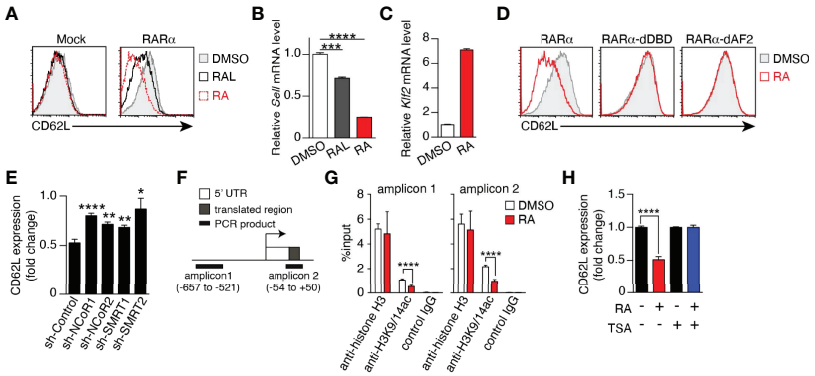

FIGURE 6 | RAR signaling-induced CD62L repression is mediated by epigenetic modifications. **(A–D)** Jurkat cells transduced with the empty vector (Mock), full-length (RARα), DBD-deficient (RARα-dDBD), or AF2-deficient RARα (RARα-dAF2) were cultured for 3–4 days in the presence of RAL (1 μM), RA (1 μM), or DMSO and the expression levels of CD62L protein **(A, D)**, CD62L mRNA **(B)**, and KLF2 mRNA **(C)** were measured. **(A, D)** Representative histograms are shown. **(B, C)** Representative CD62L and KLF2 mRNA levels in RARα-overexpressing Jurkat cells after the indicated treatments. Representative data from two independent experiments are shown **(A-D)**. **(E)** RARα-overexpressing Jurkat cells transduced with the indicated shRNAs were cultured for 4 days in the presence of RA (1 μM) or DMSO, and CD62L protein levels were measured. Data show the fold change of CD62L expression (MFIs of CD62L in RA-treated cells/those in DMSO-treated cells) in three independent experiments. **(F)** CD62L locus and positions of amplicons for the ChIP assay. **(G)** ChIP assay results from RARα-overexpressed Jurkat cells treated with DMSO or RA for 4 days. Data were obtained from two (DMSO) or three (RA) independent experiments. **(H)** CD62L expression (fold change) on RARα-overexpressing Jurkat cells cultured under the indicated conditions (RA, 1 μM; TSA, 50 nM) for 4 days. Data were obtained from three independent experiments. Data were analyzed by unpaired t-tests. Error bars show s.e.m. *$p < 0.05$; **$p < 0.01$; ***$p < 0.001$; ****$p < 0.0001$.

number of H3K9/14ac-enriched regions was lower in T_{RA} cells (1400 peak calls) than in T_{DM} (2298 peak calls) and T_{LE} cells (2590 peak calls) (**Figure 7A**). The number of H3K27me3-enriched regions was comparable among T_{DM}, T_{RA}, and T_{LE} cells, but was slightly lower in T_{LE} cells than in the other two types of cells. Analysis using the Cis-regulatory Element Annotation System (CEAS) (48) demonstrated that the proportion of the regions occupied by H3K9/14ac in both the regulatory regions (promoter and downstream) and gene bodies (UTRs, coding exons, and introns) was lower in T_{RA} cells than the other two types of cells (**Figure 7B**, upper panel). In contrast, the proportion of the regions occupied by H3K27me3 in these regions, especially in promoter regions was lower in T_{LE} cells than the other two types of cells (**Figure 7B**, lower panel). These results revealed that T_{RA} and T_{LE} cells had the "closed" and "opened" chromatin states, respectively, for gene expression.

Next, to investigate whether these chromatin states define T cell differentiation, the genes located within 10 kilobases (kb) upstream and downstream of the regions occupied by H3K9/14ac or H3K27me3 were focused. The majority of occupied genes, especially of H3K9/14ac-occupied genes, were different and unique among T_{DM}, T_{RA}, and T_{LE} cells (**Figure 7C** and **Supplementary Figure 12A**). A Metascape analysis (49) of the uniquely occupied genes showed that the cluster of T_{LE} cells was distinct from that of T_{RA} cells, but similar to that of T_{DM} cells (**Figure 7D**). T_{LE} cells had, in the uniquely H3K9/14ac-occupied genes, more highly enriched GO terms, including "cellular protein catabolic process", "protein ubiquitination involved in ubiquitin-dependent protein catabolic process", and "mitochondrion organization", which were likely to be associated with memory T cells based on the requirement for autophagy (50) and mitochondrial oxidative phosphorylation (51) for memory T cell differentiation, compared to T_{DM} cells (**Figure 7D**). Furthermore, an enrichment analysis using Reactome Gene Sets that T_{LE} cells had highly enriched memory-associated genes related to "fatty acid, triacylglycerol, and ketone body metabolism", "mitochondrial protein import", and "TCA cycle and respiratory electron transport" (**Figure 7E**). Surprisingly, the majority of GO terms for the H3K27me3-occupied genes enriched in T_{RA} and T_{DM} cells were not related to T cell biology, but rather related to the development and differentiation of organs and tissues, such as the heart, eyes, and neurons (**Supplementary Figure 12B**). To clarify epigenetic changes among T_{DM}, T_{RA} (more differentiated), and T_{LE} cells (less differentiated), the genes with two histone modifications were extracted by a comparison of differentiated T cells with less differentiated T cells (T_{DM} vs T_{LE} cells, T_{RA} vs T_{DM} cells, and T_{RA} vs T_{LE} cells), and categorized into "Opened" and "Closed" genes (**Supplementary Tables 2** and **3**). This approach also revealed that the most differentiated T_{RA} cells had the pronounced closed chromatin state, compared to T_{DM} and T_{LE} cells (**Figure 7F**). Notably, in the comparison of T_{LE} with T_{RA} cells, T_{RA} cells had the closed chromatin state in the regions of memory T cell-associated genes, including *TCF7*, *BCL2*, *KIT*, *DUSP4, CABLES1*, and *SMAD4* (52–55) (**Figure 7G** and **Supplementary Table 3**). It is well known that TCF7 is a key transcription factor for the maintenance of T cell stemness in $CD8^+$ T cells (56, 57) and the generation of memory T cells. Consistent with this, H3K27me3 at the *TCF7* locus more increased in RA-treated $CD8^+$ T cells compared to LE540- or DMSO-treated $CD8^+$ T cells

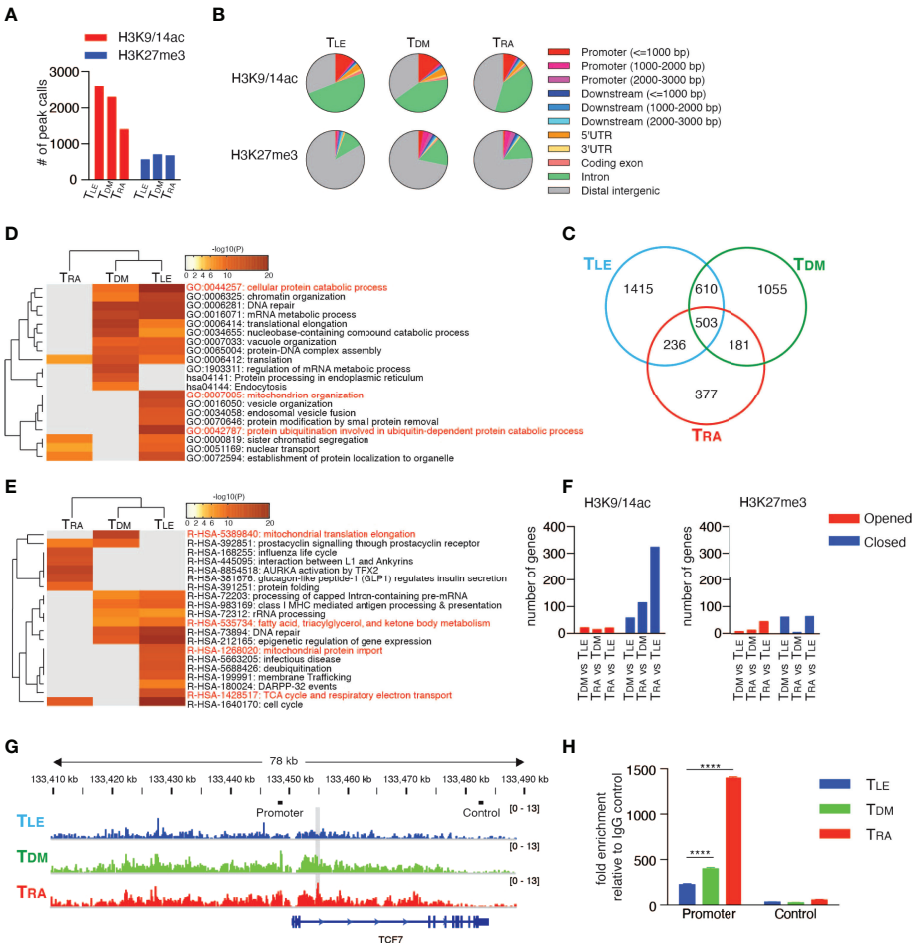

FIGURE 7 | RAR signaling deletes memory T cell profile through comprehensive histone modifications. ChIP-seq using the Illumina HiSeq2500 system was performed with T_{DM}, T_{RA}, and T_{LE} cells for both H3K9/14ac and H3K27me3. **(A)** The number of peak calls. **(B)** Pie charts show the proportion of H3K9/14ac- and H3K27me3-occupied genomic regions. **(C)** Venn diagram shows the number of genes located within ±10 kb of H3K9/14ac-occupied regions. Genes were filtered as follows: $p < 1e\text{-}5$, Fold Enrichment ≥ 5, and Peak Tag count ≥ 5. **(D, E)** Metascape analysis was performed on the uniquely H3K9/14ac-occupied genes (i.e., 1415 genes in T_{LE}, 1055 genes in T_{DM}, and 377 genes in T_{RA}, as described in **(C)**. Pathway and Process Enrichment analyses were performed using default settings without Reactome Gene Sets **(D)** and using only Reactome Gene Sets **(E)**. **(F)** Genes located within ±10 kb of H3K9/14ac- and H3K27me3-occupied regions were extracted for the indicated comparison and categorized as closed and opened genes, respectively, during differentiation. The number of closed and opened genes is shown. **(G)** The patterns of H3K27me3 peaks at the TCF7 locus are shown. The gray shadow indicates the region that was detected as a peak call in the comparison between T_{LE} and T_{RA} cells. Bars indicated as Promoter or Control are positions of amplicons for ChIP-qPCR **(H)**. **(H)** A ChIP assay was performed for H3K27me3-occupied genes in the naïve CD8+ T cells treated with DMSO, RA, or LE540. Representative data are shown from two independent experiments. Data were analyzed by one-way ANOVA with *post-hoc* tests. Error bars show SD. ****$p < 0.0001$.

(**Figure 7H**). Thus, RA signaling comprehensively induces repressive chromatin states and deletes the memory T cell profile.

DISCUSSION

Although it was well known that RAR signaling was required for eliciting effector function in both $CD4^+$ and $CD8^+$ T cells (12, 13, 58, 59), vitamin A metabolism in T cells and its role for T cell differentiation were unclear. In this study, we revealed that T cells intrinsically metabolized vitamin A to RAL by RDH10 and that this metabolism promoted T cell differentiation into terminal effector T cells. Interestingly, although RDH10 is a rate-limiting enzyme for RA production, T cells could not produce RA, which is a more potent RAR signal activator than RAL. This unique vitamin A metabolism suggests the existence of interesting and important kinetics of T cell differentiation. If T cells can produce RA upon activation, they will rapidly differentiate into terminal T_{EFF} cells and disappear by apoptosis, resulting in the discontinuation of the immune response. On the other hand, RAL not completely but appropriately induces T cell differentiation into T_{EFF} cells to keep T_{CM} cells with the avoidance of the complete T cell terminal differentiation, resulting in the continuation of the immune

response. Accordingly, T cells can protect themselves from excessive differentiation by a lack of RA production and maintain a portion of undifferentiated T_{CM} cells. These findings demonstrated a surprising dynamism of T cell differentiation.

Importantly, RA is abundant in tumors (12, 60). When T cells infiltrate into tumors, the T cells can take in the exogenous RA that abundantly exists in tumors and rapidly differentiate into T_{EFF} cells. Inflammatory stimuli can also induce RA production from dendritic cells (DCs) (61), and thus RA is abundant in inflammatory sites. Therefore, T cells infiltrated into the inflammatory sites can rapidly differentiate into T_{EFF} cells by taking in the exogenous RA and eradicate infectious agents. Moreover, RAL from T cells might be taken up and used for RA synthesis by DCs at inflammatory sites because RA production from DCs is likely to be enhanced by the interaction with T cells (17). Taken together, while T cells themselves maintain memory function with self-renewal activity and avoid complete differentiation into T_{EFF} cells by a lack of RA production, they can rapidly differentiate into T_{EFF} cells in RA-rich regions such as tumor and inflammatory sites, where prompt effector function is needed.

We demonstrated that RA signaling induced epigenetic repression of memory-associated genes *via* the decrease and increase in H3K9/14ac and H3K27me3 deposition, respectively. This finding is consistent with a recent report indicating that the accumulation of H3K27me3 deposition on "pro-memory genes", such as *Tcf7*, guides terminal effector T cell differentiation (62). In addition, the epigenetic repression by RA signaling also resulted in the disappearance of unique signatures such as the catabolic process and mitochondrial oxidative phosphorylation in memory T cells. At the effector phase, numerous effector T cells against a pathogen can be generated by clonal expansion that is supported by anabolic processes, but most of these cells subsequently die and only ~5% of them differentiate into memory T cells whose differentiation is supported by catabolic processes, such as autophagy and mitochondrial fatty acid oxidation. Importantly, recent studies have shown that T cells can become memory T cells by shifting their metabolic process from the anabolic to catabolic state (1, 63), implying that most (95%) effector T cells physiologically fail to change their metabolism to the catabolic state after pathogen clearance. Accordingly, there is surely a "gate pass" for the metabolic change. Our present results indicate that the "gate pass" should be a permissive epigenetic signature, which is turned into a repressive signature by RA signaling.

The mechanisms by which RA signaling induces comprehensive epigenetic repression of memory-associated genes remain unclear. As both the DBD and AF2 domain of RARα are required for the repression of CD62L *via* the deacetylation of H3K9/14 at the *CD62L* promoter induced by RA, it is likely that RARs bind to genome DNA and recruit functional proteins such as co-repressor proteins, resulting in the induction of comprehensive repression. However, we could not detect any functionally or evolutionarily conserved RA-responsive elements (RAREs) within ±20 kb of the *CD62L* gene (data not shown). In addition, we did not find co-localization of closed regions with RAREs (data not shown). Therefore, it is not clear whether RARs control epigenetic modifications by direct binding to RAREs. It should be noted that RA signaling alone was insufficient for the differentiation into effector T cells, and that TCR signaling was simultaneously required for it, as shown in **Supplementary Figure 8D**. Interestingly, upon TCR stimulation, the expression of *Ezh2*, which encodes a methyltransferase, is enhanced and the deposition of H3K27me3 increases in $CD8^+$ T cells (62). Furthermore, in activated T cells with TCR stimulation, HDACs co-localize with histone acetyltransferases (HATs) and RNA Pol II at transcribed regions to remove acetylation marks and reset the chromatin state (64). RAR signaling also causes long-term and stable epigenetic changes during the differentiation of stem cells into other specialized cell types, thus silencing or activating large sets of genes either directly or indirectly (65, 66). Thus, RAR signaling may exhibit cross-talk with TCR signaling in the context of epigenetic modification and achieve the directional differentiation into terminal effector T cells.

Allie et al. reported that blockage of RAR signaling enhance the development of central memory-like $CD8^+$ T cells in mouse model (59). However, it was no evidence that blockage of RAR signaling in human T cells enhance anti-tumor immunity through inducing memory T cell. We here succeeded in demonstrating for the first time that RAR signaling in human T cells is targets for improving the clinical efficacy of cancer immunotherapies such as adoptive TCR- or chimeric antigen receptor-transduced T-cell therapy, whose clinical effect is largely dependent upon the amount of memory and undifferentiated T cells (36, 67). Furthermore, we demonstrated that RDH10-dependent vitamin A metabolism in T cells is also the target. RDH10-targeted immunotherapy should be safe because the conditional RDH10 knockout adult mouse did not present any detectable organ damages (unpublished data). In fact, some chemical agents that could inhibit the RDH10 enzyme activity increased memory T cells (unpublished data). Therefore, the present study contributes to develop memory T cell-based cancer immunotherapy by *in vitro* and *in vivo* intervention of T cell differentiation.

DATA AVAILABILITY STATEMENT

The datasets presented in this study can be found in online repositories. The names of the repository/repositories and accession number(s) can be found below: https://www.ncbi.nlm.nih.gov/, GSE137142, https://www.ncbi.nlm.nih.gov/, GSE137714.

ETHICS STATEMENT

The studies involving human participants were reviewed and approved by the Ethics Committee of Osaka University Graduate School of Medicine the Osaka University Research Ethics Committee. The patients/participants provided their written informed consent to participate in this study. The animal study

was reviewed and approved by the Institutional Animal Care and Use Committee of Osaka University Graduate School of Medicine.

AUTHOR CONTRIBUTIONS

FF and HS designed experiments; FF, SM, A Katsuhara, AO, SO, EU, MM, AI, MI, SN, HN, AT, Y Oka, JN, NH, and YO performed the experiments; FF, SM, A Katsuhara, AO, SO, EU, and MM analyzed the data; Y Oka and AK contributed to conception and design of this study. FF and HS wrote the manuscript; all the authors reviewed and approved the final version of the manuscript.

FUNDING

This study was supported by the Japan Society for the Promotion of Science (JSPS) through Grants-in-Aid for Young Scientists WAKATE B-22700896, 24700991 (to FF), and 25830116 (to SM) and Scientific Research Kiban C-26430162, 17K07215, B-21H02786 (to FF), and C-17K07216 (to SM). The Department of Cancer Immunology collaborates with Otsuka Pharmaceutical Co. Ltd. and is supported by a grant from the company.

ACKNOWLEDGMENTS

The authors thank Dr. Hiroyuki Miyoshi (RIKEN Bio-Resource Center, Tsukuba, Japan) for providing the CSII-EF-MCS-IRES2-Venus, CS-RfA-EG, pCAG-HIVgp, and pCMV-VSVG-RSV-Rev plasmid. This study was also supported by Center for Medical Research and Education, Graduate School of Medicine, Osaka University.

SUPPLEMENTARY MATERIAL

The Supplementary Material for this article can be found online at: https://www.frontiersin.org/articles/10.3389/fimmu.2022.935465/full#supplementary-material

REFERENCES

1. Pearce EL, Walsh MC, Cejas PJ, Harms GM, Shen H, Wang LS, et al. Enhancing CD8 T-Cell Memory by Modulating Fatty Acid Metabolism. *Nature* (2009) 460:103–7. doi: 10.1038/nature08097
2. Chang CH, Curtis JD, Maggi LBJr, Faubert B, Villarino AV, O'Sullivan D, et al. Posttranscriptional Control of T Cell Effector Function by Aerobic Glycolysis. *Cell* (2013) 153:1239–51. doi: 10.1016/j.cell.2013.05.016
3. Cham CM, Gajewski TF. Glucose Availability Regulates IFN-Gamma Production and P70s6 Kinase Activation in CD8+ Effector T Cells. *J Immunol* (2005) 174:4670–7. doi: 10.4049/jimmunol.174.8.4670
4. Chang CH, Pearce EL. Emerging Concepts of T Cell Metabolism as a Target of Immunotherapy. *Nat Immunol* (2016) 17:364–8. doi: 10.1038/ni.3415
5. Chambon P. A Decade of Molecular Biology of Retinoic Acid Receptors. *FASEB J* (1996) 10:940–54. doi: 10.1096/fasebj.10.9.8801176
6. Collins MD, Mao GE. Teratology of Retinoids. *Annu Rev Pharmacol Toxicol* (1999) 39:399–430. doi: 10.1146/annurev.pharmtox.39.1.399
7. Morriss-Kay GM, Ward SJ. Retinoids and Mammalian Development. *Int Rev Cytol* (1999) 188:73–131. doi: 10.1016/S0074-7696(08)61566-1
8. Kastner P, Mark M, Chambon P. Nonsteroid Nuclear Receptors: What are Genetic Studies Telling Us About Their Role in Real Life? *Cell* (1995) 83:859–69. doi: 10.1016/0092-8674(95)90202-3
9. Theodosiou M, Laudet V, Schubert M. From Carrot to Clinic: An Overview of the Retinoic Acid Signaling Pathway. *Cell Mol Life Sci* (2010) 67:1423–45. doi: 10.1007/s00018-010-0268-z
10. Mucida D, Park Y, Kim G, Turovskaya O, Scott I, Kronenberg M, et al. Reciprocal TH17 and Regulatory T Cell Differentiation Mediated by Retinoic Acid. *Science* (2007) 317:256–60. doi: 10.1126/science.1145697
11. Coombes JL, Siddiqui KR, Arancibia-Carcamo CV, Hall J, Sun CM, Belkaid Y, et al. A Functionally Specialized Population of Mucosal CD103+ DCs Induces Foxp3+ Regulatory T Cells *via* a TGF-Beta and Retinoic Acid-Dependent Mechanism. *J Exp Med* (2007) 204:1757–64. doi: 10.1084/jem.20070590
12. Guo Y, Pino-Lagos K, Ahonen CA, Bennett KA, Wang J, Napoli JL, et al. A Retinoic Acid–Rich Tumor Microenvironment Provides Clonal Survival Cues for Tumor-Specific CD8(+) T Cells. *Cancer Res* (2012) 72:5230–9. doi: 10.1158/0008-5472.CAN-12-1727
13. Hall JA, Cannons JL, Grainger JR, Dos Santos LM, Hand TW, Naik S, et al. Essential Role for Retinoic Acid in the Promotion of CD4(+) T Cell Effector Responses *via* Retinoic Acid Receptor Alpha. *Immunity* (2011) 34:435–47. doi: 10.1016/j.immuni.2011.03.003
14. Pope C, Kim SK, Marzo A, Masopust D, Williams K, Jiang J, et al. Organ-Specific Regulation of the CD8 T Cell Response to Listeria Monocytogenes Infection. *J Immunol* (2001) 166:3402–9. doi: 10.4049/jimmunol.166.5.3402
15. Wang N, Strugnell R, Wijburg O, Brodnicki T. Measuring Bacterial Load and Immune Responses in Mice Infected With Listeria Monocytogenes. *J Vis Exp* (2011). doi: 10.3791/3076
16. Schule R, Rangarajan P, Yang N, Kliewer S, Ransone LJ, Bolado J, et al. Retinoic Acid is a Negative Regulator of AP-1-Responsive Genes. *Proc Natl Acad Sci USA* (1991) 88:6092–6. doi: 10.1073/pnas.88.14.6092
17. Iwata M, Hirakiyama A, Eshima Y, Kagechika H, Kato C, Song SY, et al. Retinoic Acid Imprints Gut-Homing Specificity on T Cells. *Immunity* (2004) 21:527–38. doi: 10.1016/j.immuni.2004.08.011
18. Napoli JL, Horst RL. Quantitative Analyses of Naturally Occurring Retinoids. *Methods Mol Biol* (1998) 89:29–40. doi: 10.1385/0-89603-438-0:29
19. Belyaeva OV, Johnson MP, Kedishvili NY. Kinetic Analysis of Human Enzyme RDH10 Defines the Characteristics of a Physiologically Relevant Retinol Dehydrogenase. *J Biol Chem* (2008) 283:20299–308. doi: 10.1074/jbc.M800019200
20. Farjo KM, Moiseyev G, Nikolaeva O, Sandell LL, Trainor PA, Ma JX, et al. RDH10 is the Primary Enzyme Responsible for the First Step of Embryonic Vitamin A Metabolism and Retinoic Acid Synthesis. *Dev Biol* (2011) 357:347–55. doi: 10.1016/j.ydbio.2011.07.011
21. Barnden MJ, Allison J, Heath WR, Carbone FR. Defective TCR Expression in Transgenic Mice Constructed Using cDNA-Based Alpha- and Beta-Chain Genes Under the Control of Heterologous Regulatory Elements. *Immunol Cell Biol* (1998) 76:34–40. doi: 10.1046/j.1440-1711.1998.00709.x
22. Shen H, Slifka MK, Matloubian M, Jensen ER, Ahmed R, Miller JF., et al. Recombinant Listeria Monocytogenes as a Live Vaccine Vehicle for the Induction of Protective Anti-Viral Cell-Mediated Immunity. *Proc Natl Acad Sci USA* (1995) 92:3987–91. doi: 10.1073/pnas.92.9.3987
23. Joshi NS, Cui W, Chandele A, Lee HK, Urso DR, Hagman J, et al. Inflammation Directs Memory Precursor and Short-Lived Effector CD8(+) T Cell Fates *via* the Graded Expression of T-Bet Transcription Factor. *Immunity* (2007) 27:281–95. doi: 10.1016/j.immuni.2007.07.010

24. Wirth TC, Xue HH, Rai D, Sabel JT, Bair T, Harty JT, et al. Repetitive Antigen Stimulation Induces Stepwise Transcriptome Diversification But Preserves a Core Signature of Memory CD8(+) T Cell Differentiation. *Immunity* (2010) 33:128–40. doi: 10.1016/j.immuni.2010.06.014
25. Klebanoff CA, Gattinoni L, Torabi-Parizi P, Kerstann K, Cardones AR, Finkelstein SE, et al. Central Memory Self/Tumor-Reactive CD8+ T Cells Confer Superior Antitumor Immunity Compared With Effector Memory T Cells. *Proc Natl Acad Sci USA* (2005) 102:9571–6. doi: 10.1073/pnas.0503726102
26. Kiefer FW, Vernochet C, O'Brien P, Spoerl S, Brown JD, Nallamshetty S, et al. Retinaldehyde Dehydrogenase 1 Regulates a Thermogenic Program in White Adipose Tissue. *Nat Med* (2012) 18:918–25. doi: 10.1038/nm.2757
27. Umemiya H, Fukasawa H, Ebisawa M, Eyrolles L, Kawachi E, Eisenmann G, et al. Regulation of Retinoidal Actions by Diazepinylbenzoic Acids. Retinoid Synergists Which Activate the RXR-RAR Heterodimers. *J Med Chem* (1997) 40:4222–34. doi: 10.1021/jm9704309
28. Bachmann MF, Wolint P, Schwarz K, Jager P, Oxenius A. Functional Properties and Lineage Relationship of CD8+ T Cell Subsets Identified by Expression of IL-7 Receptor Alpha and CD62L. *J Immunol* (2005) 175:4686–96. doi: 10.4049/jimmunol.175.7.4686
29. Sallusto F, Lenig D, Forster R, Lipp M, Lanzavecchia A. Two Subsets of Memory T Lymphocytes With Distinct Homing Potentials and Effector Functions. *Nature* (1999) 401:708–12. doi: 10.1038/44385
30. Hamann D, Baars PA, Rep MH, Hooibrink B, Kerkhof-Garde SR, Klein MR, et al. Phenotypic and Functional Separation of Memory and Effector Human CD8+ T Cells. *J Exp Med* (1997) 186:1407–18. doi: 10.1084/jem.186.9.1407
31. Pogenberg V, Guichou JF, Vivat-Hannah V, Kammerer S, Perez E, Germain P, et al. Characterization of the Interaction Between Retinoic Acid Receptor/Retinoid X Receptor (RAR/RXR) Heterodimers and Transcriptional Coactivators Through Structural and Fluorescence Anisotropy Studies. *J Biol Chem* (2005) 280:1625–33. doi: 10.1074/jbc.M409302200
32. Mark M, Ghyselinck NB, Wendling O, Dupe V, Mascrez B, Kastner P, et al. A Genetic Dissection of the Retinoid Signalling Pathway in the Mouse. *Proc Nutr Soc* (1999) 58:609–13. doi: 10.1017/S0029665199000798
33. Kastner P, Mark M, Ghyselinck N, Krezel W, Dupe V, Grondona JM, et al. Genetic Evidence That the Retinoid Signal is Transduced by Heterodimeric RXR/RAR Functional Units During Mouse Development. *Development* (1997) 124:313–26. doi: 10.1242/dev.124.2.313
34. Tamanaka T, Oka Y, Fujiki F, Tsuboi A, Katsuhara A, Nakajima H, et al. Recognition of a Natural WT1 Epitope by a Modified WT1 Peptide-Specific T-Cell Receptor. *Anticancer Res* (2012) 32:5201–9.
35. Morimoto S, Fujiki F, Kondo K, Nakajima H, Kobayashi Y, Inatome M, et al. Establishment of a Novel Platform Cell Line for Efficient and Precise Evaluation of T Cell Receptor Functional Avidity. *Oncotarget* (2018) 9:34132–41. doi: 10.18632/oncotarget.26139
36. Fraietta JA, Lacey SF, Orlando EJ, Pruteanu-Malinici I, Gohil M, Lundh S, et al. Determinants of Response and Resistance to CD19 Chimeric Antigen Receptor (CAR) T Cell Therapy of Chronic Lymphocytic Leukemia. *Nat Med* (2018) 24:563–71. doi: 10.1038/s41591-018-0010-1
37. Fraietta JA, Nobles CL, Sammons MA, Lundh S, Carty SA, Reich TJ, et al. Disruption of TET2 Promotes the Therapeutic Efficacy of CD19-Targeted T Cells. *Nature* (2018) 558:307–12. doi: 10.1038/s41586-018-0178-z
38. Gattinoni L, Klebanoff CA, Palmer DC, Wrzesinski C, Kerstann K, Yu Z, et al. Acquisition of Full Effector Function *In Vitro* Paradoxically Impairs the *In Vivo* Antitumor Efficacy of Adoptively Transferred CD8+ T Cells. *J Clin Invest* (2005) 115:1616–26. doi: 10.1172/JCI24480
39. Nolz JC, Harty JT. Protective Capacity of Memory CD8+ T Cells is Dictated by Antigen Exposure History and Nature of the Infection. *Immunity* (2011) 34:781–93. doi: 10.1016/j.immuni.2011.03.020
40. Sinclair LV, Finlay D, Feijoo C, Cornish GH, Gray A, Ager A, et al. Phosphatidylinositol-3-OH Kinase and Nutrient-Sensing mTOR Pathways Control T Lymphocyte Trafficking. *Nat Immunol* (2008) 9:513–21. doi: 10.1038/ni.1603
41. Carlson CM, Endrizzi BT, Wu J, Ding X, Weinreich MA, Walsh ER, et al. Kruppel-Like Factor 2 Regulates Thymocyte and T-Cell Migration. *Nature* (2006) 442:299–302. doi: 10.1038/nature04882
42. Bai A, Hu H, Yeung M, Chen J. Kruppel-Like Factor 2 Controls T Cell Trafficking by Activating L-Selectin (CD62L) and Sphingosine-1-Phosphate Receptor 1 Transcription. *J Immunol* (2007) 178:7632–9. doi: 10.4049/jimmunol.178.12.7632
43. Tsai S, Bartelmez S, Heyman R, Damm K, Evans R, Collins SJ., et al. A Mutated Retinoic Acid Receptor-Alpha Exhibiting Dominant-Negative Activity Alters the Lineage Development of a Multipotent Hematopoietic Cell Line. *Genes Dev* (1992) 6:2258–69. doi: 10.1101/gad.6.12a.2258
44. Kurokawa R, Soderstrom M, Horlein A, Halachmi S, Brown M, Rosenfeld MG, et al. Polarity-Specific Activities of Retinoic Acid Receptors Determined by a Co-Repressor. *Nature* (1995) 377:451–4. doi: 10.1038/377451a0
45. Chen JD, Evans RM. A Transcriptional Co-Repressor That Interacts With Nuclear Hormone Receptors. *Nature* (1995) 377:454–7. doi: 10.1038/377454a0
46. Guenther MG, Levine SS, Boyer LA, Jaenisch R, Young RA. A Chromatin Landmark and Transcription Initiation at Most Promoters in Human Cells. *Cell* (2007) 130:77–88. doi: 10.1016/j.cell.2007.05.042
47. Mikkelsen TS, Ku M, Jaffe DB, Issac B, Lieberman E, Giannoukos G, et al. Genome-Wide Maps of Chromatin State in Pluripotent and Lineage-Committed Cells. *Nature* (2007) 448:553–60. doi: 10.1038/nature06008
48. Shin H, Liu T, Manrai AK, Liu XS. CEAS: Cis-Regulatory Element Annotation System. *Bioinformatics* (2009) 25:2605–6. doi: 10.1093/bioinformatics/btp479
49. Tripathi S, Pohl MO, Zhou Y, Rodriguez-Frandsen A, Wang G, Stein DA, et al. Meta- and Orthogonal Integration of Influenza "OMICs" Data Defines a Role for UBR4 in Virus Budding. *Cell Host Microbe* (2015) 18:723–35. doi: 10.1016/j.chom.2015.11.002
50. Xu X, Araki K, Li S, Han JH, Ye L, Tan WG, et al. Autophagy is Essential for Effector CD8(+) T Cell Survival and Memory Formation. *Nat Immunol* (2014) 15:1152–61. doi: 10.1038/ni.3025
51. van der Windt GJ, Everts B, Chang CH, Curtis JD, Freitas TC, Amiel E, et al. Mitochondrial Respiratory Capacity is a Critical Regulator of CD8+ T Cell Memory Development. *Immunity* (2012) 36:68–78. doi: 10.1016/j.immuni.2011.12.007
52. Rutishauser RL, Martins GA, Kalachikov S, Chandele A, Parish IA, Meffre E, et al. Transcriptional Repressor Blimp-1 Promotes CD8(+) T Cell Terminal Differentiation and Represses the Acquisition of Central Memory T Cell Properties. *Immunity* (2009) 31:296–308. doi: 10.1016/j.immuni.2009.05.014
53. Zhou X, Yu S, Zhao DM, Harty JT, Badovinac VP, Xue HH., et al. Differentiation and Persistence of Memory CD8(+) T Cells Depend on T Cell Factor 1. *Immunity* (2010) 33:229–40. doi: 10.1016/j.immuni.2010.08.002
54. Turtle CJ, Swanson HM, Fujii N, Estey EH, Riddell SR. A Distinct Subset of Self-Renewing Human Memory CD8+ T Cells Survives Cytotoxic Chemotherapy. *Immunity* (2009) 31:834–44. doi: 10.1016/j.immuni.2009.09.015
55. Weng NP, Araki Y, Subedi K. The Molecular Basis of the Memory T Cell Response: Differential Gene Expression and its Epigenetic Regulation. *Nat Rev Immunol* (2012) 12:306–15. doi: 10.1038/nri3173
56. Wu T, Ji Y, Moseman EA, Xu HC, Manglani M, Kirby M, et al. The TCF1-Bcl6 Axis Counteracts Type I Interferon to Repress Exhaustion and Maintain T Cell Stemness. *Sci Immunol* (2016) 1. doi: 10.1126/sciimmunol.aai8593
57. Im SJ, Hashimoto M, Gerner MY, Lee J, Kissick HT, Burger MC, et al. Defining CD8+ T Cells That Provide the Proliferative Burst After PD-1 Therapy. *Nature* (2016) 537:417–21. doi: 10.1038/nature19330
58. Pino-Lagos K, Guo Y, Brown C, Alexander MP, Elgueta R, Bennett KA, et al. A Retinoic Acid-Dependent Checkpoint in the Development of CD4+ T Cell-Mediated Immunity. *J Exp Med* (2011) 208:1767–75. doi: 10.1084/jem.20102358
59. Allie SR, Zhang W, Tsai CY, Noelle RJ, Usherwood EJ. Critical Role for All-Trans Retinoic Acid for Optimal Effector and Effector Memory CD8 T Cell Differentiation. *J Immunol* (2013) 190:2178–87. doi: 10.4049/jimmunol.1201945
60. Devalaraja S, To TKJ, Folkert IW, Natesan R, Alam MZ, Li M, et al. Tumor-Derived Retinoic Acid Regulates Intratumoral Monocyte Differentiation to Promote Immune Suppression. *Cell* (2020) 180:1098–114.e1016. doi: 10.1016/j.cell.2020.02.042
61. Yokota A, Takeuchi H, Maeda N, Ohoka Y, Kato C, Song SY, et al. GM-CSF and IL-4 Synergistically Trigger Dendritic Cells to Acquire Retinoic Acid-

Producing Capacity. *Int Immunol* (2009) 21:361–77. doi: 10.1093/intimm/dxp003
62. Gray SM, Amezquita RA, Guan T, Kleinstein SH, Kaech SM. Polycomb Repressive Complex 2-Mediated Chromatin Repression Guides Effector CD8 + T Cell Terminal Differentiation and Loss of Multipotency. *Immunity* (2017) 46:596–608. doi: 10.1016/j.immuni.2017.03.012
63. Araki K, Turner AP, Shaffer VO, Gangappa S, Keller SA, Bachmann MF, et al. mTOR Regulates Memory CD8 T-Cell Differentiation. *Nature* (2009) 460:108–12. doi: 10.1038/nature08155
64. Wang Z, Zang C, Cui K, Schones DE, Barski A, Peng W, et al. Genome-Wide Mapping of HATs and HDACs Reveals Distinct Functions in Active and Inactive Genes. *Cell* (2009) 138:1019–31. doi: 10.1016/j.cell.2009.06.049
65. Gudas LJ. Retinoids Induce Stem Cell Differentiation via Epigenetic Changes. *Semin Cell Dev Biol* (2013) 24:701–5. doi: 10.1016/j.semcdb.2013.08.002
66. Mendoza-Parra MA, Malysheva V, Mohamed Saleem MA, Lieb M, Godel A, Gronemeyer H., et al. Reconstructed Cell Fate-Regulatory Programs in Stem Cells Reveal Hierarchies and Key Factors of Neurogenesis. *Genome Res* (2016) 26:1505–19. doi: 10.1101/gr.208926.116
67. Dudley ME, Gross CA, Somerville RP, Hong Y, Schaub NP, Rosati SF, et al. Randomized Selection Design Trial Evaluating CD8+-Enriched Versus Unselected Tumor-Infiltrating Lymphocytes for Adoptive Cell Therapy for Patients With Melanoma. *J Clin Oncol* (2013) 31:2152–9. doi: 10.1200/JCO.2012.46.6441

Conflict of Interest: FF and HS applied for a patent titled "Method for modifying T cell population".

The remaining authors declare that the research was conducted in the absence of any commercial or financial relationships that could be construed as a potential conflict of interest.

The Department of Cancer Immunology collaborates with Otsuka Pharmaceutical Co., Ltd. The company had no role in the study design, data collection and analysis, decision to publish, or preparation of the manuscript.

Publisher's Note: All claims expressed in this article are solely those of the authors and do not necessarily represent those of their affiliated organizations, or those of the publisher, the editors and the reviewers. Any product that may be evaluated in this article, or claim that may be made by its manufacturer, is not guaranteed or endorsed by the publisher.

frontiers | Frontiers in Immunology

TYPE Original Research
PUBLISHED 02 September 2022
DOI 10.3389/fimmu.2022.996348

OPEN ACCESS

EDITED BY
Claude Lambert,
Centre Hospitalier Universitaire (CHU) de Saint-Étienne, France

REVIEWED BY
Yangqiu Li,
Jinan University, China
Jimin Gao,
Wenzhou Medical University, China

*CORRESPONDENCE
Jianchun Yu
yujianchun2000@163.com

SPECIALTY SECTION
This article was submitted to Cancer Immunity and Immunotherapy, a section of the journal Frontiers in Immunology

RECEIVED 17 July 2022
ACCEPTED 16 August 2022
PUBLISHED 02 September 2022

CITATION
Zhang G, Liu A, Yang Y, Xia Y, Li W, Liu Y, Zhang J, Cui Q, Wang D, Liu X, Guo Y, Chen H and Yu J (2022) Clinical predictive value of naïve and memory T cells in advanced NSCLC. *Front. Immunol.* 13:996348. doi: 10.3389/fimmu.2022.996348

Clinical predictive value of naïve and memory T cells in advanced NSCLC

Guan Zhang[1,2], Aqing Liu[1,2], Yanjie Yang[1,2], Ying Xia[1,2], Wentao Li[1], Yunhe Liu[1], Jing Zhang[1], Qian Cui[1,2], Dong Wang[1,2], Xu Liu[3], Yongtie Guo[3], Huayu Chen[3] and Jianchun Yu[1*]

[1]Department of Oncology, First Teaching Hospital of Tianjin University of Traditional Chinese Medicine, Tianjin University of Traditional Chinese Medicine, Tianjin, China, [2]National Clinical Research Center for Chinese Medicine Acupuncture and Moxibustion, Tianjin, China, [3]Clinic Laboratory, First Teaching Hospital of Tianjin University of Traditional Chinese Medicine, Tianjin University of Traditional Chinese Medicine, Tianjin, China

Currently, there is no sensitive prognostic biomarker to screen out benefit patients from the non-benefit population in advanced non-small cell lung cancer patients (aNSCLCs). The 435 aNSCLCs and 278 normal controls (NCs) were recruited. The percentages and absolute counts (AC) of circulating naïve and memory T lymphocytes of $CD4^+$ and $CD8^+$ T cells (Tn/Tm) were measured by flow cytometry. The percentage of $CD4^+$ naïve T (Tn), $CD8^+$ Tn, $CD8^+$ T memory stem cell (Tscm), and $CD8^+$ terminal effector T cell decreased obviously. Still, all AC of Tn/Tm of aNSCLCs was significantly lower compared to NCs. Higher AC and percentage of $CD4^+$ Tn, $CD8^+$ Tn, and $CD4^+$ Tscm showed markedly longer median PFS in aNSCLCs. Statistics demonstrated the AC of $CD4^+$ Tn (≥ 3.7 cells/μL) was an independent protective factor for PFS. The analysis of the prognosis of immunotherapy showed the higher AC and percentage of $CD4^+$ Tn and $CD4^+$ Tscm and higher AC of $CD8^+$ Tscm had significantly longer median PFS and the AC of $CD4^+$ Tn (≥ 5.5 cells/μL) was an independent protective factor for PFS. Moreover, higher AC and percentages of Tn/Tm suggested higher disease control rate and lower progressive disease rate. The AC of Tn/Tm showed more regular patterns of impairment and was more relative with the disease progression than percentages in aNSCLCs. AC had a better predictive value than percentages in Tn/Tm for PFS. Notably, the AC of $CD4^+$ Tn was a potential prognostic biomarker for the PFS and efficacy of immunotherapy.

KEYWORDS

advanced non-small cell lung cancer, absolute counts, naïve $CD4^+$ T cell, immunotherapy, prognosis

Introduction

With the high incidence of cancer, the search for new oncology treatment strategies has become a challenging goal for researchers (1, 2). Now, the breakthrough advance is the programmed cell death protein 1 (PD-1)/programmed cell death-ligand 1 (PD-L1) monoclonal antibody, which is used in first-line immune checkpoint inhibitors (ICIs) in lung cancer (3–5). Histological detection of PD-L1 can guide treatment with anti-PD-1/PD-L1 antibodies. But PD-L1 is heterogeneous and unstable in tumors, and approximately 20% of PD-L1-negative patients still benefit from PD-1/PD-L1 antibody therapy (6). PD-L1 is not an ideal biomarker as some patients with low levels of PD-L1 expression respond to immunotherapy while others with high levels of PD-L1 expression do not, presenting a clinical challenge for patient stratification (7, 8). Some studies showed that high expression of tumor mutational burden (TMB) is associated with improved overall survival in patients with non-small-cell lung cancer (NSCLC) (9, 10). But others studies showed that high expression of TMB in patients with NSCLC is not associated with a prognosis of overall survival (11, 12). Valero C, et al. analyzed 10,233 patients (80% not treated with ICIs, 20% treated with ICIs) with 17 cancer types, before/without ICIs, or after ICIs. In non-ICIs-treated patients, higher TMB (higher percentile within cancer type) was not associated with better prognosis; in fact, in many cancer types, higher TMB was associated with poorer survival, in contrast to ICIs-treated patients, in whom higher TMB was associated with longer survival (13). These biomarkers suffer several well-known limitations, including result variability related to technical issues (14), the need for tumor biopsy tissue (15), and the lack of host immune status evaluation. The occurrence of high TMB does not always correspond to the response to ICIs (16). In an immunotherapy study for advanced NSCLC (aNSCLC), the objective response rate (ORR) for patients with high TMB and high PD-L1 expression was 62.5%, compared to 43.9% for patients with high TMB and low PD-L1 expression and 27.3% for patients with low TMB and high PD-L1 expression (17). However, PD-L1 and TMB expression did not allow assessment of the overall immune status of patients. In addition to intrinsic tumor resistance mechanisms, other reasons for this discrepancy may be directly related to the "quality" of the neoantigen, which activates naïve T cells (Tn) by Dendritic cells (DC) to generate eventual T helper cells (Th) cells and cytotoxic T lymphocytes (CTL) in response to the tumor (18). For patients with aNSCLC, immunotherapy alone or combined with chemotherapy (19) is currently the dominant mode of most clinal treatment (20). Nevertheless, recent advances showed immunotherapy combined with targeted therapy or radiotherapy did not increase the response in patients with PD-L1-positive in NSCLC (21, 22). Therefore, finding easily detectable and accurately prognostic biomarkers to guide immunotherapy is essential. Anti-PD-1/PD-L1 antibodies act by reliving immune suppression, activating immune cells to attack and destroy cancer cells (23). Several biomarkers had studied as potential candidates (24). Studies have shown promising results using absolute counts (AC) of lymphocytes in peripheral blood as a biomarker for patients with advanced NSCLC (aNSCLCs) (25, 26). In addition, $CD4^+$ Th play a pivotal role in the immune system due to performing multiple functions (27, 28). The percentages of lymphocyte subsets ($CD4^+$, $CD8^+$ T cells, B and NK cells) could serve as predictive biomarkers of immunotherapy efficacy and progression-free survival (PFS) in NSCLC, but it did not analyze the AC of lymphocyte subsets (29). A study reported that $CD8^+PD\text{-}1^+$ to $CD4^+PD\text{-}1^+$ ratio in peripheral blood is a prognostic indicator for aNSCLCs post ICIs (30). Different memory $CD4^+$ T cell subsets arise from the initial immune response of antigen-specific $CD4^+$ Tn (31). Baseline $CD4^+$ memory stem T cells (Tscm) in peripheral blood were associated with early screening and adjuvant diagnosis of colorectal cancer (32). The persistence of long-lived memory $CD8^+$ T cells was due to their ability for clonal expansion and cytotoxicity (33–35). Our previous study found that the AC, not the percentage of lymphocyte subsets in peripheral blood of patients with NSCLC was significantly decreased compared to healthy adults. Moreover, AC is more regular than the percentage of lymphocyte subsets. There was a positive correlation between AC of $CD4^+$ T cells and the PFS of patients (36). However, T lymphocyte subsets are heterogeneous populations, which can further divide into naive and memory T cells with different functions. Therefore, we hypothesized that the key to prolonging the survival of aNSCLCs with immunotherapy is the AC of T lymphocyte subsets.

Thus, we infer that the AC and percentages of circulating naïve and memory T lymphocytes of $CD4^+$ and $CD8^+$ T cells (Tn/Tm) could guide the clinical treatment of aNSCLCs. Hence, we explored the potential of Tn/Tm as a predictive biomarker of response to immunotherapy.

Materials and methods

Study design and patients

A total of 435 aNSCLCs and 278 normal controls (NCs) had recruited from the First Teaching Hospital of Tianjin University of Traditional Chinese Medicine and National Clinical Research Center for Chinese Medicine Acupuncture and Moxibustion, including 92 patients who received immunotherapy. All subjects were given informed consent under the Declaration of Helsinki. The clinical trial had approved by the Clinical Research Ethics Committee of the First Teaching Hospital of Tianjin University of Traditional Chinese Medicine (TYLL2021[K] 001). The inclusion criteria of aNSCLCs must meet: 1. had evidence of a pathological and immunohistochemical diagnosis, according to

Response Evaluation Criteria in Solid Tumors (RECIST; version 1.1); 2. were the absence of other malignant tumors; 3. had complete clinical and laboratory data; 4. were at least 18 years old; 5. had absence of severe cardiac, hepatic, renal, cerebral, hematopoietic and immune system disease; 6. had an Eastern Cooperative Oncology Group performance score. Exclusion criteria included an undetermined NSCLC diagnosis or NSCLC with stage I or II, other malignant tumors, or incomplete clinical and laboratory data. All inspections of the NCs enrolled were normal, including physical examination, routine blood cell testing, liver function, renal function, and blood glucose (8, 21, 30).

A total of 435 NSCLC patients with stages III and IV enrolled in the trial after screening between February 1, 2021, and March 1, 2022. Durvalumab was administered intravenously at a fixed dose of 1500 mg every four weeks for up to 4 sessions. Patients with aNCSLC stage III received Durvalumab combined with chemotherapy (concurrent or sequential chemotherapy). Patients with aNCSLC stage IV received Durvalumab monotherapy or Durvalumab in combination with chemotherapy (adenocarcinoma: pemetrexed in combination with carboplatin; squamous carcinoma: albumin paclitaxel in combination with carboplatin) (8).Treatment had discontinued if severe immune-related adverse events or disease progressive, or the patient or investigator decided to terminate treatment. A flow diagram of the subjects and analysis procedures for this study showed in Figure 1. The Tn/Tm assay had performed using flow cytometry (BD FACS Canto II: U6573380-00541, USA) with a lyse/no-wash procedure based on a single-platform technique. The known number of fluorescently labelled beads in BD Trucount tubes was the internal reference for absolute count assay.

The primary endpoint of the outcome was PFS. The second endpoints were complete response (CR), partial response (PR), stable disease (SD), and progressive disease (PD). The disease control rate (DCR) was the sum of the PR and SD rates. The differences in AC and percentages of Tn/Tm between aNSCLCs and NCs compared. In 435 aNSCLCs and 92 aNSCLCs treated with immunotherapy, PFS was compared between two groups based on the cut-off point. The baseline characteristics of patients were shown in Table 1. The 278 NCs included 175 males and 103 females with a median age of 67 years (range, 40-80). There were no significant differences between the aNSCLCs cohort and the NCs cohort in gender and age ($P > 0.05$).

Tn/Tm assay by flow cytometry

The percentages and AC of the Tn/Tm assay were performed by the single platform technique using the ten-color flow cytometer (BD FACS Canto plus: U6573380-00541) (37). The reagents include APC-H7 Mouse Anti-Human CD3 antibody (Catalog NO: 663490), PE-Cy7 Mouse Anti-Human CD4 antibody (Catalog NO: 663493), V500-C Mouse Anti-Human CD45 antibody (Catalog NO: 662912), APC Mouse Anti-Human CD8 antibody (Catalog NO: 663524), BV421 Mouse Anti-Human CD62L antibody (Catalog NO: 563862), PerCP-Cy 5.5 Mouse Anti-Human CD95 antibody (Catalog NO: 561655),

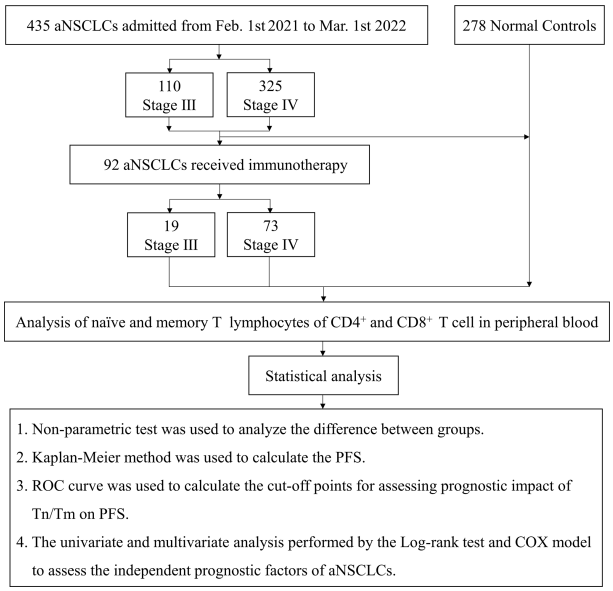

FIGURE 1
The flow chart of patient inclusion and analysis procedures in the study.

10.3389/fimmu.2022.996348

TABLE 1 The baseline characteristics of aNSCLCs.

Characteristics	N = 435	(%)
Age (years) (median, range)	67 (39–80)	
Sex		
Male	294	67.6
Female	141	32.4
Family history		
Yes	103	23.7
No	332	76.3
Smoking history		
Yes	299	68.7
No	136	31.3
Drinking history		
Yes	173	39.8
No	262	60.2
ECOG performance status		
0 or 1	362	83.2
≥ 2	73	16.8
The size of primary tumor (cm)		
< 2	19	4.4
≥ 2	416	95.6
Histological types		
Adenocarcinoma	275	63.2
Squamous carcinoma	160	36.8
Degree of differentiation		
Low	390	89.7
Moderate or High	45	10.3
TNM stage		
Ⅲ	110	25.3
Ⅳ	325	74.7
Lymph node metastasis		
Yes	320	73.6
No	115	26.4
Lung metastasis		
Yes	184	42.3
No	251	57.7
Braine metastasis		
Yes	64	14.7
No	371	85.3
Liver metastasis		
Yes	52	12
No	383	88
Bone metastasis		
Yes	128	29.4
No	307	70.6
Number of metastasis sites		
0	49	11.3
1	120	27.6
2	183	42.1
≥ 3	83	19.1

PE Mouse Anti-Human CD45RO antibody (Catalog NO: 663530), FITC Mouse Anti-Human CD45RA antibody (Catalog NO: 662840), and BD Lysing Solution (Catalog NO: 349202). The EDTA blood collecting tubes and BD Trucount tubes (Catalog NO: 340334) were also purchased from BD Biosciences, USA. The panel of phenotypic characterization of T cells was identified according to their differentiation status (Figure 2), such as naïve T cells (Tn) ($CD45RA^+$ $CD45RO^-$ $CD62L^+$ $CD95^-$), T memory stem cells (Tscm) ($CD45RA^+$ $CD45RO^-$ $CD62L^+$ $CD95^+$), central memory T cells (Tcm) ($CD45RA^-$ $CD45RO^+$ $CD62L^+$ $CD95^+$), effector memory T cells (Tem) ($CD45RA^-$ $CD45RO^+$ $CD62L^-$ $CD95^+$), and terminal effector T cells (Tte) ($CD45RA^+$ $CD45RO^-$ $CD62L^-$ $CD95^+$) (37).

Sample collection, cellular staining and analyzing

Two milliliters of fresh peripheral blood were collected from all subjects using a BD Vacutainer EDTA blood collection tube. Blood samples were taken from aNSCLCs receiving immunotherapy before treatment. Tn/Tm of peripheral blood were stained and analyzed according to BD operating instruction:

1. For each sample, the corresponding BD Trucount Tube was labeled separately;
2. 5 μL each of CD3, CD4, CD8, CD45, CD62L and CD95 antibodies, and 20 μL each of CD45RA and CD45RO reagents were respectively pipetted into the bottom of labeled BD Trucount Tubes, without touching the bead pellet;
3. Reverse pipetting method was used to drew 50 μL of well-mixed, anticoagulated whole blood into the tube just above the metal retainer;
4. The tube was capped and gently rotated to mixed the antibody and the sample;
5. The mixture was placed in the dark and incubated at room temperature between 20°C and 25°C for 15 minutes;
6. 450 μL of 1 × BD Multitest IMK Kit Lysing Solution was added into the tube, covered the tube and gently shook the tube until the liquid was uniform;
7. The tube was incubated in the dark at room temperature of 20°C-25°C for 15 minutes;
8. Samples were analyzed by a ten-color flow cytometer.

A known volume of sample was stained directly in a BD Trucount Tube. The lyophilized pellet in the tube dissolves, releasing a known number of fluorescent beads. During the

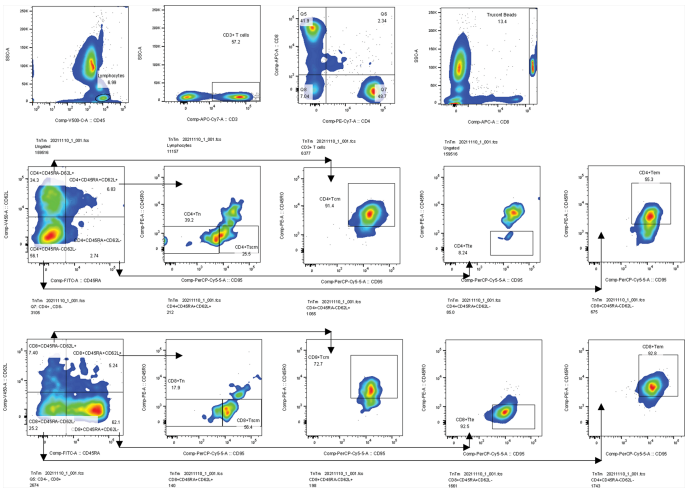

FIGURE 2
Gating strategies. Firstly, we gated lymphocytes identified by CD45 from a leukocyte, then gated $CD3^+$ T cells from a lymphocyte, and gated $CD4^+$ and $CD8^+$ T cells from $CD3^+$ T cells. Secondly, we gated Trucont Beads. Thirdly, Tn ($CD95^-CD45RO^-$) and Tscm ($CD95^+CD45RO^-$) were gated from the $CD3^+CD4^+$ $CD45RA^+CD62L^+$ T subpopulation. Tcm ($CD95^+CD45RO^+$) and Tem ($CD95^+CD45RO^+$) subpopulations were gated from $CD3^+CD4^+CD45RA^-CD62L^+$ and $CD3^+CD4^+CD45RA^-CD62L^-$ T subsets, respectively. Tte ($CD95^+CD45RO^-$) subsets were gated from the $CD3^+CD4^+CD45RA^+CD62L^-$ T subpopulation. The gating logic for each subset of $CD3^+CD8^+$ T cell is the same as above. Tcm, central memory T cells, Tem, effector memory T cells, Tte, terminal effector T cells.

analysis, the absolute number of positive cells (cells per microliter) in the sample can be determined using BD FACS Canto-specific BD clinical software. This is the formula of AC of cells:

$$\text{cell absolute count (cells/}\mu\text{L)} = \frac{Acquired\ \ cells\ \ events \times Total\ \ Beads}{Acquired\ \ beads \times Voulme\ \ of\ \ sample}$$

Statistical analysis

The comparison between groups was analyzed by non-parametric test. The median values and frequencies of the continuous and categorical variables were calculated. PFS was defined as the duration between the initiation of inclusion and the disease progression or death, whichever occurred first. PFS was calculated by Kaplan-Meier method. Patients who were still alive were reviewed at the last available follow-up. The cut-off point was calculated by ROC curve (38). Univariate and multivariate analyses were used to analyze the factors affecting disease progression. Variables with $P< 0.05$ in univariate analysis were entered for multivariate analysis. Log-rank test was used for univariate analysis and the proportional hazards regression model (COX model) was used for multivariate analysis. $P< 0.05$ were considered statistically significant. The data were analyzed by SPSS 25. 0 software and plotted by GraphPad Prism 9. 00 software.

Results

Comparison of Tn/Tm assay between aNSCLCs and normal controls

To analyze the damage status of Tn/Tm in aNSCLCs, the following comparisons were made. Compared to NCs, the percentage of $CD4^+$ Tn, $CD8^+$ Tn, $CD8^+$ Tscm and $CD8^+$ Tte in the peripheral blood of aNSCLCs decreased obviously ($P< 0.001$), the percentage of $CD4^+$ Tcm and $CD4^+$ Tem increased apparently ($P< 0.05$) (Figure 3A). Interestingly, all AC of Tn/Tm of aNSCLCs was significantly lower than NCs ($P< 0.001$), including $CD4^+$ Tn, $CD4^+$ Tscm, $CD4^+$ Tcm, $CD4^+$ Tem, $CD4^+$ Tte, $CD8^+$ Tn, $CD8^+$ Tscm, $CD8^+$ Tcm, $CD8^+$ Tem and $CD8^+$ Tte (Figure 3B). Compared to NCs, percentage of $CD4^+$ Tn, $CD8^+$ Tn and $CD8^+$ Tte in aNSCLCs with stage III was lower ($P< 0.001$), and the percentage of $CD4^+$ Tcm was higher ($P< 0.001$) (Figure 3C), whereas, the AC of $CD4^+$ Tn, $CD4^+$ Tem, $CD8^+$ Tn, $CD8^+$ Tscm, $CD8^+$ Tcm, $CD8^+$ Tem and $CD8^+$ Tte cell was significantly lower ($P< 0.05$) (Figure 3D). In NSCLCs with stage IV, the percentage of $CD4^+$ Tn, $CD8^+$ Tn, $CD8^+$ Tscm and $CD8^+$ Tte was lower ($P< 0.001$), the percentage of $CD4^+$ Tcm and $CD4^+$ Tem was higher ($P< 0.001$) (Figure 3E), however, the AC of ten Tn/Tm subsets was significantly lower than NCs ($P< 0.001$) (Figure 3F).

The above results suggested that AC showed a more regular pattern of impairment and was more relative to the progress of the tumor than percentages of Tn/Tm in aNSCLCs. Besides, the

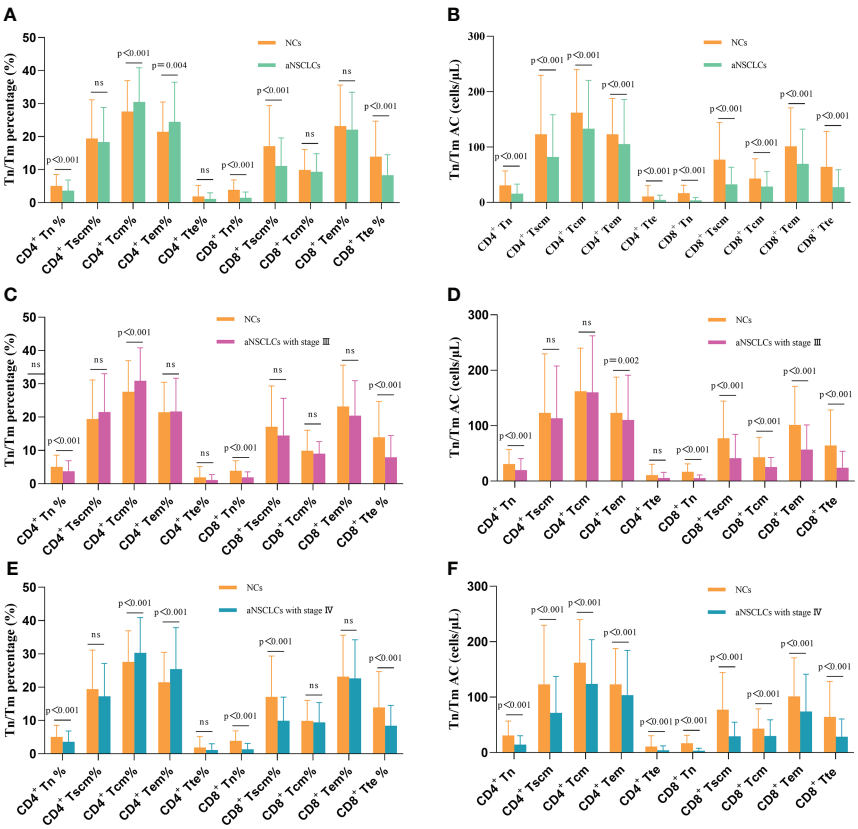

FIGURE 3
Comparison of Tn/Tm between aNSCLCs and NCs: **(A)** Comparison of percentages between aNSCLCs and NCs. **(B)** Comparison of AC between aNSCLCs and NCs. **(C)** Comparison of percentages between aNSCLCs with stage III and NCs. **(D)** Comparison of AC between aNSCLCs with stage III and NCs. **(E)** Comparison of percentages between aNSCLCs with stage IV and NCs. **(F)** Comparison of AC between aNSCLCs with stage IV and NCs. ns, no significance.

frequencies of $CD4^+$ Tn and $CD8^+$ Tn decreased obviously and were associated with the development of cancer (Table 2).

Comparison of Tn/Tm assay between stage III and IV in aNSCLCs

We further analyzed the changes in the Tn/Tm at different stages of aNSCLCs. Compared to NSCLC with stage III, the percentage of $CD4^+$ Tscm, $CD8^+$ Tn and $CD8^+$ Tscm was lower ($P< 0.001$), and the percentage of $CD4^+$ Tem was higher in NSCLC with stage IV ($P = 0.014$) (Figure 4A); while the AC of $CD4^+$ Tn, $CD4^+$ Tscm, $CD4^+$ Tcm and $CD8^+$ Tn was significantly lower ($P< 0.05$) and the AC of $CD8^+$ Tem was higher ($P = 0.031$) (Figure 4B). This research further analyzed the relationship between the expression levels of Tn/Tm and metastasis (No vs Yes = 49: 386). The results showed the percentage of $CD4^+$ Tscm, $CD8^+$ Tn, and $CD8^+$ Tscm in no metastasis was high than that in metastasis, and the frequency of $CD8^+$ Tem in no metastasis was low than that in metastasis ($P< 0.05$) (Figure 4C). The AC of $CD8^+$ Tn and $CD8^+$ Tscm was high in no metastasis. The AC of $CD8^+$ Tem was high in metastasis ($P< 0.05$) (Figure 4D).

This result suggests that the AC of Tn/Tm changes more markedly than the percentage as the disease progresses in NSCLC, and the AC of $CD4^+$ Tn and $CD8^+$ Tn showed a decline in change (Table 2). Moreover, it suggested that the percentage and AC of Tn and Tscm of $CD8^+$ correlated more significantly with metastasis.

Prognostic impact of Tn/Tm on PFS

We analyzed the relationship between AC and percentage of Tn/Tm and PFS of aNSCLCs. In Figure 5A (HR 3.142; 95% CI [2.241 to 4.406]; $P< 0.0001$), Figure 5B (HR 5.038; 95% CI [3.368 to 7.536]; $P< 0.0001$), Figure 5F (HR 2.181; 95% CI [1.554 to 3.063]; $P< 0.0001$) and Figure 5G (HR 2.245; 95% CI [1.568 to 3.217]; $P< 0.0001$), there was significantly longer median PFS for patients with higher percentage and AC of $CD4^+$ Tn (42.4 weeks,

TABLE 2 Cells impairment and prognostic cells in aNSCLCs.

Tn/Tm	Compared with the NCs						Compared with the Stage Ⅲ		PFS	
	All aNSCLCs		Stage Ⅲ		Stage Ⅳ		Stage Ⅳ		%	AC
	%	AC	%	AC	%	AC	%	AC		
$CD4^+$ Tn	★	★	★	★	★	★		★	★	★
$CD4^+$ Tscm		★				★	★	★	★	★
$CD4^+$ Tcm	★	★	★		★	★		★		
$CD4^+$ Tem	★	★		★	★	★	★		★	
$CD4^+$ Tte		★				★				
$CD8^+$ Tn	★	★	★	★	★	★	★	★	★	★
$CD8^+$ Tscm	★	★		★	★	★	★		★	
$CD8^+$ Tcm		★		★		★				
$CD8^+$ Tem		★		★		★		★		
$CD8^+$ Tte	★	★	★	★	★	★				

%: percentage; ★: P< 0.05.

95% CI, 1.715 to 3.543; 42.4 weeks, 95% CI, 2.698 to 5.313) and $CD8^+$ Tn (42.4 weeks, 95% CI, 1.145 to 2.866; 40 weeks, 95% CI, 1.462 to 2.849) compared to lower percentage and AC of $CD4^+$ Tn (17.2 weeks, 95% CI, 0.282 to 0.583;11.2 weeks, 95% CI, 0.188 to 0.371) and $CD8^+$ Tn (20.8 weeks, 95% CI, 0.349 to 0.69; 19.6 weeks, 95% CI, 0.351 to 0.684). High percentage of $CD4^+$ Tscm was associated with better median PFS (34.4 weeks, 95% CI, 1.053 to 2.087 vs 23.2 weeks, 95% CI, 0.479 to 0.949) (HR 1.737; 95% CI [1.244 to 2.427]; P=0.0012) (Figure 5C). High AC of $CD4^+$ Tscm was also associated with longer median PFS (40 weeks, 95% CI, 1.269 to 2.514 vs 22.4 weeks, 95% CI, 0.398 to 0.788) (HR 2.01; 95% CI [1.436 to 2.814]; P< 0.0001) (Figure 5D). The percentage of $CD8^+$ Tscm showed a similarly change to $CD4^+$ Tscm with a higher frequency and a longer median PFS (32.4 weeks, 95%, 0.965 to 1.889 vs 24 weeks, 95% CI, 0.529 to 1.037) (HR 1.572; 95% CI [1.124 to 2.199]; P = 0.0068) (Figure 5H). Contrarily, when the percentage of $CD4^+$ Tem was low, the median PFS was higher (33.2 weeks, 95% CI, 0.984 to 1.945 vs 24 weeks, 95% CI, 0.514 to 1.016) (HR 0.674; 95% CI [0.483 to 0.941]; P = 0.0215) (Figure 5E). The rest of the

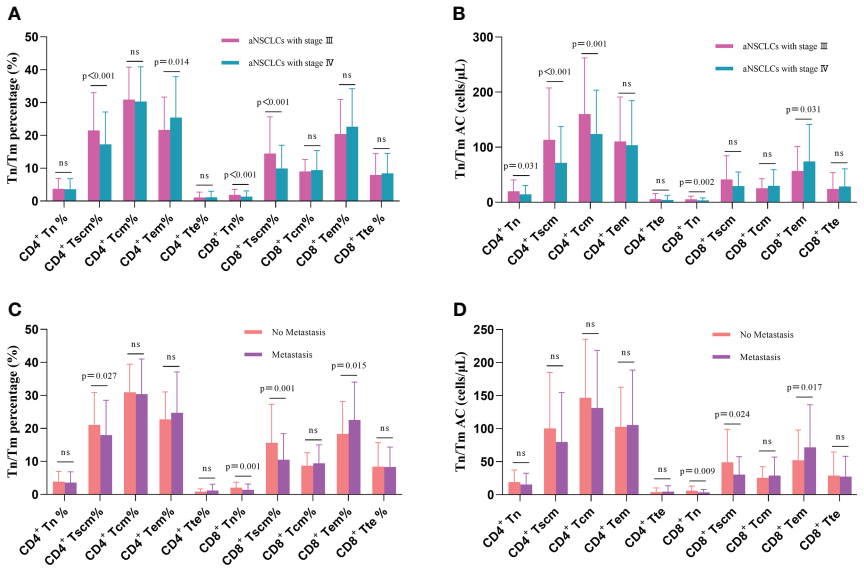

FIGURE 4
Comparison of Tn/Tm between different stages of aNSCLCs and aNSCLCs with or without metastasis: **(A)** Comparison of percentages between stages III and IV in aNSCLCs. **(B)** Comparison of AC between stages III and IV in aNSCLCs. **(C)** Comparison of percentages of aNSCLCs with or without metastasis. **(D)** Comparison of AC of aNSCLCs with or without metastasis. ns, no significance.

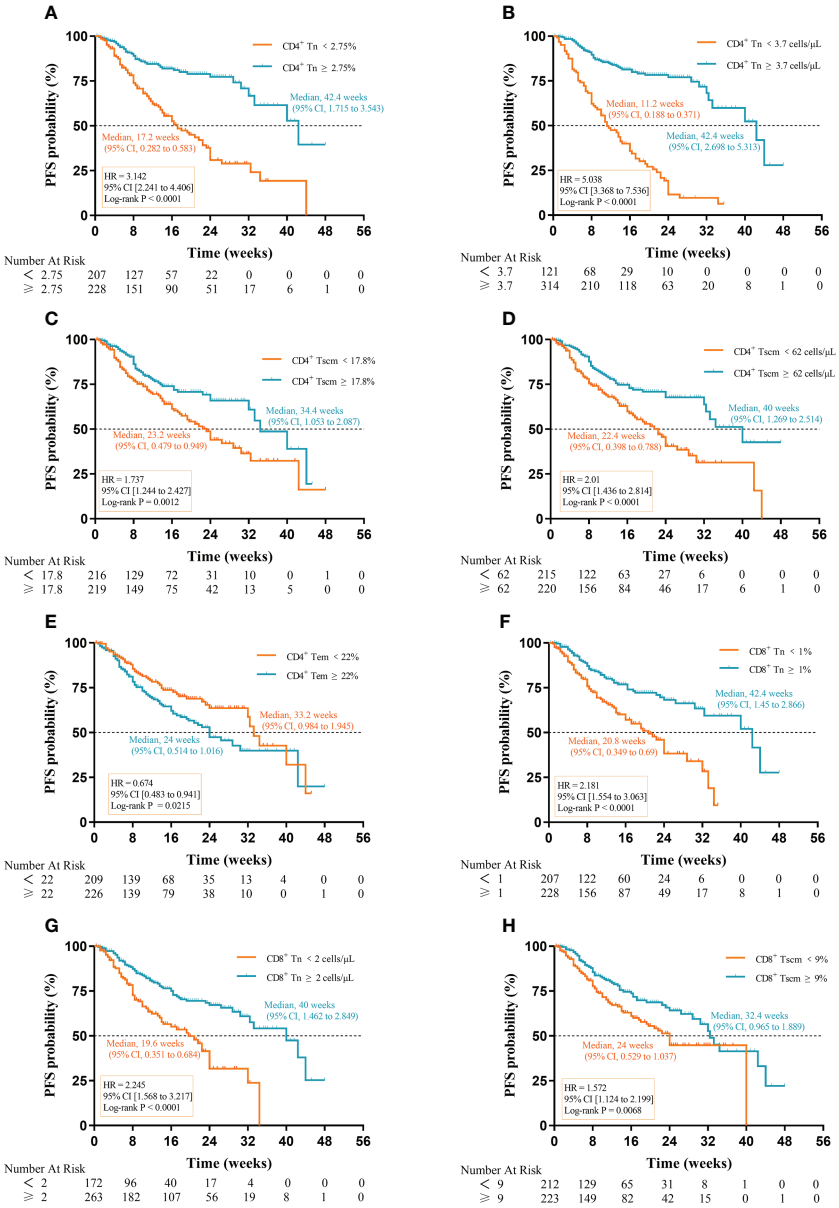

FIGURE 5
Prognostic impact of Tn/Tm on PFS of aNSCLCs: **(A)** The percentage of $CD4^+$ Tn on the prognosis of PFS. **(B)** The AC of $CD4^+$ Tn on the prognosis of PFS. **(C)** The percentage of $CD4^+$ Tscm on the prognosis of PFS. **(D)** The AC of $CD4^+$ Tscm on the prognosis of PFS. **(E)** The percentage of $CD4^+$ Tem on the prognosis of PFS. **(F)** The percentage of $CD8^+$ Tn on the prognosis of PFS. **(G)** The AC of $CD8^+$ Tn on the prognosis of PFS. **(H)** The percentage of $CD8^+$ Tscm on the prognosis of PFS.

cells, including Tcm, Tte of $CD4^+$ and $CD8^+$, the AC of $CD8^+$ Tscm and AC of $CD4^+$ Tem cells had no relationship between median PFS and cell amount (Supplementary Figure 1).

Notably, the difference in median PFS for AC of $CD4^+$ Tn (31.2 weeks) was the most apparent, followed by percentage (25.2 weeks) of $CD4^+$ Tn, percentage (21.6 weeks) of $CD8^+$ Tn, and AC (20.4 weeks) of $CD8^+$ Tn. The results suggested that high AC and percentage of Tn were conducive to prolonged PFS in aNSCLCs although the percentage and AC of $CD4^+$ Tscm, percentage of $CD4^+$ Tem, and $CD8^+$ Tscm had prognostic value in PFS of aNSCLCs too (Table 2).

Effect of variables on the PFS of aNSCLCs

Because the result had more subsets of Tn/Tm that affected the PFS of patients, it was necessary to evaluate which peripheral

Tn/Tm had the most significant impact on the PFS of aNSCLCs. This study utilized univariate analysis and a Log-rank test to analyze the variables (Table 3). The variables of P< 0.05 were input to multivariate analysis for COX model analysis, and finally, the forest plots had drawn in Figure 6. The high AC of $CD4^+$ Tn was an independent protective factor for PFS (HR 0.260; 95%CI [0.153 to 0.441]; P< 0.001), and liver metastasis (HR 1.815; 95%CI [1.094 to 3.012]; P = 0.021) was independent risk factor for PFS of aNSCLCs.

The forest plots indicated that only the AC of $CD4^+$ Tn was an independent protective factor for PFS through the AC and percentage of $CD4^+$ and $CD8^+$ Tn, as well as the frequency and AC of CD4+ Tscm, frequency of $CD4^+$ Tem, and $CD8^+$ Tscm, were correlated with PFS in aNSCLCs. Thus, more attention should be paid to the AC of $CD4^+$ Tn.

Prognosis of Tn/Tm on PFS in aNSCLCs received immunotherapy

To evaluate the prognosis of Tn/Tm on PFS in aNSCLCs received immunotherapy, we analyzed the relationship between the baseline of Tn/Tm and PFS (Table 4).

TABLE 3 Univariate analysis on PFS of aNSCLCs.

Univariate viable	Cutoff-point	Univariate analysis	
		P-value	HR
Age (≥ 67 vs< 67)	67	0.027	0.684
Sex (Male vs Female)		0.009	1.682
Family history (Yes vs No)		0.151	0.736
Smoking history (Yes vs No)		0.113	1.366
Drinking history (Yes vs No)		0.119	1.307
ECOG performance status (≥ 2 vs< 2)		< 0.001	1.964
The size of primary tumor (cm) (≥2 vs< 2)		0.033	4.57
Histological types (Adenocarcinoma vs Squamous carcinoma)		0.092	0.749
Degree of differentiation (Moderate or High vs Low)		0.955	1.015
TNM stage (Ⅳ vs Ⅲ)		0.6	1.109
Lymph node metastasis (Yes vs No)		0.036	1.531
Lung metastasis (Yes vs No)		0.445	1.14
Braine metastasis (Yes vs No)		0.061	0.554
Liver metastasis (Yes vs No)		< 0.001	3.024
Bone metastasis (Yes vs No)		0.015	1.536
Number of metastasis sites (≥ 2 vs< 2)		0.03	1.479
$CD4^+$ Tn cell (%) (High vs Low)	2.75	< 0.001	0.311
$CD4^+$ Tscm cell (%) (High vs Low)	17.8	0.002	0.575
$CD4^+$ Tcm cell (%) (High vs Low)	30	0.087	1.346
$CD4^+$ Tem cell (%) (High vs Low)	22	0.023	1.484
$CD4^+$ Tte cell (%) (High vs Low)	0.85	0.186	0.785
$CD8^+$ Tn cell (%) (High vs Low)	1	< 0.001	0.444
$CD8^+$ Tscm cell (%) (High vs Low)	9	0.008	0.629
$CD8^+$ Tcm cell (%) (High vs Low)	6.65	0.316	1.213
$CD8^+$ Tem cell (%) (High vs Low)	20.6	0.058	0.721
$CD8^+$ Tte cell (%) (High vs Low)	6.8	0.992	0.998
$CD4^+$ Tn cell (cells/μL) (High vs Low)	3.7	< 0.001	0.189
$CD4^+$ Tscm cell (cells/μL) (High vs Low)	62	< 0.001	0.493
$CD4^+$ Tcm cell (cells/μL) (High vs Low)	115	0.362	0.856
$CD4^+$ Tem cell (cells/μL) (High vs Low)	70.5	0.278	1.215
$CD4^+$ Tte cell (cells/μL) (High vs Low)	2	0.63	0.921
$CD8^+$ Tn cell (cells/μL) (High vs Low)	2	< 0.001	0.431
$CD8^+$ Tscm cell (cells/μL) (High vs Low)	23	0.099	0.753
$CD8^+$ Tcm cell (cells/μL) (High vs Low)	22	0.875	0.973
$CD8^+$ Tem cell (cells/μL) (High vs Low)	58.5	0.297	0.834
$CD8^+$ Tte cell (cells/μL) (High vs Low)	16	0.193	1.251

10.3389/fimmu.2022.996348

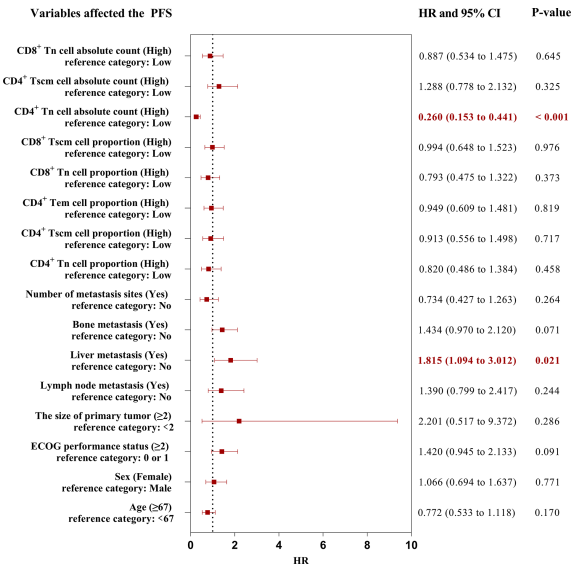

FIGURE 6
The forest plots of factors affected the PFS of aNSCLCs. HR > 1 represented variable was considered a negative factor; HR< 1 indicated variable was considered a positive factor.

When comparing the PFS in patients with PR, SD and PD, PR had the highest median PFS (NE, 95% CI, NE to NE vs 29.2 weeks, 95% CI, NE to NE vs 14 weeks, 95% CI, NE to NE) (P = 0.0002) (Figure 7A). High percentage of $CD4^+$ Tn was associated with longer median PFS (29.2 weeks, 95% CI, 1.162 to 4.212 vs 13.2 weeks, 95% CI, 0.237 to 0.861) (HR 3.591; 95% CI [1.535 to 8.399]; P< 0.0001) (Figure 7B). Patients with high AC of $CD4^+$ Tn had a better median PFS compared with patients with low AC of $CD4^+$ Tn (29.2 weeks, 95% CI, 2.14 to 7.687 vs 7.2 weeks, 95% CI, 0.13 to 0.467) (HR 4.562; 95% CI [2.099 to 9.917]; P< 0.0001) (Figure 7C). High percentage and AC of $CD4^+$ Tscm in aNSCLCs had significantly longer median PFS compared with low percentage and AC of $CD4^+$ Tscm in aNSCLCs (26.8 weeks, 95% CI, 0.902 to 3.446 vs 15.2 weeks, 95% CI, 0.29 to 1.109) (HR 2.239; 95% CI [1.183 to 4.237]; P = 0.0143, Figure 7D) (NE, 95% CI, NE to NE vs 16 weeks, 95% CI, NE to NE) (HR 3.177; 95% CI [1.68 to 6.009]; P = 0.0008, Figure 7E). There was a significant difference in PFS for patients with high or low $CD8^+$ Tscm (26.8 weeks, 95% CI, 0.845 to 3.32 vs 16 weeks, 95% CI, 0.301 to 1.183) (HR 2.56; 95% CI [1.352 to 4.845]; P = 0.0046) (Figure 7F). The Tcm, Tem, Tte of $CD4^+$ and $CD8^+$, the percentage and AC of $CD8^+$ Tn and the percentage of $CD8^+$ Tscm cells had no relationship between PFS and cell amount in aNSCLCs (Supplementary Figure 2).

Overall, this indicated that high AC and percentage of $CD4^+$ Tn and $CD4^+$ Tscm were beneficial in prolonging PFS in aNSCLCs. The AC of $CD8^+$ Tscm had prognostic value for PFS of aNSCLCs.

TABLE 4 The baseline characteristics of aNSCLCs who received immunotherapy.

Characteristics	N = 92	(%)
Age (years) (median, range)	69 (45-80)	
Sex		
Male	64	69.6
Female	28	30.4
Family history		
Yes	26	28.3
No	66	71.7
Smoking history		
Yes	61	66.3
No	31	33.7
Drinking history		
Yes	35	38
No	57	62
ECOG performance status		
0 or 1	67	72.8
≥ 2	25	27.2
The size of primary tumor (cm)		
< 2	3	3.3
≥ 2	89	96.7
Histological types		
Adenocarcinoma	59	64.1
Squamous	33	35.9
Degree of differentiation		
Low	86	93.5
Moderate or High	6	6.5
TNM stage		
Ⅲ	19	20.7
Ⅳ	73	79.3
Lymph node metastasis		
Yes	65	70.7
No	27	29.3
Lung metastasis		
Yes	39	42.4
No	53	57.6
Braine metastasis		
Yes	13	14.1
No	79	85.9
Liver metastasis		
Yes	9	9.8
No	83	90.2
Bone metastasis		
Yes	26	28.3
No	66	71.7
Number of metastasis sites		
0	12	13
1	20	21.8
2	48	52.2
≥ 3	12	13

(Continued)

TABLE 4 Continued

Characteristics	N = 92	(%)
Response evaluation		
Complete response (CR)	0	0
Partial response (PR)	19	20.6
Stable disease (SD)	34	37
Progressive disease (PD)	39	42.4

The high AC of $CD4^+$ Tn, $CD4^+$ Tscm, and $CD8^+$ Tscm and the high percentage of $CD4^+$ Tn and $CD4^+$ Tscm were associated with a better prognosis. We wondered which peripheral Tn/Tm subset was most relevant to the PFS of aNSCLCs who received immunotherapy. To answer this question, we conducted univariate analyses, using the Log-rank test to analyze the variables (Table 5). The variables with P< 0.05 entered into multivariate analysis for COX model analysis to draw forest plots. The results showed the AC of $CD4^+$ Tn ≥ 5.5 cells/μL (HR 0.248; 95% CI [0.079 to 0.775]; P = 0.017) was an independent protective factor in PFS of aNSCLCs who received immunotherapy (Figure 8).

Based on analysis above, the percentage and the AC of $CD4^+$ Tn, $CD4^+$ Tscm, $CD4^+$ Tcm, $CD4^+$ Tem, $CD4^+$ Tte, $CD8^+$ Tn, $CD8^+$ Tscm, $CD8^+$ Tcm, $CD8^+$ Tem and $CD8^+$ Tte can be divided into high and low groups according to their cutoff-point

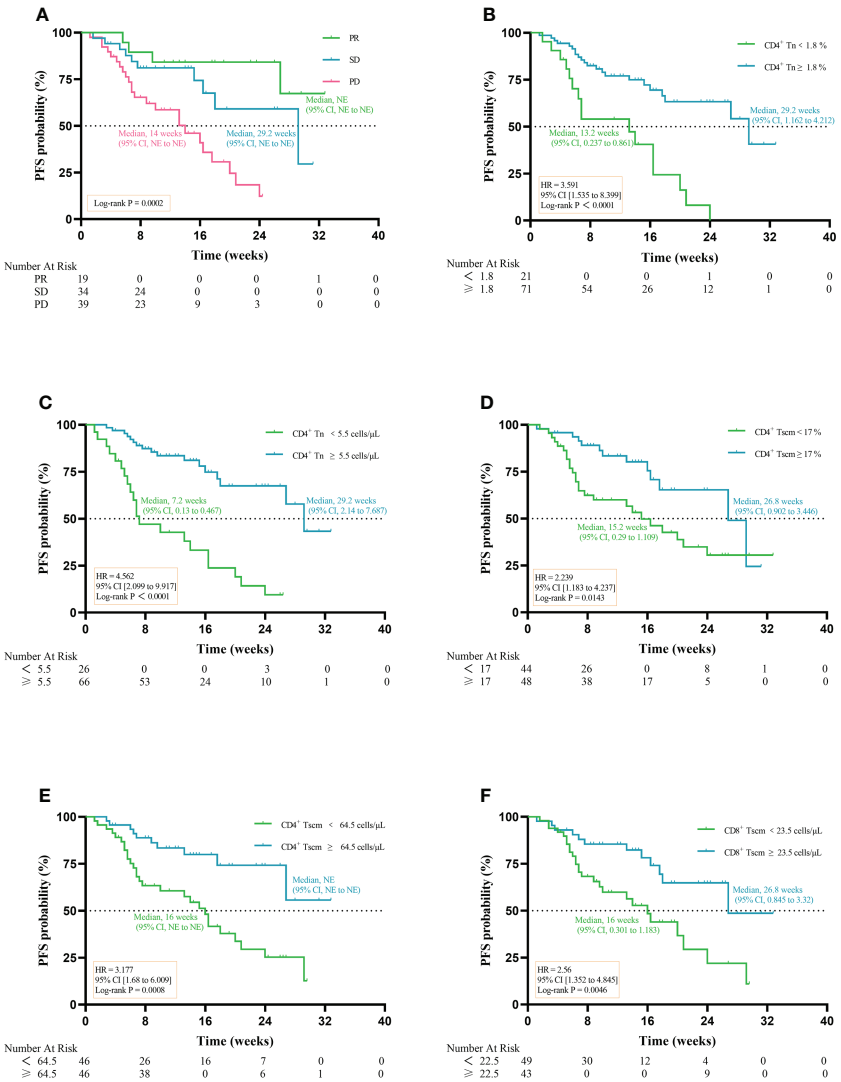

FIGURE 7
Prognostic impact of the baseline of Tn/Tm on PFS of NSCLCs: **(A)** Prognostic impact of PR, SD, and PD on PFS. **(B)** Prognostic impact in percentage of $CD4^+$ Tn on PFS. **(C)** Prognostic impact in AC of $CD4^+$ Tn on PFS. **(D)** Prognostic impact in percentage of $CD4^+$ Tscm on PFS. **(E)** Prognostic impact in AC of $CD4^+$ Tscm on PFS. **(F)** Prognostic impact in AC of $CD8^+$ Tscm on PFS. NE: not estimable.

10.3389/fimmu.2022.996348

TABLE 5 Univariate analysis on PFS of aNSCLCs who received immunotherapy.

Univariate viable	Cutoff-point	P-value	HR
$CD4^+$ Tn cell (%) (High vs Low)	1.8	< 0.001	0.266
$CD4^+$ Tscm cell (%) (High vs Low)	17	0.018	0.442
$CD4^+$ Tcm cell (%) (High vs Low)	29.85	0.542	0.819
$CD4^+$ Tem cell (%) (High vs Low)	22.1	0.702	0.882
$CD4^+$ Tte cell (%) (High vs Low)	0.35	0.214	0.659
$CD8^+$ Tn cell (%) (High vs Low)	1.35	0.077	0.494
$CD8^+$ Tscm cell (%) (High vs Low)	9.55	0.185	0.638
$CD8^+$ Tcm cell (%) (High vs Low)	9	0.741	0.896
$CD8^+$ Tem cell (%) (High vs Low)	21.3	0.064	0.538
$CD8^+$ Tte cell (%) (High vs Low)	6.55	0.923	0.969
$CD4^+$ Tn cell (cells/μL) (High vs Low)	5.5	< 0.001	0.205
$CD4^+$ Tscm cell (cells/μL) (High vs Low)	64.5	0.002	0.313
$CD4^+$ Tcm cell (cells/μL) (High vs Low)	116.5	0.071	0.548
$CD4^+$ Tem cell (cells/μL) (High vs Low)	80	0.388	0.754
$CD4^+$ Tte cell (cells/μL) (High vs Low)	2	0.14	0.616
$CD8^+$ Tn cell (cells/μL) (High vs Low)	2	0.103	0.587
$CD8^+$ Tscm cell (cells/μL) (High vs Low)	23.5	0.006	0.383
$CD8^+$ Tcm cell (cells/μL) (High vs Low)	25.5	0.715	0.887
$CD8^+$ Tem cell (cells/μL) (High vs Low)	57	0.45	0.780
$CD8^+$ Tte cell (cells/μL) (High vs Low)	15	0.978	1.009

(Table 6). In 92 patients, 71 (77%) had a high percentage of $CD4^+$ Tn (≥ 1.8%), of them 18 (25%) were PR, 31 (44%) were SD, 22 (31%) were PD, the disease control rate (DCR) reached 69%, while 21(23%) had a low percentage of $CD4^+$ Tn (< 1.8%), of them 1 (5%) were PR, 3 (14%) were SD, 17 (81%) were PD, the DCR was 19% only. Markedly, the percentage of $CD4^+$ Tn showed a positive correlation to the DCR, the higher percentage of $CD4^+$ Tn (≥ 1.8%) signified a better outcome of immunotherapy, and the lower percentage of $CD4^+$ Tn (< 1.8%) implied poorer curative effect. When the AC of $CD4^+$ Tn was higher than or equal to 5.5 cells/μL, the DCR was 71%, and the PD rate was 29%. On the contrary, the PD rate was 77% higher than the DCR (23%) when the AC of $CD4^+$ Tn was less than 5.5 cells/μL.

The AC of Tscm, Tcm, and Tem of $CD4^+$ as well as Tn, Tscm, Tcm, and Tte of $CD8^+$ all showed similar characteristics

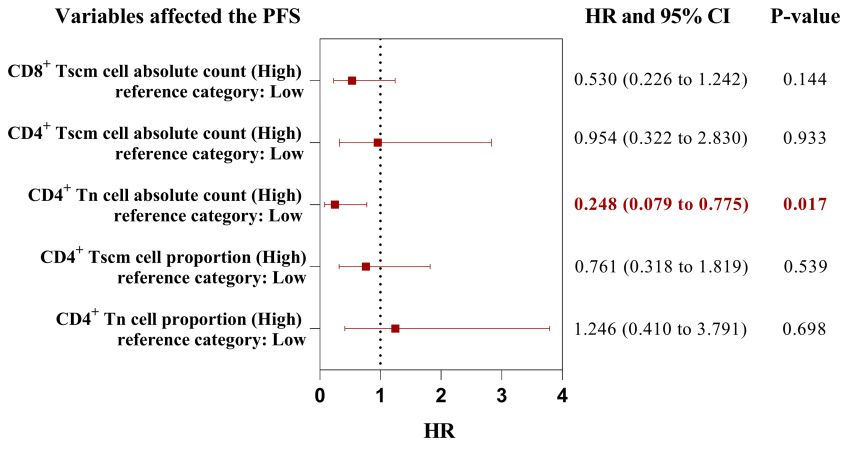

FIGURE 8
The forest plots of factors affected the PFS of aNSCLCs who received immunotherapy. HR > 1 represented variable was considered a negative factor; HR< 1 indicated variable was considered a positive factor.

10.3389/fimmu.2022.996348

TABLE 6 Evaluation response of Tn/Tm of aNSCLCs received immunotherapy.

Cells	Groups	n	Disease control		Progressive Disease
		92	PR = 19 n (%)	SD = 34 n (%)	PD = 39 n (%)
$CD4^+$ Tn %	≥ 1.8%	71	18 (25%)	31 (44%)	22 (31%)
	< 1.8%	21	1 (5%)	3 (14%)	17 (81%)
$CD4^+$ Tn	≥ 5.5 cells/μL	66	19 (29%)	28 (42%)	19 (29%)
	< 5.5 cells/μL	26	0	6 (23%)	20 (77%)
$CD4^+$ Tscm %	≥ 17%	48	10 (21%)	19 (39.5%)	19 (39.5%)
	< 17%	44	9 (20%)	15 (34%)	20 (46%)
$CD4^+$ Tscm	≥ 64.5 cells/μL	46	14 (30%)	21 (46%)	11 (24%)
	< 64.5 cells/μL	46	5 (11%)	13 (28%)	28 (61%)
$CD4^+$ Tcm %	≥ 29.85%	46	12 (26%)	19 (41%)	15 (33%)
	< 29.85%	46	7 (15%)	15 (33%)	24 (52%)
$CD4^+$ Tcm	≥ 116.5 cells/μL	46	14 (30%)	21 (46%)	11 (24%)
	< 116.5 cells/μL	46	5 (11%)	13 (28%)	28 (61%)
$CD4^+$ Tem %	≥ 22.1%	47	11 (23%)	19 (41%)	17 (36%)
	< 22.1%	45	8 (18%)	15 (33%)	22 (49%)
$CD4^+$ Tem	≥ 80 cells/μL	46	14 (30%)	21 (46%)	11 (24%)
	< 80 cells/μL	46	5 (11%)	13 (28%)	28 (61%)
$CD4^+$ Tte %	≥ 0.35%	56	11 (20%)	21 (38%)	24 (42%)
	< 0.35%	36	8 (22%)	13 (36%)	15 (42%)
$CD4^+$ Tte	≥ 2 cells/μL	50	11 (22%)	19 (38%)	20 (40%)
	< 2 cells/μL	42	8 (19%)	15 (36%)	19 (45%)
$CD8^+$ Tn %	≥ 1.35%	30	5 (17%)	16 (53%)	9 (30%)
	< 1.35%	62	14 (23%)	18 (29%)	30 (48%)
$CD8^+$ Tn	≥ 2 cells/μL	59	11 (19%)	30 (51%)	18 (30%)
	< 2 cells/μL	33	8 (24%)	4 (12%)	21 (64%)
$CD8^+$ Tscm %	≥ 9.55%	44	8 (18%)	19 (43%)	17 (39%)
	< 9.55%	48	11 (23%)	15 (31%)	22 (46%)
$CD8^+$ Tscm	≥ 23.5 cells/μL	43	11 (26%)	23 (53%)	9 (21%)
	< 23.5 cells/μL	49	8 (16%)	11 (23%)	30 (61%)
$CD8^+$ Tcm %	≥ 9%	47	10 (21%)	18 (38%)	19 (41%)
	< 9%	45	9 (20%)	16 (36%)	20 (44%)
$CD8^+$ Tcm	≥ 25.5 cells/μL	46	12 (26%)	19 (41%)	15 (33%)
	< 25.5 cells/μL	46	7 (15%)	15 (33%)	24 (52%)
$CD8^+$ Tem %	≥ 21.3%	46	10 (22%)	15 (33%)	21 (45%)
	< 21.3%	46	9 (20%)	19 (41%)	18 (39%)
$CD8^+$ Tem	≥ 57 cells/μL	47	12 (26%)	17 (36%)	18 (38%)
	< 57 cells/μL	45	7 (15%)	17 (38%)	21 (47%)
$CD8^+$ Tte %	≥ 6.55%	46	9 (20%)	20 (44%)	17 (36%)
	< 6.55%	46	10 (22%)	14 (30%)	22 (48%)
$CD8^+$ Tte	≥ 15 cells/μL	48	11 (23%)	23 (48%)	14 (29%)
	< 15 cells/μL	44	8 (18%)	11 (25%)	25 (57%)

to the AC and percentage of $CD4^+$ Tn. The same applies to the percentage of $CD4^+$ Tcm (Table 6). The higher AC (≥ cutoff-point) had better DCR than the lower AC (< cutoff-point). In other words, the lower AC had a higher PD rate.

Due to a small fraction of higher percentage and AC (≥ cutoff-point) of Tn/Tm showing no better efficacy (Table 6), to explore the cause, we further analyzed the correlation between response of immunotherapy regimes and the AC of $CD4^+$ Tn (Table 7). Here is an analysis relationship between the AC of $CD4^+$ Tn and immunotherapy only. The reason was that multivariate analysis above showed that the AC of $CD4^+$ Tn was the most significant protective factor for PFS of patients

TABLE 7 Frequency for response of treatment options in the AC of $CD4^+$ Tn cell in aNSCLCs.

Treatment regime	$CD4^+$ Tn cell					
	≥ 5.5 cells/μL (n = 66)			< 5.5 cells/μL (n = 26)		
	PR	SD	PD	PR	SD	PD
n	19	28	19	0	6	20
Immunotherapy alone	3 (16%)	5 (18%)	5 (26%)	0	1 (17%)	4 (20%)
Immunotherapy conjugate APS	5 (26%)	8 (28.5%)	3 (16%)	0	1 (17%)	1 (5%)
Immunotherapy conjugate Recombinant Human G-CSF	2 (10.5%)	3 (11%)	1 (5%)	0	0	1 (5%)
Chemotherapy followed by immunotherapy	2 (10.5%)	3 (11%)	6 (32%)	0	2 (33%)	10 (50%)
Immunotherapy followed by chemotherapy	7 (37%)	9 (31.5%)	4 (21%)	0	2 (33%)	4 (20%)

APS, Astragalus polysaccharide; G-CSF, Granulocyte Colony Stimulating Factor.

(Figures 6, 8). For high AC of $CD4^+$ Tn (≥ 5.5 cells/μL) (n = 66), immunotherapy alone achieved 3 (16%) PR, 5 (18%) SD, 5 (26%) PD; for low AC of $CD4^+$ Tn cell (< 5.5 cells/μL) (n = 26), gained 0 PR, 1 (17%) SD and 4 (20%) PD. Compared to it, immunotherapy conjugate Astragalus polysaccharide (APS) showed better efficacy with PR (5, 26%) and SD (8, 28.5%) increase, PD (3, 16%) drop for high AC of $CD4^+$ Tn (≥ 5.5 cells/μL), meanwhile PR (0), SD (1, 17%) and PD (1, 5%) decrease for low AC of $CD4^+$ Tn (< 5.5 cells/μL). Immunotherapy followed by chemotherapy showed more better efficacy with PR (7, 37%), SD (9, 31.5%) increase, PD (4, 21%) decrease for high AC of $CD4^+$ Tn (≥ 5.5 cells/μL), and SD (2, 33%) increase and PD (4, 20%) steadiness for low AC of $CD4^+$ Tn (< 5.5 cells/μL). Immunotherapy conjugate recombinant human Granulocyte Colony Stimulating Factor (G-CSF) didn't display better outcomes with PR, SD, and PD drop for high AC of $CD4^+$ Tn (≥ 5.5 cells/μL), and SD and PD decreased too for low AC of $CD4^+$ Tn (< 5.5 cells/μL). Chemotherapy followed by immunotherapy revealed poorer efficacy with PR and SD drop, PD rise for high AC of $CD4^+$ Tn cell (≥ 5.5 cells/μL), simultaneously, PD increase apparently, for low AC of $CD4^+$ Tn cell (< 5.5 cells/μL) (Table 7).

The results indicated the efficacy of immunotherapy conjugate chemotherapy was related to the AC of $CD4^+$ Tn and treatment order. The high AC of $CD4^+$ Tn, and chemotherapy used after immunotherapy predicted a better prognosis, and it was recommended options for the clinic.

Discussion

The T lymphocytes play a crucial role in protecting the body against cancer by recognizing and killing tumor cells (39, 40). T lymphocytes have mainly divided into naïve T cells (Tn) and memory T cells (Tm) based on their function and phenotype (41). Tn is a mature T cell that is resting. Tn performs the immune-surveillance function by recirculating between the blood and secondary lymphoid organs, and Tn responds only to new antigens (42). DC capture tumor antigens and present them through HLA class II or I molecules to $CD4^+$ Tn or $CD8^+$ Tn that can differentiate into Th and memory $CD4^+$ T cells or memory $CD8^+$ T cells, also known as the initial immune response (43). After 90-95% of effector T cells undergo apoptosis, only 5-10% of activated T cells were converted into long-term Tm. These Tm persisted and were involved in maintaining long-term immunity and rapid responses to antigens that had been exposed, also known as memory immune responses (44, 45). Tn and Tscm could self-renew and differentiate into all subsets of memory and effector T cells, which include Tcm, Tem, and Tte (46, 47). Tscm and Tcm undergo a memory immune response and rapidly clonally proliferate to produce Tem and Tte that specifically kill tumor cells (48). Our study showed the AC of Tn/Tn impaired significantly in aNSCLCs, the insufficient numbers of Tn or Tscm and Tcm cannot induce enough initial immune responses and memory immune responses, and cannot recognize and kill tumor cells, which may explain the development of refractory tumors. Hence, different T lymphocytes coordinate with each other and play a crucial role in the anti-tumor immune response (49, 50). Therefore, studying the number and function of Tn and Tm cells is a reference for understanding anti-tumor immunity.

Most studies have focused on the frequency of immune cells in blood or tumor-infiltrating lymphocytes (TILs) and served as biomarkers of prognosis (51–53). Liu C, et al. reported that the percentage of $CD4^+$ Tn and Tm in peripheral blood are prognostic indicators for patients with NSCLC (54–56). However, the "Tn" of these researches was a mixture of Tn and Tscm due to not using CD95 monoclonal antibodies to

discriminate Tscm from Tn according to the methods of the papers (57), while Tn and Tscm in our research had distinguished by CD95 monoclonal antibody. The "Tn" in these researches was completely different from the "Tn" of our manuscript. Meanwhile, this researches only analyzed the memory $CD4^+$ and $CD8^+$ T cells but did not fully analyze the subsets of memory cells, including Tscm, Tcm, Tem, and Tte (30, 54–56). More importantly, these studies did not analyze further the prognostic impact of each AC of the Tn/Tm subpopulation on patient survival. Therefore, naïve and memory cells of $CD4^+$ and $CD8^+$ T cells in the research are completely different from our manuscript. Wherever, the impact of AC in the Tn/Tm subpopulation of peripheral blood, which represents the overall immune status, on the prognosis of NSCLC is unclear. Chen DS, et al. indicated that possible reasons for the absence of the T-cell infiltration in the tumor microenvironment (TME) include lack of tumor antigens, defects in antigen-presenting cells (APCs), and lack of T-cell activation (58). Yost KE, et al. reported that the T-cell clones that dominate the T-cell landscape within the tumor after ICB are distinct from that before treatment, a phenomenon referred to by the authors as a clonal substitution (59). More and more evidence indicate that cloning and recruitment of T lymphocytes may be a key to disease progression during immunotherapy (60). It had suggested that the reactivation capacity of TILs was limited, and the type of expansion of T cell clones after immunotherapy had recruited from peripheral sources (59). Deep single-cell sequencing of RNA and T cell receptors in the patient's peripheral blood, tumor samples, and normal adjacent tissues confirmed the source of clonotypic amplification of TILs. The results indicated that in patients who responded, TILs were replaced by fresh non-depleted T cells from outside the tumor (61). Therefore, TILs in the local TME may be derived from Tn/Tm subsets in the peripheral blood. The immune status of the patient's TME is crucial in terms of their prognosis. We speculate that the TME combined with the systemic immune status of patients is more relevant for the prognosis of patients and the stratification of patients for immunotherapy. We hypothesized that adequate numbers of Tn/Tm are considerable for maintaining the immune homeostasis in the local TME. It is necessary to determine which AC of Tn/Tm in peripheral blood have closely associated with the prognosis of the tumor. Our previous study showed that AC of $CD4^+$ cells had a predictive value in longer PFS of NSCLC, while the percentages of $CD3^+$, $CD4^+$, $CD8^+$, B, and NK cells were the same as that in NCs, with no difference between the two groups (36). The frequency and AC of T cells reflect two aspects of immune cells: the frequency reflects mainly the development and differentiation of immune cells, while the AC shows the proliferation of immune cells. The state of immune cells requires analysis of both the percentage and AC of cells (62). Studies have shown that the AC of Tn is lower in patients with NSCLC than that in normal subjects (63).

Notably, we focused on Tn/Tm in this study. The percentage and AC of Tn/Tm had severely reduced in aNSCLCs compared to NCs, and the decrease in AC was more regular, especially the AC of $CD4^+$ Tn and $CD8^+$ Tn was associated with the disease stage of the tumor, that is, with the disease progression of aNSCLCs (Figure 3). This result suggested that aNSCLCs lack sufficient numbers of Tn to generate initial immune responses by DC recognizing and intaking new tumor antigens. This condition might cause the recurrence and metastasis of tumor cells (Figure 4). The data indicated that the initial immune response of Tn and proliferation of the T cell in aNSCLCs were severely impaired. And the inability to effectively perform immune surveillance and clearance might lead to the metastasis and progression of NSCLC.

Some studies have shown that immunotherapy conjugate with radiotherapy did not improve the outcome of aNSCLCs (21). We inferred that the ineffectiveness of immunotherapy could be due to the depletion of $CD4^+$ Tn, leading directly to desensitization to new antigens produced by recurrent tumors, which coincides with the significant impairment in AC of Tn in aNSCLCs. Therefore, it may be a crucial factor in the formation of clinically refractory tumors (Figure 6).

Multivariate analysis of all variables of Tn/Tm related to the prognosis of aNSCLCs showed that the AC of $CD4^+$ Tn (≥ cutoff-point) in peripheral blood was an independent protective factor in PFS of aNSCLCs (Figures 6, 8). Immunotherapy acts by indirectly relieving immune suppression of immune cells rather than directly killing tumor cells. These results indicated that the AC of CD4+ Tn is not only a prognostic indicator for aNSCLC but also strongly correlates with the efficacy of immunotherapy. More importantly, the population benefiting from immunotherapy can be screened out from aNSCLCs based on the AC of $CD4^+$ Tn. It is significant to improve efficacy and reduce ineffective immunotherapy in the clinic.

Studies have shown that immunotherapy can promote the differentiation of Th cells and activation of CTLs in responded patients, but that didn't happen with chemotherapy (64). Analysis of T lymphocyte subsets of peripheral blood in patients with metastatic melanoma after initial immunotherapy showed increased expansion of peripheral T lymphocyte subsets in patients who responded to treatment (65). Considering that immunotherapy strategies are also important factors, we further explored the relationship between the treatment regime and the AC of $CD4^+$ Tn.

For aNSCLC, adequate Tn is a prerequisite for immunotherapy to be effective. Immunotherapy combined with other immune-enhancing therapies can further improve outcomes, such as APS, which can significantly improve the function of humoral immunity and cellular metabolism (66, 67). Chemotherapy can shrink tumors that are sensitive to cytotoxic drugs. However, chemotherapy can cause side effects, such as bone marrow suppression (68–70). In particular, repeated chemotherapy can impair the proliferative function of cells,

including the rapidly proliferating hematopoietic stem cells in the bone marrow and Tn, Tscm, and Tcm in the peripheral blood. As a result, immune dysfunction occurs when immune cells do not complete the initial and memory immune responses performed by Tn and Tm. When $CD4^+$ Tn ≥ 5.5 cells/μL, immunotherapy followed by chemotherapy had the highest DCR in our study. Immunotherapy alone also had a higher DCR than chemotherapy followed by immunotherapy. Therefore, the sequence of treatment regimens could affect the prognosis and efficacy of patients. Chemotherapy should be avoided in patients when the AC of Tn is low, which reduces damage to immune cells, and immune-boosting therapy should be used at this time. Different clinical strategies should be used for patients at different clinical stages, depending on the patient's immune status. In brief, these results suggest that the efficacy of immunotherapy is closely related to the AC of $CD4^+$ Tn.

This study analyzed the impaired Tn/Tm in aNSCLCs, its prognostic value for immunotherapy, and implications for combination treatment strategies. However, the study has some limitations. For example, it lacks further clinical validation in large samples, a multi-center study of $CD4^+$ Tn as a biomarker, and the mechanisms of Tn/Tm impairment.

Conclusion

This study suggested that the percentage and AC of Tn/Tm, especially AC, showed varying degrees of damage in aNSCLC and were associated with tumor progression. The multivariate analysis indicated that only AC of $CD4^+$ Tn was an independent protective factor for PFS in aNSCLCs and a potential marker of efficacy and prognosis in patients receiving immunotherapy. The AC of Tn/Tm test in peripheral blood is simple to perform, cost saving and helps to assess the overall immune status of aNSCLC patients for clinical management. Moreover, our finding suggests that immunotherapy conjugate other therapies such as APS or followed by chemotherapy is of benefit for aNSCLCs.

Data availability statement

The original contributions presented in the study are included in the article/Supplementary Material. Further inquiries can be directed to the corresponding author.

Ethics statement

All enrolled participants signed the informed consent. The present study involving human samples was approved by the Ethics Committee of the First Teaching Hospital, Tianjin University of Traditional Chinese Medicine (Tianjin, China) (TYLL2021 [K] 001).

Author contributions

GZ drafted the manuscript. JY conceived and designed manuscript. AL, YY, YX, WL, YL and JZ verified the contents and revised the manuscript. QC, DW, XL, YG, HC critically revised the manuscript. All authors reviewed and approved the final manuscript. All authors contributed to the article and approved the submitted version.

Funding

This work was supported by the Scientific Research Plan Project of Tianjin Education Commission (No. 2018KJ034).

Acknowledgments

The authors thank the Scientific Research Plan Project of Tianjin Education Commission (No.2018KJ034).

Conflict of interest

The authors declare that the research was conducted in the absence of any commercial or financial relationships that could be construed as a potential conflict of interest.

Publisher's note

Supplementary material

The Supplementary Material for this article can be found online at: https://www.frontiersin.org/articles/10.3389/fimmu.2022.996348/full#supplementary-material

SUPPLEMENTARY FIGURE 1
Prognostic impact of naïve/memory T lymphocytes on PFS of NSCLCs: **(A)** The percentage of $CD4^+$ Tcm on the prognosis. **(B)** The AC of $CD4^+$ Tcm on the prognosis. **(C)** The AC of $CD4^+$ Tem on the prognosis. **(D)** The percentage of $CD4^+$ Tte on the prognosis. **(E)** The AC of $CD4^+$ Tte on the prognosis. **(F)** The AC of $CD8^+$ Tscm on the prognosis. **(G)** The percentage of $CD8^+$ Tcm on the prognosis. **(H)** The AC of $CD8^+$ Tcm on the prognosis. **(I)** The percentage of $CD8^+$ Tem on the prognosis. **(J)** The AC of $CD8^+$ Tem on the prognosis. **(K)** The percentage of $CD8^+$ Tte on the prognosis. **(L)** The AC of $CD8^+$ Tte on the prognosis.

SUPPLEMENTARY FIGURE 2

Prognostic impact of naïve/memory T lymphocytes on PFS of NSCLCs received immunotherapy: **(A)** The percentage of $CD8^+$ Tscm on the prognosis. **(B)** The percentage of $CD4^+$ Tcm on the prognosis. **(C)** The AC of $CD4^+$ Tcm on the prognosis. **(D)** The percentage of $CD4^+$ Tem on the prognosis. **(E)**The AC of $CD4^+$ Tem on the prognosis. **(F)** The percentage of $CD4^+$ Tte on the prognosis. **(G)** The AC of $CD4^+$ Tte on the prognosis. **(H)** The percentage of $CD8^+$ Tn on the prognosis. **(I)** The AC of $CD8^+$ Tn on the prognosis. **(J)** The percentage of $CD8^+$ Tcm on the prognosis. **(K)** The AC of $CD8^+$ Tcm on the prognosis. **(L)** The percentage of $CD8^+$ Tem on the prognosis. **(M)** The AC of $CD8^+$ Tem on the prognosis. **(N)** The percentage of $CD8^+$ Tte on the prognosis. **(O)** The AC of $CD8^+$ Tte on the prognosis.

References

1. Chou HL, Lin YH, Liu W, Wu CY, Li RN, Huang HW, et al. Combination therapy of chloroquine and C(2)-ceramide enhances cytotoxicity in lung cancer h460 and h1299 cells. *Cancers (Basel)* (2019) 11(3):370. doi: 10.3390/cancers11030370

2. Kim MJ, Cervantes C, Jung YS, Zhang X, Zhang J, Lee SH, et al. PAF remodels the DREAM complex to bypass cell quiescence and promote lung tumorigenesis. *Mol Cell* (2021) 81:1698–714. doi: 10.1016/j.molcel.2021.02.001

3. Ren D, Hua Y, Yu B, Ye X, He Z, Li C, et al. Predictive biomarkers and mechanisms underlying resistance to PD1/PD-L1 blockade cancer immunotherapy. *Mol Cancer* (2020) 19:19. doi: 10.1186/s12943-020-1144-6

4. Mansfield AS, Aubry MC, Moser JC, Harrington SM, Dronca RS, Park SS, et al. Temporal and spatial discordance of programmed cell death-ligand 1 expression and lymphocyte tumor infiltration between paired primary lesions and brain metastases in lung cancer. *Ann Oncol* (2016) 27:1953–8. doi: 10.1093/annonc/mdw289

5. Dong W, Wu X, Ma S, Wang Y, Nalin AP, Zhu Z, et al. The mechanism of anti-PD-L1 antibody efficacy against PD-L1-Negative tumors identifies NK cells expressing PD-L1 as a cytolytic effector. *Cancer Discov* (2019) 9:1422–37. doi: 10.1158/2159-8290.CD-18-1259

6. Walk EE, Yohe SL, Beckman A, Schade A, Zutter MM, Pfeifer J, et al. The cancer immunotherapy biomarker testing landscape. *Arch Pathol Lab Med* (2020) 144:706–24. doi: 10.5858/arpa.2018-0584-CP

7. Lee H, Wang Y, Xia W, Chen C, Rau K, Ye L, et al. Removal of n-linked glycosylation enhances PD-L1 detection and predicts anti-PD-1/PD-L1 therapeutic efficacy. *Cancer Cell* (2019) 36:168–78. doi: 10.1016/j.ccell.2019.06.008

8. Ettinger DS, Wood DE, Aisner DL, Akerley W, Bauman JR, Bharat A, et al. NCCN guidelines insights: Non-small cell lung cancer, version 2.2021. *J Natl Compr Canc Netw* (2021) 19:254–66. doi: 10.6004/jnccn.2021.0013

9. Rizvi NA, Hellmann MD, Snyder A, Kvistborg P, Makarov V, Havel JJ, et al. Cancer immunology. mutational landscape determines sensitivity to PD-1 blockade in non-small cell lung cancer. *Science.* (2015) 348:124–8. doi: 10.1126/science.aaa1348

10. Goodman AM, Kato S, Bazhenova L, Patel SP, Frampton GM, Miller V, et al. Tumor mutational burden as an independent predictor of response to immunotherapy in diverse cancers. *Mol Cancer Ther* (2017) 16:2598–608. doi: 10.1158/1535-7163.MCT-17-0386

11. Gandara DR, Paul SM, Kowanetz M, Schleifman E, Zou W, Li Y, et al. Blood-based tumor mutational burden as a predictor of clinical benefit in non-small-cell lung cancer patients treated with atezolizumab. *Nat Med* (2018) 24:1441–8. doi: 10.1038/s41591-018-0134-3

12. Carbone DP, Reck M, Paz-Ares L, Creelan B, Horn L, Steins M, et al. First-line nivolumab in stage IV or recurrent non-Small-Cell lung cancer. *N Engl J Med* (2017) 376:2415–26. doi: 10.1056/NEJMoa1613493

13. Valero C, Lee M, Hoen D, Wang J, Nadeem Z, Patel N, et al. The association between tumor mutational burden and prognosis is dependent on treatment context. *Nat Genet* (2021) 53:11–5. doi: 10.1038/s41588-020-00752-4

14. Hirsch FR, McElhinny A, Stanforth D, Ranger-Moore J, Jansson M, Kulangara K, et al. PD-L1 immunohistochemistry assays for lung cancer: Results from phase 1 of the blueprint PD-L1 IHC assay comparison project. *J Thorac Oncol* (2017) 12:208–22. doi: 10.1016/j.jtho.2016.11.2228

15. Shaverdian N, Lisberg AE, Bornazyan K, Veruttipong D, Goldman JW, Formenti SC, et al. Previous radiotherapy and the clinical activity and toxicity of pembrolizumab in the treatment of non-small-cell lung cancer: A secondary analysis of the KEYNOTE-001 phase 1 trial. *Lancet Oncol* (2017) 18:895–903. doi: 10.1016/S1470-2045(17)30380-7

16. Hellmann MD, Paz-Ares L, Bernabe CR, Zurawski B, Kim SW, Carcereny CE, et al. Nivolumab plus ipilimumab in advanced non-Small-Cell lung cancer. *N Engl J Med* (2019) 381:2020–31. doi: 10.1056/NEJMoa1910231

17. Yu Y, Zeng D, Ou Q, Liu S, Li A, Chen Y, et al. Association of survival and immune-related biomarkers with immunotherapy in patients with non-small cell lung cancer: A meta-analysis and individual patient-level analysis. *JAMA Netw Open* (2019) 2:e196879. doi: 10.1001/jamanetworkopen.2019.6879

18. Blass E, Ott PA. Advances in the development of personalized neoantigen-based therapeutic cancer vaccines. *Nat Rev Clin Oncol* (2021) 18:215–29. doi: 10.1038/s41571-020-00460-2

19. Socinski MA, Jotte RM, Cappuzzo F, Orlandi F, Stroyakovskiy D, Nogami N, et al. Atezolizumab for first-line treatment of metastatic nonsquamous NSCLC. *N Engl J Med* (2018) 378:2288–301. doi: 10.1056/NEJMoa1716948

20. Gandhi L, Rodriguez-Abreu D, Gadgeel S, Esteban E, Felip E, De Angelis F, et al. Pembrolizumab plus chemotherapy in metastatic non-Small-Cell lung cancer. *N Engl J Med* (2018) 378:2078–92. doi: 10.1056/NEJMoa1801005

21. Schoenfeld JD, Giobbie-Hurder A, Ranasinghe S, Kao KZ, Lako A, Tsuji J, et al. Durvalumab plus tremelimumab alone or in combination with low-dose or hypofractionated radiotherapy in metastatic non-small-cell lung cancer refractory to previous PD(L)-1 therapy: An open-label, multicentre, randomised, phase 2 trial. *Lancet Oncol* (2022) 23:279–91. doi: 10.1016/S1470-2045(21)00658-6

22. Howlader N, Forjaz G, Mooradian MJ, Meza R, Kong CY, Cronin KA, et al. The effect of advances in lung-cancer treatment on population mortality. *N Engl J Med* (2020) 383:640–9. doi: 10.1056/NEJMoa1916623

23. Yang Y. Cancer immunotherapy: Harnessing the immune system to battle cancer. *J Clin Invest* (2015) 125:3335–7. doi: 10.1172/JCI83871

24. Duchemann B, Remon J, Naigeon M, Mezquita L, Ferrara R, Cassard L, et al. Integrating circulating biomarkers in the immune checkpoint inhibitor treatment in lung cancer. *Cancers (Basel)* (2020) 12(12):3625. doi: 10.3390/cancers12123625

25. Oh SY, Heo J, Noh OK, Chun M, Cho O, Oh YT. Absolute lymphocyte count in preoperative chemoradiotherapy for rectal cancer: Changes over time and prognostic significance. *Technol Cancer Res Treat* (2018) 17:1077047713. doi: 10.1177/1533033818780065

26. Huemer F, Lang D, Westphal T, Gampenrieder SP, Hutarew G, Weiss L, et al. Baseline absolute lymphocyte count and ECOG performance score are associated with survival in advanced non-small cell lung cancer undergoing PD-1/PD-L1 blockade. *J Clin Med* (2019) 8(7):1014. doi: 10.3390/jcm8071014

27. Nakata Y, Brignier AC, Jin S, Shen Y, Rudnick SI, Sugita M, et al. C-myb, menin, GATA-3, and MLL form a dynamic transcription complex that plays a pivotal role in human T helper type 2 cell development. *Blood* (2010) 116:1280–90. doi: 10.1182/blood-2009-05-223255

28. Marks BR, Nowyhed HN, Choi JY, Poholek AC, Odegard JM, Flavell RA, et al. Thymic self-reactivity selects natural interleukin 17-producing T cells that can regulate peripheral inflammation. *Nat Immunol* (2009) 10:1125–32. doi: 10.1038/ni.1783

29. Yan Y, Wang X, Liu C, Jia J. Association of lymphocyte subsets with efficacy and prognosis of immune checkpoint inhibitor therapy in advanced non-small cell lung carcinoma: A retrospective study. *BMC Pulm Med* (2022) 22:166. doi: 10.1186/s12890-022-01951-x

30. Duchemann B, Naigeon M, Auclin E, Ferrara R, Cassard L, Jouniaux J, et al. CD8+ PD-1+ to CD4+ PD-1+ ratio (PERLS) is associated with prognosis of patients with advanced NSCLC treated with PD-(L)1 blockers. *J Immunother Cancer* (2022) 10:e4012. doi: 10.1136/jitc-2021-004012

31. Raphael I, Joern RR, Forsthuber TG. Memory CD4(+) T cells in immunity and autoimmune diseases. *Cells-Basel* (2020) 9(3):531. doi: 10.3390/cells9030531

32. Lu Y, Zhang Q, Zhang L. CD4(+) memory stem t cell in peripheral blood: A promising immune index for early screening and auxiliary diagnosis of colorectal cancer. *Front Oncol* (2021) 11:701738. doi: 10.3389/fonc.2021.701738

33. Ahrends T, Busselaar J, Severson TM, Babala N, de Vries E, Bovens A, et al. CD4(+) T cell help creates memory CD8(+) T cells with innate and help-independent recall capacities. *Nat Commun* (2019) 10:5531. doi: 10.1038/s41467-019-13438-1

34. Miller CH, Klawon D, Zeng S, Lee V, Socci ND, Savage PA. Eomes identifies thymic precursors of self-specific memory-phenotype CD8(+) T cells. *Nat Immunol* (2020) 21:567–77. doi: 10.1038/s41590-020-0653-1

35. Durand A, Audemard-Verger A, Guichard V, Mattiuz R, Delpoux A, Hamon P, et al. Profiling the lymphoid-resident T cell pool reveals modulation by age and microbiota. *Nat Commun* (2018) 9:68. doi: 10.1038/s41467-017-02458-4

36. Xia Y, Li W, Li Y, Liu Y, Ye S, Liu A, et al. The clinical value of the changes of peripheral lymphocyte subsets absolute counts in patients with non-small cell lung cancer. *Transl Oncol* (2020) 13:100849. doi: 10.1016/j.tranon.2020.100849

37. Xia Y, Liu A, Li W, Liu Y, Zhang G, Ye S, et al. Reference range of naïve T and T memory lymphocyte subsets in peripheral blood of healthy adult. *Clin Exp Immunol* (2021) 207(2):208–17. doi: 10.1093/cei/uxab038

38. Gong Y, Fan Z, Luo G, Huang Q, Qian Y, Cheng H, et al. Absolute counts of peripheral lymphocyte subsets correlate with the progression-free survival and metastatic status of pancreatic neuroendocrine tumour patients. *Cancer Manag Res* (2020) 12:6727–37. doi: 10.2147/CMAR.S257492

39. Chen L, Gibbons DL, Goswami S, Cortez MA, Ahn YH, Byers LA, et al. Metastasis is regulated *via* microRNA-200/ZEB1 axis control of tumour cell PD-L1 expression and intratumoral immunosuppression. *Nat Commun* (2014) 5:5241. doi: 10.1038/ncomms6241

40. Braun DA, Street K, Burke KP, Cookmeyer DL, Denize T, Pedersen CB, et al. Progressive immune dysfunction with advancing disease stage in renal cell carcinoma. *Cancer Cell* (2021) 39:632–48. doi: 10.1016/j.ccell.2021.02.013

41. Quinn KM, Fox A, Harland KL, Russ BE, Li J, Nguyen T, et al. Age-related decline in primary CD8(+) t cell responses is associated with the development of senescence in virtual memory CD8(+) t cells. *Cell Rep* (2018) 23:3512–24. doi: 10.1016/j.celrep.2018.05.057

42. Goronzy JJ, Weyand CM. Mechanisms underlying T cell ageing. *Nat Rev Immunol* (2019) 19:573–83. doi: 10.1038/s41577-019-0180-1

43. Stagg AJ, Hart AL, Knight SC, Kamm MA. The dendritic cell: Its role in intestinal inflammation and relationship with gut bacteria. *Gut* (2003) 52:1522–9. doi: 10.1136/gut.52.10.1522

44. Omilusik KD, Goldrath AW. Remembering to remember: T cell memory maintenance and plasticity. *Curr Opin Immunol* (2019) 58:89–97. doi: 10.1016/j.coi.2019.04.009

45. Zander R, Schauder D, Xin G, Nguyen C, Wu X, Zajac A, et al. CD4(+) T cell help is required for the formation of a cytolytic CD8(+) T cell subset that protects against chronic infection and cancer. *Immunity* (2019) 51:1028–42. doi: 10.1016/j.immuni.2019.10.009

46. Azevedo RI, Soares MV, Albuquerque AS, Tendeiro R, Soares RS, Martins M, et al. Long-term immune reconstitution of naive and memory t cell pools after haploidentical hematopoietic stem cell transplantation. *Biol Blood Marrow Transpl* (2013) 19:703–12. doi: 10.1016/j.bbmt.2013.01.017

47. Yamaguchi K, Mishima K, Ohmura H, Hanamura F, Ito M, Nakano M, et al. Activation of central/effector memory T cells and T-helper 1 polarization in malignant melanoma patients treated with anti-programmed death-1 antibody. *Cancer Sci* (2018) 109:3032–42. doi: 10.1111/cas.13758

48. Saxena A, Dagur PK, Biancotto A. Multiparametric flow cytometry analysis of naive, memory, and effector t cells. *Methods Mol Biol* (2019) 2032:129–40. doi: 10.1007/978-1-4939-9650-6_8

49. Kennedy R, Celis E. Multiple roles for CD4+ T cells in anti-tumor immune responses. *Immunol Rev* (2008) 222:129–44. doi: 10.1111/j.1600-065X.2008.00616.x

50. Braumuller H, Wieder T, Brenner E, Assmann S, Hahn M, Alkhaled M, et al. T-helper-1-cell cytokines drive cancer into senescence. *Nature* (2013) 494:361–5. doi: 10.1038/nature11824

51. Hu M, Eviston D, Hsu P, Marino E, Chidgey A, Santner-Nanan B, et al. Decreased maternal serum acetate and impaired fetal thymic and regulatory T cell development in preeclampsia. *Nat Commun* (2019) 10:3031. doi: 10.1038/s41467-019-10703-1

52. Zhang Y, Kurupati R, Liu L, Zhou XY, Zhang G, Hudaihed A, et al. Enhancing CD8(+) t cell fatty acid catabolism within a metabolically challenging tumor microenvironment increases the efficacy of melanoma immunotherapy. *Cancer Cell* (2017) 32:377–91. doi: 10.1016/j.ccell.2017.08.004

53. Ruhland MK, Roberts EW, Cai E, Mujal AM, Marchuk K, Beppler C, et al. Visualizing synaptic transfer of tumor antigens among dendritic cells. *Cancer Cell* (2020) 37:786–99. doi: 10.1016/j.ccell.2020.05.002

54. Lambert SL, Zhang C, Guo C, Turan T, Masica DL, Englert S, et al. Association of baseline and pharmacodynamic biomarkers with outcomes in patients treated with the PD-1 inhibitor budigalimab. *J Immunother* (2022) 45:167.

55. Xia L, Wang H, Sun M, Yang Y, Yao C, He S, et al. Peripheral CD4(+) T cell signatures in predicting the responses to anti-PD-1/PD-L1 monotherapy for Chinese advanced non-small cell lung cancer. *Sci China Life Sci* (2021) 64:1590–601. doi: 10.1007/s11427-020-1861-5

56. Liu C, Xu B, Li Q, Li A, Li L, Yue J, et al. Smoking history influences the prognostic value of peripheral naive CD4+ T cells in advanced non-small cell lung cancer. *Cancer Cell Int* (2019) 19:176. doi: 10.1186/s12935-019-0899-6

57. Gattinoni L, Speiser DE, Lichterfeld M, Bonini C. T Memory stem cells in health and disease. *Nat Med* (2017) 23:18–27. doi: 10.1038/nm.4241

58. Chen DS, Mellman I. Oncology meets immunology: The cancer-immunity cycle. *Immunity* (2013) 39:1–10. doi: 10.1016/j.immuni.2013.07.012

59. Yost KE, Satpathy AT, Wells DK, Qi Y, Wang C, Kageyama R, et al. Clonal replacement of tumor-specific T cells following PD-1 blockade. *Nat Med* (2019) 25:1251–9. doi: 10.1038/s41591-019-0522-3

60. Acharya N, Anderson AC. New clones on the block. *Immunity* (2019) 51:606–8. doi: 10.1016/j.immuni.2019.09.018

61. Wu TD, Madireddi S, de Almeida PE, Banchereau R, Chen YJ, Chitre AS, et al. Peripheral T cell expansion predicts tumour infiltration and clinical response. *Nature* (2020) 579:274–8. doi: 10.1038/s41586-020-2056-8

62. Kuss I, Hathaway B, Ferris RL, Gooding W, Whiteside TL. Decreased absolute counts of T lymphocyte subsets and their relation to disease in squamous cell carcinoma of the head and neck. *Clin Cancer Res* (2004) 10:3755–62. doi: 10.1158/1078-0432.CCR-04-0054

63. Manjarrez-Orduno N, Menard LC, Kansal S, Fischer P, Kakrecha B, Jiang C, et al. Circulating t cell subpopulations correlate with immune responses at the tumor site and clinical response to PD1 inhibition in non-small cell lung cancer. *Front Immunol* (2018) 9:1613. doi: 10.3389/fimmu.2018.01613

64. Griffiths JI, Wallet P, Pflieger LT, Stenehjem D, Liu X, Cosgrove PA, et al. Circulating immune cell phenotype dynamics reflect the strength of tumor-immune cell interactions in patients during immunotherapy. *Proc Natl Acad Sci USA* (2020) 117:16072–82. doi: 10.1073/pnas.1918937117

65. Valpione S, Galvani E, Tweedy J, Mundra PA, Banyard A, Middlehurst P, et al. Immune-awakening revealed by peripheral T cell dynamics after one cycle of immunotherapy. *Nat Cancer* (2020) 1:210–21. doi: 10.1038/s43018-019-0022-x

66. Huang WC, Kuo KT, Bamodu OA, Lin YK, Wang CH, Lee KY, et al. Astragalus polysaccharide (PG2) ameliorates cancer symptom clusters, as well as improves quality of life in patients with metastatic disease, through modulation of the inflammatory cascade. *Cancers (Basel)* (2019) 11(8):1054. doi: 10.3390/cancers11081054

67. Wang CH, Lin CY, Chen JS, Ho CL, Rau KM, Tsai JT, et al. Karnofsky performance status as a predictive factor for cancer-related fatigue treatment with astragalus polysaccharides (PG2) injection-a double blind, multi-center, randomized phase IV study. *Cancers (Basel)* (2019) 11(2):128. doi: 10.3390/cancers11020128

68. James ND, Sydes MR, Clarke NW, Mason MD, Dearnaley DP, Spears MR, et al. Addition of docetaxel, zoledronic acid, or both to first-line long-term hormone therapy in prostate cancer (STAMPEDE): Survival results from an adaptive, multiarm, multistage, platform randomised controlled trial. *Lancet* (2016) 387:1163–77. doi: 10.1016/S0140-6736(15)01037-5

69. Abdelfattah N, Rajamanickam S, Panneerdoss S, Timilsina S, Yadav P, Onyeagucha BC, et al. MiR-584-5p potentiates vincristine and radiation response by inducing spindle defects and DNA damage in medulloblastoma. *Nat Commun* (2018) 9:4541. doi: 10.1038/s41467-018-06808-8

70. Reck M, Rodriguez-Abreu D, Robinson AG, Hui R, Csoszi T, Fulop A, et al. Pembrolizumab versus chemotherapy for PD-L1-Positive non-Small-Cell lung cancer. *N Engl J Med* (2016) 375:1823–33. doi: 10.1056/NEJMoa1606774

frontiers | Frontiers in Immunology

TYPE Review
PUBLISHED 28 October 2022
DOI 10.3389/fimmu.2022.1022808

OPEN ACCESS

EDITED BY
Frederique Vegran,
U1231 Lipides, Nutrition, Cancer (LNC) (INSERM), France

REVIEWED BY
Dan Zhang,
State Key Laboratory of Molecular Developmental Biology (CAS), China
Luciana D'Apice,
National Research Council (CNR), Italy
Yishan Ye,
Zhejiang University, China

*CORRESPONDENCE
Zhijia Xia
Zhijia.Xia@med.uni-muenchen.de
Xiaosong Li
lixiaosong@cqmu.edu.cn

†These authors have contributed equally to this work

SPECIALTY SECTION
This article was submitted to Cancer Immunity and Immunotherapy, a section of the journal Frontiers in Immunology

RECEIVED 19 August 2022
ACCEPTED 17 October 2022
PUBLISHED 28 October 2022

CITATION
Zhao Y, Wei K, Chi H, Xia Z and Li X (2022) IL-7: A promising adjuvant ensuring effective T cell responses and memory in combination with cancer vaccines?
Front. Immunol. 13:1022808.
doi: 10.3389/fimmu.2022.1022808

IL-7: A promising adjuvant ensuring effective T cell responses and memory in combination with cancer vaccines?

Yue Zhao[1,2†], Kongyuan Wei[3†], Hao Chi[4], Zhijia Xia[2*] and Xiaosong Li[5*]

[1]Cancer Hospital of the University of Chinese Academy of Sciences (Zhejiang Cancer Hospital), Institute of Basic Medicine and Cancer (IBMC), Chinese Academy of Sciences, Hangzhou, Zhejiang, China, [2]Department of General, Visceral, and Transplant Surgery, Ludwig-Maximilians-University Munich, Munich, Germany, [3]Department of General, Visceral and Transplantation Surgery, University of Heidelberg, Heidelberg, Germany, [4]Clinical Medical Collage, Southwest Medical University, Luzhou, China, [5]Clinical Molecular Medicine Testing Center, The First Affiliated Hospital of Chongqing Medical University, Chongqing, China

Cancer vaccines exhibit specificity, effectiveness, and safety as an alternative immunotherapeutic strategy to struggle against malignant diseases, especially with the rapid development of mRNA cancer vaccines in recent years. However, how to maintain long-term immune memory after vaccination, especially T cells memory, to fulfill lasting surveillance against cancers, is still a challenging issue for researchers all over the world. IL-7 is critical for the development, maintenance, and proliferation of T lymphocytes, highlighting its potential role as an adjuvant in the development of cancer vaccines. Here, we summarized the IL-7/IL-7 receptor signaling in the development of T lymphocytes, the biological function of IL-7 in the maintenance and survival of T lymphocytes, the performance of IL-7 in pre-clinical and clinical trials of cancer vaccines, and the rationale to apply IL-7 as an adjuvant in cancer vaccine-based therapeutic strategy.

KEYWORDS

IL-7, adjuvant, cancer vaccines, T cell immune response, T cell memory

Introduction

Immunotherapy now is experiencing its "golden age" recently, with the immune checkpoint blocker (ICB) approved by the Food and Drug Administration for the treatment of melanoma and lung cancer, which forever changed the balance in the choice of methods of anticancer therapy (1, 2). The concept of immunotherapy

implies antitumor immune response activation or/and immunosuppression inhibition. As one of the critical components of immunotherapy in oncology, cancer vaccines show advantages in specificity, immunogenicity, and low toxicity (3, 4). Unlike ICBs, a passive immunotherapeutic strategy, cancer vaccines possess the capability to induce anti-tumor immune responses actively (5). Moreover, cancer vaccines are time- and labor-saving in manufacturing, when compared to chimeric antigen receptor T cells therapy, making it more feasible for most cancer patients. The current rapid development of the mRNA cancer vaccine brings inspiring results for cancer patients, making this field of research scorching again (6, 7). Although different types of cancer vaccines have been evaluated in clinical trials, few led to satisfying clinical benefits. One of the underlying mechanisms lies in the lack of long-term memory to maintain immune surveillance to prevent the recurrence and metastasis of cancers (3, 8). Increasing studies have revealed that the success of cancer immunotherapeutics, especially cancer vaccines, is critically dependent on the induction of memory T-cell responses against cancers (9, 10). Moreover, the administration of vaccines without immunomodulatory agents is hard to reach the greatest effectiveness to stimulate the antitumor immune response (11). Therefore, searching for adjuvants, which will augment the efficacy of cancer vaccines and contribute to building up a lasting immune memory against cancers, was an attractive issue for researchers.

IL-7, encoded by the *IL7* gene, is a 25 kDa secreted soluble protein, which was initially discovered by Hunt et al. in 1987 when they explored the latent role of bone marrow stromal cells in the development of the pre-B cell subset (12, 13). Subsequently, increasing evidence proved that except for thymocytes and stromal non-hematopoietic cells (14), IL-7 is also secreted by lymphoid organs, non-lymphoid tissues, and even cancers (15–20) (Figure 1). The receptor of IL-7 is a heterodimer complex that comprises an IL-7Rα chain (CD127, encoded by the *IL7R gene*) and a common γ chain (CD132, encoded by the *IL2RG* gene) shared with receptors for IL-2, IL-4, IL-7, IL-9, IL-15 and IL-21 (21, 22). It has been reported that the signaling of IL-7/IL-7R participates in the growth and survival of T and B cell precursors critically (21). Recently, accumulating evidence proved that IL-7 is not only the essential factor in every stage of T cell development (23, 24) but also the crucial component for the survival of naïve T cells as well as the generation and maintenance of memory T cells (25, 26). Furthermore, IL-7 was demonstrated to assist T cells to restore homeostasis *via* the signal transducer and activator of transcription 5 (STAT5)/Suppressor of cytokine signaling

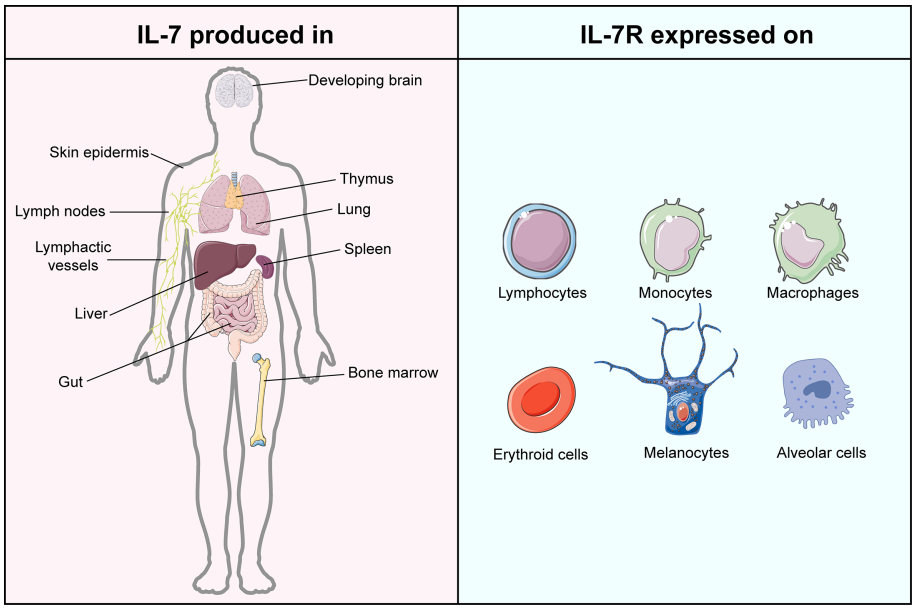

FIGURE 1
Atlas of IL-7 production and IL-7R expression. IL-7 is mainly produced in but not limited to lymphoid organs, including bone marrow, thymus, spleen, and lymphoid nodes. IL-7 is majorly generated by stromal cells but is also evidenced in epithelial cells, keratinocytes, dendritic cells, and hepatocytes. The expression of IL-7R can be found in lymphocytes, monocytes, macrophages, erythroid cells, melanocytes, and alveolar cells. This figure is created with BioRender.com and smart.servier.com.

(SOCS) pathway (27) and guide T cell homing by inducing the expression of chemokines and integrins (28, 29). In IL-7 knockout mice, a significant depletion of naïve T cells was observed, which can be restored by administrating the exogenous IL-7 (25). Except for T cells, IL-7 was also reported to regulate the immune responses of natural killer cells, dendritic cells, and B cells critically (30–32). As a cytokine therapy for cancer treatment, IL-7 exerts superior activity to induce the expansion of specific T cells against breast carcinoma than IL-2, highlighting its antitumor adjuvant molecular role in oncology (33).

Given the pleiotropic and robust biological effects of IL-7, especially its role in the survival, development, proliferation, and even maintenance of memory of T cells, several research teams apply IL-7 as a molecular adjuvant to strengthen the immunogenicity of cancer vaccines, as well as to maintain a long-term memory response against cancers. Therapeutic cancer vaccines aim to stimulate the immune responses in cancer patients, especially T-cell responses, which have been proven to be the predominant safeguard against tumors. Therefore, in this review, we summarized the biological function and mechanism of IL-7 and the signaling pathway of IL-7/IL-7R in T cells, as well as the performance of IL-7 as an adjuvant in combination with cancer vaccines in preclinical and clinical trials. The rationale to utilize IL-7 as an adjuvant in combination with cancer vaccines was also proposed.

The biological activity of IL-7 in T cells

IL-7 in T cell development

Lymphoid progenitors leave the bone marrow and migrate to the thymus for further development into naïve T cells, which were greatly influenced by IL-7 (Figure 2). In IL-7 -/- mice, the development and maturation of γδ T cells were restrained significantly, indicating the crucial role of IL-7 in T cell development (34). However, different stages of T cell development in the thymus exhibit distinct demands on IL-7. Pre-T cell progenitors lacking surface expression of CD4 and CD8 are termed double-negative (DN) cells. Based on the amount of CD44 and CD25, DN cells can be divided into four subgroups (DN1-DN4). Development of T cells from DN1-2 thymocytes showed strong dependence on IL-7 (35), while anti-IL-7 antibody led to the deprivation of T cell maturation by interrupting the expansion of T cells at the DN2 stage (36). Differentiation and proliferation of DN3-4 thymocytes also require the presence of IL-7, while the self-renewal of DN4 cells can be substituted partially by the depletion of Bcl6 in the absence of IL-7 (37). In contrast, IL-7 signaling does not participate in the positive selection of CD4 CD8 double-positive (DP), and the IL-7R is not evidenced on the surface of these cells (38). Intriguingly, cells successfully going through the

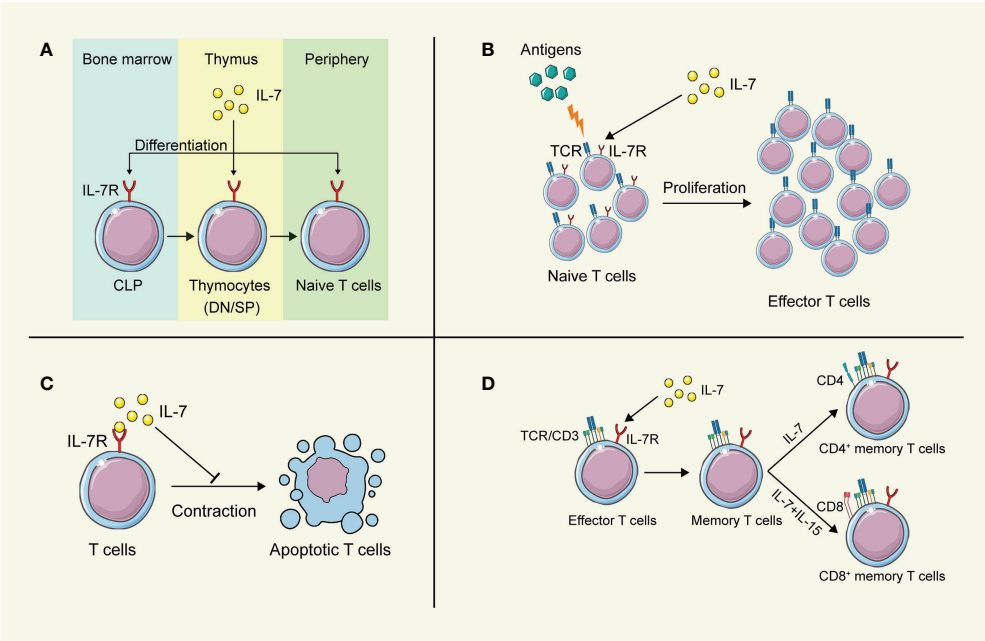

FIGURE 2
The biological function of IL-7 on T lymphocytes. **(A)** IL-7 contributes to the development of T cells in the thymus. **(B)** IL-7 boosts the proliferation of T cells after stimulation by antigens. **(C)** IL-7 prolongs the survival of T cells. **(D)** IL-7 promotes the differentiation of memory T cells. This figure is created with BioRender.com and smart.servier.com.

selection express IL-7R again modulated by developmental T cell antigen receptor (TCR)-dependent signals (39).

IL-7 in T cell survival

IL-7 was initially discovered as a survival factor for mouse T and B cell precursors. It has been demonstrated that IL-7 activates the transcription factor NFATc1 in DN thymocytes *via* phosphorylating Tyr371 to prolong the survival of DN thymocytes, while deficiency in NFATc1 blocked thymocyte development at the DN1 (40). Although DP cells are absent in the expression of IL-7R, SP cells regain it to promote their survival and induce the expression of CXCR4 to enhance the recruitment in secondary lymphoid tissues (41, 42). However, increasing evidence indicates that IL-7 fulfills its regulatory role throughout the lymphoid system. Naïve $CD4^+$ T cells consume IL-7 for survival to achieve homeostasis in bone marrow transplant recipients (43). Furthermore, IL-7 also regulates the survival of mature and memory T cells *via* upregulating the expression of Bcl-2 family proteins, leading to long-term memory (44, 45). Additionally, dendritic epidermal γδ T cells show partial dependence on IL-7 for their survival (46). Interestingly, tumor-bearing mice show a decreased level of IL-7 in the spleen, indicating that insufficient IL-7 might fails to support the survival of activated T cells, attenuating the T cell immune responses against tumors (47).

IL-7 in T cell proliferation

As a highly pleiotropic cytokine, IL-7 provides proliferation signals from hematopoietic stem cells to lymphocytes for their efficient generation (25). At the stage of DN thymocytes, IL-7 appears to promote the proliferation of these cells by upregulating the growth-facilitating genes CD98 in the Stat5-dependent manner (37). After SP thymocytes regain the IL-7R expression, IL-7 still fulfills its capability to stimulate the proliferation of these cells (41). IL-7 facilitates the proliferation of T cells in a concentration-dependent process. A higher concentration of IL-7 stimulates the proliferation of T lymphocytes, while a lower concentration maintains cell survival (48). Administration of IL-7 directly results in an increase in peripheral blood T cells and a broad TCR repertoire diversity (49, 50), while a long-term injection of IL-7 contributes to interrupting the proliferation of T cells, leading to a sharp depletion of naïve T cells (36). Furthermore, the administration of IL-7 in patients suffering from septic syndrome promotes the proliferation of $CD4^+$ and $CD8^+$ T cells in them, indicating the potential clinical application of IL-7 for septic shock (51). Interestingly, IL-7 was found to antagonize the immunosuppressive network, by abrogating the Treg-mediated suppression (52) and reducing the proportion of Treg cells and myeloid-derived suppressor cells (MDSC) (53, 54), even though IL-7 has little effect on the expansion of Treg cells and MDSCs directly (47).

IL-7 in the maintenance of T cell memory

After the clearance of pathogens or cancer cells, most of the effector T cells die, and a small proportion of them turn into memory T cells, maintaining the memory against the same antigens (55, 56). During this differentiation process, the critical role of IL-7 is highlighted. Several studies have revealed that IL-7 improves the long-term immune responses against pathogens by inducing naïve T cells to memory T cells (57, 58). A high expression of IL-7R is evidenced in the memory T cells subset, to maintain their survival by upregulating the anti-apoptotic Bcl-2 family proteins (25, 41). The homeostatic proliferation and maintenance of $CD4^+$ memory T cells heavily depend on the function of IL-7, while it has been demonstrated that these features of $CD8^+$ memory T cells require both IL-7 and IL-15 jointly (59–61). Furthermore, it has been reported that IL-7 is capable to induce more $IL\text{-}7R^+$ long-living memory stem T cells, which can self-renew and develop into effector T cells (62). Increased administration of IL-7 can boost the specific memory immune responses against cancer and viral infection (45). The adjuvanticity of IL-7 has been verified to prolong the protective effects of vaccines by inducing the production of memory T and B cells (63–65), highlighting the potential to apply IL-7 as an adjuvant in combination with cancer vaccines to struggle against cancer cells *via* long-term memory protection.

The signaling pathway of IL-7/IL-7R

The receptor of IL-7, IL-7R, is a transmembrane heterodimer composed of an IL-7Rα chain and a common γ chain. After the binding of IL-7, IL-7Rα dimerizes with the common cytokine γ chain and triggers kinase activation, while IL-7Rα alone fails to prompt the kinase activity and induce signal transduction (25, 66). The signaling of IL-7/IL-7R is mainly transduced by Janus kinase (JAK)- STAT and Phosphoinositide 3-kinase (PI3K)- Ak strain transforming (AKT) pathways in T cells to fulfill the biological functions of IL-7 (Figure 3).

When IL-7 combines with IL-7R, JAK1 and JAK3 are recruited to IL-7Rα and γ chain, and then phosphorylated, respectively. Phosphorylated JAK1 and JAK3 create the docking site for STAT5 recruitment and phosphorylation in an IL-7-dependent pattern (67–69). As a transcription factor, phosphorylated STAT5 dimerizes and translocates into the nucleus, mediating the expression of downstream targeted

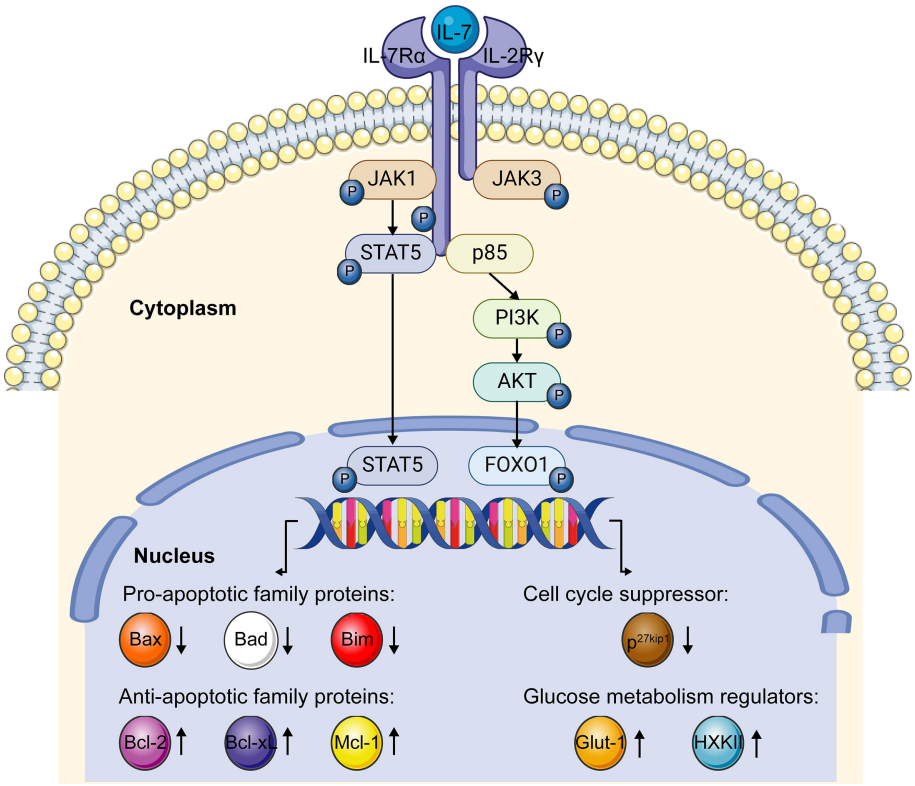

FIGURE 3
IL-7/IL-7R signaling pathway. When IL-7 interacts with the IL-7R, the α chain and γ chain dimerize. JAK1 and JAK3 were recruited to IL-7Rα and γ chains, separately. After phosphorylation, JAK1 and JAK3 phosphorylate and activate the transcription factor STAT5, which further upregulates anti-apoptotic family genes expression and downregulates pro-apoptotic family genes expression *via* the JAK-STAT5 pathway. After the interaction of IL-7 and IL-7R, recruited p85 induces the phosphorylation of the cytoplasmic tail of the IL-7Rα chain, which further triggers the phosphorylation of the PI3K-AKT pathway. Activated PI3K-AKT signaling induces glucose metabolism regulator genes expression and impedes the expression of cell cycle suppressor p27kip1 *via* FOXO1. This figure is created with BioRender.com and smart.servier.com.

genes associated with the survival and proliferation of T cells (47, 70). It has been reported that IL-7 prolongs the survival of T cells by upregulating the expression of Bcl-2, Bcl-xL, and Mcl-1 proteins *via* the JAK-STAT signaling pathway (61). Conversely, the inhibitor of JAK activation attenuates IL-7-induced Bcl-2 protein expression (71). Moreover, IL-7 downregulates the expression of the pro-apoptotic genes, like Bad, Bax, and Bim, to prevent apoptosis through the JAK-STAT signaling (72, 73). These studies taken together revealed that the survival of lymphocytes supported by IL-7 is dependent on the JAK-STAT pathway to a large extent.

Another crucial pathway involved in the IL-7/IL-7R signaling is the PI3K-AKT pathway. When IL-7 binds with IL-7R, p85, a regulatory component of PI3K, is recruited and then induces the phosphorylation of tyrosine449 in the IL-7Rα cytoplasmic tail, which triggers the activation of PI3K and then AKT (74). Subsequently, activated AKT participates in the downstream targeted gene regulation by phosphorylating transcription factor the Forkhead box protein 1 (FOXO1) (75). As a targeted molecule of the PI3K-AKT pathway, degraded p27 kinase inhibitor protein 1 (p27kip1) promotes the G1 to S phase transition of T cells in the presence of IL-7, indicating IL-7 can promote the proliferation of T lymphocytes *via* regulating the expression of p27kip1 (76). Furthermore, the PI3K-AKT signaling mediated by IL-7 was reported to regulate the expression of glycolytic enzymes hexokinase II (HXK II) and glucose transporter-1 (Glut-1), to increase the glucose uptake to support the T cells' survival and maintain homeostasis (77, 78).

IL-7 as an adjuvant for cancer vaccines in preclinical research

Numerous preclinical trials have evaluated the potential role of IL-7 as an adjuvant to strengthen the effectiveness and long-term responsiveness of cancer vaccines. Here we selectively summarized the performance of IL-7 as an adjuvant in combination with cancer vaccines in preclinical settings (Table 1).

Cancer cell vaccines transfected with the IL-7 gene to combat malignant diseases have been extensively explored (81, 82) (Figure 4A). Zhao et al. demonstrated that the production of IL-7 in the cancer cell vaccines modified with the IL-7 gene was active and stable in a soluble form, whereas tumor cells as the control settings exhibited an undetectable level of IL-7. Moreover, 10 μl supernatants of transfected cancer cells were equivalent to 1 ng recombinant human IL-7 protein in promoting T cell proliferation (82). Whole-cell cancer vaccines expressing IL-7 showed robust prophylactic and therapeutic effects against cancers, preventing tumor occurrence or prolonging the survival time in mice models. Furthermore, a higher infiltration of $CD4^+$ and $CD8^+$ T cells in the tumor regions was determined, which was correlated with a better survival outcome in the tumor-bearing mice (81, 82). Except for transfection of the IL-7 gene in tumor cell vaccines, Jeong et al. explored *Mycobacterium smegmatis* delivering a fusion protein comprising human macrophage migration inhibitory factor (MIF) and IL-7 as cancer vaccines to struggle against tumors (79) (Figure 4B). This bacterial-based cancer vaccine induced antitumor immune responses by recruiting effective T cells while reducing the infiltration of myeloid-derived suppressor cells (MDSCs) in the tumor environment. Intriguingly, an enhanced antitumor effect of the vaccine was observed in combination with programmed death-ligand 1 (PD-L1) immunotherapy.

However, the most common method to apply IL-7 as an adjuvant to enhance the antitumor effect of cancer vaccines in preclinical research was the injection of recombinant human IL-7 directly (83–86) (Figure 4C). Pellegrini and colleagues evidenced that IL-7 treatment in combination with a virus-based vaccine lead to a 3.5-10 fold increase in the number of $CD4^+$ and $CD8^+$ T cells in tumor-bearing mice, as well as higher infiltration levels of T lymphocytes in the tumor milieu compared with the PBS treatment group (83). Adjuvant IL-7 also contributed to the prolonged survival of activated T cells, enhanced effector responses, and increased production of cytokines, which boost vaccine-elicited immunity and survival in tumor-bearing mice. Furthermore, the same adjuvant effects of IL-7 were demonstrated to promote the efficacy of DC-based vaccines. Intriguingly, Pellegrini et al. also found that IL-7 possesses the capability to antagonize the Treg inhibitory network, which might promote antitumor immunity. The effects of recombinant human IL-7 as an adjuvant in augmenting the number of tumor-infiltrating T cells, specific antitumor immune responses, and survival time of tumor-bearing models also have been revealed in other published studies (84–86). Interestingly, Choi and colleagues novelly fused IL-7 with an Fc fragment to enhance the mucosal delivery across the genital epithelial barrier (Figure 4D), aiming at testing the antitumor effects of intravaginal administration of Fc-Fused IL-7 in combination with human papillomavirus (HPV) DNA vaccines against cervical cancer (80). Intravaginal administration of IL-7-Fc induces the recruitment of T cells and various cytokines and chemokines in cervicovaginal tissue, while IL-7 fails to do so. Furthermore, topical administration of IL-7-Fc in combination with the PHV vaccine increased a higher number of HPV-specific $CD8^+$ T lymphocytes and exhibited a greater therapeutic effect against cervical cancer. This research highlighted the possibility to apply Fc-fused IL-7 as an adjuvant to strengthen the cellular immunity induced by vaccines in the genital mucosa to struggle against cancers.

However, the adjuvant capability of IL-7 contributing to cancer vaccines was not only limited to inducing a short-term antitumor effect but also stimulating a long-term T cell memory against cancers. Previous studies have reported that cancer vaccines in combination with IL-7 induced a higher proportion of specific $CD8^+$ and $CD4^+$ memory T cells in mice models bearing tumors and improve the functionality of specific $CD8^+$ memory T cells by enhancing their IFN-γ secretion (81, 84). Furthermore, T cell memory elicited by cancer vaccines and IL-7 protected tumor-free mice model from a second tumor challenge (81, 85). Preclinical research highlighted that adjuvant IL-7, when combined with cancer vaccines, contributes to the generation and maintenance of T cell memory, which is the critical component to building up immune surveillance to restrict the recurrence and even metastasis of cancers. Therefore, the adjuvant value of IL-7 for cancer vaccines is further explored in clinical trials.

The advance of adjuvant IL-7 in combination with cancer vaccines in clinical trials

Preclinical studies have proved that IL-7 could serve as an ideal adjuvant for cancer vaccines to combat cancers. Therefore, based on these preclinical practices, several clinical trials utilizing IL-7 as an adjuvant for cancer vaccines to struggle against malignant diseases were initiated and some encouraging results have been achieved, as summarized in Table 2.

In the early stage, several clinical trials focus on the development of IL-7 gene-modified tumor cells as a cancer vaccine for patients with advanced malignant diseases (89–91). For instance, in a clinical phase I study launched by Westermann and colleagues, they immunized renal cell cancer (RCC) patients with IL-7 and CD80 genes cotransfected RCC tumor cells cancer vaccine (89). This vaccination has been proven to be feasible and safe with no grade III/IV adverse events (AEs) occurring. Throughout the trial, 5 out of 10 patients developed stable disease (SD) and the median time to progression was 18 weeks, while the median overall survival (OS) was 40 months in all. However, vaccination with IL-7 gene-modified RCC cells induced a TH2-predominant but not TH1-polarized immune

TABLE 1 Adjuvant effect of IL-7 in cancer vaccine treatment summarized from selective preclinical studies.

Year	Cancer vaccine	Form of IL-7	Targeted cancer cell lines	IL-7 dose/ route	Combination therapy	Study models	Study results	Reference
2021	Recombinant *Mycobacterium smegmatis* delivering a fusion protein of human MIF and IL-7	IL-7 gene inserted in Recombinant *Mycobacterium*	The MC38, LLC, and PanO2 cells	The mice were treated with peritumoral injections of mycobacterium (2×10^6 bacteria/ mice) on days 3, 7, and 14.	Anti-PD-L1 antibody	Seven-week- Old female C57BL/6 mice	Cancer vaccine treatment led to increased activation of $CD4^+$ and $CD8^+$ T cells in the tumor regions of vaccinated mice, contributing to the antitumor effect. Moreover, cancer vaccine treatment exhibited an enhanced anticancer effect with anti-PD-L1 immunotherapy, in tumor-bearing mouse models.	(79)
2016	HPV DNA vaccine	human IL-7 fused with a hybrid Fc-fragment, which contains the upper CH2 domain of IgD, and the last CH2 and CH3 domains of IgG4	The TC-1 cell line cotransformed with the HPV16 E6, E7 gene	Mice were intravaginally administered with IL-7-Fc (1 mg/kg)	None	8 to 10 weeks female C57BL/6 mice	Topical administration of IL-7-Fc after HPV DNA vaccination increased the quantity of HPV-specific $CD8^+$ T lymphocytes in the genital mucosa, resulting in a stronger anticancer immunity than HPV DNA vaccine alone. Mice cotreated with HPV vaccine and IL-7-Fc exhibited significantly attenuated tumor growth and promoted survival rate.	(80)
2016	Whole-cell cancer vaccine coexpressing IL-7 and IL-21	IL-7 gene transfected in tumor cell vaccine	Murine melanoma B16F10 cells and colon carcinoma CT26 cells	Mice were vaccinated s.c. with 1×10^6 vaccine cells twice at a one-week interval in the prophylactic setting. In the therapeutic setting, mice were treated with two doses of 1×10^7 irradiated vaccine cells	IL-21	Female C57BL/6 and Balb/c mice	Cytokine production in vaccine cell lines was confirmed. IL-21 and IL-7 co-expressing cancer cell vaccine protected mice from tumor challenges in prophylactic and therapeutic models. Furthermore, the vaccine enhanced the infiltration of $CD8^+$ and $CD4^+$ T cells in the tumor region. Notably, long-term memory antitumor immunity was demonstrated after vaccine treatment in mice.	(81)
2014	Autologous tumor cell vaccine modified with nonlytic Newcastle disease virus strain LX expressing IL-7 (LX/(IL-7))	IL-7 gene transfected in tumor cell vaccine	The EL-4 murine lymphoma cell line, and B16-F10 murine melanoma cell line	Mice were immunized with 1×10^6 irradiated cancer cell vaccine LX/(IL-7) s.c. for prophylactic or therapeutic purpose	None	Pathogen-free 6-week-old female C57BL/6 mice	The gene IL-7 product in cancer cell vaccine LX/(IL-7) was active and stable. This vaccine exhibited great prophylactic and therapeutic effects against tumors. Tumor-specific $CD8^+$ T cells with higher IFN-γ expression and cytotoxicity were evidenced in models compared to control. However, the percentage of memory T cells was not significantly modified by the vaccine treatment group.	(82)
2009	LCMV, mimicking a live viral antitumor vaccine/*In vitro*–differentiated DCs pulsed with GP33, GP276 and GP61	Recombinant human IL-7	Pancreatic β-islet cell tumors.	Eight days after vaccination, mice received 10 mg of recombinant human IL-7 s.c. daily for 2 weeks.	None	RIP-TAG2 transgenic mice	Survival of IL-7–treated mice was prolonged compared to control mice. IL-7–treated mice with tumors had a 3.5- to 10-fold increase in both $CD4^+$ and $CD8^+$ T cell numbers while tumors from IL-7–treated mice were heavily infiltrated with both $CD4^+$ and $CD8^+$ T cells, compared to PBS control mice. Furthermore, Mice receiving DC vaccination together with IL-7 also exhibited an elevated antitumor response.	(83)
2009	Recombinant lentivectors	Recombinant human IL-7	None	Mice received intraperitoneal	None	HLA-A*0201/H-	IL-7 adjuvant promoted the proliferation of the Melan-A-specific	(84)

(Continued)

TABLE 1 Continued

Year	Cancer vaccine	Form of IL-7	Targeted cancer cell lines	IL-7 dose/ route	Combination therapy	Study models	Study results	Reference
	encoding the HLA-A2–restricted Melan-A26-35 peptide			injections of 5 μg human recombinant IL-7 daily after vaccination.		2Kb transgenic mice	effector and memory $CD8^+$ T cells and enhanced their immune responses after vaccine immunization. The functionality of Melan-A-specific memory $CD8^+$ T cells was improved after IL-7 treatment.	
2007	GM-CSF expressing B16F10 and CT26 tumor cell vaccine	Recombinant human IL-7	The B16F10 melanoma and the CT26 colon carcinoma cell	Mouse received 10μg IL-7 administration by s.c. injection, three injections per week for a total of 3 weeks.	GM-CSF	8 to 12 weeks female C57BL/6 mice and BALB/c mice	IL-7 treatment increased the survival of tumor-bearing mice after vaccine administration. IL-7 augmented the number of activated and tumor-infiltrating T cells and specific immune responses in vaccine-receiving mice. Furthermore, a tumor-specific memory response induced by IL-7 protected mice from a second tumor challenge.	(85)
2006	Monocyte-derived DCs pulsed with tumor antigen KLH	Recombinant human IL-7	None	PBMCs were treated with IL-7 in a dose-dependent method	Recombinant human IL-15	PBMCs from patients with metastatic renal cell carcinoma of the clear-cell type	IL-7 induced much stronger proliferation in post- than in prevaccine PBMCs in a dose-dependent manner, while IL-7 induced IFN-γ production in postvaccine PBMCs but not in prevaccine PBMCs. However, a synergetic effect of IL-7 and IL-15 on the proliferation of PBMCs was not evidenced.	(86)

MIF, Macrophage migration inhibitory factor; PD-L1, Programmed death-ligand 1; HPV, Human papillomavirus; DNA, Deoxyribonucleic acid; s.c., subcutaneous; LCMV, Lymphocytic choriomeningitis virus; GP, Glycoprotein; RIP, Rat insulin promoter; TAG2, SV40 large T antigen; HLA, Human leukocyte antigen; DC, Dendritic cell; KLH, Keyhole limpet hemocyanin; PBMC, Peripheral blood mononuclear cell.

response against RCC in most patients. In another phase I/II clinical trial, Wittig and colleagues cotransfected IL-7 and granulocyte-macrophage colony-stimulating factor (GM-CSF) genes in autologous tumor cells as a therapeutic vaccine to immunize patients with progressive metastatic carcinoma (90). This vaccine was clinically tolerable with no AEs being observed. Increased level of IL-7 was evidenced in the serum of the patients after treatment. At the endpoint of the study, 2 out of 10 patients achieved SD while 5 remained in progressive disease. The number of $CD3^+$, $CD8^+$, and $CD56^+$ lymphocytes increased postvaccination. Intriguingly, the cytotoxicity of peripheral blood lymphocytes of patients elevated significantly during treatment, demonstrating that the IL-7-expressing tumor cell vaccine was immunological and capable to stimulate a robust immune response against metastatic cancers.

Recently, some clinical studies attempt to administer recombinant human IL-7 in cancer patients subcutaneously as an adjuvant for cancer vaccines (87, 88). In a phase I/II clinical trial (NCT00923351) (88), recombinant human IL-7 was administered to pediatric sarcoma patients on days 0, 14 ± 7 d, 28 ± 7 d, and 42 ± 7 d after receiving autologous tumor lysate-pulsed DCs vaccination. No grade III/IV AEs were reported during the treatment. Encouragingly, IL-7 recipients showed a higher number of circulating $CD4^+$, $CD8^+$ T cells, and NK cells than the subjects who did not receive IL-7, exhibiting the great potential of IL-7 to induce immunological reconstitution. Moreover, the administration of IL-7 decreased the proportion of regulatory T (Treg) cells in patients. Regrettably, there was no difference in OS between the patients treated ± IL-7. Another phase II clinical study (NCT01881867) (87), initiated by Pachynski et al., reported that subcutaneous administration of IL-7 resulted in the expansion of $CD4^+$, $CD8^+$, and γδ T cells in prostate cancer patients treated with sipuleucel-T, a therapeutic cancer vaccine proved by Food and Drug Administration (92). Furthermore, increased levels of intracellular cytokines were revealed in $CD4^+$,γδ T cells, and NK cells. Notably, increased levels of IL-2, TNF-α, IFN-γ, and IL-6 were demonstrated in the memory subsets, indicating that IL-7 possesses the capability to stimulate the memory immune responses against cancers. Although the IL-7 group does show tails of the curves in both OS and progression-free survival (PFS), this trial failed to evidence a significantly improved OS and PFS in the IL-7 arm.

Taking these clinical data together, adjuvant IL-7 exhibited great potential in immunological reconstitution, including prompting expansion of T cells, inducing cytokine production, maintaining memory response, and arousing resistance to immune suppression, when combined with cancer vaccines to struggle against tumors. Moreover, IL-7 was clinically well-

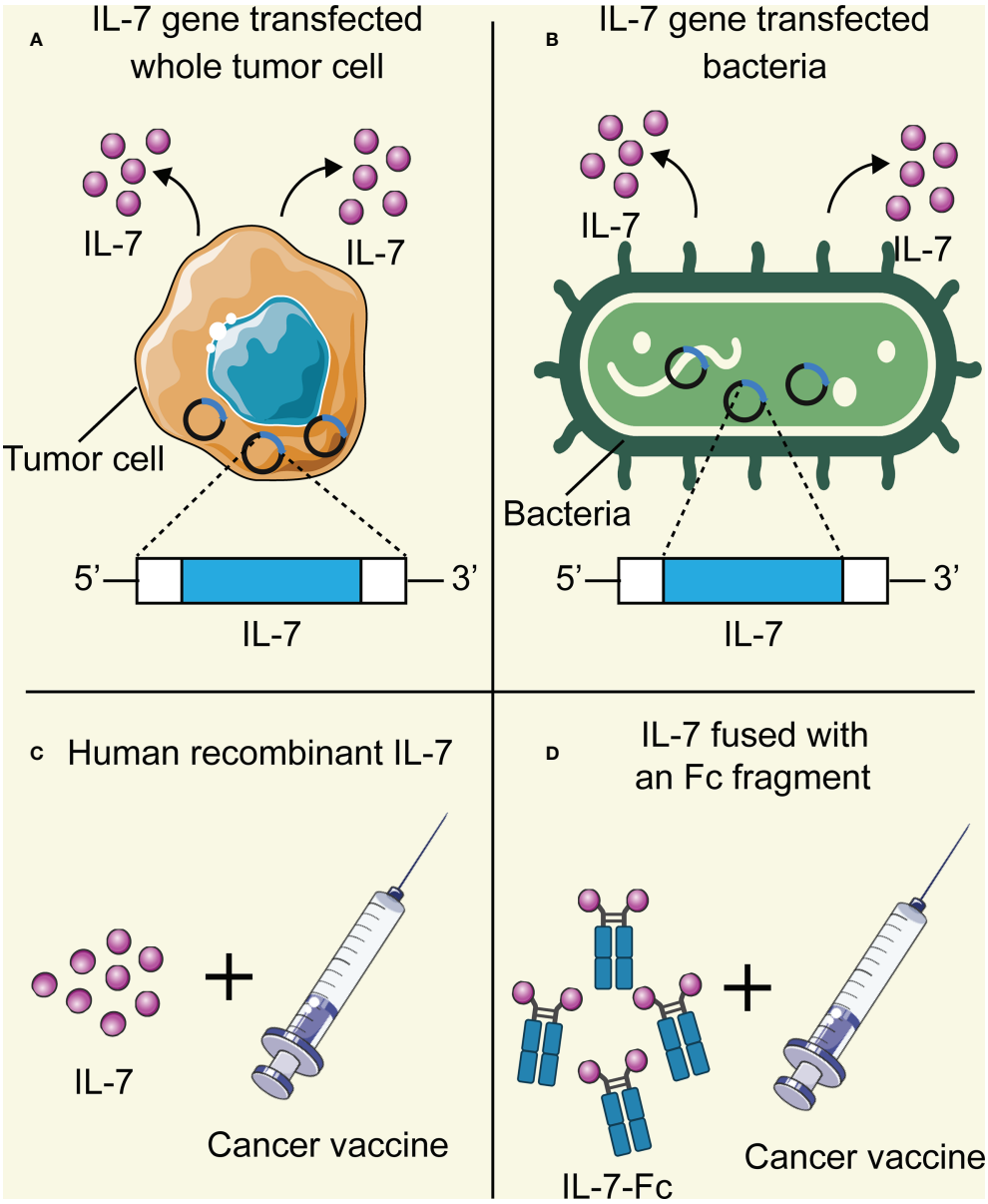

FIGURE 4
The adjuvant platform of IL-7 for cancer vaccines in preclinical and clinical trials. **(A)** Cancer vaccine tumor cells are transfected with the adjuvant IL-7 gene and then produce IL-7 stably. **(B)** Bacteria are transfected with the adjuvant IL-7 gene and then produce IL-7 stably. **(C)** Direct administration of human recombinant IL-7 as an adjuvant in combination with cancer vaccines. **(D)** IL-7 fused with the Fc region of the antibody as an adjuvant. This figure is created with BioRender.com and smart.servier.com.

tolerant for cancer patients. Unfortunately, the clinical outcome of the patients who received the IL-7 treatment is still unsatisfying, with no enhanced OS or PFS have been demonstrated. However, the population enrolled in these clinical studies is limited. With more subjects included in trials, the survival benefits of the IL-7 arm might be evidenced statistically. More preclinical and clinical studies are encouraged to explore the potential role of IL-7 as an adjuvant for the development of cancer vaccines.

Proposal of IL-7 as an adjuvant for cancer vaccines in clinical practice

The early-stage clinical trials focus on designing tumor cell cancer vaccines expressing adjuvant molecular IL-7. At least $1x10^6$ IL-7-cotransfected tumor cells were administrated subcutaneously in cancer patients with a minimum of four injections. However, in current clinical trials, direct

TABLE 2 Clinical trials of cancer vaccines combined with IL-7 as an adjuvant for the treatment of malignancy.

Vaccine	Trial ID	Phase	Enrollment status	malignancy	IL-7 dose/route	Timing/ length ofIL-7 therapy	Combination adjuvant	Study results	Enrolled population	Reference
Sipuleucel-T	NCT01881867	II	Completed	Metastatic castration-resistant prostate cancer	10 μg/kg/s.c.	IL-7 was given weekly×4 or until the unacceptable AE(s) occurred	None	Treatment with IL-7 was well tolerated. IL-7 led to a significant proliferation of $CD4^+$ and $CD8^+$ T cells. Increased expression of IL-2, TNFα, IFN-γ, and IL-6 was demonstrated in central memory and effector memory T subsets. No improved PFS or OS in the IL-7 treatment group were observed.	54	(87)
Autologous tumor lysate-pulsed DCs vaccination	NCT00923351	I/II	Completed	Metastatic and recurrent pediatric sarcomas	20μg/kg/s.c.	IL-7 was given on days 0, 14 ± 7 d, 28 ± 7 d, and 42 ± 7 d.	None	No grade 3/4 AEs were reported. An increased number of $CD4^+$ and $CD8^+$ T cells was evidenced in the IL-7 treatment group. Moreover, IL-7 down-regulates the frequency of regulatory T cells in patients. No difference in OS between subjects treated ± IL-7 was observed.	43	(88)
RCC26/IL-7/ CD80 (IL-7/ CD80 cotransfected allogeneic renal cell cancer)	NA	I	Completed	Progressive metastatic clear cell RCC	Patients were immunized with 2.5–4.0x10^6 RCC26/IL-7/ CD80, 1x10^6 RCC26/ IL-7/CD80 vaccine cells were able to produce ~4.5x10^3 pg IL-7/s.c.	2.5x10^6 cells at weeks 1, 2, 4, and 6; 10x10^6 cells at weeks 8, 10, 12, and 14; and 40x10^6 cells at weeks 18 and 22.	CD80 (cotransfected in RCC cells)	Vaccination was clinically safe, with no grade 3/4 toxicities being observed. 50% of the patients showed SD throughout the study and the median time to progression was 18 weeks while the median OS was 40 months. T cell responses were predominantly TH2 type. There was a decline of Treg cells in three patients.	10	(89)
Autologous IL-7 and GM-CSF cotransfected tumor cells	NA	I/II	Completed	Metastatic colon carcinoma, renal cancer, and melanoma	Patients received at least four injections of 1x10^6 autologous tumor cells transfected with the IL-7 gene/s.c.	Patients received four injections of vaccines on days 0, 14, 28, and 56, respectively.	GM-CSF (cotransfected in autologous tumor cells)	No AEs could be detected in all patients. IL-7 level was elevated in the serum of the patients after treatment. Two patients had SD after treatment while five patients were confirmed with PD. A significant increase in $CD3^+CD8^+$ T cells subset from 21.5 to 25.6% in all patients on day 84 was evidenced. Cytotoxicity of peripheral blood lymphocytes increased significantly during treatment.	10	(90)
MGN1601 vaccine (genetically modified allogeneic tumor cells for the expression of IL-7, GM-CSF, CD80, and CD154)	NCT01265368	I/II	Completed	Advanced renal cell carcinoma	MGN1601 was injected intradermally eight times.	Within 12 weeks.	GM-CSF, CD80, and CD154 (cotransfected in autologous tumor cells)	Administration of MGN1601 to RCC patients was well tolerated. MGN1601-treated patients showed significantly increased OS over the untreated patients. After vaccination, antibodies against TAA were demonstrated in RCC patients.	19	(91)
Melanoma peptide vaccine	NCT00091338	I	Completed	Melanoma	NA/s.c.	Patients received IL-7	Incomplete Freund's adjuvant	NA	NA	NA

(Continued)

10.3389/fimmu.2022.1022808

10.3389/fimmu.2022.1022808

TABLE 2 Continued

Vaccine	Trial ID	Phase	Enrollment status	malignancy	IL-7 dose/route	Timing/ length ofIL-7 therapy	Combination adjuvant	Study results	Enrolled population	Reference
comprising gp100 antigen and MART-1 antigen						on days 0, 3, 6, 9, 12, 15, 18, and 21.				

IL-7, interleukin 7; μg, Microgram; kg, Kilogram; s.c., Subcutaneous; AEs, Adverse events; PFS, Progression-free survival; OS, overall survival; DC, dendritic cell; RCC, Renal cell carcinoma; pg, Picogram; SD, Stable disease; TH2, T helper 2; PD, Progressive disease; TAA, Tumor-associated antigen; gp, Glycoprotein; MART-1, Melanoma antigen recognized by T cells 1; NA, Not available.

administration of human recombinant IL-7 subcutaneously as an adjuvant in combination with cancer vaccines is the preferred method. The dose of IL-7 injection varies from 10 μg/kg to 20 μg/kg in cancer patients while at least four doses were administered. Since direct injection of IL-7 as an adjuvant has been proven to be safe and effective, IL-7-cotransfected tumor cell vaccine, which is labor- and time-consuming in manufacturing, seems to be unsuitable and inconvenient in clinical practice. Although direct administration of IL-7 as an adjuvant is more practical, the dose, routine, and time length of IL-7 therapy still need to be optimized according to furthermore clinical trials.

To achieve an effective and long-lasting T cell immune response against cancer to the greatest extent, a combination with other cytokines when utilizing IL-7 as an adjuvant agent for cancer vaccines is recommended. It is crucial to choose suitable chaperone adjuvants rather than a single agent to regulate a full palette of immune responses to combat tumors comprehensively. IL-2 and IL-7 have been well demonstrated to enhance the T cell responses (93), indicating the potential role of IL-2 in combination with IL-7 as adjuvants for cancer vaccines. Another cytokine, IL-15, was also well-defined to boost T cell responses, as well as to maintain long-lasting T cell memory against cancers (94). Intriguingly, antigen-activated T lymphocytes incubated with IL-7 and IL-15 exhibited a more robust capability to induce regression of melanoma and 4T1 mammary carcinoma in comparison to IL-2 alone (33, 95). Moreover, previous studies have indicated that the proliferation and maintenance of $CD8^+$ memory T cells require IL-7 and IL-15 jointly (59–61). However, dose-related adverse events of administration of IL-2 and IL-15, like fever and serious biochemical abnormalities in the liver and kidney should not be ignored (96). Furthermore, IL-2 and IL-15 were evidenced to maintain immunosuppressive Treg cells in the periphery and induce the expression of immunosuppressive receptors, resulting in attenuated immune responses (97). To circumvent the immunosuppression induced by combined cytokines, ICB is suggested.

Although the antitumor role of IL-7 in combination with cancer vaccine has been revealed, there is still a “dark side” that needs to be emphasized. IL-7 was evidence to promote cell viability, cell cycle progression, and growth of T-cell acute lymphoblastic leukemia (T-ALL) *in vitro* (98). Moreover, *in vivo* experiments exhibited that the consumption of IL-7 contributes to the development of T-ALL, while IL-7 deficiency reduced the proliferation of leukemia cells (21, 99). Coincidently, IL-7 can also induce the expansion of B-ALL cells (100) and boost the tumorigenesis of B cells in IL-7 transgenic mice (101). These collected facts highly indicated that IL-7 acts as a tumor-promoting factor during the occurrence and progression of hematopoietic malignancy. Therefore, it is unpracticable to apply IL-7, a cytokine that contributes to leukemia development, as an adjuvant for cancer vaccines against hematopoietic malignancy for safety considerations.

Conclusion

Various factors affect the immunogenicity of cancer vaccines, like the selection of antigens (102), the choice of adjuvant (103), and even the delivery vehicles that are applied in the administration strategy (104). To stimulate an effective and long-lasting T cell memory response, cancer vaccines incorporated with adjuvant IL-7 to combat cancers were initiated in numerous experiments. The biological role of IL-7 in the development, survival, proliferation, and memory maintenance of T cells was summarized while the signaling of IL-7/IL-7R was summed up in this manuscript. These facts highlighted the feasibility to apply IL-7 as an adjuvant in combination with cancer vaccines. Preclinical researches bring inspiring results for the rationale to apply IL-7 as an adjuvant for cancer vaccines while further clinical trials enhance this notion. Although boosted T cell expansion and enhanced T cell memory were evidenced in clinical trials when administrating IL-7 as an adjuvant combined with cancer vaccines, the clinical outcomes of cancer patients are still far from satisfactory. Currently, it is still hard to give a conclusion that IL-7 can serve as an ideal adjuvant for cancer vaccines from such a limited number of clinical trials, therefore, clinical trials concerning IL-7 as an adjuvant for cancer vaccines, to fulfill efficacious T cell responses and long-lasting T cell memory against tumors, are urgently encouraged. Here, we also proposed some suggestions on how to utilize IL-7 as an adjuvant incorporated with cancer vaccines, including the form, dose, and chaperone cytokine of IL-7, which might be of value to researchers.

Author contributions

XL and ZX contributed to the study conception design. YZ, KW, and HC performed the literature search and data collection. Figures were drawn by YZ. YZ and KW prepared the draft and the manuscript was revised by XL and ZX. XL provided the funding. All authors contributed to the article and approved the submitted version.

Funding

This study was funded by the National Natural Science Foundation of China (grant number 81871653), the Natural Science Foundation of Chongqing (cstc2021jsyj-yzysbAX0018), Chongqing Science and Health Joint Medical High-end Talent Project (2022GDRC012), Science and Technology Research Program of Chongqing Municipal Education Commission (KJZD-K202100402, KJQN201900449) and CQMU Program for Youth Innovation in Future Medicine (W0073).

Conflict of interest

The authors declare that the research was conducted in the absence of any commercial or financial relationships that could be construed as a potential conflict of interest.

Publisher's note

All claims expressed in this article are solely those of the authors and do not necessarily represent those of their affiliated organizations, or those of the publisher, the editors and the reviewers. Any product that may be evaluated in this article, or claim that may be made by its manufacturer, is not guaranteed or endorsed by the publisher.

References

1. Sharma P, Allison JP. The future of immune checkpoint therapy. *Science* (2015) 348(6230):56–61. doi: 10.1126/science.aaa8172

2. Bagchi S, Yuan R, Engleman EG. Immune checkpoint inhibitors for the treatment of cancer: Clinical impact and mechanisms of response and resistance. *Annu Rev Pathol* (2021) 16:223–49. doi: 10.1146/annurev-pathol-042020-042741

3. Saxena M, van der Burg SH, Melief CJM, Bhardwaj N. Therapeutic cancer vaccines. *Nat Rev Cancer* (2021) 21(6):360–78. doi: 10.1038/s41568-021-00346-0

4. Sahin U, Türeci Ö. Personalized vaccines for cancer immunotherapy. *Science* (2018) 359(6382):1355–60. doi: 10.1126/science.aar7112

5. Baxevanis CN, Perez SA, Papamichail M. Cancer immunotherapy. *Crit Rev Clin Lab Sci* (2009) 46(4):167–89. doi: 10.1080/10408360902937809

6. Bidram M, Zhao Y, Shebardina NG, Baldin AV, Bazhin AV, Ganjalikhany MR, et al. Mrna-based cancer vaccines: A therapeutic strategy for the treatment of melanoma patients. *Vaccines (Basel)* (2021) 9(10):1060. doi: 10.3390/vaccines9101060

7. Sahin U, Karikó K, Türeci Ö. Mrna-based therapeutics–developing a new class of drugs. *Nat Rev Drug Discovery* (2014) 13(10):759–80. doi: 10.1038/nrd4278

8. Tran T, Blanc C, Granier C, Saldmann A, Tanchot C, Tartour E. Therapeutic cancer vaccine: Building the future from lessons of the past. *Semin Immunopathol* (2019) 41(1):69–85. doi: 10.1007/s00281-018-0691-z

9. Liu Q, Sun Z, Chen L. Memory T cells: Strategies for optimizing tumor immunotherapy. *Protein Cell* (2020) 11(8):549–64. doi: 10.1007/s13238-020-00707-9

10. Mami-Chouaib F, Blanc C, Corgnac S, Hans S, Malenica I, Granier C, et al. Resident memory T cells, critical components in tumor immunology. *J Immunother Cancer* (2018) 6(1):87. doi: 10.1186/s40425-018-0399-6

11. Bowen WS, Svrivastava AK, Batra L, Barsoumian H, Shirwan H. Current challenges for cancer vaccine adjuvant development. *Expert Rev Vaccines* (2018) 17(3):207–15. doi: 10.1080/14760584.2018.1434000

12. Hunt P, Robertson D, Weiss D, Rennick D, Lee F, Witte ON. A single bone marrow-derived stromal cell type supports the *in vitro* growth of early lymphoid and myeloid cells. *Cell* (1987) 48(6):997–1007. doi: 10.1016/0092-8674(87)90708-2

13. Lundström W, Fewkes NM, Mackall CL. Il-7 in human health and disease. *Semin Immunol* (2012) 24(3):218–24. doi: 10.1016/j.smim.2012.02.005

14. Huang J, Long Z, Jia R, Wang M, Zhu D, Liu M, et al. The broad immunomodulatory effects of il-7 and its application in vaccines. *Front Immunol* (2021) 12:680442. doi: 10.3389/fimmu.2021.680442

15. Lukacs-Kornek V, Malhotra D, Fletcher AL, Acton SE, Elpek KG, Tayalia P, et al. Regulated release of nitric oxide by nonhematopoietic stroma controls expansion of the activated T cell pool in lymph nodes. *Nat Immunol* (2011) 12 (11):1096–104. doi: 10.1038/ni.2112

16. Heufler C, Topar G, Grasseger A, Stanzl U, Koch F, Romani N, et al. Interleukin 7 is produced by murine and human keratinocytes. *J Exp Med* (1993) 178(3):1109–14. doi: 10.1084/jem.178.3.1109

17. Durum SK, Mazzucchelli RI. Live from the liver: Hepatocyte il-7. *Immunity* (2009) 30(3):320–1. doi: 10.1016/j.immuni.2009.03.001

18. Maeurer MJ, Walter W, Martin D, Zitvogel L, Elder E, Storkus W, et al. Interleukin-7 (Il-7) in colorectal cancer: Il-7 is produced by tissues from colorectal cancer and promotes preferential expansion of tumour infiltrating lymphocytes. *Scand J Immunol* (1997) 45(2):182–92. doi: 10.1046/j.1365-3083.1997.d01-384.x

19. Zhang W, Du JY, Yu Q, Jin JO. Interleukin-7 produced by intestinal epithelial cells in response to citrobacter rodentium infection plays a major role in innate immunity against this pathogen. *Infect Immun* (2015) 83(8):3213–23. doi: 10.1128/iai.00320-15

20. Kim GY, Hong C, Park JH. Seeing is believing: Illuminating the source of *in vivo* interleukin-7. *Immune Netw* (2011) 11(1):1–10. doi: 10.4110/in.2011.11.1.1

21. Barata JT, Durum SK, Seddon B. Flip the coin: Il-7 and il-7r in health and disease. *Nat Immunol* (2019) 20(12):1584–93. doi: 10.1038/s41590-019-0479-x

22. Li X, Bechara R, Zhao J, McGeachy MJ, Gaffen SL. Il-17 receptor-based signaling and implications for disease. *Nat Immunol* (2019) 20(12):1594–602. doi: 10.1038/s41590-019-0514-y

23. Akashi K, Kondo M, Weissman IL. Role of interleukin-7 in T-cell development from hematopoietic stem cells. *Immunol Rev* (1998) 165:13–28. doi: 10.1111/j.1600-065x.1998.tb01226.x

24. Hong C, Luckey MA, Park JH. Intrathymic il-7: The where, when, and why of il-7 signaling during T cell development. *Semin Immunol* (2012) 24(3):151–8. doi: 10.1016/j.smim.2012.02.002

25. Fry TJ, Mackall CL. Interleukin-7: From bench to clinic. *Blood* (2002) 99 (11):3892–904. doi: 10.1182/blood.v99.11.3892

26. Ribeiro D, Melão A, van Boxtel R, Santos CI, Silva A, Silva MC, et al. Stat5 is essential for il-7-Mediated viability, growth, and proliferation of T-cell acute lymphoblastic leukemia cells. *Blood Adv* (2018) 2(17):2199–213. doi: 10.1182/bloodadvances.2018021063

27. Li HB, Tong J, Zhu S, Batista PJ, Duffy EE, Zhao J, et al. M(6)a mrna methylation controls T cell homeostasis by targeting the il-7/Stat5/Socs pathways. *Nature* (2017) 548(7667):338–42. doi: 10.1038/nature23450

28. Cimbro R, Vassena L, Arthos J, Cicala C, Kehrl JH, Park C, et al. Il-7 induces expression and activation of integrin α4β7 promoting naive T-cell homing to the intestinal mucosa. *Blood* (2012) 120(13):2610–9. doi: 10.1182/blood-2012-06-434779

29. Ponte R, Rancez M, Figueiredo-Morgado S, Dutrieux J, Fabre-Mersseman V, Charmeteau-de-Muylder B, et al. Acute simian immunodeficiency virus infection triggers early and transient interleukin-7 production in the gut, leading to enhanced local chemokine expression and intestinal immune cell homing. *Front Immunol* (2017) 8:588. doi: 10.3389/fimmu.2017.00588

30. Vogt TK, Link A, Perrin J, Finke D, Luther SA. Novel function for interleukin-7 in dendritic cell development. *Blood* (2009) 113(17):3961–8. doi: 10.1182/blood-2008-08-176321

31. Meazza R, Azzarone B, Orengo AM, Ferrini S. Role of common-gamma chain cytokines in nk cell development and function: Perspectives for immunotherapy. *J BioMed Biotechnol* (2011) 2011:861920. doi: 10.1155/2011/861920

32. Kulkarni U, Herrmenau C, Win SJ, Bauer M, Kamradt T. Il-7 treatment augments and prolongs sepsis-induced expansion of il-10-Producing b lymphocytes and myeloid-derived suppressor cells. *PloS One* (2018) 13(2): e0192304. doi: 10.1371/journal.pone.0192304

33. Cha E, Graham L, Manjili MH, Bear HD. Il-7 + il-15 are superior to il-2 for the *ex vivo* expansion of 4t1 mammary carcinoma-specific T cells with greater efficacy against tumors *in vivo*. *Breast Cancer Res Treat* (2010) 122(2):359–69. doi: 10.1007/s10549-009-0573-0

34. Moore TA, von Freeden-Jeffry U, Murray R, Zlotnik A. Inhibition of gamma delta T cell development and early thymocyte maturation in il-7 -/- mice. *J Immunol* (1996) 157(6):2366–73.

35. Shitara S, Hara T, Liang B, Wagatsuma K, Zuklys S, Holländer GA, et al. Il-7 produced by thymic epithelial cells plays a major role in the development of thymocytes and tcrγδ+ intraepithelial lymphocytes. *J Immunol* (2013) 190 (12):6173–9. doi: 10.4049/jimmunol.1202573

36. Bhatia SK, Tygrett LT, Grabstein KH, Waldschmidt TJ. The effect of *in vivo* il-7 deprivation on T cell maturation. *J Exp Med* (1995) 181(4):1399–409. doi: 10.1084/jem.181.4.1399

37. Boudil A, Matei IR, Shih HY, Bogdanoski G, Yuan JS, Chang SG, et al. Il-7 coordinates proliferation, differentiation and tcra recombination during thymocyte β-selection. *Nat Immunol* (2015) 16(4):397–405. doi: 10.1038/ni.3122

38. Seddon B, Zamoyska R. Tcr and il-7 receptor signals can operate independently or synergize to promote lymphopenia-induced expansion of naive T cells. *J Immunol* (2002) 169(7):3752–9. doi: 10.4049/jimmunol.169.7.3752

39. Sinclair C, Saini M, Sakaguchi S, Seddon B. The long-term survival potential of mature T lymphocytes is programmed during development in the thymus. *Sci Signal* (2011) 4(199):ra77. doi: 10.1126/scisignal.2002246

40. Patra AK, Avots A, Zahedi RP, Schüler T, Sickmann A, Bommhardt U, et al. An alternative nfat-activation pathway mediated by il-7 is critical for early thymocyte development. *Nat Immunol* (2013) 14(2):127–35. doi: 10.1038/ni.2507

41. Mazzucchelli R, Durum SK. Interleukin-7 receptor expression: Intelligent design. *Nat Rev Immunol* (2007) 7(2):144–54. doi: 10.1038/nri2023

42. Jourdan P, Vendrell JP, Huguet MF, Segondy M, Bousquet J, Pène J, et al. Cytokines and cell surface molecules independently induce Cxcr4 expression on Cd4+ Ccr7+ human memory T cells. *J Immunol* (2000) 165(2):716–24. doi: 10.4049/jimmunol.165.2.716

43. Bolotin E, Annett G, Parkman R, Weinberg K. Serum levels of il-7 in bone marrow transplant recipients: Relationship to clinical characteristics and lymphocyte count. *Bone Marrow Transplant* (1999) 23(8):783–8. doi: 10.1038/sj.bmt.1701655

44. Ponchel F, Cuthbert RJ, Goëb V. Il-7 and lymphopenia. *Clin Chim Acta* (2011) 412(1-2):7–16. doi: 10.1016/j.cca.2010.09.002

45. Raeber ME, Zurbuchen Y, Impellizzieri D, Boyman O. The role of cytokines in T-cell memory in health and disease. *Immunol Rev* (2018) 283(1):176–93. doi: 10.1111/imr.12644

46. Sumaria N, Roediger B, Ng LG, Qin J, Pinto R, Cavanagh LL, et al. Cutaneous immunosurveillance by self-renewing dermal gammadelta T cells. *J Exp Med* (2011) 208(3):505–18. doi: 10.1084/jem.20101824

47. Gao J, Zhao L, Wan YY, Zhu B. Mechanism of action of il-7 and its potential applications and limitations in cancer immunotherapy. *Int J Mol Sci* (2015) 16 (5):10267–80. doi: 10.3390/ijms160510267

48. Swainson L, Kinet S, Mongellaz C, Sourisseau M, Henriques T, Taylor N. Il-7-Induced proliferation of recent thymic emigrants requires activation of the Pi3k pathway. *Blood* (2007) 109(3):1034–42. doi: 10.1182/blood-2006-06-027912

49. Sportès C, Hakim FT, Memon SA, Zhang H, Chua KS, Brown MR, et al. Administration of rhil-7 in humans increases *in vivo* tcr repertoire diversity by preferential expansion of naive T cell subsets. *J Exp Med* (2008) 205(7):1701–14. doi: 10.1084/jem.20071681

50. Tan JT, Dudl E, LeRoy E, Murray R, Sprent J, Weinberg KI, et al. Il-7 is critical for homeostatic proliferation and survival of naive T cells. *Proc Natl Acad Sci USA* (2001) 98(15):8732–7. doi: 10.1073/pnas.161126098

51. Venet F, Foray AP, Villars-Méchin A, Malcus C, Poitevin-Later F, Lepape A, et al. Il-7 restores lymphocyte functions in septic patients. *J Immunol* (2012) 189 (10):5073–81. doi: 10.4049/jimmunol.1202062

52. Heninger AK, Theil A, Wilhelm C, Petzold C, Huebel N, Kretschmer K, et al. Il-7 abrogates suppressive activity of human Cd4+Cd25+Foxp3+ regulatory T cells and allows expansion of alloreactive and autoreactive T cells. *J Immunol* (2012) 189(12):5649–58. doi: 10.4049/jimmunol.1201286

53. Andersson A, Yang SC, Huang M, Zhu L, Kar UK, Batra RK, et al. Il-7 promotes Cxcr3 ligand-dependent T cell antitumor reactivity in lung cancer. *J Immunol* (2009) 182(11):6951–8. doi: 10.4049/jimmunol.0803340

54. Habibi M, Kmieciak M, Graham L, Morales JK, Bear HD, Manjili MH. Radiofrequency thermal ablation of breast tumors combined with intralesional administration of il-7 and il-15 augments anti-tumor immune responses and inhibits tumor development and metastasis. *Breast Cancer Res Treat* (2009) 114 (3):423–31. doi: 10.1007/s10549-008-0024-3

55. Williams MA, Bevan MJ. Effector and memory ctl differentiation. *Annu Rev Immunol* (2007) 25:171–92. doi: 10.1146/annurev.immunol.25.022106.141548

56. Gerlach C, Rohr JC, Perié L, van Rooij N, van Heijst JW, Velds A, et al. Heterogeneous differentiation patterns of individual Cd8+ T cells. *Science* (2013) 340(6132):635–9. doi: 10.1126/science.1235487

57. Colpitts SL, Dalton NM, Scott P. Il-7 receptor expression provides the potential for long-term survival of both Cd62lhigh central memory T cells and Th1 effector cells during leishmania major infection. *J Immunol* (2009) 182(9):5702–11. doi: 10.4049/jimmunol.0803450

58. Terrazzini N, Mantegani P, Kern F, Fortis C, Mondino A, Caserta S. Interleukin-7 unveils pathogen-specific T cells by enhancing antigen-recall responses. *J Infect Dis* (2018) 217(12):1997–2007. doi: 10.1093/infdis/jiy096

59. Bradley LM, Haynes L, Swain SL. Il-7: Maintaining T-cell memory and achieving homeostasis. *Trends Immunol* (2005) 26(3):172–6. doi: 10.1016/j.it.2005.01.004

60. Tan JT, Ernst B, Kieper WC, LeRoy E, Sprent J, Surh CD. Interleukin (Il)-15 and il-7 jointly regulate homeostatic proliferation of memory phenotype Cd8+ cells but are not required for memory phenotype Cd4+ cells. *J Exp Med* (2002) 195 (12):1523–32. doi: 10.1084/jem.20020066

61. Chetoui N, Boisvert M, Gendron S, Aoudjit F. Interleukin-7 promotes the survival of human Cd4+ Effector/Memory T cells by up-regulating bcl-2 proteins and activating the Jak/Stat signalling pathway. *Immunology* (2010) 130(3):418–26. doi: 10.1111/j.1365-2567.2009.03244.x

62. Cieri N, Camisa B, Cocchiarella F, Forcato M, Oliveira G, Provasi E, et al. Il-7 and il-15 instruct the generation of human memory stem T cells from naive precursors. *Blood* (2013) 121(4):573–84. doi: 10.1182/blood-2012-05-431718

63. Melchionda F, Fry TJ, Milliron MJ, McKirdy MA, Tagaya Y, Mackall CL. Adjuvant il-7 or il-15 overcomes immunodominance and improves survival of the Cd8+ memory cell pool. *J Clin Invest* (2005) 115(5):1177–87. doi: 10.1172/jci23134

64. Nanjappa SG, Walent JH, Morre M, Suresh M. Effects of il-7 on memory Cd8 T cell homeostasis are influenced by the timing of therapy in mice. *J Clin Invest* (2008) 118(3):1027–39. doi: 10.1172/jci32020

65. Singh V, Gowthaman U, Jain S, Parihar P, Banskar S, Gupta P, et al. Coadministration of interleukins 7 and 15 with bacille calmette-guérin mounts enduring T cell memory response against mycobacterium tuberculosis. *J Infect Dis* (2010) 202(3):480–9. doi: 10.1086/653827

66. Jiang Q, Li WQ, Aiello FB, Mazzucchelli R, Asefa B, Khaled AR, et al. Cell biology of il-7, a key lymphotrophin. *Cytokine Growth Factor Rev* (2005) 16(4-5):513–33. doi: 10.1016/j.cytogfr.2005.05.004

67. Leonard WJ, Imada K, Nakajima H, Puel A, Soldaini E, John S. Signaling *Via* the il-2 and il-7 receptors from the membrane to the nucleus. *Cold Spring Harb Symp Quant Biol* (1999) 64:417–24. doi: 10.1101/sqb.1999.64.417

68. Mohamed MF, Beck D, Camp HS, Othman AA. Preferential inhibition of Jak1 relative to Jak3 by upadacitinib: Exposure-response analyses of *ex vivo* data from 2 phase 1 clinical trials and comparison to tofacitinib. *J Clin Pharmacol* (2020) 60(2):188–97. doi: 10.1002/jcph.1513

69. Osborne LC, Dhanji S, Snow JW, Priatel JJ, Ma MC, Miners MJ, et al. Impaired Cd8 T cell memory and Cd4 T cell primary responses in il-7r alpha mutant mice. *J Exp Med* (2007) 204(3):619–31. doi: 10.1084/jem.20061871

70. Zaunders JJ, Lévy Y, Seddiki N. Exploiting differential expression of the il-7 receptor on memory T cells to modulate immune responses. *Cytokine Growth Factor Rev* (2014) 25(4):391–401. doi: 10.1016/j.cytogfr.2014.07.012

71. Crawley AM, Vranjkovic A, Faller E, McGuinty M, Busca A, Burke SC, et al. Jak/Stat and Pi3k signaling pathways have both common and distinct roles in il-7-Mediated activities in human Cd8+ T cells. *J Leukoc Biol* (2014) 95(1):117–27. doi: 10.1189/jlb.0313122

72. Pellegrini M, Bouillet P, Robati M, Belz GT, Davey GM, Strasser A. Loss of bim increases T cell production and function in interleukin 7 receptor-deficient mice. *J Exp Med* (2004) 200(9):1189–95. doi: 10.1084/jem.20041328

73. Lu L, Chaudhury P, Osmond DG. Regulation of cell survival during b lymphopoiesis: Apoptosis and bcl-2/Bax content of precursor b cells in bone marrow of mice with altered expression of il-7 and recombinase-activating gene-2. *J Immunol* (1999) 162(4):1931–40.

74. Venkitaraman AR, Cowling RJ. Interleukin-7 induces the association of phosphatidylinositol 3-kinase with the alpha chain of the interleukin-7 receptor. *Eur J Immunol* (1994) 24(9):2168–74. doi: 10.1002/eji.1830240935

75. Yang F, Chen E, Yang Y, Han F, Han S, Wu G, et al. The Akt/Foxo/P27 (Kip1) axis contributes to the anti-proliferation of pentoxifylline in hypertrophic scars. *J Cell Mol Med* (2019) 23(9):6164–72. doi: 10.1111/jcmm.14498

76. Li WQ, Jiang Q, Aleem E, Kaldis P, Khaled AR, Durum SK. Il-7 promotes T cell proliferation through destabilization of P27kip1. *J Exp Med* (2006) 203(3):573–82. doi: 10.1084/jem.20051520

77. Wofford JA, Wieman HL, Jacobs SR, Zhao Y, Rathmell JC. Il-7 promotes Glut1 trafficking and glucose uptake *Via* Stat5-mediated activation of akt to support T-cell survival. *Blood* (2008) 111(4):2101–11. doi: 10.1182/blood-2007-06-096297

78. Chehtane M, Khaled AR. Interleukin-7 mediates glucose utilization in lymphocytes through transcriptional regulation of the hexokinase ii gene. *Am J Physiol Cell Physiol* (2010) 298(6):C1560–71. doi: 10.1152/ajpcell.00506.2009

79. Jeong H, Lee SY, Seo H, Kim BJ. Recombinant mycobacterium smegmatis delivering a fusion protein of human macrophage migration inhibitory factor (Mif) and il-7 exerts an anticancer effect by inducing an immune response against mif in a tumor-bearing mouse model. *J Immunother Cancer* (2021) 9(8):e003180. doi: 10.1136/jitc-2021-003180

80. Choi YW, Kang MC, Seo YB, Namkoong H, Park Y, Choi DH, et al. Intravaginal administration of fc-fused Il7 suppresses the cervicovaginal tumor by recruiting hpv DNA vaccine-induced Cd8 T cells. *Clin Cancer Res* (2016) 22 (23):5898–908. doi: 10.1158/1078-0432.CCR-16-0423

81. Gu YZ, Fan CW, Lu R, Shao B, Sang YX, Huang QR, et al. Forced Co-expression of il-21 and il-7 in whole-cell cancer vaccines promotes antitumor immunity. *Sci Rep* (2016) 6:32351. doi: 10.1038/srep32351

82. Zhao L, Mei Y, Sun Q, Guo L, Wu Y, Yu X, et al. Autologous tumor vaccine modified with recombinant new castle disease virus expressing il-7 promotes antitumor immune response. *J Immunol* (2014) 193(2):735–45. doi: 10.4049/jimmunol.1400004

83. Pellegrini M, Calzascia T, Elford AR, Shahinian A, Lin AE, Dissanayake D, et al. Adjuvant il-7 antagonizes multiple cellular and molecular inhibitory networks to enhance immunotherapies. *Nat Med* (2009) 15(5):528–36. doi: 10.1038/nm.1953

84. Colombetti S, Levy F, Chapatte L. Il-7 adjuvant treatment enhances long-term tumor-Antigen-Specific Cd8+ T-cell responses after immunization with recombinant lentivector. *Blood* (2009) 113(26):6629–37. doi: 10.1182/blood-2008-05-155309

85. Li B, VanRoey MJ, Jooss K. Recombinant il-7 enhances the potency of gm-Csf-Secreting tumor cell immunotherapy. *Clin Immunol* (2007) 123(2):155–65. doi: 10.1016/j.clim.2007.01.002

86. Leonhartsberger N, Ramoner R, Putz T, Gander H, Rahm A, Falkensammer C, et al. Antigen-independent immune responses after dendritic cell vaccination. *Cancer Immunol Immunother* (2007) 56(6):897–903. doi: 10.1007/s00262-006-0245-4

87. Pachynski RK, Morishima C, Szmulewitz R, Harshman L, Appleman L, Monk P, et al. Il-7 expands lymphocyte populations and enhances immune responses to sipuleucel-T in patients with metastatic castration-resistant prostate cancer (Mcrpc). *J Immunother Cancer* (2021) 9(8):e002903. doi: 10.1136/jitc-2021-002903

88. Merchant MS, Bernstein D, Amoako M, Baird K, Fleisher TA, Morre M, et al. Adjuvant immunotherapy to improve outcome in high-risk pediatric sarcomas. *Clin Cancer Res* (2016) 22(13):3182–91. doi: 10.1158/1078-0432.CCR-15-2550

89. Westermann J, Florcken A, Willimsky G, van Lessen A, Kopp J, Takvorian A, et al. Allogeneic gene-modified tumor cells (Rcc-26/Il-7/Cd80) as a vaccine in patients with metastatic renal cell cancer: A clinical phase-I study. *Gene Ther* (2011) 18(4):354–63. doi: 10.1038/gt.2010.143

90. Wittig B, Märten A, Dorbic T, Weineck S, Min H, Niemitz S, et al. Therapeutic vaccination against metastatic carcinoma by expression-modulated and immunomodified autologous tumor cells: A first clinical phase I/Ii trial. *Hum Gene Ther* (2001) 12(3):267–78. doi: 10.1089/10430340150218404

91. Volz B, Schmidt M, Heinrich K, Kapp K, Schroff M, Wittig B. Design and characterization of the tumor vaccine Mgn1601, allogeneic fourfold gene-modified vaccine cells combined with a tlr-9 agonist. *Mol Ther Oncolytics* (2016) 3:15023. doi: 10.1038/mto.2015.23

92. Higano CS, Small EJ, Schellhammer P, Yasothan U, Gubernick S, Kirkpatrick P, et al. Sipuleucel-T. *Nat Rev Drug Discov* (2010) 9(7):513–4. doi: 10.1038/nrd3220

93. Kim J-H, Lee K-J, Lee S-W. Cancer immunotherapy with T-cell targeting cytokines: Il-2 and il-7. *BMB Rep* (2021) 54(1):21–30. doi: 10.5483/BMBRep.2021.54.1.257

94. Waldmann TA, Dubois S, Miljkovic MD, Conlon KC. Il-15 in the combination immunotherapy of cancer. *Front Immunol* (2020) 11:868. doi: 10.3389/fimmu.2020.00868

95. Le HK, Graham L, Miller CH, Kmieciak M, Manjili MH, Bear HD. Incubation of antigen-sensitized T lymphocytes activated with bryostatin 1 + ionomycin in il-7 + il-15 increases yield of cells capable of inducing regression of melanoma metastases compared to culture in il-2. *Cancer Immunol Immunother* (2009) 58(10):1565–76. doi: 10.1007/s00262-009-0666-y

96. Rosenberg SA. Il-2: The first effective immunotherapy for human cancer. *J Immunol* (2014) 192(12):5451–8. doi: 10.4049/jimmunol.1490019

97. Waldmann TA. The shared and contrasting roles of Il2 and Il15 in the life and death of normal and neoplastic lymphocytes: Implications for cancer therapy. *Cancer Immunol Res* (2015) 3(3):219–27. doi: 10.1158/2326-6066.Cir-15-0009

98. Oliveira ML, Akkapeddi P, Ribeiro D, Melão A, Barata JT. Il-7r-Mediated signaling in T-cell acute lymphoblastic leukemia: An update. *Adv Biol Regul* (2019) 71:88–96. doi: 10.1016/j.jbior.2018.09.012

99. Silva A, Laranjeira AB, Martins LR, Cardoso BA, Demengeot J, Yunes JA, et al. Il-7 contributes to the progression of human T-cell acute lymphoblastic leukemias. *Cancer Res* (2011) 71(14):4780–9. doi: 10.1158/0008-5472.Can-10-3606

100. Digel W, Schmid M, Heil G, Conrad P, Gillis S, Porzsolt F. Human interleukin-7 induces proliferation of neoplastic cells from chronic lymphocytic leukemia and acute leukemias. *Blood* (1991) 78(3):753–9. doi: 10.1182/blood.V78.3.753.753

101. Rich BE, Campos-Torres J, Tepper RI, Moreadith RW, Leder P. Cutaneous lymphoproliferation and lymphomas in interleukin 7 transgenic mice. *J Exp Med* (1993) 177(2):305–16. doi: 10.1084/jem.177.2.305

102. Zhao Y, Baldin AV, Isayev O, Werner J, Zamyatnin AAJr., Bazhin AV. Cancer vaccines: Antigen selection strategy. *Vaccines (Basel)* (2021) 9(2):85. doi: 10.3390/vaccines9020085

103. Paston SJ, Brentville VA, Symonds P, Durrant LG. Cancer vaccines, adjuvants, and delivery systems. *Front Immunol* (2021) 12:627932. doi: 10.3389/fimmu.2021.627932

104. Ye T, Li F, Ma G, Wei W. Enhancing therapeutic performance of personalized cancer vaccine *Via* delivery vectors. *Adv Drug Del Rev* (2021) 177:113927. doi: 10.1016/j.addr.2021.113927

frontiers | Frontiers in Immunology

TYPE Original Research
PUBLISHED 23 March 2023
DOI 10.3389/fimmu.2023.1137054

OPEN ACCESS

EDITED BY
Anna Pasetto,
Oslo University Hospital, Norway

REVIEWED BY
Maki Nakayama,
University of Colorado Denver, United States
Will Hudson,
Baylor College of Medicine, United States

*CORRESPONDENCE
Ira Bergman
ira.bergman@chp.edu

SPECIALTY SECTION
This article was submitted to Cancer Immunity and Immunotherapy, a section of the journal Frontiers in Immunology

RECEIVED 03 January 2023
ACCEPTED 13 March 2023
PUBLISHED 23 March 2023

CITATION
Gao Y and Bergman I (2023) Anti-tumor memory CD4 and CD8 T-cells quantified by bulk T-cell receptor (TCR) clonal analysis.
Front. Immunol. 14:1137054.
doi: 10.3389/fimmu.2023.1137054

Anti-tumor memory CD4 and CD8 T-cells quantified by bulk T-cell receptor (TCR) clonal analysis

Yanhua Gao[1] and Ira Bergman[1,2,3]*

[1]Department of Pediatrics, Children's Hospital of Pittsburgh, University of Pittsburgh School of Medicine, Pittsburgh, PA, United States, [2]Department of Neurology, University of Pittsburgh School of Medicine, Pittsburgh, PA, United States, [3]Department of Immunology, University of Pittsburgh School of Medicine, Pittsburgh, PA, United States

Simple, reliable methods to detect anti-tumor memory T-cells are necessary to develop a clinical tumor vaccination program. A mouse model of curative viral onco-immunotherapy found that peritoneal tumor challenge following cure identified an oligoclonal anti-tumor memory CD4 and CD8 T-cell response. Clonotypes differed among the challenged animals but were congruent in blood, spleen and peritoneal cells (PC) of the same animal. Adoptive transfer demonstrated that the high-frequency responding T-cells were tumor specific. Tetramer analysis confirmed that clonotype frequency determined by T-cell receptor (TCR)- chain (TRB) analysis closely approximated cell clone frequency. The mean frequency of resting anti-tumor memory CD4 T-cells in unchallenged spleen was 0.028% and of memory CD8 T-cells was 0.11% which was not high enough to distinguish them from background. Stimulation produced a mean ~10-fold increase in splenic and 100-fold increase in peritoneal anti-tumor memory T-cell clonotypes. This methodology can be developed to use blood and tissue sampling to rapidly quantify the effectiveness of a tumor vaccine or any vaccine generating therapeutic T-cells.

KEYWORDS

memory T cells, T-cell receptor clonotypes, immune repertoire analysis, tumor vaccination, clonotype analysis

Introduction

Vaccination to generate antibody-mediated protection from infectious diseases has been a spectacularly successful, inexpensive, public health measure, rivaled in effectiveness only by cleanliness of water and society. T-cells, the alternative effector of the adaptive immune system, have not been harnessed to prevent human disease. The only possible exception may be BCG vaccination which, in some populations, has reduced the incidence of severe tuberculosis (1). One reason for this failure is the lack of a simple, reliable and valid measure of T-cell memory (2). EliSpot is widely used but long incubations with

multiple cell types and biologic reagents make it a complex procedure that is difficult to standardize. Validation of high EliSpot response with clinical effectiveness has not been consistently shown. Tetramer analysis, once the tetramer is compounded, is simple and reliable but not available for almost any CD4 antigens and only a small number of CD8 antigens. The lack of a quantifiable memory T-cell response prevents incremental progress in vaccine development because the only outcome measure is clinical success or failure. The goal of this project was to use recent developments in next generation sequencing (NGS) and TCR clonal analysis to develop a simple, easily standardized measure of anti-tumor CD4 and CD8 memory T-cell response.

Materials and methods

Cells, antibodies, chemicals and animals

D2F2/E2 cells, a mouse mammary tumor line that has been stably transfected with a vector expressing the human HER2/neu gene and its parent cell line, D2F2 were a generous gift from Dr. Wei-Zen Wei, (Karmanos Cancer Institute, Wayne State University, Detroit, MI USA). Early passage cells were frozen and periodically thawed for experimental use or restocking. Mycoplasma testing was negative using the Impact III PCR profile from IDEXX (RADIL, Columbia, MO, USA). Anti-CTLA4 monoclonal antibody (mAb 9H10) was obtained commercially (BioXcell Fermentation/Purification Services #BE0131, West Lebanon, NH, USA) as was cyclophosphamide (Bristol-Myers Squibb Co., Princeton, NJ, USA). Mice were 8 to 20 weeks of age and weighed 20-25 g. Thy 1.2 BALB/c were obtained from Taconic (Hudson, NY). Animal studies were approved by the University of Pittsburgh institutional Animal Care and Use Committee (IACUC Protocol #: 21028761).

Replicating recombinant vesicular stomatitis virus (rrVSV)

A replicating virus expressing the following properties was created from vector components as previously described (3): Preferential infection of cells expressing human HER2/neu, expression of mouse granulocyte-macrophage colony-stimulating factor, and expression of enhanced green fluorescent protein. Construction used vectors generously supplied by Dr. John K. Rose (Department of Pathology, Yale University, New Haven, CT, USA) and Genentech Inc., South San Francisco, CA, USA).

Tumor implants and treatment

Female BALB/c mice weighing 20-25g and aged 8-20 weeks were implanted intraperitoneally (IP) with 2 x 10^6 D2F2/E2 cells in 300 µl PBS. Viral immune-oncotherapy consisted of treatment on day 3 after peritoneal implant with IP rrVSV, 1 x 10^8 ID, on day 4 with 200 µg anti-CTLA4 mAb IP and on day 5 with cyclophosphamide (CTX), ~100 mg/kg IP. Cure was defined by survival without any symptoms of disease for >100 days after tumor cell implantation. Control mice received the same viral immune-oncotherapy but were never implanted with tumor.

Memory T-cells

Memory T-cells were obtained from spleens, peritoneal cells or blood of cured animals and controls. Animals were sacrificed prior to spleen cell harvesting. Spleens were harvested, minced and ground through a 70 µM nylon cell strainer (#352350, BD Falcon, Franklin Lakes, NJ). Red blood cells were removed using RBC lysis buffer (Alfa Aesar, J62150AP). Peritoneal washings were performed by injecting 10 ml of sterile PBS into the peritoneum through a 16-gauge needle which was left in place. Two minutes later all the fluid that could be aspirated easily into the syringe was collected, ~ 9 ml. All cells were washed twice with PBS and re-suspended in PBS. Peripheral blood was collected by submandibular punch and dripping the blood into a heparinized tube. Mononuclear cells were separated using Lymphocytes Separation Medium. CD4 and CD8 T-cells were isolated by flow cytometry (see below).

Adoptive therapy and tumor challenge

Peritoneal tumors were established in host animals and treated 3 days later by adoptive transfer of splenocytes from cured animals. As previously described, host animals were pre-treated with cyclophosphamide one day before transfer of memory cells (4). Tumor challenge to cured or control mice was achieved by injecting 2 x 10^6 D2F2/E2 cells IP.

Flow cytometry

Peritoneal cells were suspended in ice-cold PBS/0.1% BSA/0.2% Azide and stained with combinations of the following antibodies: CD4- APC-eFluor 780 (eBioscience 47-0041-82), CD8a- PE-Cyanine7 (eBioscience 25-0081-82), CD90.2-PE (BD 553006), Live-Dead fixable red Kit (Life Science, NC0836452) and H-2K (d)/TYLPTNASL, human HER2 p63 tetramer conjugated with APC (NIH Tetramer Core Facility at Emory University). Immunofluorescence was quantified using a LSR Fortesa (Becton Dickinson, Mountainview, CA, USA) and cell sorting was performed using a FACSAria II machine (Becton Dickinson) (5).

RNA extraction

RNA extraction was completed using Qiagen's RNeasy Plus Micro kit (Qiagen:74034), according to the manufacturer's instructions with DNA elimination columns. Briefly, cells were pelleted in a centrifuge at 4°C for 8 minutes at 800xg, then lysed in RLT buffer with beta- mercaptoethanol. RNA was eluted with 22 µl of RNase/DNase free H_20. RNA quality was assessed using an

Agilent HS RNA ScreenTape (Agilent: 5067-5579) on an Agilent 2200 TapeStation. RNA concentration was quantified with a Qubit HS RNA assay kit (Invitrogen: Q32855) on a Qubit 4 (Invitrogen: Q33238).

TCR-seq library generation

Libraries were generated with the Takara SMARTer Mouse TCR a/b profiling kit (Takara: 634403) according to the manufacturer's instructions. Twenty-one cycles were used for PCR1, after which 1 µl of product was used for indexing PCR2 with 19 cycles. Samples with RNA concentrations ≤ 1.0 ng/µl RNA used 22 cycles for PCR1, after which 2 µl of product was used for indexing PCR2 with 19 cycles. Library assessment and quantification was done using Qubit 1x HS DNA assay kit (Invitrogen: Q33231) on a Qubit 4 fluorometer, and a HS NGS Fragment kit (Agilent: DNF-474-1000) on an Agilent 5300 Fragment Analyzer. Libraries were normalized and pooled by calculating the nM concentration based off the fragment size (base pairs) and the concentration (ng/µl) of the libraries.

TCR-seq library sequencing

Sequencing was performed on an Illumina MiSeq using a MiSeq 600 v3 flow cell (Illumina: MS-102-3003). The pooled library was loaded at 13.5nM with 10% PhiX, generating 2x300 bp paired-end reads. Library generation and sequencing was performed by the University of Pittsburgh Health Sciences Sequencing Core (HSSC), Rangos Research Center, UPMC Children's Hospital of Pittsburgh, Pittsburgh, Pennsylvania, United States of America.

TCR repertoire analysis

MiXCR (platform 3.0.13; MiLaboratories Inc, Sunnyvale, CA, USA) was used to align and assemble the raw paired-end Fastq files sequencing reads and assemble identical and homologous reads into clonotypes, correcting for PCR and sequencing errors. The program provided detailed information for each clone, including fractions, counts, nucleotide sequence, and amino acid sequence, as well as alignments for multiple samples, repertoire overlap analysis, diversity estimation and segment usage (6). Mouse NKT TRA clonotypes, identified by the canonical CDR3 sequence, CVVGDRGSALGRLHF, were excluded from analysis (7, 8) as were mouse MAIT TRA clonotypes, identified by the canonical CDR3 sequence, CAVRDSNYQLIW (9). This methodology does not exclude TRB clonotypes associate with NKT or MAIT cells but the NKT TRA clonotype was never found at high frequency in peritoneal cells following tumor stimulation indicating that the high frequency response did not contain any NKT cells. Mouse MAIT TRA clonotypes were never found at high frequency in any sample suggesting that these cells were not a confounder in this work. Finally, results for TRA clonotypes, which have definitely excluded NKT and MAIT cells are provided for all analysis and do not change any of the conclusions.

Statistics

GraphPad Prism version 7.0 (GraphPad Software, Inc., San Diego, CA, USA) was used for presentation and statistical analysis of the data.

Results

Tumor challenge in cured mice stimulates a large oligoclonal CD4 and CD8 memory T-cell response in spleen cells

Viral immuno-oncotherapy consisting of a replicating recombinant VSV (rrVSV) targeted to Her2, and single doses of anti-CTLA4 Mab and cyclophosphamide cures 3 day implanted Her2+ peritoneal tumors in Balb/c mice. Cure is immunologically dependent, requires both CD4 and CD8 T-cells and generates memory T-cells by 90 days after treatment (5, 10, 11). The anti-tumor memory response was assessed by re-challenging tumor-cured mice with IP administration of tumor cells. TCR clonal analysis, TCRα (TRA) and TCRβ (TRB), was performed on spleen cells harvested 5 days after challenge. A control group consisted of animals who received targeted rrVSV oncolytic immunotherapy, at least 100 days prior to challenge but were never implanted with tumor (virus control mice). All animals in the tumor- cured group showed an oligoclonal set of high-responding splenic TCR clones for CD4 and CD8 T-cells that was not observed in the control group (Figures 1–3). The mean clone fractions of the top 3 clones was 5-fold higher for CD4 T-cells and 8-10 fold higher in CD8 T-cells in tumor-cured mice compared with virus control mice (Figure 3). The high responder response to challenge varied among the cured animals but was uniformly low among the control animals (Figure 2). At least one high frequency clone was higher than the highest control value in 5/5 mice (100%) for CD8 T-cells and 4/5 mice (80%) for CD4 T-cells (Figure 2). This highest frequency oligoclonal response in spleen varied from 2-18 CD8 and 0-5 CD4 T-cell anti-tumor TRA or TRB clonotypes per animal (median CD8 = 2.5 and CD4 = 1.5).

The oligoclonal high-responder spleen response to tumor challenge reflects the peritoneal anti-tumor response and is distinct for each animal

Our previous work in this model system has shown that anti-tumor memory CD4 and CD8 T-cells accumulate in the peritoneum following IP tumor challenge in tumor-cured mice (5, 11). In this study, the peritoneal cell response to tumor challenge in experimental and control groups is displayed in Supplemental Figure S1. The specific migration of anti-tumor memory T-cells to the peritoneum following stimulation was

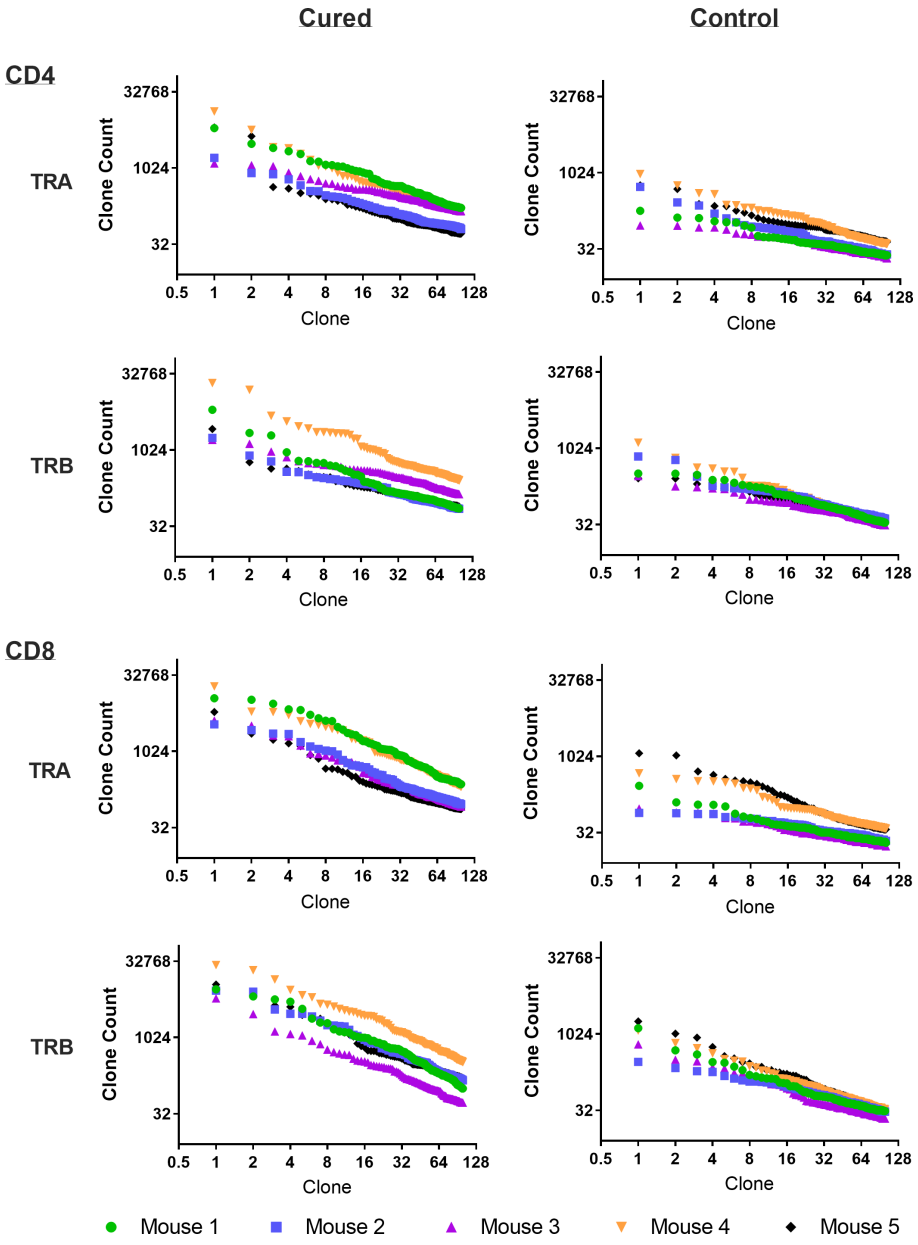

FIGURE 1
Frequency analysis of tumor-challenged spleen T-cells. Intraperitoneal tumor challenge in mice who had received rrVSV oncolytic immunotherapy to cure implanted tumor (tumor-cured mice) compared to mice with full viral therapy but no tumor implant (virus control mice). Splenic CD4 and CD8 T-cells were harvested 5 days after challenge and TCR clones quantified. The top 100 clones are plotted and results shown separately for CD4 and CD8 T-cells and TCR-α (TRA) and TCR-β (TRB) receptors (Log2 scale for X and Y axes).

supported by the absence of high frequency peritoneal NKT cells, which could easily be identified by an invariant clonotype and were abundant in the spleens of experimental and control animals (12). Clonal overlap was determined between the spleen and peritoneal response in the same animals to show that the anti-tumor response seen in the peritoneum was reflected in the spleen, providing evidence that the spleen response was an anti-tumor response (Table 1). In total, 70% of high-responding T-cells in the peritoneum were also high-responders in the spleen (62.5% of the CD4 and 82% of the CD8 T-cells). Each animal with a high-responding clonotype in the peritoneum had at least one identical high-responding clonotype in the spleen. The spleen response was therefore an excellent surrogate for the peritoneal response.

Clonal overlap was also determined between the peritoneal cell response among the different animals (Figure 4). These results show that none of the highest-responder clonotypes in one animal were also high-responders in a different animal. As illustrated in Figure 4, some of the high-responder clonotypes were found in other animals but only at low frequency. Basically, each animal had a private set of high-frequency tumor-responding CD4 and CD8 TCR clonotypes.

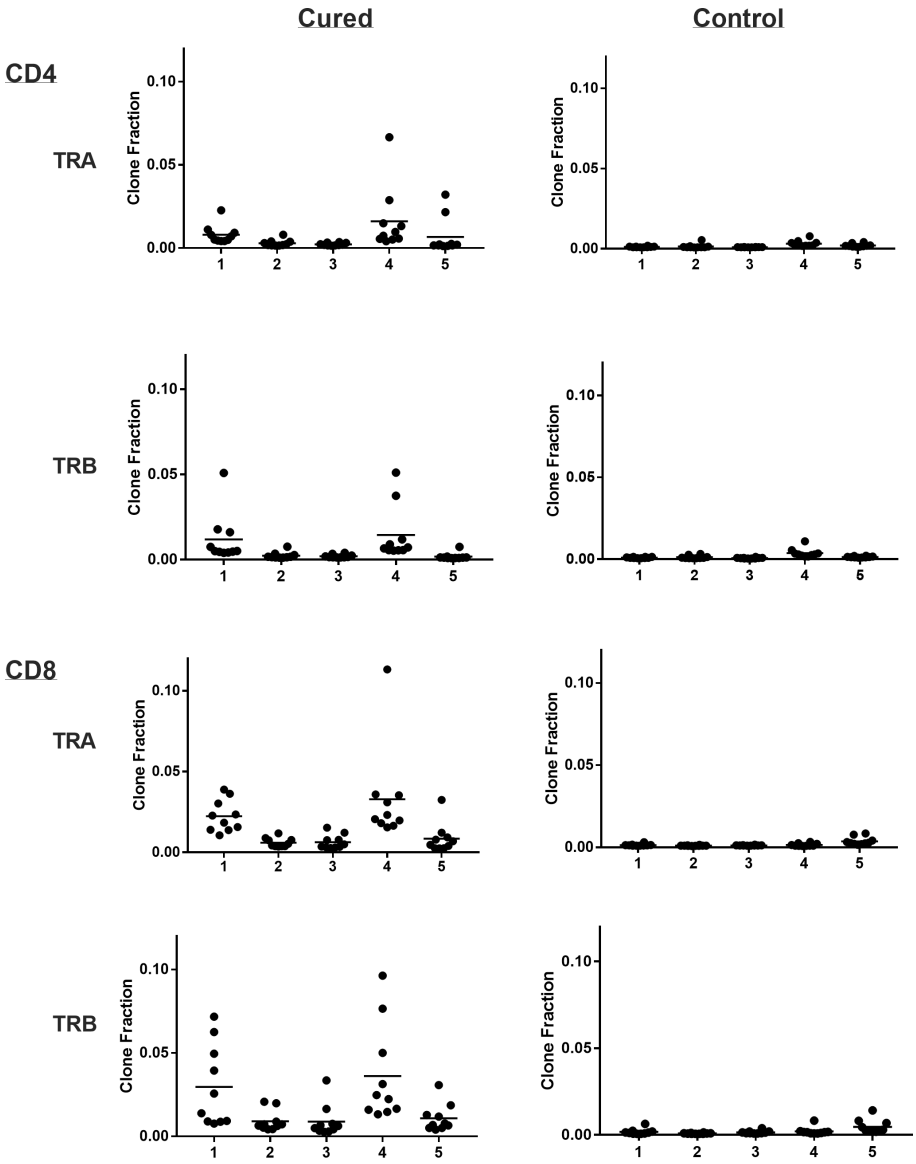

FIGURE 2
Clone frequency following challenge in spleens of tumor-cured mice compared with virus control mice. Scatter plot of the top 10 clones. Results are shown separately for CD4 and CD8 T-cells; TRA and TRB. Each number represents a single cured or control mouse.

Tetramer analysis demonstrates that high responder peritoneal CD8 T-cells were anti-tumor memory T-cells and had distinct clonotypes for each animal

Tumor-cured mice (n=4) received peritoneal tumor challenge followed 5 days later by isolation of CD8 T-cells from peritoneal lavage. Each sample was divided in half. One half from each animal had flow cytometry tetramer analysis and TCR clonotyping performed individually for each animal. The other individual samples were combined and tetramer+ CD8 T-cells were identified and separated by flow cytometry. Flow cytometry tetramer analysis and TCR clonotyping was then performed on this mixed sample from 4 mice (Figure 5). A combined sample of tetramer+ CD8 T-cells was required to assure an adequate concentration of mRNA for TCR clonotyping analysis. Purity of the tetramer+ mixture was 86.9% and the delineation between tetramer-positive and tetramer-negative cells with flow cytometry was not absolute (Figure 5B), leading to false positive clonotypes in the tetramer+ mixture. True positives were determined by using all high-frequency clonotypes (>1%) in the individual animals as index cases, determining the frequencies of the identical clonotypes in the tetramer+ mix and plotting the inverse ratio (Supplemental Figure S2). High ratios were easily separated from low ratios and had similar patterns in TRA and TRB for each animal. Clonotypes with ratios 0.18 were considered true positives.

Analysis of the 3 highest clonotypes in each animal showed that 5/12 TRB clonotypes and 3/12 TRA clonotypes were tetramer+ (Figure 6). None of these 8 highest frequency responding tetramer+ clonotypes had the same TCR peptide sequence and, in fact each of the 24 highest frequency responding clonotypes had a unique sequence

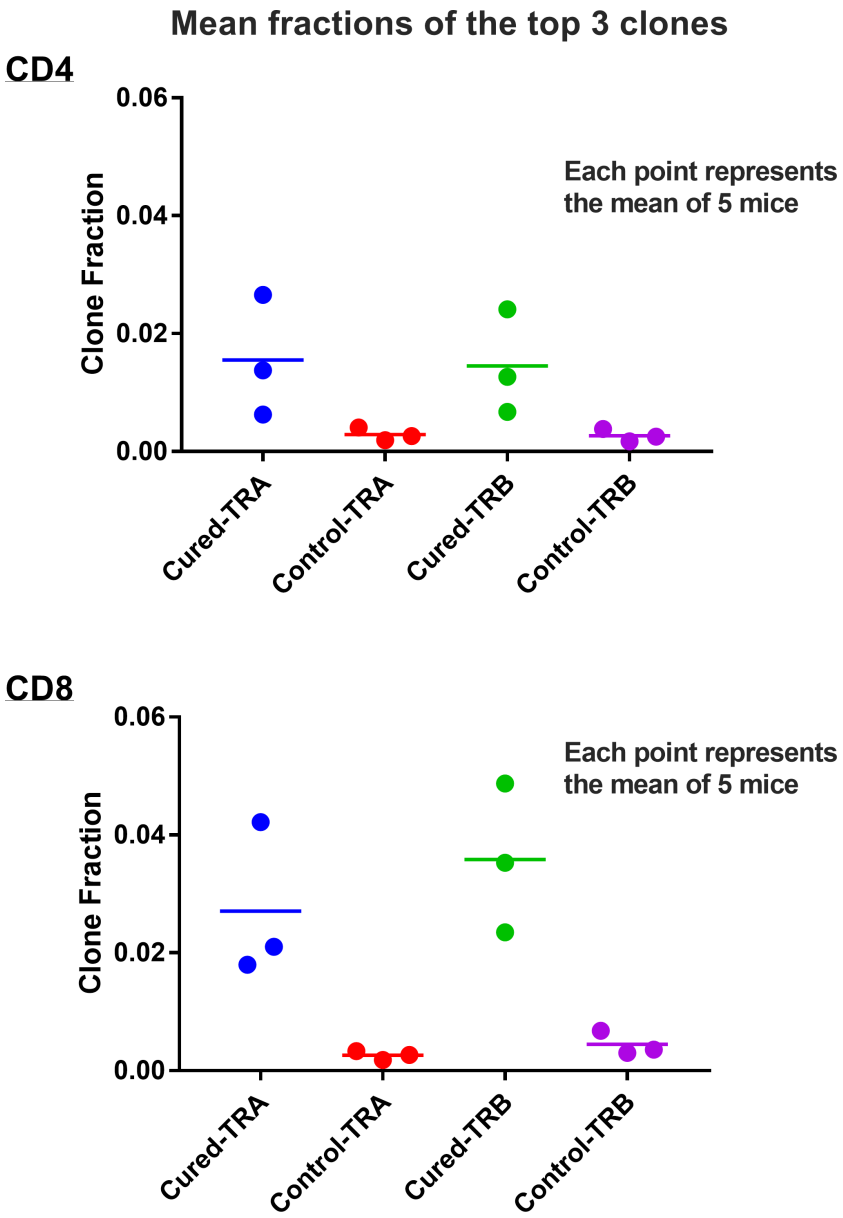

FIGURE 3
Mean fractions of the responding clones in spleens of tumor-cured mice compared with virus control mice. Scatter plot of the top 3 clones. Results are shown separately for CD4 and CD8 T-cells and TRA and TRB receptors. The mean fractions of the top 3 clones were 5.4-fold higher for CD4 T-cells and 8-10 fold higher in CD8 T-cells in tumor-cured mice compared with virus control mice (all difference were significantly different; p=0.05 and 0.04 for TRA and TRB CD4 T-cells, and p= 0.0164 and 0.0066 for TRA and TRB CD8 T-cells; unpaired, one-tailed t test; n=5 for each group).

TABLE 1 Comparison of high-responding clones in the spleen and peritoneum of the same animal.

Number of high responding peritoneal clones and number of identical clones in spleen*		
	PC	Spleen
CD4	16	11
CD8	11	9

*n=5 animals except for peritoneal CD8 T-cells which were inadequate for testing on one animal. Clonotypes were considered high-responders when their frequency was greater than the mean of the top 2 clones, of the same T-cell category, in the virus-control group.

(13). An analysis of all tetramer+ clonotypes found 11 TRB clonotypes and 12 TRA clonotypes with frequency > 1% (Figure 7). The number of these tetramer+ clonotypes per mouse varied from 2 to 4 (median = 3) and each clonotype was unique (Figure 7). The same clonotype was sometimes found in other animals (5 TRA and 5 TRB) but never at frequency >0.15% and usually much lower (Figure 7). In summary, each animal had its own private high-frequency tetramer+ sequence and some had more than one. An unexpected finding was that tetramer + frequency based on TRB clonotype frequency closely matched clone frequency results based on flow cytometry (Figure 7). TRA frequency was not as closely matched probably because ~30% of T-cells express 2 functionally rearranged TRA mRNAs (14, 15).

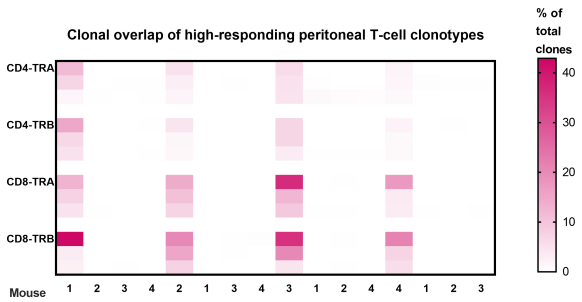

FIGURE 4
Clonal overlap of high-responding peritoneal T-cell clonotypes. The top 3 responding clonotypes in each animal were the index clones for heatmap comparison with each of the other animals. There is no overlap of high-frequency T-cell clonotypes in peritoneal cells from different animals. Clonotypes were considered peritoneal high-responders when their frequency was greater than the mean of the top 2 clones in the virus-control group. (Scale is % of total clones; n=4; a 5th animal was excluded because collection of peritoneal CD8 T-cells was inadequate for analysis.).

Transfer experiments demonstrate that high responder splenic CD4 and CD8 T-cells were anti-tumor memory T-cells

The CD4 and CD8 TCR clonotype response in spleen and peritoneum to IP tumor challenge was compared in donor animals cured of implanted tumor by rrVSV oncolytic immunotherapy and host animals cured by T-cell transfer from the donor animals (Figure 8). The critical finding was that the same high-responding TCR clonotypes were found in all 4 samples (Figure 9 for TRB and Supplemental Figure S3 for TRA), strongly suggesting that they represented anti-tumor memory clones. The high responder peritoneal CD4 and CD8 T-cells in the host animals were derived from the donor mice because they had matching clonotypes. Independent clones arising from the hosts would have had their own private sequences as shown in the previous sections. These were the therapeutic T-cells because cure was obtained solely by transfer of donor spleen cells. These cells were first recognized by IP challenge in the donor mice demonstrating that a high clonotype response to challenge is a reliable method to identify anti-tumor CD4 and CD8 T-

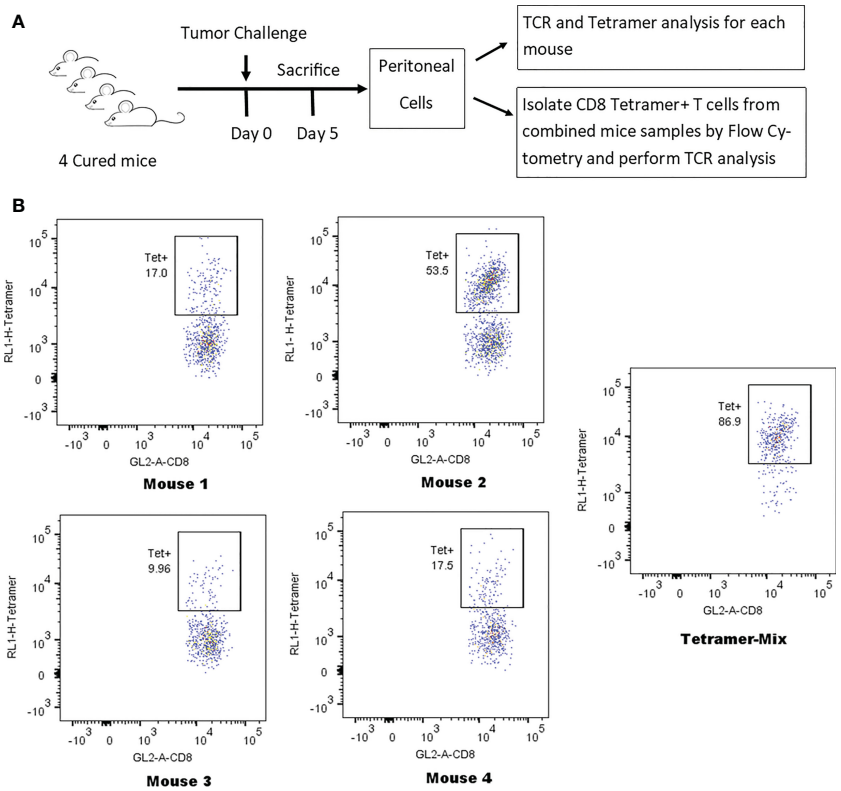

FIGURE 5
Identification of tetramer+ clonotypes within the total CD8 T-cell population. **(A)** Illustration of experiment identifying TCR clones of tetramer+ CD8 T-cells. **(B)** Anti-tumor memory CD8 T-cells identified by flow cytometry following staining with the human HER2 p63 tetramer conjugated with APC. The percent tetramer-positive cells is noted for the peritoneal cells of each individual mouse and for the tetramer-positive mix from all 4 mice.

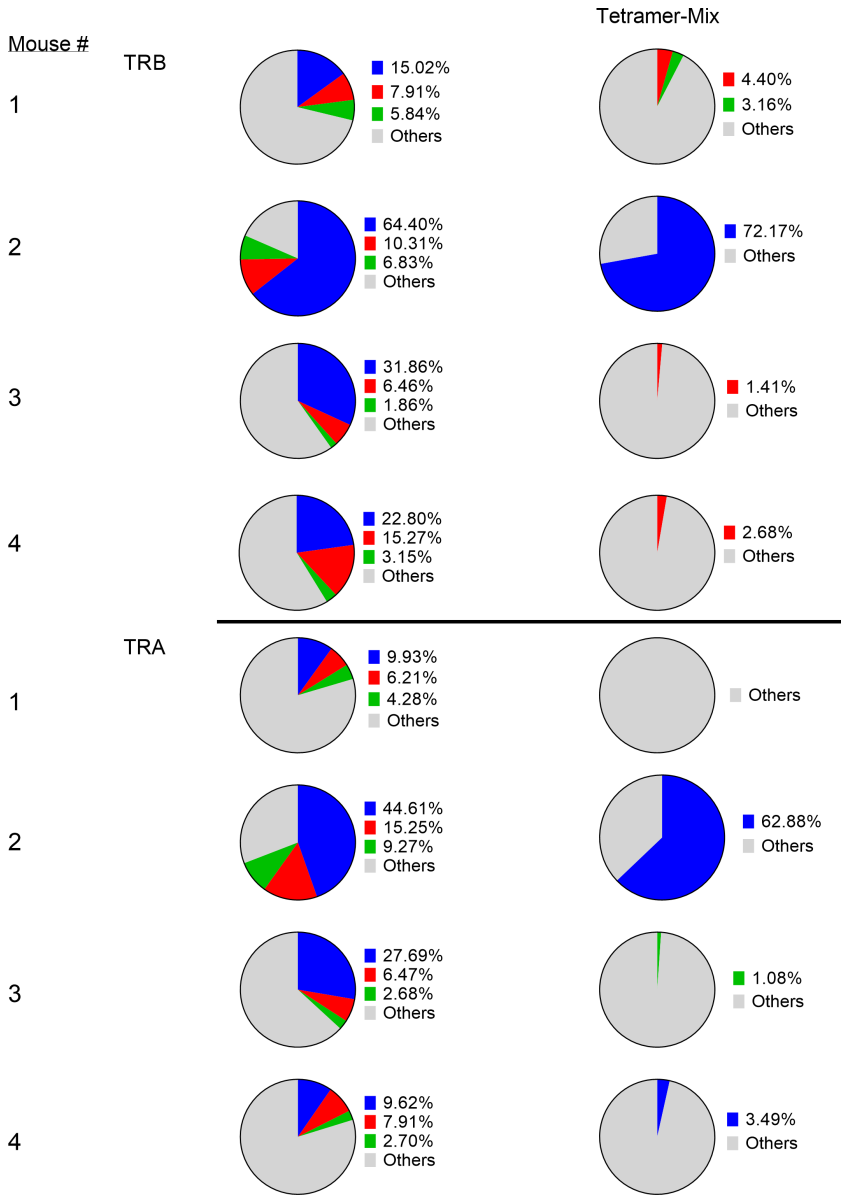

FIGURE 6
Identification of tetramer^{+} clonotypes within the total CD8 T-cell population. The left column displays the top 3 CD8 T-cell clonotypes in peritoneum in 4 cured animals challenged with IP tumor cells. The right column displays matching TCR clonotypes in the tetramer+ mix from the 4 animals. The blue, red and green colors represent the top 3 clones in each animal and are unique high-frequency clonotypes in each animal.

cell clones. Peritoneal clonotypes were classified as definite, active anti-tumor memory if they appeared in both donor and host peritoneal cells at a frequency greater than the mean of the top 10 clonotypes from all control animals (Figure 9). The number of unique high-frequency anti-tumor memory TRB clonotypes in the peritoneum varied from 1 to 8 in CD4 and 4-8 in CD8 T-cells with a median of 4 CD4 T-cells and 6 CD8 T-cells. Donor spleen and host peritoneal clonotypes were also classified as definite, active anti-tumor memory if they appeared in both host PC and donor spleen at a frequency greater than the mean of the top 10 clonotypes from all control animals (Figure 9). The number of high-frequency unique anti-tumor memory TRB clonotypes in the donor spleen varied from 1 to 8 for CD4 and 5-7 for CD8 T-cells with a median of 3 CD4 T-cells and 6 CD8 T-cells. The frequency of anti-tumor CD4 TRB clonotypes was 12.7-fold higher in host peritoneum than host spleen and 7.9-fold higher for CD8 TRB clonotypes, confirming our previous work, that anti-tumor memory CD4 and CD8 T-cells migrate to and expand at the site of challenge in tumor-cured mice (5, 11). TRB clonotypes were used in these analyses because their frequency had the best correspondence with clone frequency, as determined above. Importantly, the anti-tumor memory clonotypes were also found in blood, at similar frequencies to spleen, indicating that these analyses may be practical clinically (Figure 9 and Supplemental Figure S3).

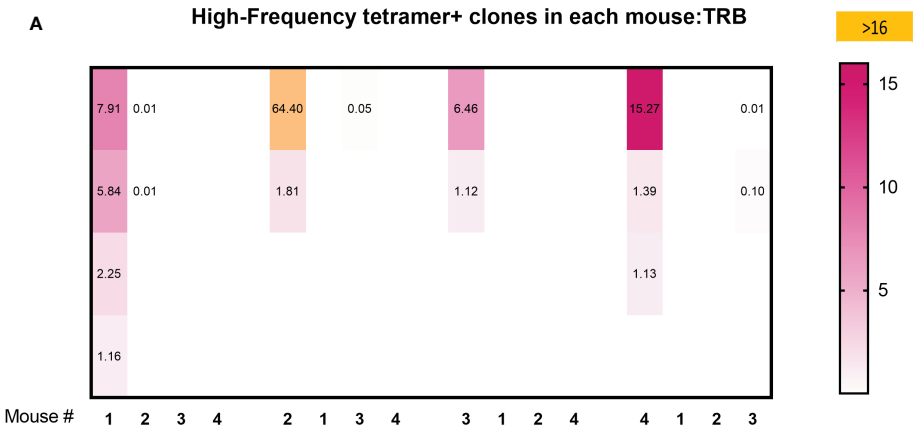

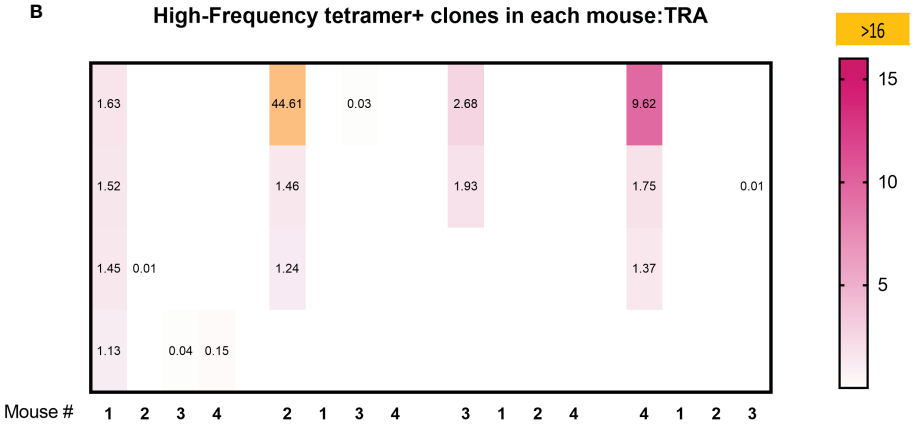

C.

tetramer+(%)				
Flow Cytometry	17	53.5	9.96	17.5
TRB	17.15	66.21	7.58	17.79
TRA	5.73	47.31	4.61	12.74

FIGURE 7
Clonal overlap of high frequency tetramer+ CD8 T-cells clonotypes among 4 animals. Tetramer+ CD8 T-cells from each mouse (the first column in each set) was heatmap compared with the top 20 responding clonotypes in each of the other mice. **(A)** TRB clonotypes. **(B)** TRA clonotypes. **(C)** A comparison of the percentage of high frequency tetramer+ CD8 T-cells identified by fluorescence activated cell sorting (FACS) and by TRB or TRA clonotype analyis.

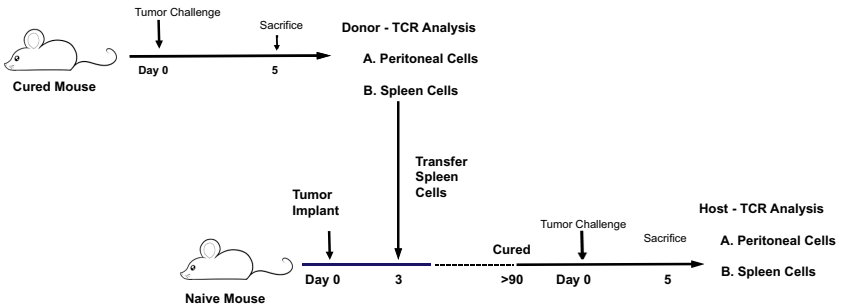

FIGURE 8
Illustration of experiment comparing the CD4 and CD8 TCR clonotype response to IP tumor challenge in donor animals cured of implanted tumor by rrVSV oncolytic immunotherapy and host animals cured by T-cell transfer from the donor animals.

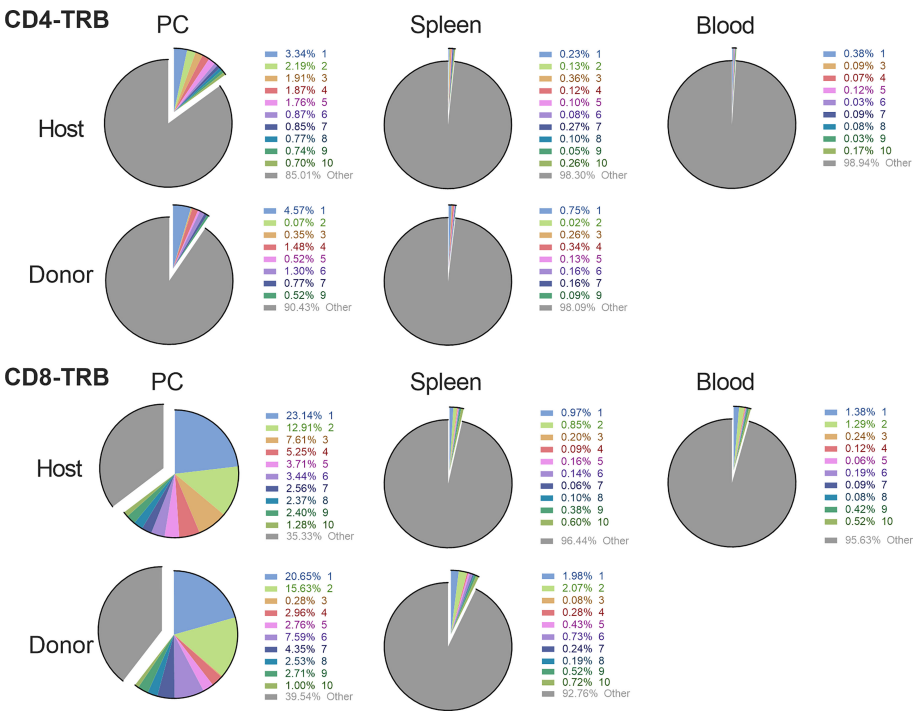

FIGURE 9
Comparison of the high frequency clonotypes following challenge in donor animals cured of implanted tumor by rrVSV oncolytic immunotherapy and host animals cured by T-cell transfer from the donor animals. Graphs show CD4 and CD8 T-cell TRB data from one representative pair of animals of three total pairs. The top 10 most frequent clones in the host peritoneal cells are the index clones and are compared with the donor peritoneal and spleen cells and the host spleen and blood cells. Identical numbers and colors within the CD4 and CD8 sets refer to identical clonotypes.

The mean resting frequency of anti-tumor memory T-cells in spleen is 0.028% for CD4 T-cells and 0.11% for CD8 T-cells

The resting frequency of anti-tumor memory T-cells was determined by harvesting spleen cells from cured, unchallenged, resting, donor mice and assaying TCR clonotypes from one aliquot of 1 x 10^7 cells. A second aliquot of 5 x 10^7 spleen cells were challenged by transfer to a host animal with a 3 day implanted peritoneal tumor. Host spleen and peritoneal TCR clonotypes were assayed 5 days later (Figure 10). Clonotypes in the resting donor cured tumor mice that were identical to high frequency clonotypes in the peritoneum of challenged mice were anti-tumor memory clonotypes. Independent clones arising from the hosts would have had their own private sequences as shown in the previous sections. In addition, only memory cells from the donors and not naïve cells from the hosts, could be present at sufficient concentration and multiply rapidly enough in 5 days to produce the high frequency clones found in the peritoneum. Challenge of naïve animals with peritoneal tumor cells produced only low clonotype frequencies at 5 days (data not

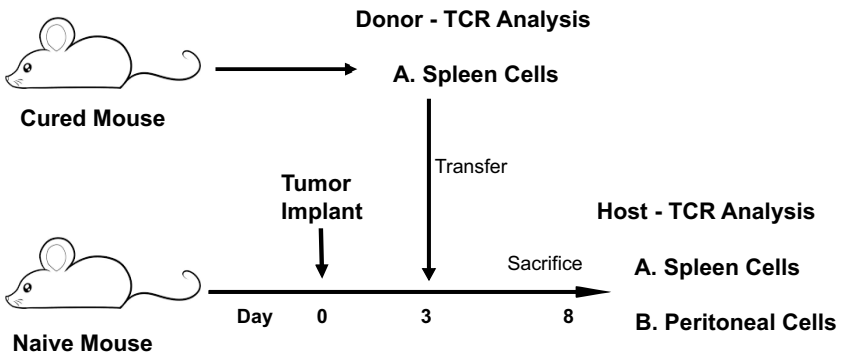

FIGURE 10
Identifying and determining the frequency of resting and challenged anti-tumor memory T-cells. Illustration of experiment comparing a TCR frequency analysis of memory anti-tumor T-cells in resting spleens of donor mice with challenged spleen and peritoneal T-cells of host mice.

shown). Finally, our current and previous work has shown that spleens from donor mice cured of tumor by rrVSV oncolytic immunotherapy contain potent therapeutic anti-tumor memory T-cells (4, 5, 10, 11, 16, 17). Using the top 5 peritoneal clonotypes as index clonotypess, all CD4 and CD8 T-cell TRB clonotypes had identical clones in the donor unchallenged mice, although 2 CD4 clonotypes from one animal had notably lower resting frequencies than all the others (Figure 11 for TRB and Supplemental Figure S4 for TRA). The mean frequency of these anti-tumor memory T-cells in resting T-cells averaged 0.028% for CD4 T-cells and 0.11% for CD8 T-cells (Figure 12). The highest frequency clone for CD4 T-cells was 0.15% and for CD8 T-cells was 0.34%. These findings match well with tetramer-based studies of anti-viral human memory CD4 and CD8 T-cells and mouse CD4 T-cells but are 30-fold lower than several previous reports of mouse anti-viral memory CD8 T-cells. All studies agree that resting memory CD8 T-cells form a higher fraction of total CD8 T-cells than resting memory CD4 T-cells form of total CD4 T-cells (13, 18–24). TRA data was similar (Supplemental Figure S4) but we focused on TRB clonotypes as the best surrogate for TCR clones for several reasons: T-cells almost invariable express a single TRB mRNA but ~1/3 express 2 TRA mRNA (14, 15); the main contribution to TCR-peptide binding comes from the TRB CD3 sequence (25); and data presented above showed a close correspondence between TRB clonotype frequency and cell clonal frequency.

Resting donor spleen TRB clonotypes had ~ 1/10 the frequency of challenged memory clonotypes in spleen and ~1/100 the frequency of challenged memory clonotypes in the peritoneum (Figure 12 for TRB and Supplemental Figure S5 for TRA). CD4 T-cells increased from 0.028% to 0.26% to 2.44% and CD8 T-cells

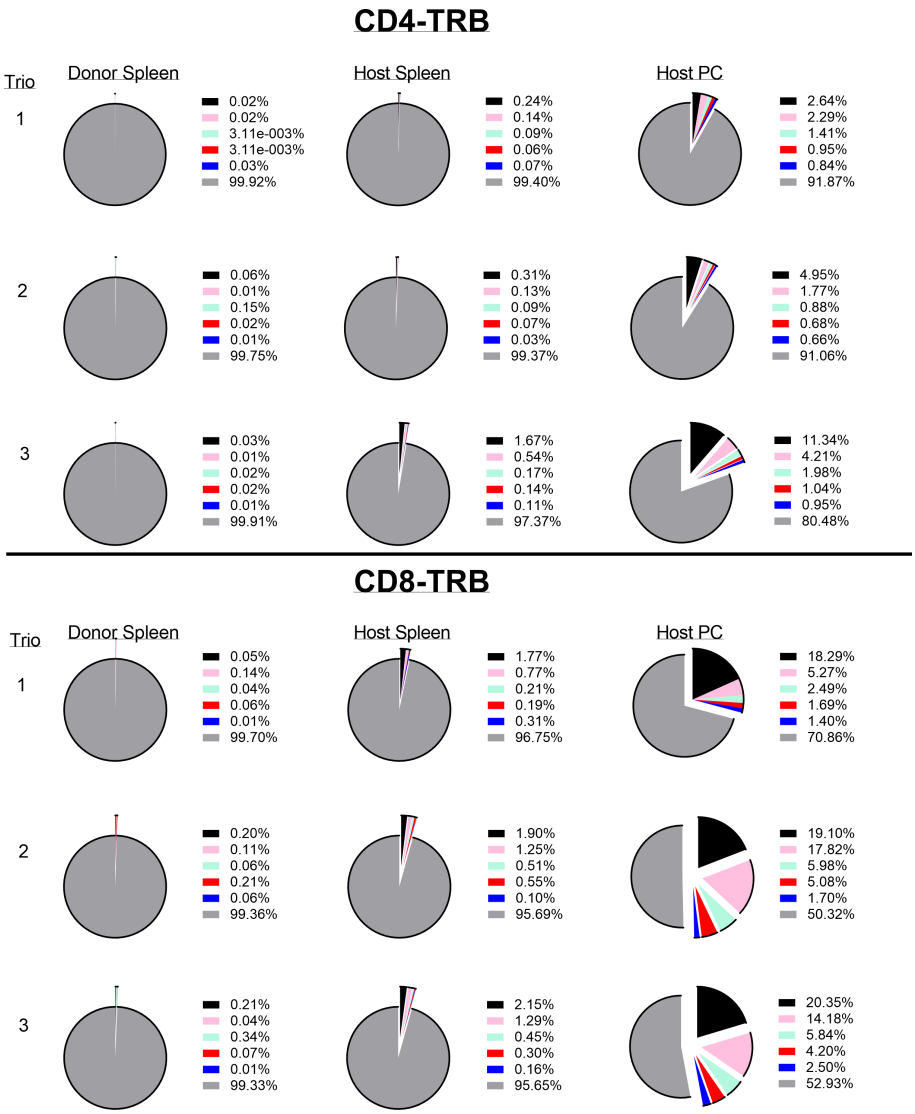

FIGURE 11
Identifying and determining the frequency of resting and challenged anti-tumor memory T-cells. The top 5 most frequent clones in the host challenged peritoneal T-cells are the index clones and are compared with the frequency of the same clones in the spleens of challenged host and unchallenged donor mice. Three trios of animals are shown in separate rows with the CD4 T-cells in the top half and the CD8 T-cells in the bottom half of the figure (TRB only). Identical numbers and colors within the CD4 and CD8 pairs refer to identical clonotypes.

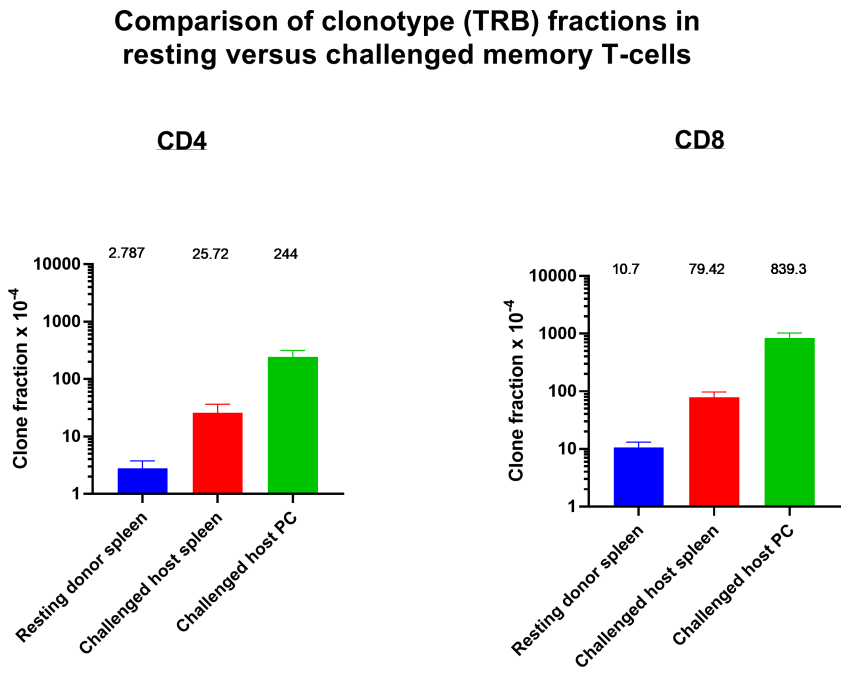

FIGURE 12
Identifying and determining the frequency of resting and challenged anti-tumor memory T-cells. The frequency of the top 5 anti-tumor memory T-cells in the peritoneum of host challenged mice are compared with the frequency of the same clones in the spleen of host challenged mice and the spleen of resting donor mice. (n=3 in each group, CD4 and CD8, TRB only); mean values and SEM bars above the column for each group).

increased from 0.11% to 0.79% to 8.39%. The mean increase in TRB clonotype count from transferred donor T-cells to combined harvested spleen and peritoneal T-cells was 65-fold for both CD4 and CD8 memory T-cells (Figure 13 for TRB and Supplemental Figure S6 for TRA). This indicated a minimum mean number of 6 doublings in 5 days because potential anti-tumor T-cells in other tissues such as lymph nodes, bone marrow and blood were not harvested. Doublings in individual clones varied from 2 to 8 (Figure 13).

Frequency analysis of resting T-cells does not distinguish anti-tumor memory T-cells from background (Figure 14 for TRB and Supplemental Figure S7 for TRA). The top 5 most frequent CD4 and CD8 TRA clonotypes from 3 animals are highlighted by large bold red, green or black diamonds within the frequency distribution of all resting spleen cells from the same animal. A stimulation is required to identify and quantify anti-tumor memory T-cells (Figures 1, 6, 9, 11). In this sample size of 30, potential resting anti-tumor memory T-cell clones, 28 were found within the top 625 clones. As expected, following initial expansion, these resting memory cells did not diminish to rare frequency but neither did they stand out from the mixed background of resting frequencies.

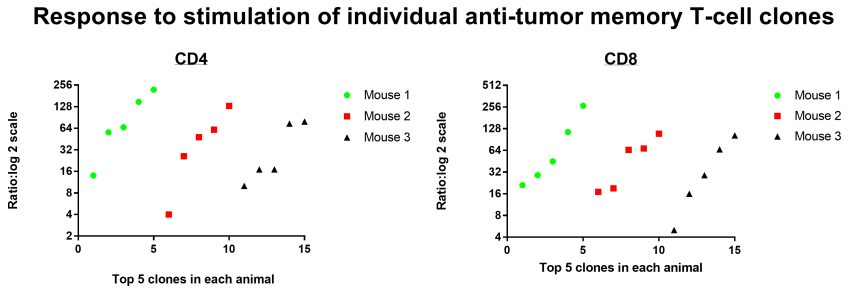

FIGURE 13
Response to stimulation of individual anti-tumor memory T-cell clones. The total number of memory T-cells in transferred donor spleen cells were compared with total number of stimulated host memory T-cells harvested from spleen and peritoneum. The top 5 most frequent CD4 and CD8 memory T-cell clones for each of 3 animals are plotted separately (TRB clonotypes). The mean increase in clone count was 65-fold for both CD4 and CD8 T-cells.

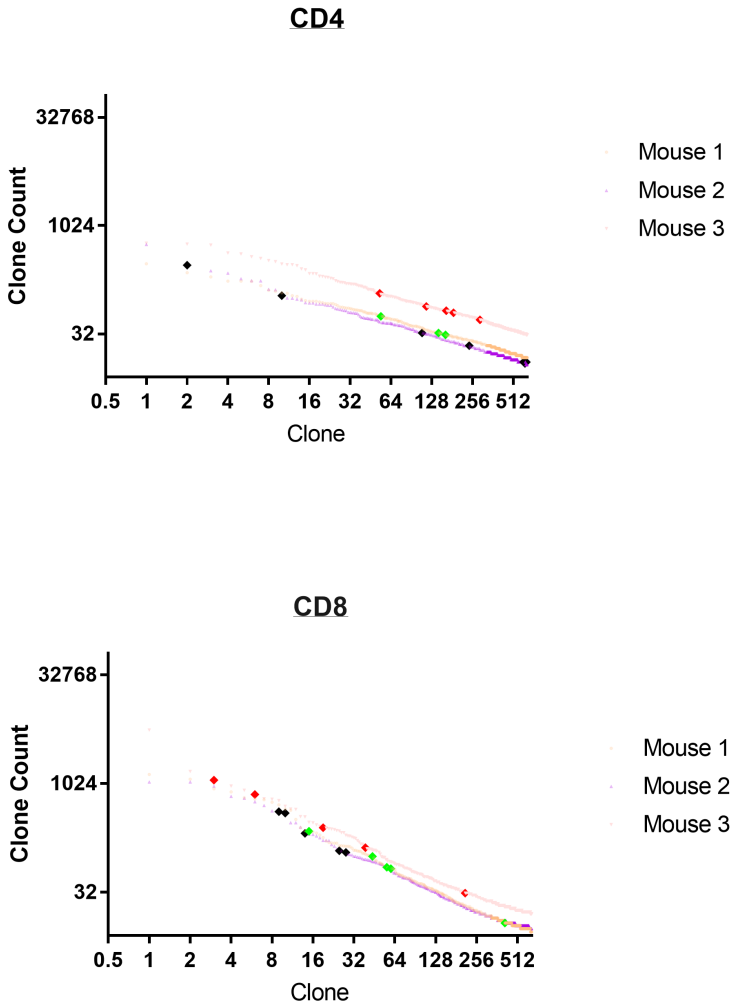

FIGURE 14
Frequency distribution of resting anti-tumor memory T-cells. The top 5 most frequent memory anti-tumor CD4 and CD8 TRB clonotypes from 3 animals are highlighted by large bold red, green or black diamonds within the frequency distribution of all resting spleen cells from the same animal.

Discussion

This study found that curative viral onco-immunotherapy generated an oligoclonal anti-tumor memory response that could be quantified by bulk TCR clonal analysis following antigen stimulation. Frequency analysis of resting T-cells cannot distinguish these anti-tumor memory T-cells from background but antigen stimulation increases their frequency 10-fold, on average, in spleen and clearly identifies the most numerous of these cells. The high frequency T-cell clonotypes were higher than the highest control value for 100% of CD8 T-cells and 80% of CD4 T-cells showing that an effective anti-tumor response was identifiable in all animals. Multiple lines of evidence indicated that the high frequency clones were anti-tumor memory T-cells. First and most directly, one third of the high frequency CD8 T-cells were also identified by a known anti-tumor CD8 tetramer. Second, the high frequency spleen CD4 and CD8 T-cells were often identical to the peritoneal T-cells which have previously been shown to be anti-tumor memory T-cells. Third, transfer experiments showed that the same transferred clonotypes which cured tumors in host animals displayed high frequencies following stimulation in donor animals. Previous work with viruses and neoplasms, such as HIV and melanoma, has also used TCR clonotyping to track the anti-tumor and anti-virus T-cell response over time (26–31).

The total number of unique high-frequency anti-tumor memory clones can only be approximated from this data. Tetramer analysis, a direct measure of anti-tumor T-cells, found 2-4 (median = 3) peritoneal CD8 T-cell clones per animal. This is a minimum estimate because only a single antigen was interrogated. A second method, using a stringent standard that labeled as

memory anti-tumor only clonotypes that reached a higher frequency following stimulation than any control values, found that unique clonotypes varied from 0-18 CD8 and 0-5 CD4 T-cell TRA or TRB anti-tumor clonotypes per animal (median CD8 = 2.5 and CD4 = 1.5). This estimate is also certainly low because some tetramer positive CD8 T-cells did not meet this stringent criteria. Effective anti-tumor clones that have low initial resting frequency or those that are less responsive to tumor antigen presented in the format used in this model system might not reach the stringent threshold values. A third method analyzing donor memory cells that cured tumor in host animals classified peritoneal cells as definite, active anti-tumor memory if they appeared in high frequency following stimulation in both donor and host. The number of unique anti-tumor memory clonotypes in the peritoneum varied from 1 to 8 in CD4 and 4-8 in CD8 T-cells with a median of 4 CD4 T-cells and 6 CD8 T-cells. Donor spleen cells were classified as anti-tumor memory if they appeared in high frequency following stimulation in both donor spleen and host peritoneum. The number of high-frequency unique anti-tumor memory TRB clonotypes in the donor spleen varied from 1 to 8 for CD4 and 5-7 for CD8 T-cells with a median of 3 CD4 T-cells and 6 CD8 T-cells. Overall, it is clear that stimulation elicits a high-frequency oligoclonal anti-tumor response of at least 1 CD4 and 3 CD8 memory T-cell clones. Memory CD4 T-cells are certainly present and necessary for an effective anti-tumor response, as shown in our previous work (4, 5, 10). The results are not comprehensive because sampling was obtained at only 2 tissue sites, at only one time point and with predominantly indirect identification of anti-tumor memory T-cells. In this study, anti-tumor memory CD8 T-cells were more frequently identified than CD4 T-cells but lymph node or blood may be a better tissue to sample for these cells than spleen or peritoneum. A more direct methodology to identify unique anti-tumor memory clones is required for a more precise count. Single cell RNA sequence analysis can add breadth by identifying unique TRA/TRB combinations as well as multiple receptor and transcription markers but is currently much more expensive than bulk TCR analysis (32, 33).

The resting frequency of memory CD4 T-cells (mean = 0.028%) and CD8 T-cells (mean = 0.11%) was low but still usually within the top 625 clones in each animal, as expected for memory T-cells (34). Stimulation produced a minimum of 6 doublings in 5 days with doublings in individual clones varying from 2 to 8. These doubling rates in memory T-cells closely match previous work assessing anti-virus memory T-cells in mice (22, 35–37). This response rate provides an effective immune response to tumor cells, which grow much more slowly than microorganisms, as shown by the consistent ability of cured animals to resist tumor rechallenge and of transferred T-cells to cure established implanted tumors (4, 5, 10, 16).

Tetramer analysis and stimulation assays showed that the oligoclonal high-frequency anti-tumor memory T-cells consisted predominantly of private clonotypes unique to each animal (7, 13, 38, 39). This result is not surprising because, as our tetramer data shows, many different clonotypes, even within a single animal, can create a set of CD8 T-cells with the same antigen specificity (13, 40). The number of unique clonotypes in the naïve T-cell population is extremely large and clonotypes expressed on just a small number of T-cells can expand to generate effective, permanent memory T-cells (18, 34). Previous studies have shown that the human CMV and Influenza virus T-cell responses also involve mainly private TCR clones but some public clones or clones biased to particular variable-gene usage are found and might be used to identify an anti-viral response in a population (41–45). Our data in a mouse tumor model of limited sample size hints that it will be difficult to find a set of high-frequency clonotypes that can be used to identify anti-tumor memory T-cells in a population. However, private clonotypes, once identified in an individual, can be tracked over time and location, in that individual. This study shows that these anti-tumor clonotypes can be identified initially by a very high-frequency response to tumor antigen stimulation.

Tetramer analysis confirmed that clonotype frequency determined by T-cell receptor (TCR)-β (TRB) analysis closely approximated cell clone frequency determined by flow cytometry. Clonotype frequency depends on the number of mRNA molecules per cells and efficiency of PCR amplification as well as the number of T-cells expressing the clonotype but these factors did not greatly alter the correspondence between cell and clonotype frequency in this experimental system (33). Clonotype analysis has the advantage that it can approximate the number of unique memory T-cell clones and their frequency without requiring knowledge of the specific tumor antigens. TRB analysis was superior to TRA analysis in estimating clone frequency perhaps because T-cells almost invariable express a single TRB mRNA but ~30% express 2 TRA mRNA (14, 15) and because the main contribution to TCR-peptide binding comes from the TRB CD3 sequence (25).

The methodology described in this report can be used immediately in pre-clinical work in mice to quantify the amplitude and diversity of the anti-tumor memory response in spleen to vaccination or treatment. Clinical application, however, will be confounded by a circulating repertoire in humans enriched in virus-reactive specificities (31, 42, 43) and requires further work to develop a practical method of stimulation in humans that produces a clear, acute response of anti-tumor T-cells in blood. Repeated blood testing is practical in humans and allows testing before and after stimulation, which will create a more sensitive test that can detect not only clonotypes with a large absolute oligoclonal response but also clonotypes that show a 10-fold increase following stimulation. Repeated blood testing will also allow following unique anti-tumor memory T-cell clonotypes in an individual over time.

Data availability statement

The data presented in this paper are deposited with the NCBI BioProject with BioProject ID: PRJNA930664 and Submission ID: SUB12529129 and release date of 2023-03-17.

Ethics statement

The animal study was reviewed and approved by Institutional Animal Research and Care Committee Protocol #: 21028761.

Author contributions

YG is credited with contributing to the development of the idea for the article, as well as designing and performing experiments, preparing TCR data for analysis, analyzing all data and editing the manuscript. IB is credited with contributing to the development of the idea for the article, designing experiments, analyzing all data, and writing the paper. All authors contributed to the article and approved the submitted version.

Acknowledgments

Amanda C. Poholek, PhD, Director and William A. MacDonald PhD, Managing Director of the University of Pittsburgh Health Sciences Sequencing Core (HSSC), Rangos Research Center, UPMC Children's Hospital of Pittsburgh, provided invaluable advice and technical assistance for next generation sequencing. Kaylie Yu Wu helped with figure preparation. The Authors thank Stanislav Poslavsky and the MiXCR team for providing technical assistance and free use of the MiXCR program. The Authors gratefully acknowledge the assistance of the NIH Tetramer Core Facility at Emory University and Dale Long, facility manager, for generously supplying all the tetramer reagents. The NIH Tetramer Facility is supported by contract HHSN272201300006C from the National Institute of Allergy and Infectious Diseases, a component of the National Institutes of Health in the Department of Health and Human Services. Drs. Wei-Zen Wei and John K. Rose and Genentech Inc. generously supplied materials as noted in the text.

Conflict of interest

The authors declare that the research was conducted in the absence of any commercial or financial relationships that could be construed as a potential conflict of interest.

Publisher's note

Supplementary material

The Supplementary Material for this article can be found online at: https://www.frontiersin.org/articles/10.3389/fimmu.2023.1137054/full#supplementary-material

SUPPLEMENTARY FIGURE 1
Frequency analysis of tumor-challenged peritoneal T-cells. Intraperitoneal tumor challenge in mice who had received rrVSV oncolytic immunotherapy to cure implanted tumor (tumor-cured mice) compared to mice with with full viral therapy but no tumor implant (virus control mice). Peritoneal CD4 and CD8 T-cells were harvested 5 days after challenge and TCR clones quantified. The top 100 clones are plotted and results shown separately for CD4 and CD8 T-cells and TCR-α (TRA) and TCR-β (TRB) receptors (Log2 scale for X and Y axes).

SUPPLEMENTARY FIGURE 2
Distinguishing true-positive tetramer+ clonotypes from contaminants in the sample mixture. High-frequency clonotypes (>1%) in individual animals were the index cases and the inverse ratio of the frequency of this clonotype in the individual mouse compared with the same clonotype in the tetramer+ mix was plotted.

SUPPLEMENTARY FIGURE 3
Comparison of the high frequency clonotypes following challenge in donor animals cured of implanted tumor by rrVSV oncolytic immunotherapy and host animals cured by T-cell transfer from the donor animals. Graphs show CD4 and CD8 T-cell TRA data from the same representative pair of animals of three total pairs shown in Fig. 9. The top 10 most frequent clones in the host peritoneal cells are the index clones and are compared with the donor peritoneal and spleen cells and the host spleen and blood cells. Identical numbers and colors within the CD4 and CD8 sets refer to identical clonotypes.

SUPPLEMENTARY FIGURE 4
Identifying and determining the frequency of resting and challenged anti-tumor memory T-cells. The top 5 most frequent clones in the host challenged peritoneal T-cells are the index clones and are compared with the frequency of the same clones in the spleens of challenged host and unchallenged donor mice. Three trios of animals are shown in separate rows with the CD4 T-cells in the top half and the CD8 T-cells in the bottom half of the figure (TRA only). Identical numbers and colors within the CD4 and CD8 pairs refer to identical clonotypes.

SUPPLEMENTARY FIGURE 5
Identifying and determining the frequency of resting and challenged anti-tumor memory T-cells. The frequency of the top 5 anti-tumor memory T-cells in the peritoneum of host challenged mice are compared with the frequency of the same clones in the spleen of host challenged mice and the spleen of resting donor mice. (n=3 in each group, CD4 and CD8, TRA only); mean values and SEM bars above the column for each group).

SUPPLEMENTARY FIGURE 6
Response to stimulation of individual anti-tumor memory T-cell clones. The total number of memory T-cells in transferred donor spleen cells were compared with total number of stimulated host memory T-cells harvested from spleen and peritoneum. The top 5 most frequent CD4 and CD8 memory T-cell clones for each of 3 animals are plotted separately (TRA clonotypes). The mean increase in clone count was 41-fold for CD4 and 67-fold for CD8 T-cells.

SUPPLEMENTARY FIGURE 7
Frequency distribution of resting anti-tumor memory T-cells. The top 5 most frequent CD4 and CD8 TRA clonotypes from 3 animals are highlighted by large bold red, green or black diamonds within the frequency distribution of all resting spleen cells from the same animal.

References

1. Steigler P, Verrall AJ, Kirman JR. Beyond memory T cells: Mechanisms of protective immunity to tuberculosis infection. *Immunol Cell Biol* (2019) 97:647–55. doi: 10.1111/imcb.12278

2. Clemens EB, de Sandt Cv, Wong SS, Wakim LM, Valkenburg SA. Harnessing the power of T cells: The promising hope for a universal influenza vaccine. *Vaccines* (2018) 6:26. doi: 10.3390/vaccines6020018

3. Bergman I, Whitaker-Dowling P, Gao Y, Griffin JA. Preferential targeting of vesicular stomatitis virus to breast cancer cells. *Virology* (2004) 330:24–33. doi: 10.1016/j.virol.2004.06.048

4. Gao Y, Whitaker-Dowling P, Griffin JA, Bergman I. Treatment with targeted vesicular stomatitis virus generates therapeutic multifunctional anti-tumor memory CD4 T cells. *Cancer Gene Ther* (2012) 19:282–91. doi: 10.1038/cgt.2011.90

5. Gao Y, Bergman I. Potent antitumor T-cell memory is generated by curative viral oncolytic immunotherapy but not curative chemotherapy. *Anticancer Res* (2018) 38:6621–9. doi: 10.21873/anticanres.13029

6. Izraelson M, Nakonechnaya TO, Moltedo B, Egorov ES, Kasatskaya SA, Putintseva EV, et al. Comparative analysis of murine T-cell receptor repertoires. *Immunology* (2018) 153:133–44. doi: 10.1111/imm.12857

7. Stubbington MJT, Lonnberg T, Proserpio V, Clare S, Speak AO, Dougan G, et al. T Cell fate and clonality inference from single-cell transcriptomes. *Nat Methods* (2016) 13:329–32. doi: 10.1038/nmeth.3800

8. Zhang J, Bedel R, Krovi SH, Tuttle KD, Zhang B, Gross J, et al. Mutation of the Traj18 gene segment using TALENs to generate natural killer T cell deficient mice. *Sci Rep* (2016) 6:27375. doi: 10.1038/srep27375

9. Xiao X, Li K, Ma X, Liu B, He X, Yang S, et al. Mucosal-associated invariant T cells expressing the TRAV1-TRAJ33 chain are present in pigs. *Front Immunol* (2019) 10:2070. doi: 10.3389/fimmu.2019.02070

10. Gao Y, Whitaker-Dowling P, Griffin JA, Barmada MA, Bergman I. Recombinant vesicular stomatitis virus targeted to Her2/neu combined with anti-CTLA4 antibody eliminates implanted mammary tumors. *Cancer Gene Ther* (2009) 16:44–52. doi: 10.1038/cgt.2008.55

11. Gao Y, Barmada MA, Bergman I. Antitumor memory T-cells become functionally mature from 30 to 100 days in a mouse model of neoplasia. *Anticancer Res* (2018) 38:147–57. doi: 10.21873/anticanres.12202

12. Zhang H, Zhu Z, Modrak S, Little A. Tissue-resident memory CD4+ T cells play a dominant role in the initiation of antitumor immunity. *J Immunol* (2022) 208:2837–46. doi: 10.4049/jimmunol.2100852

13. Bunztman A, Vincent BG, Krovi H, Steele S, Frelinger JA. The LCMV gp33-specific memory T cell repertoire narrows with age. *Immun Ageing [Electronic Resource]: I A* (2012) 9:17. doi: 10.1186/1742-4933-9-17

14. Schuldt NJ, Binstadt BA. Dual TCR T cells: Identity crisis or multitaskers? *J Immunol* (2019) 202:637–44. doi: 10.4049/jimmunol.1800904

15. Dupic T, Marcou Q, Walczak AM, Mora T. Genesis of the alphabeta T-cell receptor. *PloS Comput Biol* (2019) 15:e1006874. doi: 10.1371/journal.pcbi.1006874

16. Gao Y, Whitaker-Dowling P, Barmada MA, Basse PH, Bergman I. Viral infection of implanted meningeal tumors induces antitumor memory T-cells to travel to the brain and eliminate established tumors. *Neuro Oncol* (2015) 17:536–44. doi: 10.1093/neuonc/nou231

17. Gao Y, Whitaker-Dowling P, Bergman I. Memory antitumor T-cells resist inhibition by immune suppressor cells. *Anticancer Res* (2015) 35:4593–7.

18. Pan YG, Aiamkitsumrit B, Bartolo L, Wang Y, Lavery C, Marc A, et al. Vaccination reshapes the virus-specific T cell repertoire in unexposed adults. *Immunity* (2021) 54:1245–1256.e5. doi: 10.1016/j.immuni.2021.04.023

19. Dan JM, Mateus J, Kato Y, Hastie KM, Yu ED, Faliti CE, et al. Immunological memory to SARS-CoV-2 assessed for up to 8 months after infection. *Science* (2021) 1:371. doi: 10.1126/science.abf4063

20. Miller JD, van der Most RG, Akondy RS, Glidewell JT, Albott S, Masopust D, et al. Human effector and memory CD8+ T cell responses to smallpox and yellow fever vaccines. *Immunity* (2008) 28:710–22. doi: 10.1016/j.immuni.2008.02.020

21. Eberhardt CS, Wieland A, Nasti TH, Grifoni A, Wilson E, Schmid DS, et al. Persistence of varicella-zoster virus-specific plasma cells in adult human bone marrow following childhood vaccination. *J Virol* (2020) 94:16. doi: 10.1128/JVI.02127-19

22. Homann D, Teyton L, Oldstone MB. Differential regulation of antiviral T-cell immunity results in stable CD8+ but declining CD4+ T-cell memory. *Nat Med* (2001) 7:913–9. doi: 10.1038/90950

23. Whitmire JK, Murali-Krishna K, Altman J, Ahmed R. Antiviral CD4 and CD8 T-cell memory: differences in the size of the response and activation requirements. *Philos Trans R Soc London - Ser B: Biol Sci* (2000) 355:373–9. doi: 10.1098/rstb.2000.0577

24. De Boer RJ, Homann D, Perelson AS. Different dynamics of CD4+ and CD8+ T cell responses during and after acute lymphocytic choriomeningitis virus infection. *J Immunol* (2003) 171:3928–35. doi: 10.4049/jimmunol.171.8.3928

25. Springer I, Tickotsky N, Louzoun Y. Contribution of T cell receptor alpha and beta CDR3, MHC typing, V and J genes to peptide binding prediction. *Front Immunol* (2021) 12:664514. doi: 10.3389/fimmu.2021.664514

26. Wieland A, Kamphorst AO, Adsay NV, Masor JJ, Sarmiento J, Nasti TH, et al. T Cell receptor sequencing of activated CD8 T cells in the blood identifies tumor-infiltrating clones that expand after PD-1 therapy and radiation in a melanoma patient. *Cancer Immunol Immunother* (2018) 67:1767–76. doi: 10.1007/s00262-018-2228-7

27. Hohn H, Neukirch C, Freitag K, Necker A, Hitzler W, Seliger B, et al. Longitudinal analysis of the T-cell receptor (TCR)-VA and -VB repertoire in CD8+ T cells from individuals immunized with recombinant hepatitis b surface antigen. *Clin Exp Immunol* (2002) 129:309–17. doi: 10.1046/j.1365-2249.2002.01841.x

28. Kalams SA, Johnson RP, Trocha AK, Dynan MJ, Ngo HS, D'Aquila RT, et al. Longitudinal analysis of T cell receptor (TCR) gene usage by human immunodeficiency virus 1 envelope-specific cytotoxic T lymphocyte clones reveals a limited TCR repertoire. *J Exp Med* (1994) 179:1261–71. doi: 10.1084/jem.179.4.1261

29. Pauken KE, Shahid O, Lagattuta KA, Mahuron KM, Luber JM, Lowe MM, et al. Single-cell analyses identify circulating anti-tumor CD8 T cells and markers for their enrichment. *J Exp Med* (2021) 218:05. doi: 10.1084/jem.20200920

30. Lucca LE, Axisa PP, Lu B, Harnett B, Jessel S, Zhang L, et al. Circulating clonally expanded T cells reflect functions of tumor-infiltrating T cells. *J Exp Med* (2021) 218:05. doi: 10.1084/jem.20200921

31. Oliveira G, Stromhaug K, Klaeger S, Kula T, Frederick DT, Le PM, et al. Phenotype, specificity and avidity of antitumour CD8+ T cells in melanoma. *Nature* (2021) 596:119–25. doi: 10.1038/s41586-021-03704-y

32. Wu TD, Madireddi S, de Almeida PE, Banchereau R, Chen YJ, Chitre AS, et al. Peripheral T cell expansion predicts tumour infiltration and clinical response. *Nature* (2020) 579:274–8. doi: 10.1038/s41586-020-2056-8

33. Ma KY, He C, Wendel BS, Williams CM, Xiao J, Yang H, et al. Immune repertoire sequencing using molecular identifiers enables accurate clonality discovery and clone size quantification. *Front Immunol* (2018) 9:33. doi: 10.3389/fimmu.2018.00033

34. Kirchenbaum JHGA, Roen DR, Lehmann PV. Detection of antigen-specific T cell lineages and effector functions based on secretory signature. *J Immunol Sci* (2019) 3:14–20. doi: 10.29245/2578-3009/2019/2.1168

35. Tubo NJ, Fife BT, Pagan AJ, Kotov DI, Goldberg MF, Jenkins MK. Most microbe-specific naive CD4+ T cells produce memory cells during infection. *Science* (2016) 351:511–4. doi: 10.1126/science.aad0483

36. Obar JJ, Khanna KM, Lefrancois L, Obar JJ, Khanna KM, Lefrancois L. Endogenous naive CD8+ T cell precursor frequency regulates primary and memory responses to infection. *Immunity* (2008) 28:859–69. doi: 10.1016/j.immuni.2008.04.010

37. Moon JJ, Chu HH, Pepper M, McSorley SJ, Jameson SC, Kedl RM, et al. Naive CD4(+) T cell frequency varies for different epitopes and predicts repertoire diversity and response magnitude. *Immunity* (2007) 27:203–13. doi: 10.1016/j.immuni.2007.07.007

38. Sun Y, Best K, Cinelli M, Heather JM, Reich-Zeliger S, Shifrut E, et al. Specificity, privacy, and degeneracy in the CD4 T cell receptor repertoire following immunization. *Front Immunol* (2017) 8:430. doi: 10.3389/fimmu.2017.00430

39. Pogorelyy MV, Minervina AA, Touzel MP, Sycheva AL, Komech EA, Kovalenko EI, et al. Precise tracking of vaccine-responding T cell clones reveals convergent and personalized response in identical twins. *Proc Natl Acad Sci USA* (2018) 115:12704–9. doi: 10.1073/pnas.1809642115

40. Hu Z, Leet DE, Allesoe RL, Oliveira G, Li S, Luoma AM, et al. Personal neoantigen vaccines induce persistent memory T cell responses and epitope spreading in patients with melanoma. *Nat Med* (2021) 27:515–25. doi: 10.1038/s41591-020-01206-4

41. Becher LRE, Nevala WK, Sutor SL, Abergel M, Hoffmann MM, Parks CA, et al. Public and private human T-cell clones respond differentially to HCMV antigen when boosted by CD3 copotentiation. *Blood Adv* (2020) 4:5343–56. doi: 10.1182/bloodadvances.2020002255

42. Attaf M, Roider J, Malik A, Rius Rafael C, Dolton G, Predergast AJ, et al. Cytomegalovirus-mediated T cell receptor repertoire perturbation is present in early life. *Front Immunol* (2020) 11:1587. doi: 10.3389/fimmu.2020.01587

43. Chen G, Yang X, Ko A, Sun X, Gao M, Zhang Y, et al. Sequence and structural analyses reveal distinct and highly diverse human CD8+ TCR repertoires to immunodominant viral antigens. *Cell Rep* (2017) 19:569–83. doi: 10.1016/j.celrep.2017.03.072

44. Greenshields-Watson A, Attaf M, MacLachlan BJ, Whalley T, Rius C, Wall A, et al. CD4+ T cells recognize conserved influenza a epitopes through shared patterns of V-gene usage and complementary biochemical features. *Cell Rep* (2020) 32:107885. doi: 10.1016/j.celrep.2020.107885

45. Valkenburg SA, Josephs TM, Clemens EB, Grant EJ, Nguyen TH, Wang GC, et al. Molecular basis for universal HLA-a 0201-restricted CD8+ T-cell immunity against influenza viruses. *Proc Natl Acad Sci USA* (2016) 113:4440–5. doi: 10.1073/pnas.1603106113

frontiers | Frontiers in Immunology

TYPE Original Research
PUBLISHED 11 May 2023
DOI 10.3389/fimmu.2023.1057292

OPEN ACCESS

EDITED BY
Catherine Sautes-Fridman,
INSERM U1138 Centre de Recherche des Cordeliers (CRC), France

REVIEWED BY
Datian Chen,
Haimen City People's Hospital, China
Kevin D. Pavelko,
Mayo Clinic, United States

*CORRESPONDENCE
Judith M. Ramage
Judith.ramage@nottingham.ac.uk

RECEIVED 29 September 2022
ACCEPTED 21 April 2023
PUBLISHED 11 May 2023

CITATION
Talhouni S, Fadhil W, Mongan NP, Field L, Hunter K, Makhsous S, Maciel-Guerra A, Kaur N, Nestarenkaite A, Laurinavicius A, Willcox BE, Dottorini T, Spendlove I, Jackson AM, Ilyas M and Ramage JM (2023) Activated tissue resident memory T-cells (CD8+CD103+CD39+) uniquely predict survival in left sided "immune-hot" colorectal cancers.
Front. Immunol. 14:1057292.
doi: 10.3389/fimmu.2023.1057292

Activated tissue resident memory T-cells (CD8+CD103+CD39+) uniquely predict survival in left sided "immune-hot" colorectal cancers

Shahd Talhouni[1,2], Wakkas Fadhil[3], Nigel P. Mongan[4,5], Lara Field[1], Kelly Hunter[6], Sogand Makhsous[1], Alexandre Maciel-Guerra[7], Nayandeep Kaur[1], Ausrine Nestarenkaite[8], Arvydas Laurinavicius[8], Benjamin E. Willcox[6,9], Tania Dottorini[7], Ian Spendlove[1], Andrew M. Jackson[10], Mohammad Ilyas[3] and Judith M. Ramage[1*]

[1]Cancer Immunology Group, School of Medicine, University of Nottingham Biodiscovery Institute, Nottingham, United Kingdom, [2]Faculty of Pharmacy, Al-Zaytoonah University of Jordan, Amman, Jordan, [3]Academic Unit of Translational Medical Sciences, School of Medicine, Queens Medical Centre, University of Nottingham, Nottingham, United Kingdom, [4]School of Veterinary Medicine and Sciences, University of Nottingham Biodiscovery Institute, Nottingham, United Kingdom, [5]Department of Pharmacology, Weill Cornell Medicine, New York, NY, United States, [6]Birmingham Tissue Analytics, College of Medical and Dental Sciences, University of Birmingham, Birmingham, United Kingdom, [7]School of Veterinary Medicine and Science, University of Nottingham, Sutton Bonington, United Kingdom, [8]Faculty of Medicine, Institute of Biomedical Sciences, Vilnius University, Vilnius, Lithuania, [9]Institute of Immunology and Immunotherapy, University of Birmingham, Birmingham, United Kingdom, [10]Host-Tumour Interactions Group, School of Medicine, University of Nottingham Biodiscovery Institute, Nottingham, United Kingdom

Introduction: Characterization of the tumour immune infiltrate (notably CD8+ T-cells) has strong predictive survival value for cancer patients. Quantification of CD8 T-cells alone cannot determine antigenic experience, as not all infiltrating T-cells recognize tumour antigens. Activated tumour-specific tissue resident memory CD8 T-cells (T_{RM}) can be defined by the co-express of CD103, CD39 and CD8. We investigated the hypothesis that the abundance and localization of T_{RM} provides a higher-resolution route to patient stratification.

Methods: A comprehensive series of 1000 colorectal cancer (CRC) were arrayed on a tissue microarray, with representative cores from three tumour locations and the adjacent normal mucosa. Using multiplex immunohistochemistry we quantified and determined the localization of T_{RM}.

Results: Across all patients, activated T_{RM} were an independent predictor of survival, and superior to CD8 alone. Patients with the best survival had immune-hot tumours heavily infiltrated throughout with activated T_{RM}. Interestingly, differences between right- and left-sided tumours were apparent. In left-sided CRC, only the presence of activated T_{RM} (and not CD8 alone) was prognostically significant. Patients with low numbers of activated T_{RM} cells had a poor prognosis even with high CD8 T-cell

infiltration. In contrast, in right-sided CRC, high CD8 T-cell infiltration with low numbers of activated T_{RM} was a good prognosis.

Conclusion: The presence of high intra-tumoural CD8 T-cells alone is not a predictor of survival in left-sided CRC and potentially risks under treatment of patients. Measuring both high tumour-associated T_{RM} and total CD8 T-cells in left-sided disease has the potential to minimize current under-treatment of patients. The challenge will be to design immunotherapies, for left-sided CRC patients with high CD8 T-cells and low activate $T_{RM,}$that result in effective immune responses and thereby improve patient survival.

KEYWORDS

colorectal cancer, T-cells, multiplex IHC/IF, tissue resident T cells, immune microenvironment, CD8 T-cells, cancer

Introduction

Colorectal cancers (CRC) have traditionally been grouped together as one disease due to the anatomic continuity of the colon into the rectum. However, right and left colon differ in terms of their embryonic origin, vascular and nervous supplies, and gut flora (1). Increasing evidence has pointed to the location of the tumour affecting cancer pathology, progression and prognosis (2, 3), and ultimately patient's response to different cancer treatments (4, 5). This in part may be due to the molecular variations and difference in mutational profiles between right and left-sided colon cancer (3, 6, 7). There is, however, increasing recognition in the literature that the differences in CRC may go beyond currently defined molecular subtypes (7) and that for cancer treatment right and left-sided colon cancer should be treated as separate diseases (3).

It is generally accepted that tumour progression may be influenced by non-malignant cells found in the tumour environment, especially the immune cells (8). T-cell infiltration has been shown to be superior to tumour staging as a prognostic factor (9, 10). Furthermore, responses to immune checkpoint blockade have been shown to be associated with patients having a pre-existing anti-tumour T-cell repertoire (11, 12). There is a strong correlation between the mutational load of a cancer type, the presence of neoepitopes and the response to immune check point blockade (13–15). Currently, only CRC patients with microsatellite instability (MSI), arising through loss of DNA mismatch repair function, are treated with checkpoint inhibitors (14). MSI is predominately found in right-sided colon cancers and tumours with MSI have been shown to have high T-cell infiltration (16, 17). Reflecting this, higher CD8 gene expression has also been demonstrated in right-sided colon cancer compared to the left-side (18).

Based on immune infiltration, tumours have been classified as: "immune-hot" (heavily infiltrated by lymphocytes); "immune-cold" (low levels of lymphocyte infiltration) (19). Since "immune-hot" tumours generally have a better prognosis than immune-cold tumours, this would imply that these immune cells – especially the CD8 T-cells – are activated and have anti-tumour activity. However, it has been shown that some tumour infiltrating T-cells may be inactive bystander cells which recognize viral antigens rather than cancer antigens (20).

Discriminating tumour-specific T-cells from bystander T-cells using markers of activation could aid in defining their role in the tumour microenvironment and patient outcome. One possible marker of activated CD8 T-cells is the co-expression of CD39 and CD103 (21). CD39 is an ectonucleotidase present on activated CD4 and CD8 T-cells following TCR stimulation (22). $CD8^+CD103^+$ have been defined as a tissue resident memory T-cell (T_{RM}) signature (23). T_{RM} have been described as T-cells that no-longer circulate but develop and reside in the peripheral tissues as part of the memory response (24). CD103 (integrin alpha E), binds to E-cadherin and is important in retaining T_{RM} in the peripheral tissues (25).

The presence of $CD103^+$ TIL in ovarian (26, 27), breast (26) lung (23, 28) and head and neck cancers (21) has shown a stronger correlation with survival than canonical T-cell markers such as CD3 or CD8. However, in a study in head and neck cancer, Duhen et al. (21) demonstrated that not all $CD8^+CD103^+$ T-cells were tumour-specific, and that some were the result of bystander recruitment. An increase in 4-1BB and Ki-67 expression on $CD8^+CD103^+CD39^+$ T-cells lead the authors to hypothesize that these cells had recently encountered cognate antigen and were proliferating in the tumour. Moreover, these cells expressed granzyme and were cytotoxic. These tumour specific T-cells had an oligoclonal T-cell receptor (TCR) repertoire (21), and were associated with improved survival. Similarly, T-cells recognizing neoepitopes isolated from CRC patients expressed CD103 and CD39 (29), whereas bystander T_{RM} that were specific for viral antigens and not tumour antigens had diverse phenotypes that lacked CD39 expression (20). There is therefore substantial evidence that co-expression of CD103/CD39 can be used as a marker of activated T_{RM} in the tumour environment. Though these studies investigated tumour infiltrating lymphocytes they did not analyze the cells *in situ*. We hypothesized that intra-tumoural activated T_{RM} confer a survival advantage (by virtue of their tumour-specificity) in patients with

CRC. Using multiplex immunohistochemistry, on a tissue microarray (TMA) containing cores from 1000 CRC patients, we quantified the activated and non-activated intra-tumoural CD8 T-cells in 891 cases. This study demonstrated that while high numbers of activated T_{RM} is a good predictor of survival in the overall cohort, there is a difference in the size of the effect depending on tumour location. In left-sided colon cancer high numbers of activated T_{RM} was the sole marker of enhanced survival irrespective of total CD8 T-cell infiltration. In contrast, in the right-sided colon cancer, both high numbers of activated T_{RM} and high total CD8 T-cell infiltration (even with low numbers of activated T_{RM}) predicted good survival. This suggests that there is a fundamental difference in biology between right and left-sided colon cancers.

Materials and methods

Patient cohorts

Cohort 1 consisted of a consecutive series of 1000 CRC patients presenting at Nottingham University Hospitals NHS trust between 2008 and 2012 (53.6 months mean follow up). Cancer specific survival was measured from the date of primary surgical treatment to time of death due to cancer. Ethical approval was obtained for the study (reference no. 05/Q1605/66). The median age was 69 (range 16-94) with TMN stages: 16% stage I, 40% stage II, 32% stage III and 12% stage IV. For clinicopathological details refer to Table 1; Supplementary Table 1. Cohort 2 was obtained from the TCGA database containing mRNA sequencing data and clinicopathological characteristics (Table 1) of 515 colon adenocarcinomas (TCGA-COAD) (Cancer genome Atlas).

Tissue microarrays and immunohistochemistry

All tumours were formalin-fixed and processed into paraffin blocks. The histology of all cases was reviewed, appropriate donor blocks selected and marked to enable sampling of tumours from the luminal surface, center, advancing edge and adjacent normal mucosa. Tissue cores (0.6mm) were obtained from representative tumour regions of each donor block and arrayed into new recipient paraffin block using a tissue microarrayer (Beecher Instruments). Primary antibodies concentrations were optimized using chromogenic immunohistochemistry (30).

Multiplex immunohistochemistry

Multiplex immunohistochemistry was performed using the Opal 4-colour manual IHC kit (Akoya Bioscience) for simultaneous detection of CD8, CD103 and CD39 on a single TMA section. Extensive optimization achieved fluorescence staining with optimal intensity and no bleed-through into other channels. Slides were deparaffinized in xylene and rehydrated in three baths of 100%, 90%, and 70% ethanol. Antigen retrieval was performed with EDTA (pH:9, 35 minutes, 100°C). TMA sections were incubated overnight (4°C) with anti-CD39 [Abcam, EPR20627, 1:300 in antibody diluent/blocking solution], washed with TBST buffer, incubated with anti-mouse-HRP conjugate, washed and incubated with Opal 570 (1:100) for 10 minutes. Antibody stripping was performed by microwaving (100W microwave: 100% for 45 seconds, 20% for 14 minutes) in antigen retrieval buffer (AR9, Akoya Bioscience) (31). Sides were cooled, washed and the procedure repeated with anti-CD103 antibody [Abcam: EPR4166(2) 1 hour, room temperature] paired with Opal 690 (1:100) and then with anti-CD8 [Agilent DAKO clone: C8/144b (M7103) 1 hour, room temperature] paired with Opal 520 (1:100). Slides were counterstained with Spectra DAPI, and coverslips were mounted with ProLong® Diamond Antifade Mountant (Thermo Fisher Scientific). To obtain a spectral library anti-CD8 antibody was paired with each Opal fluorophore (without DAPI counterstain) as a singleplex.

Image acquisition and scoring

TMA slides were scanned (Vectra 3, Akoya Biosciences) at 20 times resolution. The quality of the spectral library was evaluated by reviewing the unmixed images to confirm the absence of spectral

TABLE 1 Clinicopathological Characteristics of patient Cohorts 1 and 2.

Clinicopathological parameters		Cohort 1 All patients N (%)	Cohort 1 Left-sided CRC N (%)	Cohort 1 Right-sided CRC N (%)	Cohort 2 All patients N (%)	Cohort 2 Left-sided CRC N (%)	Cohort 2 Right-sided CRC N (%)
Sex	Male	568 (56.8%)	212 (58.4%)	236 (51.2%)	234 (52%)	65 (51.2%)	115 (52.8%)
	Female	432 (43.2%)	151 (41.6%)	225 (48.8%)	216 (48%)	62 (48.8%)	103 (47.2%)
	Overall	1000	363	461	450	127	218
Age	¾69	508 (50.8%)	196 (54%)	204 (44.3%)	240 (53.3%)	76 (59.8%)	104 (47.7%)
	>69	492 (49.2%)	167 (46%)	257 (55.7%)	210 (46.7%)	51 (40.2%)	114 (52.3%)
	Overall	1000	363	461	450	127	218

(Continued)

10.3389/fimmu.2023.1057292

TABLE 1 Continued

Clinicopathological parameters		Cohort 1 All patients N (%)	Cohort 1 Left-sided CRC N (%)	Cohort 1 Right-sided CRC N (%)	Cohort 2 All patients N (%)	Cohort 2 Left-sided CRC N (%)	Cohort 2 Right-sided CRC N (%)
Site of Primary tumour	Right colon	461 (46.1%)	N/A	N/A	218 (48.4%)	N/A	N/A
	Left colon	363 (36.3%)	N/A	N/A	127 (28.25)	N/A	N/A
	Rectal	147 (14.7%)	N/A	N/A	1 (0.25)	N/A	N/A
	Unknown	29 (2.9%)	N/A	N/A	104 (23.15)	N/A	N/A
	Overall	1000	N/A	N/A	450	N/A	N/A
N-regional Lymph nodes	N0	570 (58.5%)	197 (56.3%)	274 (59.6%)	265 (58.9)	68 (53.5%)	133 (61%)
	N1	243 (24.9%)	106 (30.3%)	96 (20.9%)	104 (23.1)	40 (31.5%)	47 (21.6%)
	N2	162 (16.6%)	47 (13.4%)	90 (19.6%)	81 (18%)	19 (15%)	38 (17.4%)
	Overall	975	350	460	450	127	218
Metastases (M)	M0 (no distant metastasis)	881 (88.1%)	315 (86.8%)	406 (88.1%)	331(75.2%)	92 (73%)	159 (74%)
	M1 (Distant Metastasis)	119 (11.9%)	48 (13.2%)	55 (11.9%)	63 (14.3%)	23 (18.3%)	26 (12.1%)
	MX (unknown)				46 (10.5%)	11 (8.7%)	30 (13.9%)
	Overall	1000	363	461	440	126	215
T stage	T1	74 (7.4%)	35 (9.6%)	19 (4.1%)	11 (2.5%)	4 (3.1%)	5 (2.3%)
	T2	106 (10.6%)	31 (8.5%)	34 (7.4%)	77 (17.1%)	24 (18.9%)	35 (16.1%)
	T3	526 (52.6%)	190 (52.3%)	251 (54.4%)	308 (68.6%)	87 (68.5%)	143 (65.9%)
	T4	294 (29.4%)	107 (29.5%)	157 (34.1%)	53 (11.8%)	12 (9.4%)	34 (15.7%)
	overall	1000	363	461	449	127	217
TNM stage	I	161 (16.1%)	60 (16.5%)	47 (10.2%)	Not reported	Not reported	Not reported
	II	402 (40.2%)	138 (38%)	215 (46.6%)			
	III	319 (31.9%)	117 (32.2%)	145 (31.5%			
	IV	118 (11.8%)	48 (13.2%)	54 (11.7%)			
	Overall	1000	363	461			
Vascular invasion	Absent	502 (50.9%)	179 (50.1%)	228 (49.7%)	Not reported	Not reported	Not reported
	Present	483 (49%)	178 (49.9%)	231 (50.3%)			
	Overall	985	357	459			
Microsatellite Status	MSS	818 (83.6%)	336 (94.1%)	318 (70.4%)	Not reported	Not reported	Not reported
	MSI	160 (16.4%)	21 (5.9%)	134 (29.6%)			
	Overall	978	357	452			
Treatment type	Pharmaceutical	Not reported	Not reported	Not reported	231 (51.3%)	69 (54.3%)	110 (50.5%)
	Radiation				219 (48.7%)	58 (45.7%)	108 (49.5%)
	Overall				450	127	218

NA, not applicable.

overlap or bleed-through between channels. Machine learning (Inform® software, Akoya Biosciences) enabled quantification of cells in the stroma and epithelium. This consisted of training the software to recognize: stroma and epithelial cells; individual cells and phenotype different cells based on fluorescence (Figure 1; Supplementary Figure 1). Tissue segmentation involved training the program to detect differences between the stroma and epithelial cells based on tissue morphologies. DAPI staining allowed nuclei detection which was used to determine the cell segmentation. One schema was used to phenotype all the different subsets. They were trained as following: CD8+CD103+CD39+; CD8+CD103+CD39-; CD8+CD103-CD39+; CD8+CD103-CD39-; CD8-CD103+CD39-; CD8-CD103-CD39+ and other (any other cell). This allowed training to ensure that all double and triple positive cells were as phenotyped and that membrane staining was around the whole cell and not fluorescence from a neighbouring cell (Supplementary Figure 2). A separate schema was used to identify total CD8+ T-cells. All cores were visually inspected to determine agreement with machine learning: any that did not pass initial quality control were trained again (Supplementary Figure 1). The main reason for rejection was tissue segmentation (Supplementary Figure 3 shows examples of failed and retrained images). Out of 4000 TMA cores, 3708 cores were accepted with the rest rejected due to loss of tissue or inaccurately trained after second training. The data from Inform® was merged and processed using phenoptrReports (Akoya Biosciences)

Statistical analysis

Optimal cut-off points were determined using X-tile bioinformatics software (version 3.4.7). Statistical analysis was

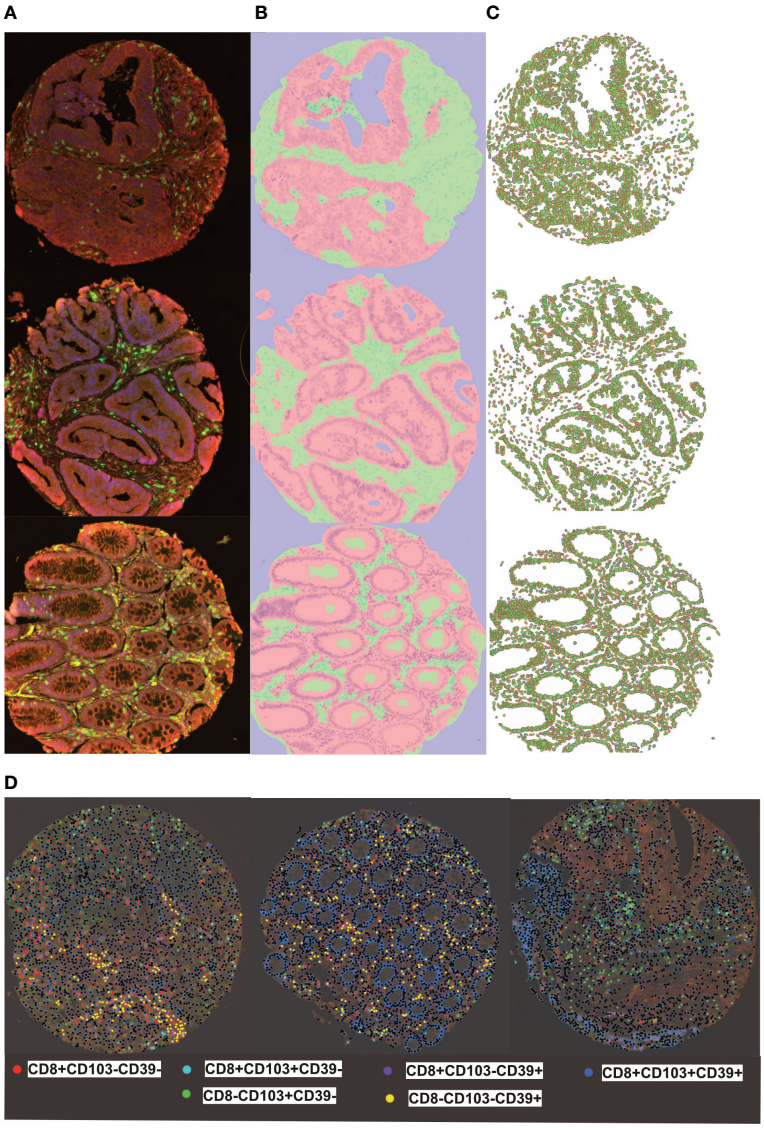

FIGURE 1
inform training stages for automated detection of tissues, cells and phenotyping individual cells **(A)** representive multiplex view of tumour cores with multi-stained cells, **(B)** Tissue segmentation of tumour epithelium (pink) and stroma (green) using pattern recognition **(C)** Cell segmentation was used to identify individual cell types **(D)** Training and phenotyping multi-stained and single stained cells was performed using a coloring- code method on infrom software. Black dots represent other cells.

performed using the SPSS 21.0 software (SPSS, USA). Univariant and multivariant analyses were determined by chi-squared, log rank and Cox regression analysis, respectively. A p-value<0.05 was considered significant. GraphPad PRISM version 8 was used to compare the densities of different CD8+ T-cells. Statistical differences were assessed by two tailed paired T-test; One way Anova with Turkey's multiple comparison test or Kruskal-Wallis with Dunn's multiple comparison test.

TCGA analysis

Using the medical reports from the TCGA-COAD database, patients were sorted according to primary tumour location: right-sided (228 patients) or left-sided (131 patients). HTSeq data were used as the gene expression count. Differentially expressed genes were determined in each sample group using Deseq2 (32). These groups were defined in terms of CD8 and CD103 expression: high (4^{th} Quartile) or low (1^{st} Quartile). Inclusion criteria for differentially expressed genes (DEG) was an FDR < 0.05, Log_2 FC < -1 and Log_2 FC < +1. FDR were analyzed with ClueGO (33), Cytoscape (34) and Webgestalt (http://www.webgestalt.org/) (35).

Results

Multiplex immunohistochemistry

Multiplex IHC was performed on a TMA containing tumour cores from 1000 colorectal cancer patients (cohort 1), each of which was represented by four cores from different tumour regions (see Supplementary Figure 4): luminal side; center of the tumour; invasive margin and adjacent pathologically normal. Representative examples of fluorescently labelled cells are shown in Figure 2. The following subsets were classified: CD8+CD103+CD39+ (activated T_{RM}) CD8+CD103+CD39-, CD8+CD103-

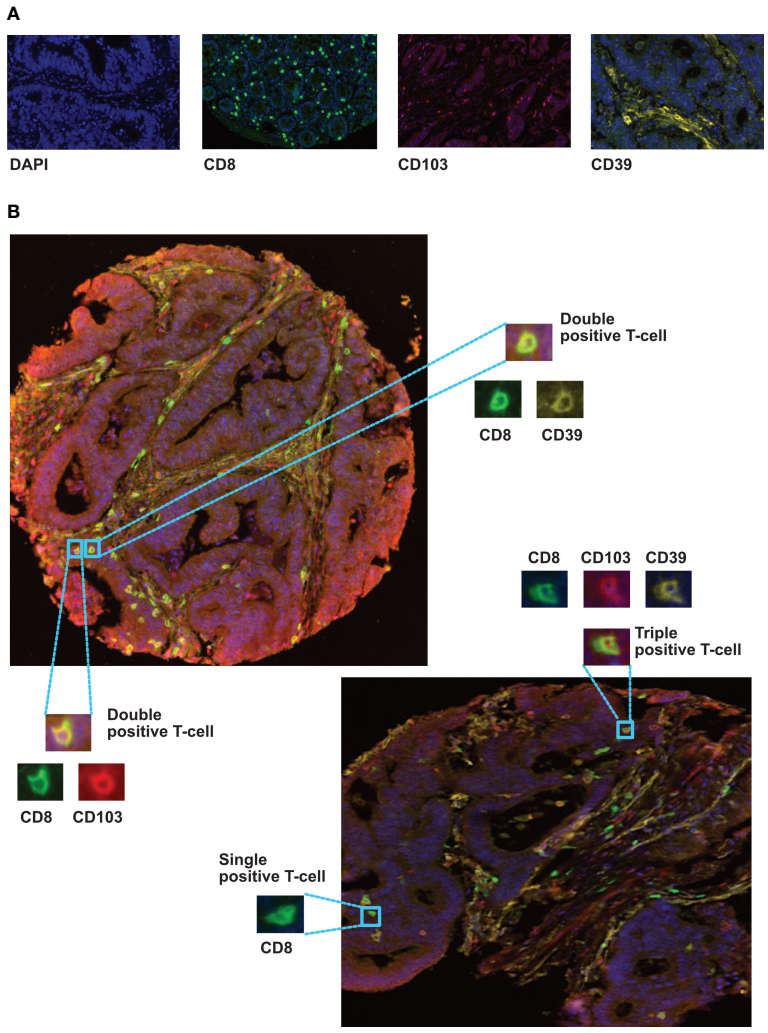

FIGURE 2
Immunolocalization of different CD8+ phenotypes in colorectal cancer tissues. **(A)** representive monoplex expression of CD8, CD103 and CD39 markers, and the tissue nuclear counterstain (DAPI) using fluorescence setting (Inserts x40). **(B)** Multiplex staining of different CRC TMA cores presenting triple, double and single stained cells with CD8 (green), CD103 (red) and CD39 (yellow) biomarkers. Training and phenotyping multi-stained and single stained cells were performed using coloring- code method on inform software.

CD39+, CD8+CD103-CD39-, and total CD8+ T-cells. Cores from 891 patients remained available to analysis due to the loss of cores during processing and quality control for machine learning.

Activated T_{RM} T-cells are an independent predictor of survival in CRC

Across the whole cohort, Kaplan Meier analysis indicated high numbers of activated T_{RM} in the epithelium (Figure 3A, p=0.004) and stroma (Supplementary Figure 5, p=0.006) were associated with increased survival. Patients with high numbers of activated T_{RM} in their tumours had a 10-year survival of 92% compared with 79% for total CD8+ T-cells (Figures 3A, B).

The abundant presence of high numbers of CD8 T-cells of any phenotype in the intra-epithelial region was significantly associated with disease-free survival (Supplementary Figure 6 CD8+CD103+CD39- p<0.001; CD8+CD103-CD39+ p=0.017; CD8+CD103-CD39- p=0.006). In the stroma only high CD8 T-cells, activated T_{RM} and high CD8+CD103+CD39- T-cells were significantly associated with disease free survival (Supplementary Figure 7). Furthermore, all CD8 T-cell subsets were significantly correlated (p<0.05) with TNM stage, metastases, vascular invasion and microsatellite instability. High infiltration of activated T_{RM} was significantly associated with primary tumour location (see Supplementary Table 2). However, on their own neither MSI nor primary location predicted survival (Supplementary Figure 8). High numbers of intraepithelial activated T_{RM} was an independent prognostic factor (Figure 3C p=0.05). In agreement with the literature (36), high numbers of intraepithelial CD8+ T-cells was also an independent prognostic factor (Figure 3D p=0.05).

Right-sided CRC patients with high CD8 and high CD103 gene expression have increased expression of genes involved in immune pathways

We utilized the data available in the cancer genome atlas (https://portal.gdc.cancer.gov/) to determine the differentially expressed genes (DEG) associated with high (4th Quartile) and low (1st Quartile) expression of CD8 and/or CD103 and the primary tumour location: right-sided (228 patients) or left-sided (131 patients). All groups were compared with CD8 low CD103 low from the same tumour side. Differential analysis identified 7272 DEG in the right-sided CD8 high CD103 high group. This contrast with only 877 DEG identified in the left-sided CD8 high CD103 high. The right- and left-sided CRC patients with CD8 high CD103 low expression had 260 DEG and 201 DEG respectively (Supplementary Figures 9, 10 and Supplementary Table 3). Gene pathway comparison showed the right-sided CRC CD8 high CD103 high group had predominately more gene pathways than the comparable left-sided group (Figures 4A, B). Most of the pathways were associated with immunity. Pathways that are present in right but not left-sided CRC include: protein processing in ER; autophagy; ubiquitin mediated proteolysis;

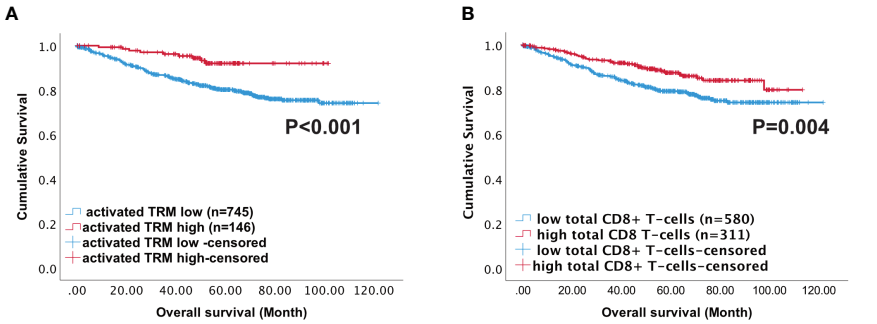

C

Variable	HR	95% CI		P-value
		Lower	Upper	
TNM stage	4.099	2.639	4.099	<0.001
Vascular invasion	2.454	1.173	2.454	0.005
Tumour grade	3.953	1.427	3.953	0.001
MMR status	1.287	0.426	1.287	0.287
Total Intraepithelial CD8+T-cells	1.008	0.476	1.008	**0.05**

D

Variable	HR	95% CI		P-value
		Lower	Upper	
TNM stage	3.429	2.738	4.295	<0.001
Vascular invasion	1.588	1.095	2.302	0.015
Tumour grade	2.624	1.537	4.480	<0.001
MMR status	0.656	0.369	1.163	0.149
Intraepithelial Activated T_{RM}T-cells	0.449	0.228	0.883	**0.02**

FIGURE 3
Prognostic impact of activated T_{RM} T-cells in CRC patients. Kaplan-Meier plots represent the probability of disease-specific survival for **(A)** Activated T_{RM} (CD8+CD103+CD39+) T-cells and **(B)** total CD8+ T-cells in the tumour epithelium. Cut-off points used to stratify CRC patients into high and low-density groups were determined using X-tile. The cut-off point for total CD8+ T cells was 222 cell/mm^2 and for activated TRM cells was 74 cell/mm^2. The log-rank test was used to compare curves, and p values <0.05 were considered statistically significant. **(C)** Multivariate analysis (Cox regression) of Intraepithelial total CD8 T cells with vascular invasion, TNM stage, tumour grade, microsatellite status and colorectal cancer-specific survival **(D)** Multivariate analysis (Cox regression) of Intraepithelial activated T_{RM} with vascular invasion, TNM stage, tumour grade, microsatellite status and colorectal cancer-specific survival.

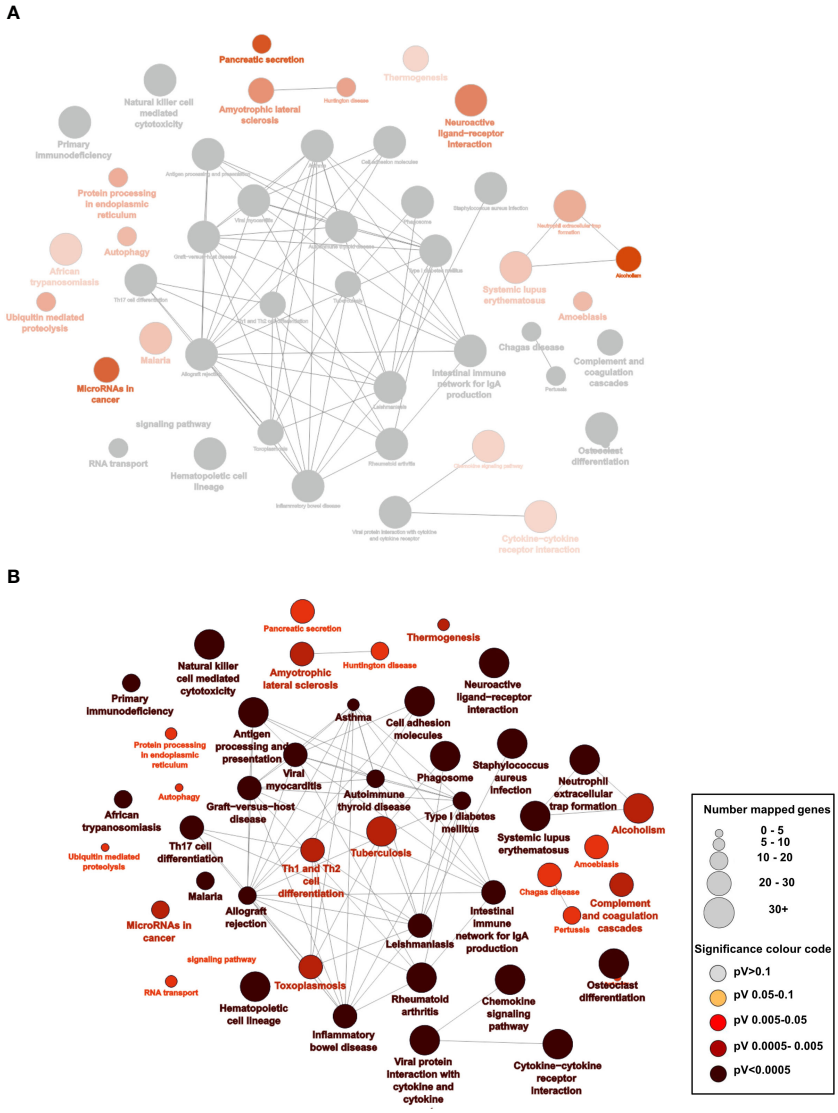

FIGURE 4
Overexpression of pathways predominately in right-sided CRC patients who have high CD8 and CD103 expression: **(A)** Analysis of the RNAseq data from the TCGA database of right- and left-sided CRC patients: 7245 differentially expressed genes (DEG) for right-sided CD8 high (4^{th} quartile) CD103 high (4^{th} quartile) patients compared with 877 DEG from left-sided CD8 high CD103 high CRC patients ($p<0.05$ and a logfold at least =1). There were predominately more significant enriched KEGG pathways on the right (shown in red) as opposed to left (where none were significant). The grey nodes represent overlapping pathways. The network of pathways was created using Cytoscape and ClueGo **(B)** Statistically enriched KEGG pathways with the larger the nodes representing more genes and the darker the red the more significant the pathway.

chemokine signaling pathways; cytokine-cytokine interaction and micro RNAs in cancer. There were limited pathways (Supplementary Figure 10) identified in the other groups and this included the high CD8 low CD103 expression group.

Only activated T_{RM} T-cells predict survival in left-sided colon cancer

The TCGA analysis indicated the prevalence of immune pathways and DEG associated with high CD8 and high CD103 infiltration in right- versus left-sided CRC. We therefore analysed survival in our patient cohort in terms of tumour location. Although, high numbers of either total CD8+ T-cells or activated T_{RM} predicted survival this was not maintained in left-sided tumours. Indeed, although high infiltration of all immune phenotypes predicted survival in right-sided tumours, activated T_{RM} was the only phenotype that significantly predicted survival in left-sided disease ($p=0.008$) (Figure 5).

Disparity between CD8 "immune-hot tumours" and T_{RM} T-cell infiltration

To assess if all "immune-hot" tumours contained elevated numbers of activated $T_{RM,}$ heat maps were employed for all

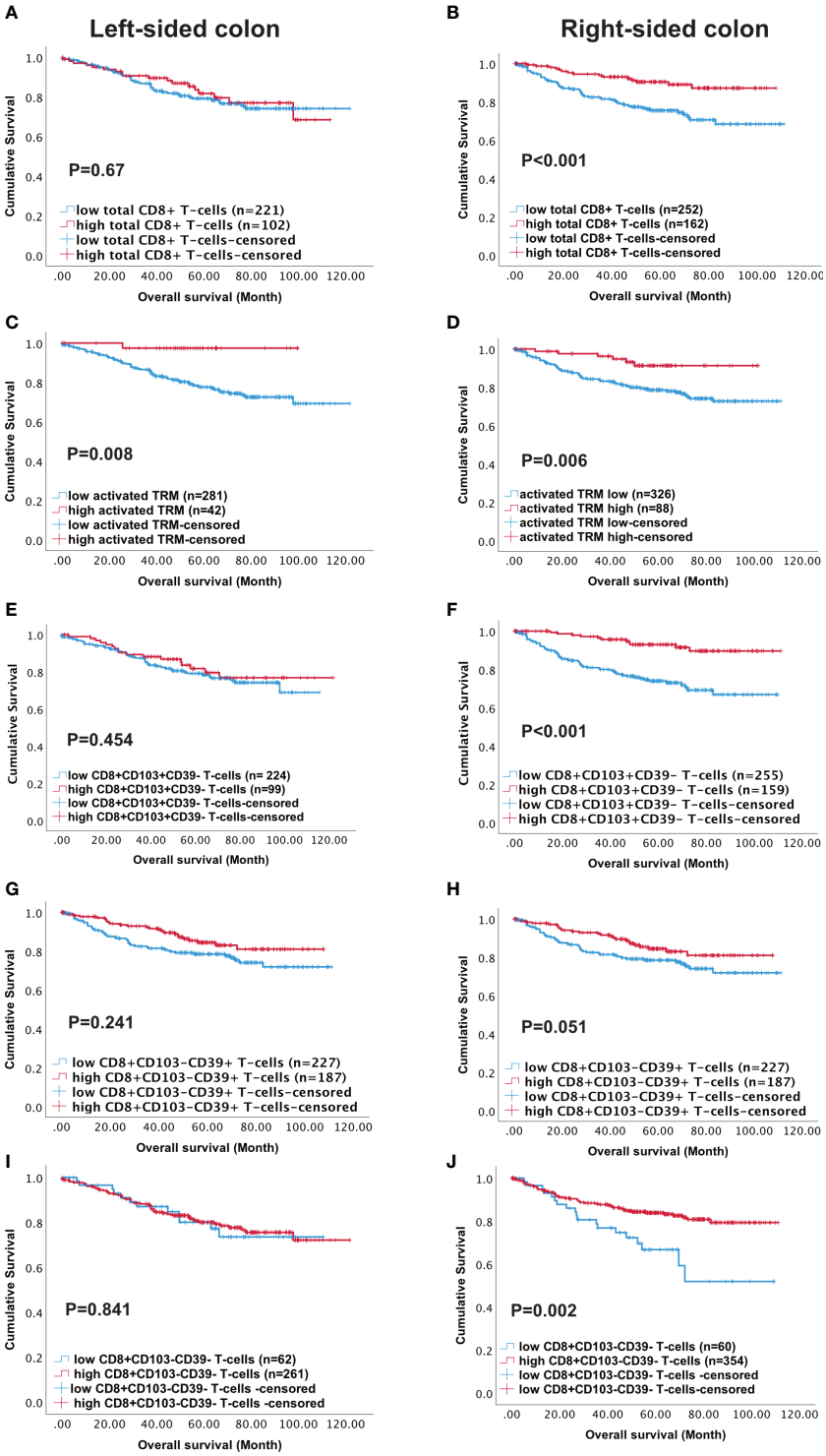

FIGURE 5
High density of activated T_{RM} T-cells predicts better survival in Left-sided colon cancer patients. Kaplan-Meier plots represent the probability of disease-specific survival for total CD8+ T-cells **(A, B)**, Activated T_{RM} (CD8+CD103+CD39+) T-cells **(C, D)**, CD8+CD103+CD39- T-cells **(E, F)**, CD8 +CD103-CD39+ T cells **(G, H)** and CD8+CD103-CD39- T-cells **(I, J)** in the tumour epithelium of right-sided colon cancer and Left-sided colorectal cancer patients. Cut-off points used to stratify CRC patients into high and low-density groups were determined using X-tile. The cut-off points for total CD8+ T cells, activated T_{RM}, CD8+CD103+CD39- T-cells, CD8+CD103-CD39+ T-cells and CD8+CD103-CD39- T-cells were 222, 74, 21, 19 and 7 cell/mm^2, respectively. The log-rank test was used to compare curves, and p values <0.05 were considered statistically significant.

phenotypes. While the majority of patients with increased activated T_{RM} had corresponding elevations of total CD8 T-cells (Supplementary Figure 11), not all patients with high total CD8 T-cells had high levels of activated T_{RM}. Neither the tumour location or MSI status was associated with any of the groups (Supplementary Figure 9).

The absence of activated T_{RM} infiltration associates with poor prognosis irrespective of total CD8 infiltration

Survival was studied in patients with high ("immune-hot") or low ("immune-cold") total CD8 T-cells and high or low numbers of activated T_{RM} in the tumour epithelium resulting in 4 groups of patients. Group-1 patients (high CD8 T-cell infiltration and high activated T_{RM}) had the best survival overall Figures 6A(i), B(i) p=0.003). The major CD8+ subset in the tumours were activated T_{RM}. Furthermore, there was greater infiltration of these cells in the epithelial than stroma (p<0.0001) Figure 6B(i): such tumours could be conventionally classified as "immune-hot".

Group-2 tumours lacked pronounced CD8+ T-cell infiltration but nevertheless exhibited high numbers of activated T_{RM} Figures 6A(i), B(ii). These tumours displayed significantly greater CD8 infiltration than Group-4 (low total CD8 low activated T_{RM}) (p<0.0001) Figure 6B(iv). Survival in Group-2 patients was not significantly different to Group-1 indicating that the presence of activated T_{RM} (as opposed to total CD8) are important for survival.

Group-3 had high total CD8 T-cell infiltration but low numbers of activated T_{RM}. Most cells were single positive (CD8+) with few CD8 +CD103+ or CD8+CD39+ cells Figure 6B(iii). They had a similar pattern of infiltration in the intraepithelial and stroma. However, despite having high total CD8+ T cells, patients in this group had poor survival. Lastly, group-4 displayed both low total CD8+ infiltration and low numbers of activated T_{RM} with corresponding poor survival Figure 6B. This group were conventional "immune-cold" tumours Figure 6B(iv). Therefore, only patients with high numbers of CD8 T-cells and/or high numbers of activated T_{RM} had improved survival (truly hot tumours). Importantly, patients whose tumours exhibited high total CD8 T-cells in the absence of activated T_{RM} had poor survival Figure 6A(i).

Activated T_{RM} are required for better survival prognosis in left-sided but not right-sided colon cancer

Sub-classification of patients into right and left-sided disease revealed differential survival Figures 6A(ii), (iii). For patients with left-sided tumours survival depended on infiltration by activated T_{RM}. In contrast, for right-sided disease a group of patients exhibited good survival with high total CD8+ T-cells but low activated T_{RM} infiltration. There was no difference in overall number of infiltrating cells between right- and left-sided tumours in any group (data not shown). However, survival was poor in patients with left-sided disease (Figure 6C, Group 3).

The presence of CD39+ on non-lymphocyte stromal cells was associated with poor survival

CD39 and CD73 ectonucleotidases operate in concert to produce immunosuppressive metabolite adenosine in tumour environments (37). We hypothesized that high levels of CD39+ cells in the non-lymphoid stroma cells (e.g., fibroblast) associated with poor survival. As shown in Figure 6D higher numbers of CD39 + cells were observed in group-3 and group-4 patients: those that lacked abundant activated T_{RM}.

Infiltration of total CD8 and activated T_{RM} T-cells consistent across the cores

Colorectal tumours have been shown to exhibit higher levels of immune infiltrate at the invasive margins (38). However, in this study infiltration of both total CD8 and activated T_{RM} was consistent throughout the tumours (Figure 7). Group-1," immune-hot tumours", had high numbers of CD8+ T-cells throughout the tumour with lower numbers in adjacent normal tissue. These tumours also had corresponding elevated levels of activated T_{RM} even in the adjacent pathologically normal tissue. Group-3 tumours were characterized by high levels of CD8 T-cells in all cores with no significant difference in any location and limited activated T_{RM} irrespective of region. In contrast, Group 4 "immune-cold" had scant CD8 T-cells throughout, but in adjacent normal tissue these cells were as abundant as those observed in Group-1 and Group-3. This group also had limited infiltration with activated T_{RM}.

Discussion

Our study of T_{RM} cells within the tumour environment is the largest and most detailed study of its kind, having determined the *in-situ* localization of CD8 T-cell subsets in tissue from nearly 900 CRC patients. We addressed whether the presence of all CD8 T-cells within the tumour are beneficial for survival or whether activated T_{RM} are a better predictor of survival. Using multiplex IHC we established the prognostic significance of activated T_{RM} in CRC. The presence of activated T_{RM} independently predicted survival. Furthermore, the presence of high numbers of activated T_{RM} was a better overall predictor of survival than total CD8+ T-cells. Tumours with high numbers of activated T_{RM} were predominately "immune-hot" (tumours with high total CD8+ T-cell counts), and were highly infiltrated throughout (luminal side, center of the tumour and invasive margins) with both total CD8+ T-cells and activated T_{RM}. While CD8+ T-cells alone did not predict survival in left-sided tumours, activated T_{RM} were uniquely able to predict survival. This contrasted with right-sided tumours where patients exhibiting high total CD8+ T-cells (even with low numbers of activated T_{RM}) had good overall survival.

It has previously been shown that CD8+CD103+CD39+ T-cells identifies tumour reactive T-cells in both head and neck cancer (21) and breast cancer (39), and that their presence associates with

10.3389/fimmu.2023.1057292

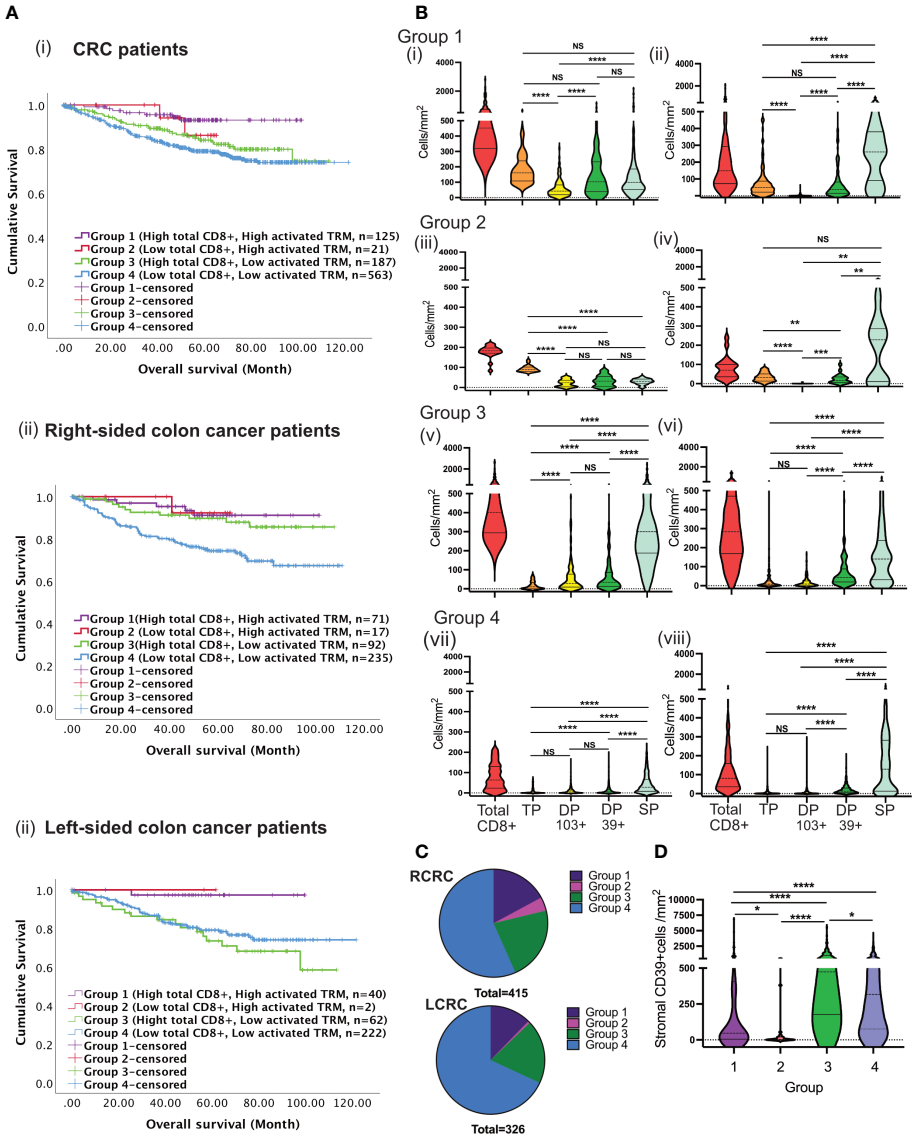

FIGURE 6
Tumours with high total CD8 T-cells and low activated TRM cells infiltration predict disease prognosis differently between RCRC and LCRC. **(A)** CRC patients were classified into four groups depending on total CD8 TILs, and activated TRM infiltration into the TME followed by the assessment of their correlation to survival using Kaplan Meier analysis for the entire (i) CRC cohort, (ii)Right sided and left sided colon cancer patients. **(B)** The violin plots represent the average densities of the respective CD8+ TIL subsets in the TME for each of the four groups using the Wilcoxon Test: Group 1((i) and (ii); Group 2 ((iii) and (iv)); Group 3 ((v) and (vi)); Group 4 ((vii) and (viii), The left column depicts intraepithelial CD8+ TIL ((i), (iii), (v) and (vii)) and the right column depicts stromal CD8+ TIL ((ii), (iv), (vii) and (viii) (TP: triple positive (CD8+CD103+CD39+), DP 103+ : double positive CD103(CD8+CD103+CD39-), DP 39+: double positive CD39+ (CD8+CD103-CD39+), SP: single positive (CD8+CD103-CD39+)) **(C)** The pie charts illustrate the numerical proportion of the four groups within RCRC (right-sided colon cancer patient) (n=415) and LCRC (left sided colon cancer patients) (n=326). **(D)** Comparison of average densities of CD39+ non-lymphoid cells in the stroma of group 1, group 2, group 3 and group 4 tumours. One way Anova/mixed effect analysis with Turkey correction for multiple comparison was used for statistical comparisons in B, while a Kruskal-wallis test with Dunn's multiple comparison test was used in **(D)** p-values <0.05 were considered statistically significant. (ns if $p > 0.05$, *$p \leq 0.05$, **$p \leq 0.01$, ***$p \leq 0.001$, ****$p \leq 0.0001$).

survival. While those studies showed the functionality of the activated T_{RM}, we focused on their survival advantage and location in tumours. Our findings that activated T_{RM} are an independent predictor would support the concept that these T-cells have been active in the tumour environment.

The immunoscore uses the presence of CD3 and CD8 T-cell in the invasive margins and center of the tumour to predict survival in CRC (40–42). As far as we are aware we are the first to show that CD8 alone does not predict survival in left-sided colon cancer and that T_{RM} uniquely predict survival. Other studies have shown an increase in CD8 gene expression in right-sided CRC and suggested that these patients have a better immune response (18). Indeed, TCGA analysis of right-sided CRC patients with high CD8 and high CD103 compared to the low CD8 low CD103 had significantly more immune pathway involvement than patients with left-sided tumours, suggesting greater immune responses in right-sided disease. This is the first time both high CD8 and high CD103 expression have been analysed together using data from the TCGA

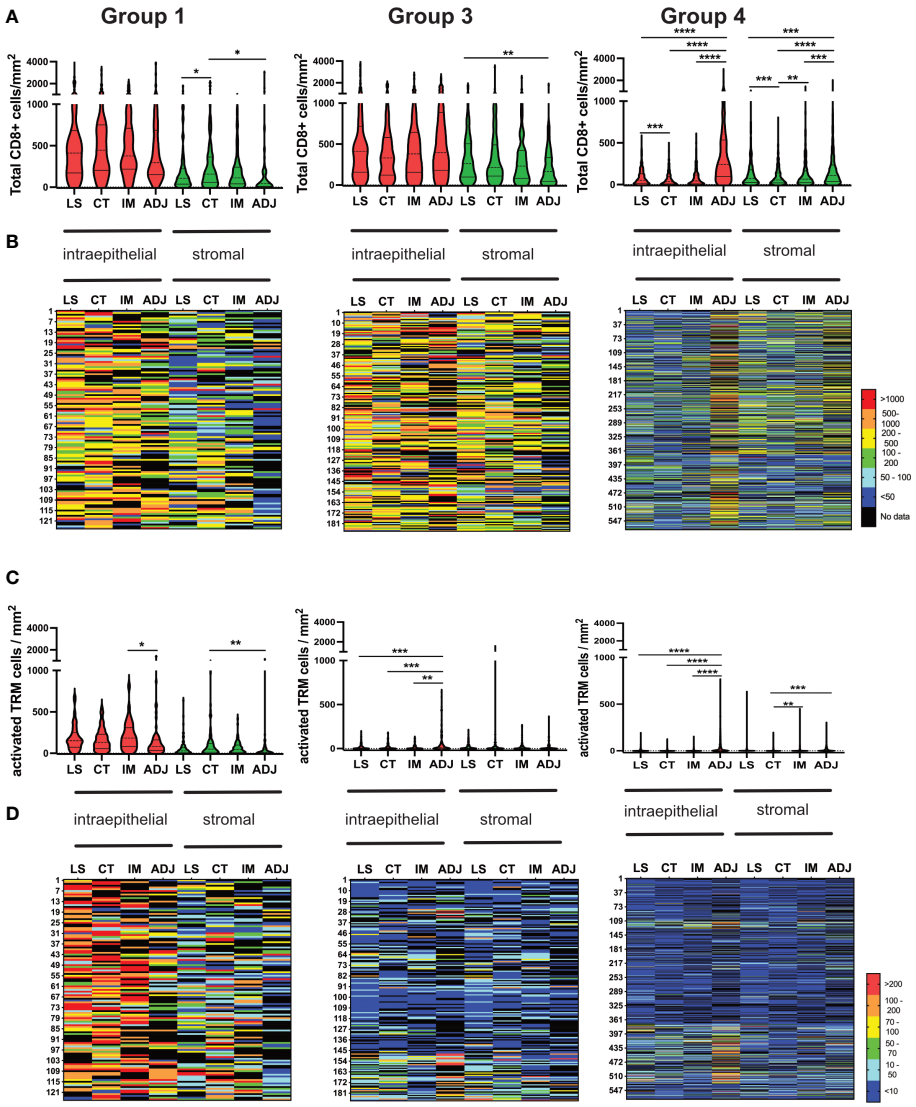

FIGURE 7
Consistent Infiltration of recently activated TRM cells across different tumour regions (LS, CT, IM and ADJ) within the four groups of CRC cohort. **(A)** The violin plots represent the median density of total CD8 TILs in the respective tumour region matched to the density of total CD8 TILs infiltrating the same tumour region in each patient mapped one below each other in the heat maps **(B)**. Group 1 and group 3 tumours had no significant difference in total CD8 TILs infiltration between LS, CT and IM. The normal adjacent tissue had significantly higher total CD8 TILs infiltration compared to other tumour regions in group 4 tumours (Cold tumours). **(C)** The violin plots represent the median density of TP TRM cells in the respective tumour region matched to the density of TILs infiltrating the same tumour region in each patient in the heat maps **(D)**. Group 1 tumours (hot tumours) had significantly higher TRM cell infiltration in the LS, CT and IM as compared to ADJ. Meanwhile, group 3 and group 4 tumours had significantly higher activated TRM cell infiltration in the AJD as compared to other regions of the tumour. Mixed effect analysis with Turkeys multiple comparison correction test was used to test for significance. P values <0.05 were considered statistically significant. (*p ≤0.05, **p ≤ 0.01,***p ≤ 0.001, ****p ≤ 0.0001) (LS, luminal side; CT, center of tumour; IM, invasive margin and ADJ, adjacent normal).

database for CRC and the results are consistent with our data showing that there are differences in immune responses between right and left-sided CRC.

The presence of high CD8 T-cells irrespective of subtype predicts survival in right-sided CRC. Intriguingly, "immune-hot" tumours with low numbers of activated T_{RM} had good survival, suggesting that although activated T_{RM} are important as predictors of survival there may be other markers of antigen specificity and activation that need to be defined for these patients. Why infiltration of high total CD8+ T-cells without T_{RM} is a good prognosis on right-sided but not left-sided colon cancer is unclear, however, other leukocytes within the tumours may be contributing factors. These could include T-regs and tumour associated macrophages. In a study in breast cancer, the presence of T-regs was responsible for the loss of prognostic significance of high numbers of T_{RM} (39).

The difference in survival relating to T-cell infiltration in the right versus the left CRC could be due to differences in somatic mutations and neoantigen generation. The mutations rates in *BRAF*, *POLE*, *POLD1* and *PIK3CA* genes associate with right-sided CRC. Patients with these mutations (43) have elevated expression of helper T-cells, class II-related genes, chemokines and inhibitory molecules. In contrast,

RAS mutant (KRAS, NRAS) tumours (which are more frequent on the left) associate with poor immune infiltration, low inhibitory molecule expression (43) and recruitment of suppressive myeloid cells. Nevertheless, this does not explain why CRC patients with tumours heavily infiltrated with CD8 T-cells but lacking activated T_{RM} have good prognosis if their tumour is right-sided. It is not that the T_{RM} have not upregulated CD39 in these tumours, but that there are low levels of T_{RM}: most cells are single positive CD8 T-cells. The literature would support the theory that CD8+CD103+CD39- T-cells are bystander without specificity for tumour antigens (20) while activated T_{RM} are tumour specific. Left-sided CRC generally exhibit lower mutational burden, and therefore may present less antigenic opportunity for antigen specific T_{RM}. The association between the absence of activated T_{RM} with high levels of CD39+ stromal cells (e.g. fibroblasts) may reflect the role of CD39 in ATP depletion and suppression of T-cell activation and may consequently account for the lack of T_{RM} in these patients. Quantifying activated T_{RM} in CRC patients may therefore permit stratification of tumours with strong immunity genuinely focused on the tumour.

Bindea et al. (38) in a study of 107 patients, showed elevated total CD8+ cells in the invasive margins than the rest of the tumour. In contrast, we observed in 9-fold more patients that high total CD8+ T-cells were homogeneously distributed throughout the "immune-hot" tumours. Whereas in "immune-cold" tumours there were higher numbers of CD8+ T-cells present in pathological adjacent normal tissue than in the tumours. The difference could be due to their analysis of the whole cohort of CRC patients together compared to our analysis of patients with high and low total CD8 T-cell separately.

CD39 and CD103 upregulation on tumour infiltrating CD8 T-cells is due to TGFβ and chronic TCR stimulation (21). Once a cell is activated it displays markers of exhaustion. The expression of CD39 and TIM3 have been shown to discriminate exhausted cells from memory/effector T-cells (44). Expression of other markers of exhaustion such as PD-1 associate with terminal exhaustion (45). It is of note that in our study the "immune-hot" tumours had high levels of all CD8 phenotypes including both CD8+CD103+ and CD8+CD39+. This could suggest an active immune response in the tumour environment of these patients and therefore the reason activated T_{RM} herald survival is that they have previously responded to the tumour. It can be argued that patients who have previously mounted an immune response could continue to mount new T-cell responses.

Clinical use of immune checkpoint inhibitors has revolutionized the treatment of solid tumours. However, future work is needed to identify CRC patients suitable for immunotherapy and characterize repertoires of T-cells to be targeted, a point illustrated by studies showing the presence of intra-tumoural CD103+CD8+ T cells predicts responses to PDL-1 blockade (46, 47). We have already argued that activated T_{RM} have markers of exhaustion, and that the presence of T_{RM} in the tumour is indicative of active immunity. While there is evidence that exhausted T-cells can respond to checkpoint blockade (48, 49), there is also evidence that these cells are not readily reactivated (50). Indeed, recent studies show that new responses to checkpoint inhibitors involve CD8 T-cells actively replenished from outside the tumour (50) and not from the pre-existing repertoire of exhausted T-cells (51). Patients who have previously mounted an immune response could continue to mount new responses with appropriate immunotherapy. In this paper we have shown over 90% survival in the group of patients with high numbers of total CD8 and high numbers of activated T_{RM}. Therefore, patients who may benefit from future immunotherapies may not be the ones with activated T_{RM} who already have generated a good immune prognosis but those patients who have shown the ability to recruit CD8 T-cells but have so far failed to convert this to a survival advantage: the left-sided colon cancer patients with high CD8 T-cells and low recently activated T_{RM}. The challenge will be to generate activated tumour specific T_{RM} in these patients.

Data availability statement

The raw data supporting the conclusions of this article will be made available by the authors, without undue reservation.

Ethics statement

The studies involving human participants were reviewed and approved by Oxford Rec B, NHS (reference 05/Q1605/66). The patients/participants provided their written informed consent to participate in this study.

Author contributions

Data acquisition: ST, NM, KH, SM, AN, AL. Analysis and interpretation of data: JR, ST, NM, LF, NK, IS, AJ, MI, AM-G, TD. Building the patient cohort: WF, MI, Conception/design of work: JR, AJ, ST. Oversight of entire project: JR. Manuscript preparation and review: JR, ST, AJ, MI, IS, BW. All authors contributed to the article and approved the submitted version.

Funding

This work was supported by the Medical Research Council, UK grant to MI (grant code: MR/N005953/1). Multiplex imaging was supported by a Wellcome Trust Multi-User Equipment Grant awarded to BW. This research was funded in whole, or in part, by the Wellcome Trust (Grant number 218287/Z/19/Z). For the purpose of open access, the author has applied a CC BY public copyright license to any Author Accepted Manuscript version arising from this submission.

Acknowledgments

The authors would like to acknowledge Akoya Biosciences and particularly Roslyn Lloyd for advice and training with the inform software and Matt's Fund (in memory of Matthew Boulton, raising awareness of Malignant Melanoma and funding related research) for their donation to support the computer analysis.

Conflict of interest

The authors declare that the research was conducted in the absence of any commercial or financial relationships that could be construed as a potential conflict of interest.

Publisher's note

All claims expressed in this article are solely those of the authors and do not necessarily represent those of their affiliated organizations, or those of the publisher, the editors and the reviewers. Any product that may be evaluated in this article, or claim that may be made by its manufacturer, is not guaranteed or endorsed by the publisher.

Supplementary material

The Supplementary Material for this article can be found online at: https://www.frontiersin.org/articles/10.3389/fimmu.2023.1057292/full#supplementary-material

References

1. Flemer B, Lynch DB, Brown JM, Jeffery IB, Ryan FJ, Claesson MJ, et al. Tumour-associated and non-tumour-associated microbiota in colorectal cancer. *Gut* (2017) 66:633–43. doi: 10.1136/gutjnl-2015-309595

2. Mukund K, Syulyukina N, Ramamoorthy S, Subramaniam S. Right and left-sided colon cancers - specificity of molecular mechanisms in tumorigenesis and progression. *BMC Cancer* (2020) 20:317. doi: 10.1186/s12885-020-06784-7

3. Narayanan S, Gabriel E, Attwood K, Boland P, Nurkin S. Association of clinicopathologic and molecular markers on stage-specific survival of right versus left colon cancer. *Clin Colorectal Cancer* (2018) 17:e671–e8. doi: 10.1016/j.clcc.2018.07.001

4. Arnold D, Lueza B, Douillard JY, Peeters M, Lenz HJ, Venook A, et al. Prognostic and predictive value of primary tumour side in patients with RAS wild-type metastatic colorectal cancer treated with chemotherapy and EGFR directed antibodies in six randomized trials. *Ann Oncol* (2017) 28:1713–29. doi: 10.1093/annonc/mdx175

5. Baran B, Mert Ozupek N, Yerli Tetik N, Acar E, Bekcioglu O, Baskin Y. Difference between left-sided and right-sided colorectal cancer: a focused review of literature. *Gastroenterol Res* (2018) 11:264–73. doi: 10.14740/gr1062w

6. Salem ME, Weinberg BA, Xiu J, El-Deiry WS, Hwang JJ, Gatalica Z, et al. Comparative molecular analyses of left-sided colon, right-sided colon, and rectal cancers. *Oncotarget* (2017) 8:86356–68. doi: 10.18632/oncotarget.21169

7. Cancer Genome Atlas N. Comprehensive molecular characterization of human colon and rectal cancer. *Nature* (2012) 487:330–7. doi: 10.1038/nature11252

8. McAllister SS, Weinberg RA. The tumour-induced systemic environment as a critical regulator of cancer progression and metastasis. *Nat Cell Biol* (2014) 16:717–27. doi: 10.1038/ncb3015

9. Galon J, Costes A, Sanchez-Cabo F, Kirilovsky A, Mlecnik B, Lagorce-Pages C, et al. Type, density, and location of immune cells within human colorectal tumors predict clinical outcome. *Science* (2006) 313:1960–4. doi: 10.1126/science.1129139

10. Simpson JA, Al-Attar A, Watson NF, Scholefield JH, Ilyas M, Durrant LG, et al. Intratumoral T cell infiltration and STAT1 as biomarkers of good prognosis in colorectal cancer. *Gut* (2010) 59:926–33. doi: 10.1136/gut.2009.194472

11. Herbst RS, Soria JC, Kowanetz M, Fine GD, Hamid O, Gordon MS, et al. Predictive correlates of response to the anti-PD-L1 antibody MPDL3280A in cancer patients. *Nature* (2014) 515:563–7. doi: 10.1038/nature14011

12. Tumeh PC, Harview CL, Yearley JH, Shintaku IP, Taylor EJ, Robert L, et al. PD-1 blockade induces responses by inhibiting adaptive immune resistance. *Nature* (2014) 515:568–71. doi: 10.1038/nature13954

13. Alexandrov LB, Nik-Zainal S, Wedge DC, Aparicio SA, Behjati S, Biankin AV, et al. Signatures of mutational processes in human cancer. *Nature* (2013) 500:415–21. doi: 10.1038/nature12477

14. Le DT, Durham JN, Smith KN, Wang H, Bartlett BR, Aulakh LK, et al. Mismatch repair deficiency predicts response of solid tumors to PD-1 blockade. *Science* (2017) 357:409–13. doi: 10.1126/science.aan6733

15. Van Allen EM, Miao D, Schilling B, Shukla SA, Blank C, Zimmer L, et al. Genomic correlates of response to CTLA-4 blockade in metastatic melanoma. *Science* (2015) 350:207–11. doi: 10.1126/science.aad0095

16. Maby P, Tougeron D, Hamieh M, Mlecnik B, Kora H, Bindea G, et al. Correlation between density of CD8+ T-cell infiltrate in microsatellite unstable colorectal cancers and frameshift mutations: a rationale for personalized immunotherapy. *Cancer Res* (2015) 75:3446–55. doi: 10.1158/0008-5472.CAN-14-3051

17. Mlecnik B, Bindea G, Angell HK, Maby P, Angelova M, Tougeron D, et al. Integrative analyses of colorectal cancer show immunoscore is a stronger predictor of patient survival than microsatellite instability. *Immunity* (2016) 44:698–711. doi: 10.1016/j.immuni.2016.02.025

18. Zhang L, Zhao Y, Dai Y, Cheng JN, Gong Z, Feng Y, et al. Immune landscape of colorectal cancer tumor microenvironment from different primary tumor location. *Front Immunol* (2018) 9:1578. doi: 10.3389/fimmu.2018.01578

19. Galon J, Bruni D. Approaches to treat immune hot, altered and cold tumours with combination immunotherapies. *Nat Rev Drug Discovery* (2019) 18:197–218. doi: 10.1038/s41573-018-0007-y

20. Simoni Y, Becht E, Fehlings M, Loh CY, Koo SL, Teng KWW, et al. Bystander CD8(+) T cells are abundant and phenotypically distinct in human tumour infiltrates. *Nature* (2018) 557:575–9. doi: 10.1038/s41586-018-0130-2

21. Duhen T, Duhen R, Montler R, Moses J, Moudgil T, de Miranda NF, et al. Co-Expression of CD39 and CD103 identifies tumor-reactive CD8 T cells in human solid tumors. *Nat Commun* (2018) 9:2724. doi: 10.1038/s41467-018-05072-0

22. Raczkowski F, Rissiek A, Ricklefs I, Heiss K, Schumacher V, Wundenberg K, et al. CD39 is upregulated during activation of mouse and human T cells and attenuates the immune response to listeria monocytogenes. *PloS One* (2018) 13:e0197151. doi: 10.1371/journal.pone.0197151

23. Ganesan AP, Clarke J, Wood O, Garrido-Martin EM, Chee SJ, Mellows T, et al. Tissue-resident memory features are linked to the magnitude of cytotoxic T cell responses in human lung cancer. *Nat Immunol* (2017) 18:940–50. doi: 10.1038/ni.3775

24. Schenkel JM, Masopust D. Tissue-resident memory T cells. *Immunity* (2014) 41:886–97. doi: 10.1016/j.immuni.2014.12.007

25. Okla K, Farber DL, Zou W. Tissue-resident memory T cells in tumor immunity and immunotherapy. *J Exp Med* (2021) 218(4): e20201605. doi: 10.1084/jem.20201605

26. Wang ZQ, Milne K, Derocher H, Webb JR, Nelson BH, Watson PH. CD103 and intratumoral immune response in breast cancer. *Clin Cancer Res* (2016) 22:6290–7. doi: 10.1158/1078-0432.CCR-16-0732

27. Webb JR, Milne K, Watson P, Deleeuw RJ, Nelson BH. Tumor-infiltrating lymphocytes expressing the tissue resident memory marker CD103 are associated with increased survival in high-grade serous ovarian cancer. *Clin Cancer Res* (2014) 20:434–44. doi: 10.1158/1078-0432.CCR-13-1877

28. Djenidi F, Adam J, Goubar A, Durgeau A, Meurice G, de Montpreville V, et al. CD8+CD103+ tumor-infiltrating lymphocytes are tumor-specific tissue-resident memory T cells and a prognostic factor for survival in lung cancer patients. *J Immunol* (2015) 194:3475–86. doi: 10.4049/jimmunol.1402711

29. van den Bulk J, Verdegaal EME, Ruano D, Ijsselsteijn ME, Visser M, van der Breggen R, et al. Neoantigen-specific immunity in low mutation burden colorectal cancers of the consensus molecular subtype 4. *Genome Med* (2019) 11:87. doi: 10.1186/s13073-019-0697-8

30. Popple A, Durrant LG, Spendlove I, Rolland P, Scott IV, Deen S, et al. The chemokine, CXCL12, is an independent predictor of poor survival in ovarian cancer. *Br J Cancer* (2012) 106:1306–13. doi: 10.1038/bjc.2012.49

31. Mori H, Bolen J, Schuetter L, Massion P, Hoyt CC, VandenBerg S, et al. Characterizing the tumor immune microenvironment with tyramide-based multiplex immunofluorescence. *J Mammary Gland Biol Neoplasia* (2020) 25:417–32. doi: 10.1007/s10911-021-09479-2

32. Love MI, Huber W, Anders S. Moderated estimation of fold change and dispersion for RNA-seq data with DESeq2. *Genome Biol* (2014) 15:550. doi: 10.1186/s13059-014-0550-8

33. Bindea G, Mlecnik B, Hackl H, Charoentong P, Tosolini M, Kirilovsky A, et al. ClueGO: a cytoscape plug-in to decipher functionally grouped gene ontology and pathway annotation networks. *Bioinformatics* (2009) 25:1091–3. doi: 10.1093/bioinformatics/btp101

34. Shannon P, Markiel A, Ozier O, Baliga NS, Wang JT, Ramage D, et al. Cytoscape: a software environment for integrated models of biomolecular interaction networks. *Genome Res* (2003) 13:2498–504. doi: 10.1101/gr.1239303

35. Liao Y, Wang J, Jaehnig EJ, Shi Z, Zhang B. WebGestalt 2019: gene set analysis toolkit with revamped UIs and APIs. *Nucleic Acids Res* (2019) 47:W199–205. doi: 10.1093/nar/gkz401

36. Bruni D, Angell HK, Galon J. The immune contexture and immunoscore in cancer prognosis and therapeutic efficacy. *Nat Rev Cancer* (2020) 20:662–80. doi: 10.1038/s41568-020-0285-7

37. Ghiringhelli F, Bruchard M, Chalmin F, Rebe C. Production of adenosine by ectonucleotidases: a key factor in tumor immunoescape. *J BioMed Biotechnol* (2012) 2012:473712. doi: 10.1155/2012/473712

38. Bindea G, Mlecnik B, Tosolini M, Kirilovsky A, Waldner M, Obenauf AC, et al. Spatiotemporal dynamics of intratumoral immune cells reveal the immune landscape in human cancer. *Immunity* (2013) 39:782–95. doi: 10.1016/j.immuni.2013.10.003

39. Losurdo A, Scirgolea C, Alvisi G, Brummelman J, Errico V, Di Tommaso L, et al. Single-cell profiling defines the prognostic benefit of CD39(high) tissue resident memory CD8+ T cells in luminal-like breast cancer. *Commun Biol* (2021) 4:1117. doi: 10.1038/s42003-021-02595-z

40. Pages F, Mlecnik B, Marliot F, Bindea G, Ou FS, Bifulco C, et al. International validation of the consensus immunoscore for the classification of colon cancer: a prognostic and accuracy study. *Lancet* (2018) 391:2128–39. doi: 10.1016/S0140-6736(18)30789-X

41. Galon J, Pages F, Marincola FM, Angell HK, Thurin M, Lugli A, et al. Cancer classification using the immunoscore: a worldwide task force. *J Transl Med* (2012) 10:205. doi: 10.1186/1479-5876-10-205

42. Angell HK, Bruni D, Barrett JC, Herbst R, Galon J. The immunoscore: colon cancer and beyond. *Clin Cancer Res* (2020) 26:332–9. doi: 10.1158/1078-0432.CCR-18-1851

43. Lal N, Beggs AD, Willcox BE, Middleton GW. An immunogenomic stratification of colorectal cancer: implications for development of targeted immunotherapy. *Oncoimmunology* (2015) 4:e976052. doi: 10.4161/2162402X.2014.976052

44. Sade-Feldman M, Yizhak K, Bjorgaard SL, Ray JP, de Boer CG, Jenkins RW, et al. Defining T cell states associated with response to checkpoint immunotherapy in melanoma. *Cell* (2018) 175:998–1013.e20. doi: 10.1016/j.cell.2018.10.038

45. Gupta PK, Godec J, Wolski D, Adland E, Yates K, Pauken KE, et al. CD39 expression identifies terminally exhausted CD8+ T cells. *PloS Pathog* (2015) 11:e1005177. doi: 10.1371/journal.ppat.1005177

46. Banchereau R, Chitre AS, Scherl A, Wu TD, Patil NS, de Almeida P, et al. Intratumoral CD103+ CD8+ T cells predict response to PD-L1 blockade. *J Immunother Cancer* (2021) 9:e002231. doi: 10.1136/jitc-2020-002231

47. Hsu CL, Ou DL, Bai LY, Chen CW, Lin L, Huang SF, et al. Exploring markers of exhausted CD8 T cells to predict response to immune checkpoint inhibitor therapy for hepatocellular carcinoma. *Liver Cancer* (2021) 10:346–59. doi: 10.1159/000515305

48. Nelson CE, Mills LJ, McCurtain JL, Thompson EA, Seelig DM, Bhela S, et al. Reprogramming responsiveness to checkpoint blockade in dysfunctional CD8 T cells. *Proc Natl Acad Sci U.S.A.* (2019) 116:2640–5. doi: 10.1073/pnas.1810326116

49. Kallies A, Zehn D, Utzschneider DT. Precursor exhausted T cells: key to successful immunotherapy? *Nat Rev Immunol* (2020) 20:128–36. doi: 10.1038/s41577-019-0223-7

50. Yost KE, Satpathy AT, Wells DK, Qi Y, Wang C, Kageyama R, et al. Clonal replacement of tumor-specific T cells following PD-1 blockade. *Nat Med* (2019) 25:1251–9. doi: 10.1038/s41591-019-0522-3

51. Wu TD, Madireddi S, de Almeida PE, Banchereau R, Chen YJ, Chitre AS, et al. Peripheral T cell expansion predicts tumour infiltration and clinical response. *Nature* (2020) 579:274–8. doi: 10.1038/s41586-020-2056-8

frontiers | Frontiers in Immunology

TYPE Original Research
PUBLISHED 21 September 2023
DOI 10.3389/fimmu.2023.1236595

OPEN ACCESS

EDITED BY
Shiki Takamura,
RIKEN Yokohama, Japan

REVIEWED BY
Toshiro Hirai,
Osaka University, Japan
Henrique Borges da Silva,
Mayo Clinic Arizona, United States

*CORRESPONDENCE
Heather D. Hickman
hhickman@mail.nih.gov

RECEIVED 08 June 2023
ACCEPTED 31 August 2023
PUBLISHED 21 September 2023

CITATION
Lujan RA, Pei L, Shannon JP, Dábilla N, Dolan PT and Hickman HD (2023) Widespread and dynamic expression of granzyme C by skin-resident antiviral T cells.
Front. Immunol. 14:1236595.
doi: 10.3389/fimmu.2023.1236595

Widespread and dynamic expression of granzyme C by skin-resident antiviral T cells

Ramon A. Lujan[1,2], Luxin Pei[1], John P. Shannon[1], Nathânia Dábilla[3], Patrick T. Dolan[3] and Heather D. Hickman[1*]

[1]Viral Immunity and Pathogenesis Unit, Laboratory of Clinical Immunology and Microbiology, National Institute of Allergy and Infectious Diseases (NIAID), National Institutes of Health (NIH), Bethesda, MD, United States, [2]School of Nursing, Duke University, Durham, NC, United States, [3]Quantitative Virology and Evolution Unit, Laboratory of Viral Diseases, NIAID, NIH, Bethesda, MD, United States

After recognition of cognate antigen (Ag), effector CD8$^+$ T cells secrete serine proteases called granzymes in conjunction with perforin, allowing granzymes to enter and kill target cells. While the roles for some granzymes during antiviral immune responses are well characterized, the function of others, such as granzyme C and its human ortholog granzyme H, is still unclear. Granzyme C is constitutively expressed by mature, cytolytic innate lymphoid 1 cells (ILC1s). Whether other antiviral effector cells also produce granzyme C and whether it is continually expressed or responsive to the environment is unknown. To explore this, we analyzed granzyme C expression in different murine skin-resident antiviral lymphocytes. At steady-state, dendritic epidermal T cells (DETCs) expressed granzyme C while dermal γδ T cells did not. CD8$^+$ tissue-resident memory T cells (T_{RM}) generated in response to cutaneous viral infection with the poxvirus vaccinia virus (VACV) also expressed granzyme C. Both DETCs and virus-specific CD8$^+$ T_{RM} upregulated granzyme C upon local VACV infection. Continual Ag exposure was not required for maintained T_{RM} expression of granzyme C, although re-encounter with cognate Ag boosted expression. Additionally, IL-15 treatment increased granzyme C expression in both DETCs and T_{RM}. Together, our data demonstrate that granzyme C is widely expressed by antiviral T cells in the skin and that expression is responsive to both environmental stimuli and TCR engagement. These data suggest that granzyme C may have functions other than killing in tissue-resident lymphocytes.

KEYWORDS

granzymes, antiviral immunity, unconventional T cells, poxvirus, microscopy

Introduction

Granzymes are a family of serine proteases that are expressed by both innate and adaptive cytotoxic lymphocytes (1–3). There are 11 granzymes in mice (A-G, K-N) and 5 granzymes in human (A, B, H, K, M). Granzymes A and B have been the most extensively studied of the family, primarily in the context of killing infected or neoplastic cells (4).

However, there are several family members, including granzyme C in mice and granzyme H in humans, with currently unknown function(s) (5).

Granzymes are expressed by different innate and adaptive immune cells, with unique cellular populations expressing different granzymes. Granzymes A and B are highly expressed by cytotoxic effector cells, including T cells and natural killer (NK) cells (6). Murine $CD8^+$ T cells can also express Granzyme K, which has been associated with inflammatory aging (7). Human $CD8^+$ T cells produce granzyme K in inflamed tissues (8). Human NK cells have been demonstrated to translate high levels of granzymes H and M in certain conditions (9, 10). Mouse $CD4^+$ and $CD8^+$ T cells synthesize granzyme C primarily *in vitro* or in the context of mixed lymphocyte reactions (2, 11, 12). Recently, mouse granzyme C was shown to be constitutively expressed by cytolytic group 1 innate lymphoid cells (ILC1s) in the liver and salivary gland (13). Thus, the unique tissue environments and cellular functions of lymphocytes support the differential expression of granzyme family members.

Mechanistically, granzymes have been shown to function primarily during cytolysis. Cytotoxic lymphocytes recognizing cognate Ag form an immune synapse and directionally secrete granzymes toward target cells along with the pore-forming protein perforin (14). Perforin/granzyme secretion is critical for the control of some viral infections, including ectromelia virus (mousepox) and lymphocytic choriomeningitis virus (LCMV) (15, 16). However, numerous studies have now demonstrated that granzymes possess non-canonical activities as well (6, 17). For example, $CD8^+$ T cells and NK cells use granzyme B independently from perforin to extravasate into the tissues and traffic to sites of infection *in vivo* (18). Granzyme B can degrade extracellular matrix proteins and may affect various physiological processes such as basement membrane degradation, collagen disorganization, and wound healing (18–20). Additionally, granzyme A can reach high levels in human serum during infection with human immunodeficiency virus (HIV), Epstein-Barr virus (EBV), and Chikungunya virus (CHIKV) (6). Exogenously produced granzyme K can induce inflammation in non-lymphoid cells such as fibroblasts and activate endothelial cells (7, 21). Thus, granzymes can remodel the tissue environment through their protease activity.

In addition to granzyme C function, the regulation of its expression is also unknown. Some ILC1s constitutively produce granzyme C *in vivo* (13). ILC1s do not express the rearranged Ag receptors of adaptive lymphocytes, suggesting that factors other than Ag recognition might drive granzyme C production. Granzyme C expression may be developmentally hard-wired in some cells, or it may occur in response to changes in the local environment. Here, we sought to understand 1) whether ILC1s are the only tissue-resident lymphocytes that express granzyme C and 2) what factors regulate granzyme C expression. To do this, we analyzed granzyme C expression in different T cell populations present in the mouse skin: activated effector $CD8^+$ T cells, tissue-resident memory (T_{RM}) $CD8^+$ T cells, and γδ T cells. Although the level and frequency of granzyme C expression varied, a percentage of each skin-resident T cell population expressed granzyme C. Interestingly, skin-resident γδ T cells and $CD8^+$ αβ T_{RM} expressed granzyme C at steady-state and upregulated granzyme C following primary or secondary infection. Exposure to cognate Ag in the absence of virus-driven inflammation also increased granzyme C expression in $CD8^+$ αβ T_{RM}. However, a proportion of $CD8^+$ αβ T cells maintained granzyme C expression in the skin in an Ag-independent manner. Furthermore, IL-15 administration led to granzyme C upregulation in skin-resident T cells. Thus, the local tissue environment also modulates granzyme C expression in antiviral T cells. These results provide insight into the regulation of expression of granzyme C during antiviral immune responses and suggest a more ubiquitous function for granzyme C than the killing of virus-infected cells.

Results

Gamma-delta T cells express granzyme C in the epidermis at steady-state

Gamma-delta T cells seed tissues perinatally and can protect against murine poxvirus infection (22, 23). In the skin, $V\gamma5^+$ dendritic epidermal T cells (DETCs) and $V\gamma4^+/V\gamma6^+$ γδ T cells occupy the epidermis and dermis, respectively (24, 25). We first analyzed granzyme C expression in both populations using flow cytometry of single-cell suspensions of dissociated skin from wild-type C57BL/6 mice (Figures 1A–D). Prior to tissue harvest, we injected a CD45.2-specific antibody (Ab) intravenously (IV) to identify and exclude cells circulating in the vasculature from analysis, as previously described (26). We first gated on CD45.2 IV^-, $CD45^+$, $CD3^+$ lymphocytes and used Vγ5 TCR staining to identify TCR $\gamma\delta^+$ DETCs (with dermal γδ T cells being Vγ5 TCR^-) (Figure 1A). At steady-state in naïve, specific pathogen-free C57BL/6 mice, from 15 to 35% of DETCs expressed granzyme C (Figure 1B). Conversely, we did not observe significant frequencies or numbers of granzyme C-expressing dermal γδ T cells (Figures 1B, C). Likewise, DETCs expressed significantly higher levels of granzyme C per cell than the few positive dermal γδ T cells, determined by the mean fluorescent intensity (MFI) of intracellular granzyme C staining (Figure 1D). As tissue-resident cells can be perturbed by the enzymatic digestion needed to liberate them for flow cytometry (27), we also examined γδ T cells using confocal microscopy of frozen cross-sections of the ear skin (Figure 1E). Confocal images corroborated our flow cytometry findings, with a subset of DETCs expressing granzyme C in the epidermis. Interestingly, we often detected granzyme C localized to the dendritic cellular extensions between epidermal keratinocytes (Figure 1E). Thus, even naïve, specific-pathogen free mice have granzyme C-expressing skin-resident lymphocytes.

Gamma-delta T cells increase granzyme C expression during VACV skin infection

Gamma-delta T cells upregulate IFN-γ, granzymes A and B, and perforin during viral infection or in response to PAMPs (28–30). To understand the kinetics of granzyme C expression by DETCs and dermal γδ T cells during VACV infection, we first characterized the

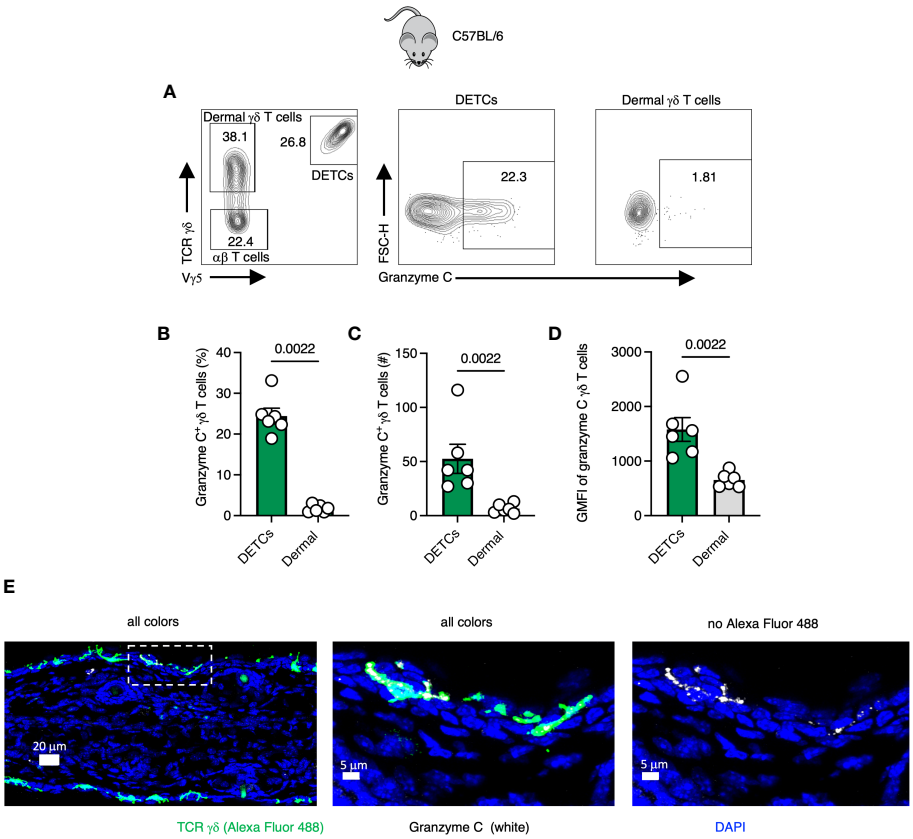

FIGURE 1
Gamma-delta T cells express granzyme C in the epidermis at steady-state. **(A)** Flow cytometry plots of cutaneous T cells isolated from sex- and age-matched naïve specific-pathogen free C57BL/6 mice. Cells were gated on CD45$^+$ CD45.2 IV$^-$ CD3$^+$. DETCs were gated on CD45$^+$ CD45.2 IV$^-$ CD3$^+$ TCRγδ$^+$ Vγ5$^+$. Dermal γδ T cells were gated on CD45$^+$ CD45.2 IV$^-$ CD3$^+$ TCRγδ+ Vγ5–. **(B–D)** Percentages, numbers, and mean florescence intensities (MFI) of granzyme C in γδ T cells. Dots represent individual ears. Error bars show the SEM. Results are representative of 3 experiments with 3 mice/group. Statistics = Mann-Whitney tests. **(E)** Confocal images of frozen cross-sections of uninfected ear skin from naïve specific-pathogen free C57BL/6 mice. Boxed area is magnified in panels to the right. Scale bars represent 20 µm (left panel), 5 µm (middle panel), and 5 µm (right panel). Images are representative of at least 3 images taken from 3 mice.

γδ T cell response in the skin. We infected C57BL/6 mice with VACV-SIINFEKL (expressing a minigene containing residues 257-264 of ovalbumin) in the ear pinna using a bifurcated needle as previously described (31–33). We used VACV as a viral infection model because this virus infects cells in both the epidermis and dermis where DETCs and dermal γδ T cells reside, respectively (Figure S1). We analyzed the single-cell suspensions generated from VACV-infected ears at 0-, 1-, 3-, and 5- days post-infection (dpi) (Figures S1C–G). Flow cytometry results revealed that the frequency of DETCs and dermal γδ T cells amongst total leukocytes in the skin decreased significantly at 5 dpi (Figures S1D–E). Nevertheless, the total number of DETCs and dermal γδ T cells was significantly higher at 5 dpi (Figures S1F–G). Thus, both DETCs and dermal γδ T cells in the skin expand in number during VACV infection but constitute a smaller frequency of CD45$^+$ CD3$^+$ lymphocytes as new T cells are recruited into the skin.

We next analyzed granzyme C expression in both γδ T cell populations after infection (Figures 2A–F). We observed the highest average frequency of granzyme C$^+$ DETCs on 5 dpi (~36% compared to ~27% in naïve tissue) (Figure 2C). In contrast, the highest frequency of granzyme C$^+$ dermal γδ T cells was observed on 1 dpi (5.4 ± 0.81% compared to 3.05 ± 0.71% in naïve tissue) (Figure 2D). DETCs expressed more granzyme C per cell than dermal γδ T cells, with the highest granzyme C MFI on 5 dpi (Figure 2E). Dermal γδ T cells did not increase granzyme C expression levels by MFI during VACV infection (Figure 2F). These data show that epidermal DETCs are the only cutaneous γδ T cell population to upregulate granzyme C during local VACV infection.

We also analyzed the frequencies and numbers of endogenous TCR αβ CD8$^+$ T cells that had entered the skin at the same timepoints post-VACV infection (Figures S2A–F). At 5 dpi a significant number of CD8$^+$ T cells, defined as CD45.2 IV$^-$, CD45$^+$, CD3$^+$, Vγ5$^-$, TCR γδ–, CD8β$^+$, TCRβ$^+$, were recruited to the infected skin (Figures S2A–C). Few CD8$^+$ T cells expressed granzyme C at this timepoint and the frequency of expression was not increased by infection (Figures S2D–F). Together, these data show that epidermal DETCs specifically respond to cutaneous poxvirus infection with enhanced granzyme C production during the first 5 days post-infection.

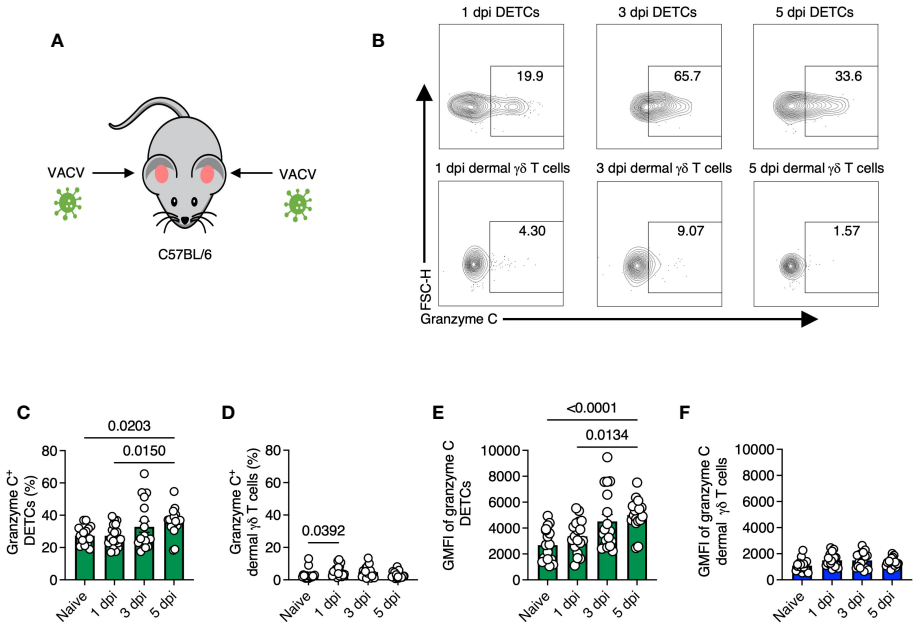

FIGURE 2
Gamma-delta T cells maintain granzyme C expression during VACV skin infection. **(A)** Diagram of experimental design. Ear pinna of sex- and age-matched C57BL/6 mice were infected epicutaneously with VACV-SIINFEKL. **(B)** Flow cytometry plots of cutaneous γδ T cells isolated from ear pinna of C57BL/6 mice at 1-, 3- 5-dpi with VACV-SIINFEKL. DETCs were gated on $CD45^+$ CD45.2 IV^- $CD3^+$ $TCR\gamma\delta^+$ $V\gamma5^+$. Dermal γδ T cells were gated on $CD45^+$ CD45.2 IV^- $CD3^+$ $TCR\gamma\delta^+$ $V\gamma5^-$. **(C–F)** Percentages and MFIs of granzyme C in γδ T cells at indicated dpi. MFIs were determined from the entire population (not granzyme C^+ cells). Dots represent individual ears. Error bars show SEM. Statistics = Kruskal-Wallis tests. Data are pooled from 3 experiments with 3 mice/timepoint.

Tissue-resident memory $CD8^+$ T cells express granzyme C in the skin at steady-state

We next analyzed $CD8^+$ T_{RM} in the skin, another epidermal lymphocyte population with notable antiviral activity (34, 35). We infected mice with VACV-SIINFEKL and allowed for the endogenous polyclonal VACV-specific $CD8^+$ T cell response to develop and T_{RM} to form (36). On 28 dpi or greater, we harvested skin, generated single-cell suspensions via enzymatic digestion, and analyzed the frequency of granzyme C expressing T cells using flow cytometry (Figures 3A–F). We first gated on $CD45^+$, CD45.2 IV^-, $CD8\beta^+$ cells. Both CD103 and CD69 are commonly used as tissue residency markers to identify T_{RM} in the skin (37). Therefore, we classified $CD8^+$ T cells in the skin based on CD103 and CD69 expression and analyzed granzyme C expression in each population (Figures 3B–F). $CD69^+$ $CD103^+$ T_{RM} had the highest frequency of granzyme C expression at approximately 54% of the population. Cells that did not express either CD69 or CD103 had the lowest frequency of granzyme C expression at 11.8 ± 1.5%. We also analyzed granzyme C expression in $CD62L^+$ $CD44^+$ central memory T cells in the cervical lymph node and spleen. These non-tissue-resident memory $CD8^+$ T cells scantly expressed granzyme C (Figures S3A–C). Furthermore, circulating $CD62L^+$ $CD44^-$ naïve, $CD62L^+$ $CD44^+$ central memory, and $CD62L^-$ $CD44^+$ effector memory $CD8^+$ T cell subsets expressed little granzyme C (Figures S3D–F).

As before, we verified granzyme C expression using confocal imaging. For these experiments, we first transferred 1 x 10^4 dsRed-expressing OT-I TCR transgenic $CD8^+$ T cells (recognizing K_b-SIINFEKL) into *Cd8a*$^{-/-}$ mice (deficient in $CD8^+$ αβ T cells) to allow easy microscopic visualization of T_{RM} cells in the skin. In contrast to DETCs, we detected OT-I $CD8^+$ T cells that expressed granzyme C in both the dermis and epidermis at 28 dpi (Figure 3G). We next quantified granzyme C expression in dermal and epidermal OT-I T_{RM} using confocal microscopy (Figure S4A). Both dermal and epidermal cells expressed similar levels of granzyme C based on the quantified intensity of granzyme C fluorescence per cell (Figures S4B–C).

To complement our confocal and flow cytometric analyses of granzyme C protein expression, we performed single-cell RNAseq on OT-I $CD8^+$ T_{RM} isolated from the skin (Figure S5). At the mRNA level, approximately 12% of *Cd3e*$^+$ cells also expressed detectable message for granzyme C. OT-I $CD8^+$ T cells expressing *Gzmc* also co-expressed *Cd69* and *Itgae* (CD103), consistent with our flow cytometry data. Other additional transcripts that were highly co-expressed with *Gzmc* included *Gzmb, Il2rb, Ifng*, and *Prf1* (perforin).

Together these data show that granzyme C is expressed by resting $CD8^+$ T_{RM} in mouse skin.

OT-I $CD8^+$ T_{RM} upregulate granzyme C during secondary VACV infection

We next examined whether VACV-specific T_{RM} would, like DETCs, upregulate granzyme C during VACV infection, or whether

10.3389/fimmu.2023.1236595

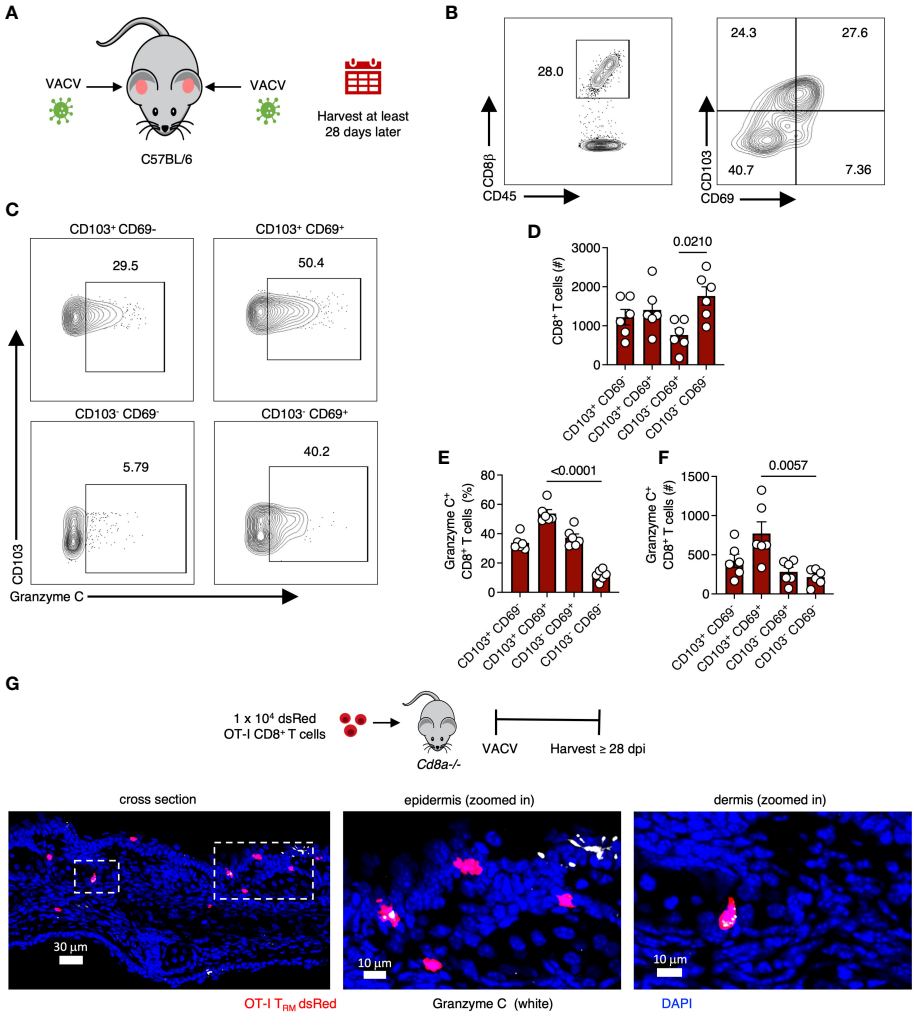

FIGURE 3
VACV-specific CD8$^+$ T cells express granzyme C in the skin. **(A)** Diagram of VACV-SIINFEKL infection model to establish CD8$^+$ T_{RM} in the ear pinna of age- and sex- matched C57BL/6 mice. Mice were infected using a bifurcated needle in the ear pinna with VACV-SIINFEKL. T_{RM} were allowed to develop for at least 28 dpi. **(B)** Flow cytometry plots of cutaneous CD8$^+$ T cells. Cells were gated on CD45$^+$ CD45.2 IV$^-$ CD8β$^+$. **(C)** Flow cytometry plots showing cutaneous granzyme C$^+$ CD8$^+$ T cells. CD8$^+$ T cells were gated into four quadrants as shown based on the differential expression of CD103 and CD69. **(D)** Total number of CD8$^+$ T cells based on differential expression of CD103 and CD69. Dots represent individual ears. Error bars show SEM. Statistics = Kruskal-Wallis tests. Results are representative of 3 independent experiments with 3 mice/group. **(E, F)** As in **(D)** but percentages and numbers of granzyme C$^+$ CD8$^+$ T cells based on the differential expression of CD103 and CD69. **(G)** Confocal images of frozen cross-sections of ear skin of *Cd8a*$^{-/-}$ mice that received 1 x 10^4 dsRed OT-I CD8$^+$ T cells prior to epicutaneous infection with VACV-NP-S-eGFP (containing SIINFEKL). Images were acquired at 28 dpi. Boxed areas are magnified in panels to the right. Scale bars represent 30 µm (left panel), 10 µm (middle panel), and 10 µm (right panel). Images are representative of at least 5 images taken from 2 mice.

this was a specific feature of γδ T cells. For these experiments, we continued analyses of CD103$^+$ CD69$^+$ VACV-specific CD8$^+$ T_{RM} in the skin (37). On 28 dpi or greater, we reinfected the ear pinna of mice with the same VACV that was used for initial infection and analyzed T cells on day 2 post-reinfection (Figures 4A–C). Secondary infection increased both the frequency and expression level (MFI) of granzyme C in T_{RM} compared to T_{RM} from mice only infected once (Figures 4D–F). Secondary infection also increased the frequency and expression level of granzyme B- and IFN-γ -producing T_{RM} (Figures 4G–J). Together, these data demonstrate that CD8$^+$ T_{RM} upregulate granzyme C (along with known effector molecules) during re-exposure to VACV.

OT-I CD8$^+$ T_{RM} maintain granzyme C expression in an Ag-independent manner

Although our data thus far suggested that granzyme C can be upregulated in some antiviral T cells during viral infection, it was unclear whether this was a response to recognition of cognate Ag or inflammation induced by infection. To test whether Ag sensing in the tissue was needed for increased granzyme C expression, we again transferred 1 x 10^4 naïve OT-I CD8$^+$ T cells into *Cd8a*$^{-/-}$ mice. We then infected one ear with VACV-NP-S-eGFP (expressing a fusion protein consisting of the nucleoprotein from influenza virus, the SIINFEKL OT-I CD8$^+$ T cell

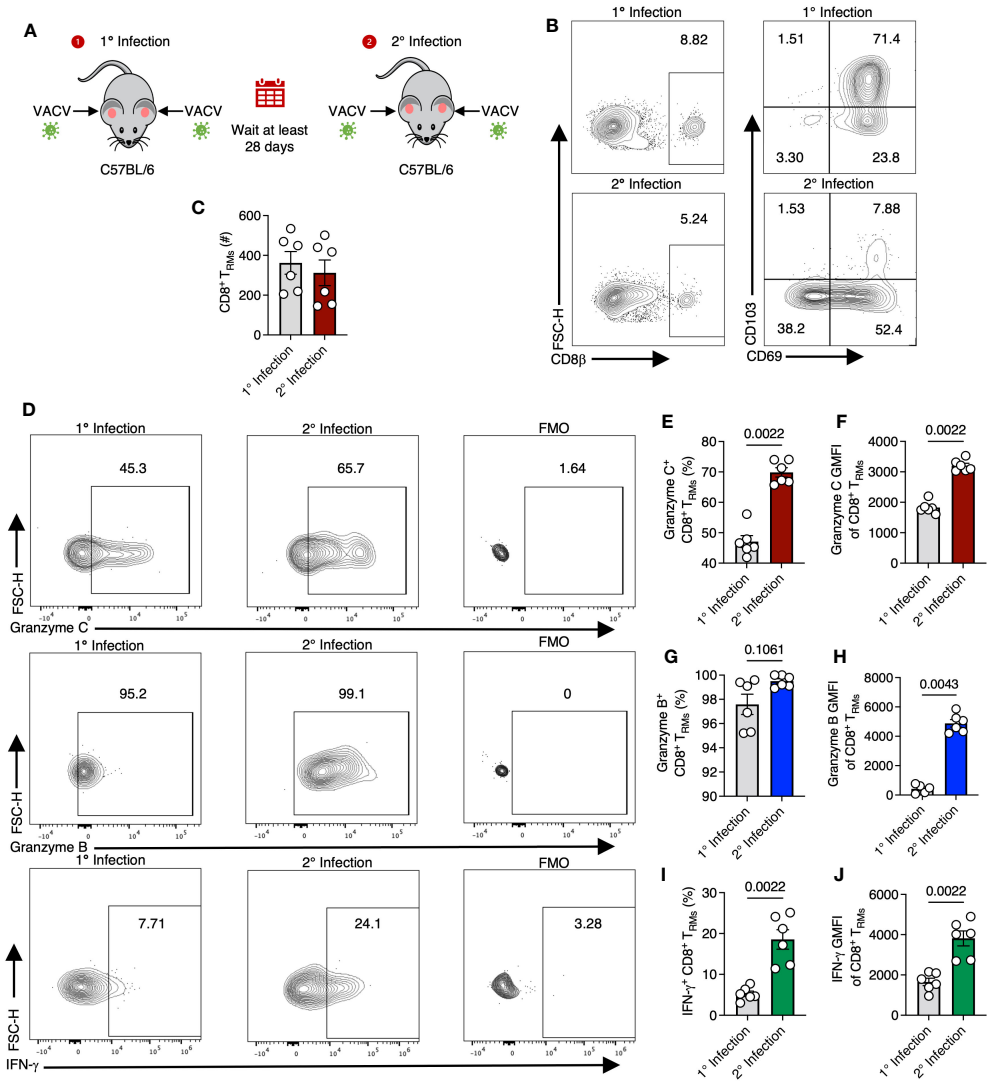

FIGURE 4
T_{RM} upregulate granzyme C during secondary VACV infection. **(A)** Diagram depicting primary and secondary infection with VACV. C57BL/6 mice were epicutaneously infected in both ears with VACV-SIINFEKL. At least 28 days later, mice were reinfected epicutaneously with the same virus. Ears were removed for analyses on day 2 after secondary infection. **(B)** Flow cytometry plots of cutaneous $CD8^+$ T cells after primary or secondary infection with VACV-SIINFEKL. Initial gating was on $CD45^+$ CD45.2 IV^- cells. **(C)** Total number of $CD8^+$ T_{RM} cells gated as $CD45^+$ CD45.2 IV^- $CD8\beta^+$ $CD103^+$ $CD69^+$. Dots show individual ears. Error bars show SEM. Statistics = Mann-Whitney test. Results are representative of 1 experiment of 3 with 3 mice/group. **(D)** Flow cytometry plots showing staining for granzyme C (top panels), granzyme B (middle panels), and IFN-γ (bottom panels) in cutaneous $CD8^+$ T_{RM} during initial (left panels) or secondary (right panels) VACV infection and corresponding FMOs. **(E–J)** As in **(C)** but percentages and MFIs of $CD8^+$ T_{RM} expressing granzymes C, B, and IFN-γ.

determinant, and eGFP) and the other ear with VACV-NP-eGFP (an identical virus that lacks SIINFEKL) as previously described (32) (Figure 5A). On 7-, 14-, 21-, and 28- dpi, we removed each ear (keeping them separate), created single-cell suspensions, and analyzed cells via flow cytometry (Figures 5B–F). The number of OT-I $CD8^+$ T cells per ear were similar between ears infected with virus expressing or lacking cognate Ag on days 7 and 14 dpi (Figure 5C). On 21 and 28 dpi, we noted a significant increase in the number of OT-I $CD8^+$ T cells in the ears infected with VACV-NP-S-eGFP compared to the ears infected with VACV lacking cognate Ag, consistent with previous reports (38) (Figure 5C). Granzyme C expression was detectable in OT-I $CD8^+$ T cells in the skin by 7 dpi and occurred in T cells present in ears lacking cognate Ag expression (Figures 5D–F). Over time, granzyme C expression was maintained in ears lacking cognate Ag expression, although frequencies of granzyme C^+ OT-I $CD8^+$ T cells were slightly higher in ears containing cognate Ag. Accordingly, there were higher numbers of OT-I $CD8^+$ T cells expressing granzyme C in the ears containing cognate Ag at 21 and 28 dpi (Figure 5F). These data show that $CD8^+$ T cells do not require cognate Ag expression in the skin to produce granzyme C; however, cognate Ag may bolster expression.

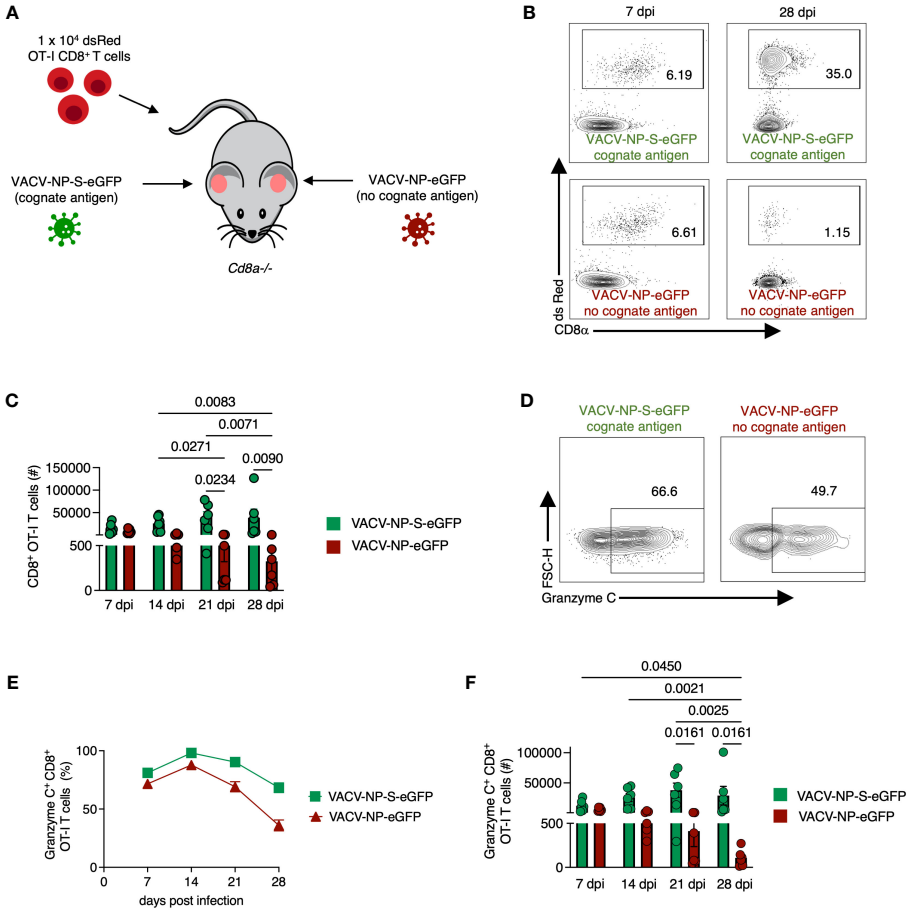

FIGURE 5
CD8$^+$ OT-I T cells recruited to the skin express granzyme C in an antigen-independent manner. **(A)** Experimental design. *Cd8a*$^{-/-}$ mice received 1 x 10^4 dsRed OT-I CD8$^+$ T cells prior to epicutaneous infection in one ear with VACV-NP-S-eGFP (expressing the cognate Ag SIINFEKL) and the other ear with VACV-NP-eGFP (no cognate Ag). Ears were harvested at various times post-infection to examine granzyme C expression in ears with or without cognate Ag expression. **(B)** Flow cytometry plots of cutaneous dsRed OT-I CD8$^+$ T cells at 7 dpi and 28 dpi isolated from separate ears infected with VACV-NP-S-eGFP (with cognate Ag) or VACV-NP-eGFP (no cognate Ag). Cells initially gated as CD45$^+$ CD45.2 IV$^-$. **(C)** Numbers of OT-I CD8$^+$ T cells present in ears infected with VACV-NP-S-eGFP (with cognate Ag, green bars) or VACV-NP-eGFP (no cognate Ag, red bars) at 7-, 14-, 21-, and 28-dpi. OT-I CD8$^+$ T cells were gated as CD45$^+$ CD45.2 IV$^-$ dsRed$^+$ CD8α^+. Dots represent individual ears. Error bars show SEM. Pooled data are shown from 2 independent timecourse experiments with 3 mice/group. Statistics = Kruskal-Wallis tests. **(D)** Flow cytometry plots of dsRed OT-I CD8$^+$ T cells at 28 dpi gated on granzyme C. **(E, F)** As in **(C)** but frequencies and numbers of granzyme C$^+$ dsRed OT-I CD8$^+$ T cells on the indicated dpi.

OT-I CD8$^+$ T_{RM} upregulate granzyme C in response to both viral infection and TCR engagement

Although cognate Ag was not needed for continued granzyme C expression, we next queried whether TCR engagement during secondary infection could upregulate granzyme C. As before, we transferred 1 x 10^4 naïve OT-I CD8$^+$ T cells into *Cd8a*$^{-/-}$ mice and infected both ears with VACV-NP-S-eGFP (containing cognate Ag) to establish OT-I CD8$^+$ T_{RM} in both ears under the same conditions. Beyond 28 dpi, we reinfected one ear with VACV-NP-S-eGFP and the other ear with VACV-NP-eGFP (lacking cognate Ag) (Figure 6A). Flow cytometric analysis revealed no statistical difference in the frequency of granzyme B and C expressing CD8$^+$ T_{RM} in the skin during secondary infection in the presence or absence of cognate Ag (Figures 6B–E). Granzyme A expression, however, trended toward increased expression in the absence of cognate Ag (Figures 6B, C). Thus, viral infection alone can drive the upregulation of granzyme C in CD8$^+$ T_{RM}.

In the converse experiment, we assessed whether cognate Ag alone could drive upregulation of granzyme C (without virus-induced inflammation). After the establishment of OT-I CD8$^+$ T_{RM}, we injected SIINFEKL peptide intravenously and harvested the ear pinna 6 hours post-injection (Figure 6F). Flow cytometric analyses revealed significant upregulation of granzyme C$^+$ OT-I CD8$^+$ T_{RM} after peptide injection (Figures 6G–J). The frequency of granzyme B$^+$ T_{RM} also increased even more dramatically, while granzyme A remained relatively unchanged. Together, these data suggest granzyme C can be upregulated by both virally induced inflammation or TCR stimulation in the absence of other inflammatory stimuli. Furthermore, they reveal differential regulation of specific granzyme expression in response to different stimulation.

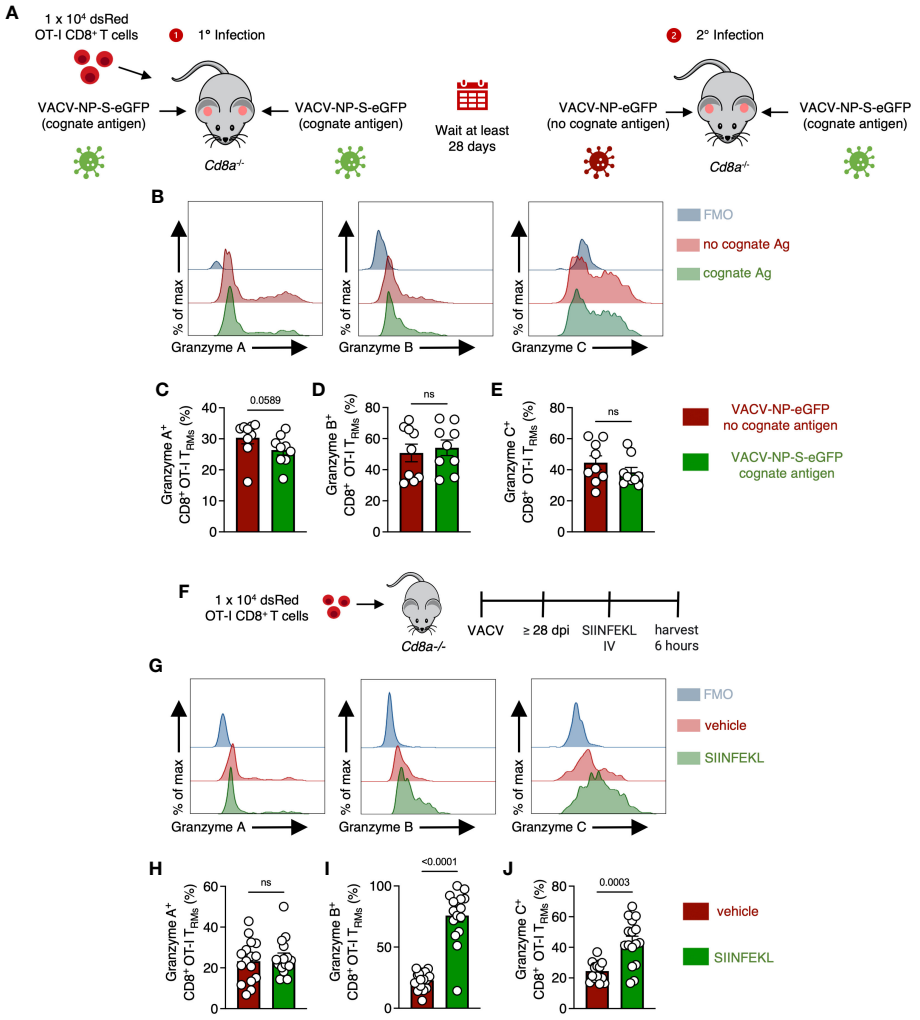

FIGURE 6
OT-I CD8$^+$ T_{RM} can upregulate granzyme C in response to either viral infection or cognate Ag. **(A)** Experimental design. *Cd8a*$^{-/-}$ mice received 1 x 10^4 dsRed OT-I CD8$^+$ T cells prior to epicutaneous infection in both ears with VACV-NP-S-eGFP (expressing the cognate Ag SIINFEKL) to establish OT-I CD8$^+$ T_{RM}. At least 28 days later, mice were infected in one ear with VACV-NP-S-eGFP (expressing the cognate Ag SIINFEKL) and the other ear with VACV-NP-eGFP (no cognate Ag). Ears were removed for analyses on day 2 after secondary infection. **(B)** Overlaid histograms showing expression of granzymes A, B, and C along with corresponding FMOs in OT-I CD8$^+$ T_{RM} from ears expressing or lacking cognate antigen. OT-I CD8$^+$ T_{RMs} were gated as CD45.2 IV$^-$ CD45$^+$ CD8β$^+$ dsRed$^+$ CD69$^+$ CD103$^+$. **(C–E)** Frequencies of granzyme A$^+$ B$^+$ or C$^+$ OT-I CD8$^+$ T_{RM} from ears infected with either VACV-NP-S-eGFP or VACV-NP-eGFP. Dots represent individual ears. Error bars = SEM. Statistics = Mann-Whitney tests. Data are pooled from 2 experiments with 4 or 5 mice/group. **(F)** Experimental design. *Cd8a*$^{-/-}$ mice received 1 x 10^4 dsRed OT-I CD8$^+$ T cells prior to epicutaneous infection in both ears with VACV-SIINFEKL. At least 28 days later, mice were IV injected with either SIINFEKL peptide or vehicle control and harvested 6 hours after injection. OT-I CD8$^+$ T_{RMs} were gated as CD45.2 IV$^-$ CD45$^+$ CD8β$^+$ dsRed$^+$ CD69$^+$ CD103$^+$. **(G)** As in **(B)** but histograms of granzymes A, B, and C between mice treated with SIINFEKL peptide or vehicle control. **(H–J)** As in **(C–E)** but frequencies of granzyme A$^+$, B$^+$, or C$^+$ OT-I CD8$^+$ T_{RM} between mice having received SIINFEKL peptide or vehicle control. Dots represent individual ears. Error bars = SEM. Statistics = Mann-Whitney tests. ns, not statistically significant. Data are pooled from 2 experiments with 4 mice/group.

Skin-resident T cells upregulate granzyme C in response to IL-15 administration

We next explored whether local cytokine changes could promote granzyme C expression in the absence of cognate Ag recognition. The cytokine IL-15 is induced during many acute viral infections and is important for tissue-resident lymphocyte maintenance (39, 40). *In vitro*, IL-15 upregulates granzyme C expression in isolated liver ILC1s (13). We therefore explored whether *in vivo* treatment with IL-15 alone could induce granzyme C expression. We first assessed the effect of IL-15 administration on DETCs. We intraperitoneally (IP) injected naïve wild-type C57BL/6 mice with exogenous IL-15 every 48 hr (three treatments) and harvested the ear pinna on day 7 (Figure 7A). Mice from the IL-15 treatment group had a higher number but not frequency of DETCs compared to the vehicle control (Figures 7B–D). DETCs in mice treated with IL-15 had an increased frequency of granzyme C expression and MFI compared to DETCs in mice receiving vehicle control (Figures 7E, F). IL-15 treatment also increased the expression level (MFI) and frequency of dermal γδ T cells expressing granzyme C, though this remained low compared to DETCs (Figure S6). Confocal imaging also revealed numerous granzyme C$^+$ DETCs in IL-15-treated mice (Figure 7G).

10.3389/fimmu.2023.1236595

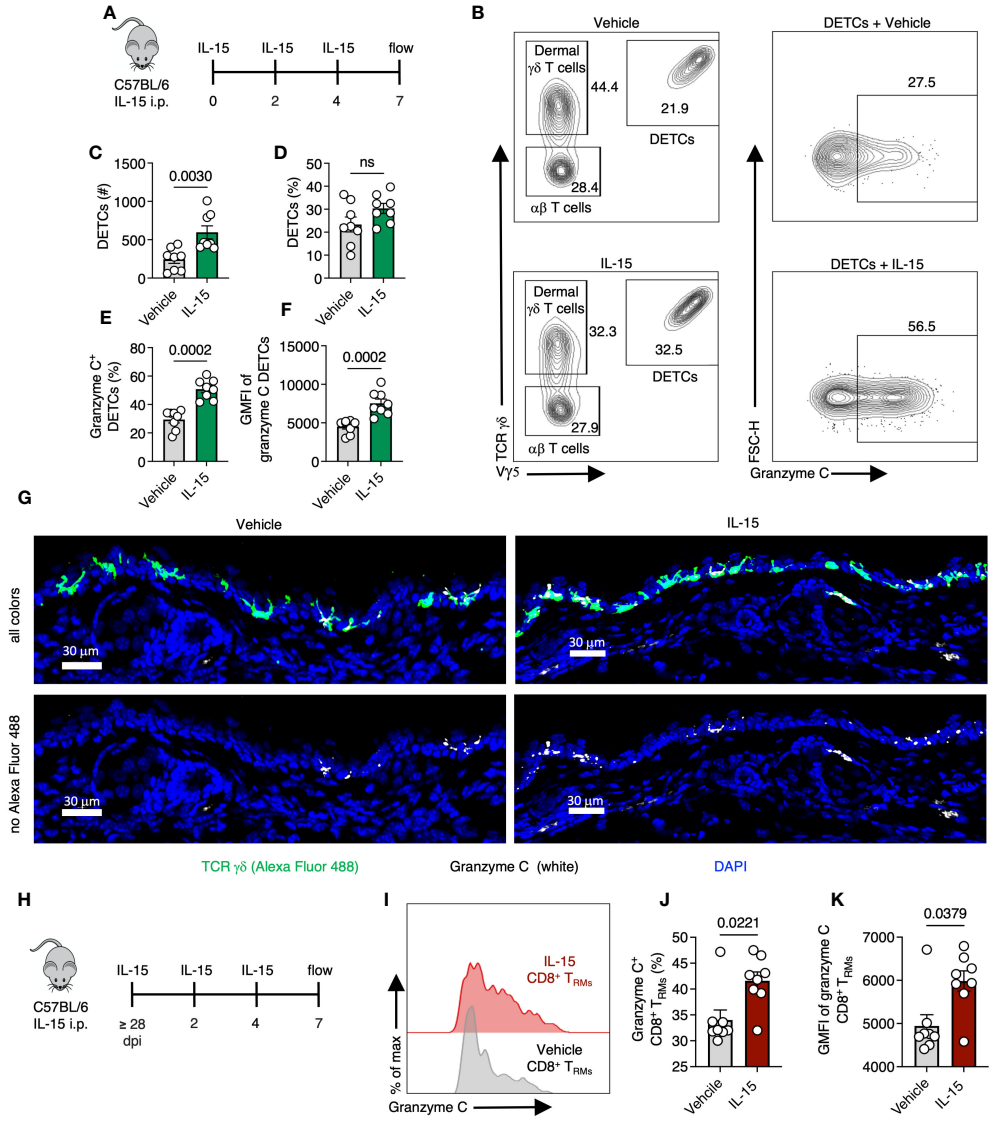

FIGURE 7
Skin-resident T cells upregulate granzyme C after IL-15 administration. **(A)** Experimental design. Naïve C57BL/6 mice were injected IP with 5 µg of recombinant IL-15 every 48 hr (three treatments). Ear pinna were harvested on day 7 post-treatment. **(B)** Flow cytometry plots of cutaneous T cells from C57BL/6 mice either treated with IL-15 or vehicle control. Cells were gated on $CD45^+$ CD45.2 IV^- $CD3^+$. DETCs were gated on $CD45^+$ CD45.2 IV^- $CD3^+$ $TCR\gamma\delta^+$ $V\gamma5^+$. **(C, D)** Numbers and frequencies of DETCs isolated C57BL/6 mice either treated with IL-15 or vehicle control. Dots represent individual ears. Error bars = SEM. Statistics = Mann-Whitney tests. ns, not statistically significant. Data representative of 2 independent experiments with 4 mice/group. **(E, F)** As in **(C, D)** but frequencies of granzyme C^+ DETCs and MFIs of granzyme C in all DETCs in IL-15- or vehicle-treated mice. **(G)** Confocal images of frozen cross-sections of ears of naive C57BL/6 mice either treated with IL-15 or vehicle control. Top images show all colors green (TCR γδ AlexFluor 488), white (granzyme C), blue (DAPI-nuclear stain). Bottom images remove green (TCR γδ AlexFluor 488) channel to better reveal granzyme C signal (white). Scale bars represent 30 µm. Images are representative of at least 3 images taken from 3 mice/group. **(H)** Experimental design. Age- and sex- matched C57BL/6 mice were infected with VACV-SIINFEKL for at least 28 days for T_{RM} formation. At least 28 days post-infection, mice were injected IP with IL-15 every 48 hr. Ear pinna were harvested on day 7 post-treatment. **(I)** Overlaid histograms of granzyme C expression in $CD8^+$ T_{RM} in IL-15- or vehicle-treated mice. $CD8^+$ T_{RM} gated on CD45.2 IV^-, $CD45^+$, $CD3^+$, $V\gamma5^-$, TCR $\gamma\delta^-$, $CD8\beta^+$, $CD103^+$, $CD69^+$ cells. **(J, K)** Frequencies of granzyme C^+ $CD8^+$ T_{RM} and granzyme C MFIs in all T_{RM} between treatment groups. Dots represent individual ears. Error bars = SEM. Statistics = Mann-Whitney tests. Data representative of 2 independent experiments with 4 mice/group.

Having demonstrated exogenous IL-15 administration could upregulate granzyme C expression in skin-resident γδ T cells, we examined whether IL-15 would have the same effect in $CD103^+$ $CD69^+$ $CD8^+$ T_{RM}. As before, we infected C57BL/6 mice with VACV-SIINFEKL and allowed for the endogenous polyclonal VACV-specific $CD8^+$ T cell response to develop (36). On 28 dpi or greater, we administered IL-15 via IP injection as before, generated single-cell suspensions via enzymatic digestion from the ear pinna and analyzed the frequency of granzyme C-expressing T cells using flow cytometry (Figures 7H–K). Like the DETCs, IL-15 increased T_{RM} expression of granzyme C (in both frequency and MFI) compared to vehicle controls (Figures 7I–K). Thus, granzyme C expression is also cytokine responsive *in vivo*.

Discussion

Mice can express many different granzymes, some of which do not have established function or known immunological roles. One of these, granzyme C was recently identified as a definitive marker for mature antiviral ILC1s as these cells continually produce granzyme C in the liver (13). However, it was unknown if other antiviral lymphocytes express granzyme C and whether its expression is regulated *in vivo* by viral infection. Here, using flow cytometry, confocal microscopy, and single-cell RNA-seq, we demonstrate that different innate and adaptive antiviral T cell subsets express granzyme C in the skin. During homeostasis, some DETCs and most T_{RM} present in the epidermis expressed granzyme C. Poxvirus infection of the skin upregulated granzyme C production by both DETCs and T_{RM}. Interestingly, cognate Ag recognition in the tissue was not required for maintained granzyme C expression by TCR-transgenic OT-I $CD8^+$ T cells. Nonetheless, cognate Ag recognition enhanced granzyme C expression. Additionally, IL-15 treatment also enhanced granzyme C expression by DETCs and virus-specific T_{RM}. Together, our data reveal that granzyme C expression is more widespread than previously appreciated and is responsive to both environmental cues and TCR engagement.

An important question remains: what is the function of homeostatic granzyme C expression? Other studies have shown that granzyme C can be expressed without contact with tumor or virally infected cells, hinting at other roles for granzyme C besides the direct cytolysis of target cells. Most experiments examining granzyme C-mediated cytolysis have been performed *in vitro* (3, 11, 13, 41, 42). The most compelling *in vivo* data for granzyme C-mediated killing demonstrated that the constitutive activation of granzyme C^+ cells led to perforin-dependent lethality in uninfected neonatal mice (13). However, perforin knockout mice also succumbed to death in this model, albeit with a delay of several weeks. Furthermore, the crystal structure of granzyme C has revealed that this protease may be auto-inhibited under normal circumstances (43). Thus, the function of granzyme C may be multifactorial but remains unestablished.

There are demonstrated non-canonical roles for other granzymes. Some have been shown to play a pro-inflammatory role during infection. Granzymes A and B in humans and mice are produced at high levels during various viral infections including HIV, CHIKV, and EBV (6, 44, 45). In a mouse model of CHIKV infection, granzyme A promoted arthritic foot swelling but not viral clearance (45). Granzyme K is a marker of a unique age-associated $CD8^+$ T cell population in both humans and mice, which may induce fibroblast secretion the pro-inflammatory cytokines IL-6, CCL2, and CXCL1 (7). Granzyme C can be upregulated in mast cells activated with IL-33 (46).

Granzymes can also directly inhibit viruses via the cleavage of viral proteins (6). Murine granzyme B degrades the herpes simplex virus type 1 (HSV-1) immediate early protein ICP4 (needed for transcription of early and late viral genes) (47, 48). Granzyme M inhibits human cytomegalovirus (HCMV) replication through the cleavage of the viral protein pp71 (49). Additionally, granzyme H, the human ortholog of granzyme C, can cleave DNA-binding protein and the granzyme B-inhibiting 100k assembly protein of adenovirus (50). Future studies will be needed to determine whether granzyme C also has direct antiviral effects through the degradation of specific viral proteins.

IL-15 is an important cytokine for tissue-resident antiviral protection. DETCs, T_{RM}, and ILC1s all reside in barrier epithelia, and all require IL-15 for their development and/or maintenance (25, 51–53). Originally identified as a T cell proliferation factor, IL-15 can be expressed throughout the body by antigen-presenting cells (APCs), bone-marrow stromal cells, and epithelial lineages such as human and mouse epidermal keratinocytes (54–57). IL-15 is expressed as both soluble and trans-presented forms, the latter of which is thought to represent the most physiologically relevant form of the cytokine (58). During IL-15 trans-presentation, IL-15 is bound to the IL-15 receptor α (IL-15Rα) and traffics to the cell surface as an IL-15/IL-15Rα complex (58). Stimulation by IL-15 therefore requires contact between the recipient cells and IL-15/IL-15Rα trans-presenting cell (59). We show here that IL-15 upregulates granzyme C expression in tissue-resident lymphocytes *in vivo*. IL-15 may enhance granzyme C expression independent from its canonical function, for example as a consequence of cytokine-driven cellular expansion. Alternatively, granzyme C, a serine protease, may help to liberate this or other cytokines for use by tissue-resident lymphocytes. The unique positioning of DETCs within the epidermis and the expression of granzyme C along their dendritic extensions of DETCs might also suggest a strategy to distribute granzyme C as widely as possible in the epidermis.

Granzyme C upregulation after IL-15 stimulation suggests that granzyme C expression might serve as a surrogate to identify cells receiving IL-15 during homeostasis, infection, and inflammation. Interestingly, human granzyme K expression was identified as a feature of both γδ T cell and innate $CD8^+$ T cell subsets and is upregulated in response to cytokine stimulation rather than TCR stimulation (60). Our data reveal that a smaller percentage of DETCs express granzyme C than $CD8^+$ T_{RM}, at least at the timepoints we examined. This may reflect the recent development of T_{RM} in the epidermis and more recent IL-15 acquisition by T_{RM}. Interestingly, T_{RM} and DETCs exhibit different motility in the epidermis (35), which might cause differences in IL-15 acquisition as these cells perambulate through the keratinocytes.

Our data provide a framework for understanding granzyme C expression by antiviral lymphocytes in the skin. Rather than being developmentally programmed, granzyme C expression was dynamic and reflected the current tissue status. Given the functional versatility of granzymes, the deletion of granzyme C in select lymphocyte populations may disrupt viral clearance either through reduced lysis of virally infected cells or the inhibition/degradation of viral proteins. Alternatively, knocking out granzyme C may impair pro-inflammatory pathways or reduce the ability of lymphocytes to migrate through the dense tissue microenvironment. Although CRISPR editing is an attractive approach to knockout granzyme C expression in OT-I $CD8^+$ T_{RM}, granzyme gene homology will necessitate careful validation to ensure proper targeting of only granzyme C. Furthermore, this

approach could not be employed for other tissue-resident cells that are seeded embryonically or neonatally. Therefore, the creation of animal models deleting granzyme C expression will be required to fully unravel the role(s) of this enigmatic protease during antiviral immune responses. Nonetheless, the widespread increase in granzyme C expression in skin-resident lymphocytes in response to viral infection or cytokine stimulation suggests that this protease, like other granzymes, could be an important contributor to antiviral immunity in the tissue.

Materials and methods

Mice

Specific pathogen-free C57BL/6N mice were obtained from Taconic Farms. dsRed (Stock Tg(CAG-DsRed*MST)1Nagy/J, #5441); *Cd8a*$^{-/-}$ *(B6.129S2-Cd8a*^{tm1Mak}*/J*, #2665*)*; and albino C57BL/6 (B6(Cg)-*Tyr*$^{c-2J}$/J, #58) mice were obtained from Jackson Laboratories. *Rag1*$^{-/-}$ (Line 146); *Rag2*$^{-/-}$*Il2rg*$^{-/-}$ (Line 111); *T-betZsGreen* (Line 8419); and OT-I TCR transgenic (C57BL/6NAi-[Tg]TCR OT-1-[KO]RAG1, Line 175) mice were obtained from the NIAID Intramural Research Repository at Taconic Farms. dsRed mice were crossed with OT-I TCR transgenic mice to create dsRed OT-I mice. *Rag1*$^{-/-}$ mice were crossed with *T-betZsGreen* mice and bred to homozygosity to create *Rag1*$^{-/-}$ *T-betZsGreen* mice. *Cd8a*$^{-/-}$ mice were crossed with B6 albino mice and bred to homozygosity to create albino *Cd8a*$^{-/-}$ mice. 6- to 20-week-old male and female mice were used in experiments. All mice were maintained on standard rodent chow and water supplied as necessary. All animal studies were approved by and performed in accordance with the Animal Care and Use Committee of NIAID.

Microbe strains

Viruses used for this study included VACV-NP-S-eGFP (expressing a fusion protein consisting of influenza nucleoprotein, the SIINFEKL T cell determinant, and eGFP); VACV-NP-eGFP (an identical virus to VACV-NP-S-eGFP that lacks SIINFEKL); VACV-SIINFEKL (expressing residues 257-264 of ovalbumin). Recombinant VACV viruses were generated as TK^{-} viruses using the Western Reserve strain of VACV and have been previously described (32, 61).

Method details

Viral infections and enzymatic tissue dissociation

Mice were infected in the dorsal ear pinna as previously described (33, 62) with 5 pokes of a bifurcated needle dipped in VACV. VACV infection was performed with VACV-SIINFEKL (1 x 10^8 pfu), VACV-NP-S-eGFP (2.1 x 10^8 pfu), or VACV-NP-eGFP (2.4 x 10^8 pfu). At the indicated time, ears were harvested, separated into dorsal and ventral sides, diced, and digested in RPMI containing 7.5% fetal bovine serum (FBS), collagenase I (Worthington), DNAse (Worthington), and brefeldin A solution 1000x (Biolegend) at a 1:1000 dilution for 1 hr at 37°C. Spleens and cervical lymph nodes were harvested and homogenized using a pestle in RPMI containing 7.5% FBS and brefeldin A solution 1000x (Biolegend) at a 1:1000 dilution.

Blood collection and lymphocyte isolation

Prior to blood collection mice were IV injected with 200 µls of saline containing brefeldin A solution (Biolegend) at a 1:100 dilution. Mice were immediately placed under isoflurane anesthesia and blood was collected through terminal retro-orbital eye bleeds. BioWhittaker Lymphocyte Separation Medium (LSM) (Lonza) was then used to isolate lymphocytes.

Flow cytometry analyses

To distinguish IV^{+} cells, mice were injected with 3 µgs of pacific blue-conjugated CD45.2 (clone 104.2) intravenously as previously described 3 minutes prior to tissue isolation (63). Suspensions were filtered through 70 µm nylon cell strainers. Cells were stained with a combination of the following antibodies: CD45 (clone 30-F11), CD45.2 (clone 104), CD3 (clone 17A2), CD8β (clone H35-17.2 or YTS156.7.7), CD8α (clone 53-6.7), CD69 (clone H1.2F3), CD103 (clone 2E7), Vα2 (clone B20.1), TCRβ (clone H57-597), TCR γδ (clone GL3), Vγ5 (Tonegawa's nomenclature (clone 536)), granzyme A (GzA-3G8.5), granzyme B (clone 16G6 or NGZB), granzyme C (clone SFC1D8), IFN-γ (clone XMG1.2), Armenian Hamster IgG Isotype Control (clone HTK888), CD62L (clone MEL-14), CD44 (clone IM7) and fixable viability dyes (Zombie Aqua) from Biolegend, eBiosciences, Invitrogen, or BD Biosciences diluted in PBS and brefeldin A solution (Biolegend) at a 1:1000 dilution. Cells were fixed with 3.2% paraformaldehyde for 15 minutes and intracellular staining was done using 0.5% saponin in Hanks Balanced Salt Solution (HBSS) + 0.1% Bovine Serum Albumin (BSA) for 1 hr at room temperature. dsRed^{+} cells were identified based upon fluorescent protein expression. Cells were analyzed on a Fortessa flow cytometer (BD Biosciences) or 5L 16UV-16V-14B-10YG-8R Aurora (Cytek) and resultant data analyzed using FlowJo software (Treestar).

Drug and Peptide treatment

Recombinant murine IL-15 (PeproTech) was reconstituted in water and diluted in sterile saline solution prior to intraperitoneal (IP) injection of 5 µg/mouse every 48 hr for a total of 3 treatments. Ears were harvested 7 days after the start of the first treatment. SIINFEKL peptide (GenScript) was reconstituted in dimethyl sulfoxide (DMSO) and diluted in sterile saline solution prior to one time IV injection of 200 µg of peptide/mouse. Ears were harvested 6 hours after peptide injection.

Adoptive transfer of OT-I CD8$^+$ T cells

CD8$^+$ T cells were purified from spleens and lymph nodes using an EasySep Mouse CD8$^+$ T cell Isolation Kit (Negative Selection) according to the manufacturer's instructions (Stem Cell Technologies). Cells were naïve (CD69$^-$) (antibody information clone: H1.2F3) and > 90% pure by flow cytometry prior to IV transfer. Unless otherwise noted, mice received a standard dose of 1 x 10^4 OT-I CD8$^+$ T cells prior to infection.

Confocal microscopy of frozen tissue sections

Ears were removed on the indicated dpi, fixed in periodate-lysine-paraformaldehyde (PLP) for 24 hr, and moved to 30% sucrose/PBS solution for 24 hr. Ears were embedded in optimal-cutting-temperature (OCT) medium (Electron Microscopy Sciences) in cross-section orientation and frozen in dry-ice-cooled 2-methylbutane. 16-µm sections were cut on a Leica cryostat (Leica Microsystems), blocked with HBSS, 0.1% BSA, 10% bovine and donkey serum, 0.05% Triton X. Tissues were stained with a combination of the following antibodies: purified granzyme C (clone SFC1D8), Alexa Fluor 647 AffiniPure Goat Anti-Armenian Hamster IgG (H+L) or Alexa Fluor® 594 AffiniPure Goat Anti-Armenian Hamster IgG (H+L), purified Cytokeratin 6 (clone SP87), Alexa Fluor 647 AffiniPure Donkey Anti-Rabit IgG (H+L), conjugated Alexa Fluor 488 anti-mouse TCR γ/δ (clone GL3) antibody, and nuclei stained using DAPI from Biolegend, ThermoFisher, or Jackson ImmunoResearch. Antibodies were diluted in HBSS, 0.1% BSA, 10% bovine and donkey serum, 0.05% Triton X. Images were acquired on a Leica SP8 confocal microscope equipped with hybrid detectors or a Leica Stellaris 8.

Cell sorting and single-cell RNA-seq

Rag1$^{-/-}$ *T-betZsGreen* mice received 1 x 10^4 dsRed OT-I CD8$^+$ T cells prior to infection with VACV-SIINFEKL. At the indicated time post infection, mice were injected with 3 µgs of pacific blue-conjugated CD45.2 (clone 104.2) IV as previously described 3 minutes prior to tissue isolation to distinguish IV$^+$ cells (63). Ears were harvested, separated into dorsal and ventral sides, diced, and digested in RPMI containing 7.5% fetal bovine serum (FBS), collagenase I (Worthington), and DNAse (Worthington) for 1 hr at 37°C. Suspensions were filtered through 70 µm nylon cell strainers. Cells were stained with a combination of the following antibodies: CD45 (clone 30-F11), CD8α (clone 53-6.7) along with Zombie Aqua viability dye. Using a BD FACS Aria III Cell Sorter, OT-I CD8$^+$ T cells and Tbet-ZsGreen group I ILCs were sorted as Viability Dye$^-$ CD45.2 IV$^-$ CD45$^+$ dsRed$^+$ CD8α$^+$ or ZsGreen$^+$ cells, respectively, into RPMI containing 10% FBS and HEPES (25 mM). Cells were centrifuged and resuspended in RPMI containing 10% FBS and HEPES (25 mM) at a 1000 cells/µl concentration.

Single-cell RNA-seq library generation

Two technical replicates of the *Rag1*$^{-/-}$ *T-betZsGreen* ear samples were collected for single-cell RNA sequencing using Chromium Next GEM Single Cell 3' v3.1 standard kit (10X Genomics, Pleasanton, CA). Approximately 3000 cells were targeted in each single-cell preparation. For the preparation of the cDNA and sequencing library generation, libraries were prepared as described in the Chromium Next GEM Single Cell 3' Reagent Kit v3.1 (Dual Index) user guide to produce barcoded cDNA and perform Illumina sequencing library preparation.

Single-cell RNA-seq library sequencing, and analysis

The Illumina library quality was assessed by TapeStation D1000 high sensitivity reagent kit (Agilent, Santa Clara, CA), and DNA concentration was measured by Qubit High Sensitivity reagent kit (Thermo Fisher, Waltham, MA). Samples were diluted for sequencing and pooled equimolarly according to Illumina sequencing protocol to a final concentration of approximately 650 pM. Sequencing was performed NextSeq2000 instrument using two P3 200 cycle kits (Illumina, San Diego, CA) to target approximately 50,000 reads per cell.

After sequencing, the FastQ files were submitted to Cell Ranger 'count' and 'aggregate' functions. Sample *Rag1*$^{-/-}$ *T-betZsGreen* Ear_1 had 2,744 passing cells with 1,986 median genes per cell and *Rag1*$^{-/-}$ *T-betZsGreen* Ear _2 had 1,910 passing cells with 2,180 median genes per cell. Sequencing saturation for both libraries were 64.8% and 76.8%, respectively. After all quality control of the replicates, the expression of granzyme C and other genes were analyzed in the *Loupe* browser (10X Genomics, Pleasanton, CA).

Statistical analyses

Significances were assessed using Prism software (GraphPad) using a Kruskal-Wallis Test (3 or more groups) or unpaired two-tail Mann-Whitney test (2 groups) as indicated in the figure legends. Exact P values are shown throughout, statistical significance was set at $P \leq 0.05$.

Data availability statement

The raw data supporting the conclusions of this article will be made available by the authors, without undue reservation.

Ethics statement

The animal study was approved by the Animal Care and Use Committee of NIAID, NIH. The study was conducted in accordance with the local legislation and institutional requirements.

Author contributions

RL and HH conceived and designed the study. RL, PD, and HH analyzed the data. RL and HH drafted the manuscript. RL, LP, JS, and ND performed experiments. HH provided reagents, experimental expertise, and reviewed the manuscript. All authors contributed to the article and approved the submitted version.

Funding

RL is supported by a Dean's Graduate Fellowship, The Graduate School, Duke University and by an NIH Intramural Training Fellowship. HH and PD are funded by the Division of Intramural Research, NIAID, NIH. This work was supported by the Intramural Research Program of NIAID, NIH.

Acknowledgments

We thank the members of the Viral Immunity and Pathogenesis Unit for their helpful feedback and support.

Conflict of interest

The authors declare that the research was conducted in the absence of any commercial or financial relationships that could be construed as a potential conflict of interest.

Publisher's note

Supplementary material

The Supplementary Material for this article can be found online at: https://www.frontiersin.org/articles/10.3389/fimmu.2023.1236595/full#supplementary-material

References

1. Johnson BJ, Costelloe EO, Fitzpatrick DR, Haanen JB, Schumacher TN, Brown LE, et al. Single-cell perforin and granzyme expression reveals the anatomical localization of effector CD8+ T cells in influenza virus-infected mice. *Proc Natl Acad Sci USA* (2003) 100(5):2657–62. doi: 10.1073/pnas.0538056100

2. Cai SF, Fehniger TA, Cao X, Mayer JC, Brune JD, French AR, et al. Differential expression of granzyme B and C in murine cytotoxic lymphocytes. *J Immunol* (2009) 182(10):6287. doi: 10.4049/jimmunol.0804333

3. Friedrich C, Taggenbrock RLRE, Doucet-Ladevèze R, Golda G, Moenius R, Arampatzi P, et al. Effector differentiation downstream of lineage commitment in ILC1s is driven by Hobit across tissues. *Nat Immunol* (2021) 22(10):1256–67. doi: 10.1038/s41590-021-01013-0

4. Martínez-Lostao L, Anel A, Pardo J. How do cytotoxic lymphocytes kill cancer cells? *Clin Cancer Res* (2015) 21(22):5047–56. doi: 10.1158/1078-0432.CCR-15-0685

5. Grossman WJ, Revell PA, Lu ZH, Johnson H, Bredemeyer AJ, Ley TJ. The orphan granzymes of humans and mice. *Curr Opin Immunol* (2003) 15(5):544–52. doi: 10.1016/S0952-7915(03)00099-2

6. de Jong LC, Crnko S, ten Broeke T, Bovenschen N. Noncytotoxic functions of killer cell granzymes in viral infections. *PloS Pathogens* (2021) 17(9):e1009818. doi: 10.1371/journal.ppat.1009818

7. Mogilenko DA, Shpynov O, Andhey PS, Arthur L, Swain A, Esaulova E, et al. Comprehensive profiling of an aging immune system reveals clonal GZMK+ CD8+ T cells as conserved hallmark of inflammaging. *Immunity* (2021) 54(1):99–115.e12. doi: 10.1016/j.immuni.2020.11.005

8. Jonsson AH, Zhang F, Dunlap G, Gomez-Rivas E, Watts GFM, Faust HJ, et al. Granzyme K(+) CD8 T cells form a core population in inflamed human tissue. *Sci Transl Med* (2022) 14(649):eabo0686. doi: 10.1126/scitranslmed.abo0686

9. Voigt J, Malone DFG, Dias J, Leeansyah E, Björkström NK, Ljunggren HG, et al. Proteome analysis of human CD56(neg) NK cells reveals a homogeneous phenotype surprisingly similar to CD56(dim) NK cells. *Eur J Immunol* (2018) 48(9):1456–69. doi: 10.1002/eji.201747450

10. Enomoto Y, Li P, Jenkins LM, Anastasakis D, Lyons GC, Hafner M, et al. Cytokine-enhanced cytolytic activity of exosomes from NK Cells. *Cancer Gene Ther* (2022) 29(6):734–49. doi: 10.1038/s41417-021-00352-2

11. Getachew Y, Stout-Delgado H, Miller BC, Thiele DL. Granzyme C supports efficient CTL-mediated killing late in primary alloimmune responses. *J Immunol* (2008) 181(11):7810. doi: 10.4049/jimmunol.181.11.7810

12. Kelso A, Costelloe EO, Johnson BJ, Groves P, Buttigieg K, Fitzpatrick DR. The genes for perforin, granzymes A–C and IFN-γ are differentially expressed in single CD8 + T cells during primary activation. *Int Immunol* (2002) 14(6):605–13. doi: 10.1093/intimm/dxf028

13. Nixon BG, Chou C, Krishna C, Dadi S, Michel AO, Cornish AE, et al. Cytotoxic granzyme C-expressing ILC1s contribute to antitumor immunity and neonatal autoimmunity. *Sci Immunol* (2022) 7(70):eabi8642. doi: 10.1126/sciimmunol.abi8642

14. Voskoboinik I, Whisstock JC, Trapani JA. Perforin and granzymes: function, dysfunction and human pathology. *Nat Rev Immunol* (2015) 15(6):388–400. doi: 10.1038/nri3839

15. Müllbacher A, Waring P, Tha Hla R, Tran T, Chin S, Stehle T, et al. Granzymes are the essential downstream effector molecules for the control of primary virus infections by cytolytic leukocytes. *Proc Natl Acad Sci* (1999) 96(24):13950–5. doi: 10.1073/pnas.96.24.13950

16. Storm P, Bartholdy C, Sørensen MR, Christensen JP, Thomsen AR. Perforin-deficient CD8+ T cells mediate fatal lymphocytic choriomeningitis despite impaired cytokine production. *J Virol* (2006) 80(3):1222–30. doi: 10.1128/JVI.80.3.1222-1230.2006

17. Boivin WA, Cooper DM, Hiebert PR, Granville DJ. Intracellular versus extracellular granzyme B in immunity and disease: challenging the dogma. *Lab Invest* (2009) 89(11):1195–220. doi: 10.1038/labinvest.2009.91

18. Prakash MD, Munoz MA, Jain R, Tong PL, Koskinen A, Regner M, et al. Granzyme B promotes cytotoxic lymphocyte transmigration via basement membrane remodeling. *Immunity* (2014) 41(6):960–72. doi: 10.1016/j.immuni.2014.11.012

19. Hiebert PR, Wu D, Granville DJ. Granzyme B degrades extracellular matrix and contributes to delayed wound closure in apolipoprotein E knockout mice. *Cell Death Differ* (2013) 20(10):1404–14. doi: 10.1038/cdd.2013.96

20. Hiebert PR, Boivin WA, Abraham T, Pazooki S, Zhao H, Granville DJ. Granzyme B contributes to extracellular matrix remodeling and skin aging in apolipoprotein E knockout mice. *Exp Gerontol* (2011) 46(6):489–99. doi: 10.1016/j.exger.2011.02.004

21. Sharma M, Merkulova Y, Raithatha S, Parkinson LG, Shen Y, Cooper D, et al. Extracellular granzyme K mediates endothelial activation through the cleavage of protease-activated receptor-1. *FEBS J* (2016) 283(9):1734–47. doi: 10.1111/febs.13699

22. Dai R, Huang X, Yang Y. γδT cells are required for CD8+ T cell response to vaccinia viral infection. *Front Immunol* (2021) 12. doi: 10.3389/fimmu.2021.727046

23. Woodward Davis AS, Bergsbaken T, Delaney MA, Bevan MJ. Dermal-resident versus recruited γδ T cell response to cutaneous vaccinia virus infection. *J Immunol* (2015) 194(5):2260–7. doi: 10.4049/jimmunol.1402438

24. Qu G, Wang S, Zhou Z, Jiang D, Liao A, Luo J. Comparing mouse and human tissue-resident γδ T cells. *Front Immunol* (2022) 13:891687. doi: 10.3389/fimmu.2022.891687

25. Sumaria N, Roediger B, Ng LG, Qin J, Pinto R, Cavanagh LL, et al. Cutaneous immunosurveillance by self-renewing dermal gammadelta T cells. *J Exp Med* (2011) 208(3):505–18. doi: 10.1084/jem.20101824

26. Shannon JP, Vrba SM, Reynoso GV, Wynne-Jones E, Kamenyeva O, Malo CS, et al. Group 1 innate lymphoid-cell-derived interferon-gamma maintains anti-viral vigilance in the mucosal epithelium. *Immunity* (2021) 54(2):276–90 e5. doi: 10.1016/j.immuni.2020.12.004

27. Steinert Elizabeth M, Schenkel Jason M, Fraser Kathryn A, Beura Lalit K, Manlove Luke S, Igyártó Botond Z, et al. Quantifying memory CD8 T cells reveals regionalization of immunosurveillance. *Cell* (2015) 161(4):737–49. doi: 10.1016/j.cell.2015.03.031

28. Hildreth AD, O'Sullivan TE. Tissue-resident innate and innate-like lymphocyte responses to viral infection. *Viruses* (2019) 11(3):272. doi: 10.3390/v11030272

29. Hernández-Castañeda MA, Happ K, Cattalani F, Wallimann A, Blanchard M, Fellay I, et al. γδ T Cells Kill Plasmodium falciparum in a Granzyme- and Granulysin-Dependent Mechanism during the Late Blood Stage. *J Immunol* (2020) 204(7):1798–809. doi: 10.4049/jimmunol.1900725

30. Hu MD, Golovchenko NB, Burns GL, Nair PM, Kelly T, Agos J, et al. γδ Intraepithelial lymphocytes facilitate pathological epithelial cell shedding via CD103-mediated granzyme release. *Gastroenterology* (2022) 162(3):877–89.e7. doi: 10.1053/j.gastro.2021.11.028

31. Shannon JP, Kamenyeva O, Reynoso GV, Hickman HD. Intravital imaging of vaccinia virus-infected mice. *Methods Mol Biol* (2019) 2023:301–11. doi: 10.1007/978-1-4939-9593-6_19

32. Hickman HD, Reynoso GV, Ngudiankama BF, Cush SS, Gibbs J, Bennink JR, et al. CXCR3 chemokine receptor enables local CD8(+) T cell migration for the destruction of virus-infected cells. *Immunity* (2015) 42(3):524–37. doi: 10.1016/j.immuni.2015.02.009

33. Hickman HD, Reynoso GV, Ngudiankama BF, Rubin EJ, Magadan JG, Cush SS, et al. Anatomically restricted synergistic antiviral activities of innate and adaptive immune cells in the skin. *Cell Host Microbe* (2013) 13(2):155–68. doi: 10.1016/j.chom.2013.01.004

34. Wu X, Wu P, Shen Y, Jiang X, Xu F. CD8(+) resident memory T cells and viral infection. *Front Immunol* (2018) 9:2093. doi: 10.3389/fimmu.2018.02093

35. Zaid A, Mackay LK, Rahimpour A, Braun A, Veldhoen M, Carbone FR, et al. Persistence of skin-resident memory T cells within an epidermal niche. *Proc Natl Acad Sci* (2014) 111(14):5307–12. doi: 10.1073/pnas.1322292111

36. Jiang X, Clark RA, Liu L, Wagers AJ, Fuhlbrigge RC, Kupper TS. Skin infection generates non-migratory memory CD8+ TRM cells providing global skin immunity. *Nature* (2012) 483(7388):227–31. doi: 10.1038/nature10851

37. Topham DJ, Reilly EC. Tissue-resident memory CD8(+) T cells: from phenotype to function. *Front Immunol* (2018) 9:515. doi: 10.3389/fimmu.2018.00515

38. Khan TN, Mooster JL, Kilgore AM, Osborn JF, Nolz JC. Local antigen in nonlymphoid tissue promotes resident memory CD8+ T cell formation during viral infection. *J Exp Med* (2016) 213(6):951–66. doi: 10.1084/jem.20151855

39. Verbist KC, Klonowski KD. Functions of IL-15 in anti-viral immunity: multiplicity and variety. *Cytokine* (2012) 59(3):467–78. doi: 10.1016/j.cyto.2012.05.020

40. Schenkel JM, Fraser KA, Casey KA, Beura LK, Pauken KE, Vezys V, et al. IL-15-independent maintenance of tissue-resident and boosted effector memory CD8 T cells. *J Immunol* (2016) 196(9):3920–6. doi: 10.4049/jimmunol.1502337

41. Dadi S, Chhangawala S, Whitlock BM, Franklin RA, Luo CT, Oh SA, et al. Cancer immunosurveillance by tissue-resident innate lymphoid cells and innate-like T cells. *Cell* (2016) 164(3):365–77. doi: 10.1016/j.cell.2016.01.002

42. Johnson H, Scorrano L, Korsmeyer SJ, Ley TJ. Cell death induced by granzyme C. *Blood* (2003) 101(8):3093–101. doi: 10.1182/blood-2002-08-2485

43. Kaiserman D, Buckle AM, Van Damme P, Irving JA, Law RH, Matthews AY, et al. Structure of granzyme C reveals an unusual mechanism of protease autoinhibition. *Proc Natl Acad Sci USA* (2009) 106(14):5587–92. doi: 10.1073/pnas.0811968106

44. Spaeny-Dekking EHA, Hanna WL, Wolbink AM, Wever PC, Kummer AJ, Swaak AJG, et al. Extracellular granzymes A and B in humans: detection of native species during CTL responses *in vitro* and *in vivo*1. *J Immunol* (1998) 160(7):3610–6. doi: 10.4049/jimmunol.160.7.3610

45. Wilson JAC, Prow NA, Schroder WA, Ellis JJ, Cumming HE, Gearing LJ, et al. RNA-Seq analysis of chikungunya virus infection and identification of granzyme A as a major promoter of arthritic inflammation. *PloS Pathogens* (2017) 13(2):e1006155. doi: 10.1371/journal.ppat.1006155

46. Phair Iain R, Sumoreeah Megan C, Scott N, Spinelli L, Arthur JSimon C. IL-33 induces granzyme C expression in murine mast cells via an MSK1/2-CREB-dependent pathway. *Biosci Rep* (2022) 42(12):BSR20221165. doi: 10.1042/BSR20221165

47. Knickelbein JE, Khanna KM, Yee MB, Baty CJ, Kinchington PR, Hendricks RL. Noncytotoxic lytic granule–mediated CD8+ T cell inhibition of HSV-1 reactivation from neuronal latency. *Science* (2008) 322(5899):268–71. doi: 10.1126/science.1164164

48. Gerada C, Steain M, Campbell Tessa M, McSharry B, Slobedman B, Abendroth A. Granzyme B cleaves multiple herpes simplex virus 1 and varicella-zoster virus (VZV) gene products, and VZV ORF4 inhibits natural killer cell cytotoxicity. *J Virol* (2019) 93(22):e01140–19. doi: 10.1128/JVI.01140-19

49. van Domselaar R, Philippen LE, Quadir R, Wiertz EJHJ, Kummer JA, Bovenschen N. Noncytotoxic inhibition of cytomegalovirus replication through NK cell protease granzyme M-mediated cleavage of viral phosphoprotein 71. *J Immunol* (2010) 185(12):7605–13. doi: 10.4049/jimmunol.1001503

50. Andrade F, Fellows E, Jenne DE, Rosen A, Young CSH. Granzyme H destroys the function of critical adenoviral proteins required for viral DNA replication and granzyme B inhibition. *EMBO J* (2007) 26(8):2148–57. doi: 10.1038/sj.emboj.7601650

51. De Creus A, Van Beneden K, Stevenaert F, Debacker V, Plum J, Leclercq G. Developmental and functional defects of thymic and epidermal Vγ3 cells in IL-15-deficient and IFN regulatory factor-1-deficient mice1. *J Immunol* (2002) 168(12):6486–93. doi: 10.4049/jimmunol.168.12.6486

52. Klose CSN, Flach M, Möhle L, Rogell L, Hoyler T, Ebert K, et al. Differentiation of type 1 ILCs from a common progenitor to all helper-like innate lymphoid cell lineages. *Cell* (2014) 157(2):340–56. doi: 10.1016/j.cell.2014.03.030

53. Mackay Laura K, Wynne-Jones E, Freestone D, Pellicci Daniel G, Mielke Lisa A, Newman Dane M, et al. T-box transcription factors combine with the cytokines TGF-β and IL-15 to control tissue-resident memory T cell fate. *Immunity* (2015) 43(6):1101–11. doi: 10.1016/j.immuni.2015.11.008

54. Mohamadzadeh M, Takashima A, Dougherty I, Knop J, Bergstresser PR, Cruz PD Jr. Ultraviolet B radiation up-regulates the expression of IL-15 in human skin. *J Immunol* (1995) 155(9):4492–6. doi: 10.4049/jimmunol.155.9.4492

55. Fehniger TA, Caligiuri MA. Interleukin 15: biology and relevance to human disease. *Blood* (2001) 97(1):14–32. doi: 10.1182/blood.V97.1.14

56. Wang Y, Bai Y, Li Y, Liang G, Jiang Y, Liu Z, et al. IL-15 enhances activation and IGF-1 production of dendritic epidermal T cells to promote wound healing in diabetic mice. *Front Immunol* (2017) 8. doi: 10.3389/fimmu.2017.01557

57. Liu Z, Liang G, Gui L, Li Y, Liu M, Bai Y, et al. Weakened IL-15 production and impaired mTOR activation alter dendritic epidermal T cell homeostasis in diabetic mice. *Sci Rep* (2017) 7(1):6028. doi: 10.1038/s41598-017-05950-5

58. Piera Filomena F, Sabina Di M, Nicola T, Francesca Romana M, Gabriella P, Selene O, et al. Interleukin-15 and cancer: some solved and many unsolved questions. *J ImmunoTher Cancer* (2020) 8(2):e001428. doi: 10.1136/jitc-2020-001428

59. Tamzalit F, Barbieux I, Plet A, Heim J, Nedellec S, Morisseau S, et al. IL-15.IL-15Rα complex shedding following trans-presentation is essential for the survival of IL-15 responding NK and T cells. *Proc Natl Acad Sci* (2014) 111(23):8565–70. doi: 10.1073/pnas.1405514111

60. Duquette D, Harmon C, Zaborowski A, Michelet X, O'Farrelly C, Winter D, et al. Human granzyme K is a feature of innate T cells in blood, tissues, and tumors, responding to cytokines rather than TCR stimulation. *J Immunol* (2023) 211(4):633–47. doi: 10.4049/jimmunol.2300083

61. Cush SS, Reynoso GV, Kamenyeva O, Bennink JR, Yewdell JW, Hickman HD. Locally produced IL-10 limits cutaneous vaccinia virus spread. *PloS Pathogens* (2016) 12(3):e1005493. doi: 10.1371/journal.ppat.1005493

62. Shannon JP, Cherry CR, Vrba SM, Hickman HD. Protocol for analyzing and visualizing antiviral immune responses after acute infection of the murine oral mucosa. *STAR Protoc* (2021) 2(4):100790. doi: 10.1016/j.xpro.2021.100790

63. Anderson KG, Mayer-Barber K, Sung H, Beura L, James BR, Taylor JJ, et al. Intravascular staining for discrimination of vascular and tissue leukocytes. *Nat Protoc* (2014) 9(1):209–22. doi: 10.1038/nprot.2014.005

frontiers | Frontiers in Immunology

TYPE Original Research
PUBLISHED 20 November 2023
DOI 10.3389/fimmu.2023.1303724

OPEN ACCESS

EDITED BY
Chaofan Li,
University of Virginia, United States

REVIEWED BY
Wei Su,
Stanford University, United States
Yusuke Endo,
Kazusa DNA Research Institute, Japan

*CORRESPONDENCE
David Lopez-Perez
dlopezperez@ugr.es

†These authors have contributed equally to this work and share first authorship

‡These authors have contributed equally to this work and share senior authorship

RECEIVED 28 September 2023
ACCEPTED 01 November 2023
PUBLISHED 20 November 2023

CITATION
Redruello-Romero A, Benitez-Cantos MS, Lopez-Perez D, García-Rubio J, Tamayo F, Pérez-Bartivas D, Moreno-SanJuan S, Ruiz-Palmero I, Puentes-Pardo JD, Vilchez JR, López-Nevot MÁ, García F, Cano C, León J and Carazo Á (2023) Human adipose tissue as a major reservoir of cytomegalovirus-reactive T cells. *Front. Immunol.* 14:1303724. doi: 10.3389/fimmu.2023.1303724

Human adipose tissue as a major reservoir of cytomegalovirus-reactive T cells

Anaïs Redruello-Romero[1†], Maria S. Benitez-Cantos[1,2,3†], David Lopez-Perez[1,4*], Jesús García-Rubio[5], Francisco Tamayo[5], Daniel Pérez-Bartivas[1], Sara Moreno-SanJuan[1,6], Isabel Ruiz-Palmero[1], Jose D. Puentes-Pardo[1,4], Jose R. Vilchez[1,7], Miguel Á. López-Nevot[1,2,7], Federico García[1,8,9], Carlos Cano[10], Josefa León[1,11‡] and Ángel Carazo[1,8‡]

[1]Research Unit, Biosanitary Research Institute of Granada (ibs.GRANADA), Granada, Spain, [2]Department of Biochemistry and Molecular Biology III and Immunology, Faculty of Medicine, University of Granada, Granada, Spain, [3]GENYO, Centre for Genomics and Oncological Research: Pfizer/University of Granada/Andalusian Regional Government, Granada, Spain, [4]Department of Pharmacology, Faculty of Pharmacy, University of Granada, Granada, Spain, [5]Surgery Unit, San Cecilio University Hospital, Granada, Spain, [6]Cytometry and Microscopy Research Service, Biosanitary Research Institute of Granada (ibs.GRANADA), Granada, Spain, [7]Clinical Analyses and Immunology Unit, Virgen de las Nieves University Hospital, Granada, Spain, [8]Clinical Microbiology Unit, San Cecilio University Hospital, Granada, Spain, [9]Centro de Investigación Biomédica en Red (CIBER) of Infectious Diseases, Health Institute Carlos III, Madrid, Spain, [10]Department of Computer Science and Artificial Intelligence, University of Granada, Granada, Spain, [11]Digestive Unit, San Cecilio University Hospital, Granada, Spain

Introduction: Cytomegalovirus (CMV) is a common herpesvirus with a high prevalence worldwide. After the acute infection phase, CMV can remain latent in several tissues. CD8 T cells in the lungs and salivary glands mainly control its reactivation control. White adipose tissue (WAT) contains a significant population of memory T cells reactive to viral antigens, but CMV specificity has mainly been studied in mouse WAT. Therefore, we obtained blood, omental WAT (oWAT), subcutaneous WAT (sWAT), and liver samples from 11 obese donors to characterize the human WAT adaptive immune landscape from a phenotypic and immune receptor specificity perspective.

Methods: We performed high-throughput sequencing of the T cell receptor (TCR) locus to analyze tissue and blood TCR repertoires of the 11 donors. The presence of TCRs specific to CMV epitopes was tested through ELISpot assays. Moreover, phenotypic characterization of T cells was carried out through flow cytometry.

Results: High-throughput sequencing analyses revealed that tissue TCR repertoires in oWAT, sWAT, and liver samples were less diverse and dominated by hyperexpanded clones when compared to blood samples. Additionally, we predicted the presence of TCRs specific to viral epitopes, particularly from CMV, which was confirmed by ELISpot assays. Remarkably, we found that oWAT has a higher proportion of CMV-reactive T cells than blood or sWAT. Finally, flow cytometry analyses indicated that most WAT-infiltrated lymphocytes were tissue-resident effector memory CD8 T cells.

Discussion: Overall, these findings postulate human oWAT as a major reservoir of CMV-specific T cells, presumably for latent viral reactivation control. This study enhances our understanding of the adaptive immune response in human WAT and highlights its potential role in antiviral defense.

KEYWORDS

T cell receptor, adipose tissue, cytomegalovirus, tissue-resident memory T cells, antigen prediction

1 Introduction

Cytomegalovirus (CMV) is a common type of herpesvirus that has a high prevalence in the population, infecting 50-90% of adults in developing countries (1). In most cases, patients are asymptomatic. In immunocompetent conditions, the viral reactivation is controlled by blood-circulating and tissue-resident leukocytes, particularly by CD8+ T cells (2). However, infections in immunocompromised individuals can lead to severe conditions and even death (3). In this context, studies of latent infection control among the body have pinpointed adipose tissue as a relevant reservoir of adaptive immune cells for lifelong control of CMV infection (4, 5).

The understanding of white adipose tissue (WAT) has noticeably evolved. Initially regarded as a mere storage of neutral lipids, it is currently considered an endocrine organ, essential in regulating systemic energy homeostasis (6). In addition, WAT plays a role in non-shivering thermogenesis by the generation of a particular kind of thermogenic adipocyte (7). This multi-functional vision of WAT is still changing since a new role as an immune organ is emerging (8).

Different cell types occur in WAT, including white and thermogenic adipocytes, fibroblasts, endothelial cells, different populations of stem cells and a wide variety of leukocytes (from both, adaptive and innate immune systems) (9). They all contribute to the main functions of WAT: energy storage, endocrine regulation, non-shivering thermogenesis, and host defense. Therefore, WAT is currently seen as a complex tissue full of synergistic interactions between different cell types (8, 10–13).

WAT contains a lymphoid structure called fat-associated lymphoid clusters (FALCs) or milky spots (8, 14, 15). Regarding immune defense, FALCs resemble secondary or tertiary lymphoid organs. They are particularly interesting in the peritoneal cavity since they filter peritoneal fluid and capture soluble antigens (16). When microbial antigens are detected, fibroblastic reticular cells in FALCs recruit peripheral monocytes and promote the formation of new FALCs. This is followed by rapid activation of T and B cells.

FALCs contain a huge amount of memory T cells (8, 9, 17). Most of them belong to the resident memory compartment and do not recirculate. This accumulation of tissue-resident memory T cells (Trm) in FALCs has two advantages. Firstly, WAT connects all organs with lymphoid structures and, during inflammation, lymph leak from vessels reaching WAT lymphatics and FALCs. Therefore, this mechanism works synergistically with classic lymphatic drainage. Secondly, the main source of energy in Trm is mitochondrial fatty acid oxidation (17). Interestingly, upon microbial challenge, adipocytes increase lipolysis making fatty acids available to Trm (13). In a nutshell, T cells in FALCs are located in a strategic location full of fuel to respond to microbes' reencounter. Besides, CD8+ Trm in WAT shows a higher proliferative potential than Trm in other locations and co-expresses IFN-γ and TNF-alfa 1h after activation (17).

A fraction of WAT-resident memory T cells has been demonstrated to be reactive to viral antigens (17, 18). At present, only a few works (mainly in murine models) have studied the WAT reservoir of viral-specific memory T cells (4, 17). Murine CMV-specific CD8 T cells have been identified in mice adipose tissue and have been associated with the control of lifelong infection (4). Some studies in humans have described the role of a minor subpopulation of CMV-specific CD4+ T cells in sWAT of patients coinfected with human immunodeficiency viruses (HIV) and CMV (5), and the presence of Trm cells reactive to CMV antigens in respiratory mucosa (19).

The antigen specificity of a T cell is determined by its T cell receptor (TCR) sequence. High-throughput sequencing of the TCR repertoire can provide a snapshot of the clonal expansion level of an immune reservoir, as well as its antigen specificities if a given TCR has a known, experimentally determined, cognate antigen. In the present work we have generated TCR libraries of 11 donors from blood, omental WAT (oWAT), subcutaneous WAT (sWAT) and liver to study the adaptive immunity landscape of tissue reservoirs. We found T cells annotated to be specific to common viral pathogens in WAT, specially to CMV antigens. The presence of CMV-specific T cells in human WAT was confirmed by ELISpot

Abbreviations: BC, barcode; BMI, Body Mass Index; C, Constant gene segment of TCR; CDR, Complementary Determining Region; CMV, cytomegalovirus; EBV, Epstein-Barr virus; FALCs, Fat-Associated Lymphoid Clusters; HbA1c, glycated hemoglobin; HDL, High-Density Lipoprotein; HIV, human immunodeficiency viruses; J, Joining gene segment of TCR; LDL, Low-Density Lipoprotein; oWAT, omental White Adipose Tissue; PBMCs, Peripheral Blood Mononuclear Cells; SVF, Stromal Vascular Fraction; sWAT, subcutaneous White Adipose Tissue; Tcm, T central memory; TCR, T cell receptor; Tem, T effector memory; Temra, T effector memory re-expressing CD45RA; Treg, T regulatory cell; Trm, tissue-resident memory T cell; UTR, untranslated region; V, Variable gene segment of TCR; WAT, White Adipose Tissue.

10.3389/fimmu.2023.1303724

TABLE 1 Clinical baseline characteristics of patients.

Variables	Patient										
	#1	#2	#3	#4	#5	#6	#7	#8	#9	#10	#11
Age (years)	37	36	55	55	53	50	44	65	38	48	55
Female/Male	F	F	M	M	F	M	F	F	M	F	F
T2D	+	–	–	+	–	+	–	–	–	–	–
Hypertension	+	–	+	–	+	+	–	+	–	–	+
BMI (kg/m2)	38.2	39	33.8	50	36.9	40.6	45.5	37.1	48.1	41.8	42.8
Glucose (mg/dL)	151	88	75	98	92	318	116	88	90	105	101
Hb1Ac (%)	5.5.	5	5.7	7	5.4	5.5	5.7	6.2	5.4	5.5	5.5
CRP (mg/L)	18.7	5	9.3	22	11.9	2.7	20.9	5.9	5.3	4.1	16.6
Cholesterol (mg/dL)	128	118	156	125	125	201	131	143	143	188	149
Triglycerides (mg/dL)	175	156	104	105	48	12	202	175	85	264	120
HDL (mg/dL)	39	29	39	41	61	34	27	52	35	34	38
LDL (mg/dL)	54	58	96	63	80	134	64	56	91	101	87
CMV (IgG/IgM)	+/-	+/-	+/-	+/-	+/-	+/-	+/-	+/-	-/-	+/-	+/-
EBV (IgG/IgM)	+/-	+/-	+/-	+/-	+/-	+/-	+/-	+/-	-/-	+/-	+/-

assays in all CMV-seropositive donors. Moreover, we characterized the phenotype of WAT-infiltrating T cells by flow cytometry. The fact that tissue-resident effector memory T cells (Tem) are the most abundant population in WAT, together with the enrichment in CMV-specific T lymphocytes, supports the hypothesis that WAT contains an immunological reservoir responsible for controlling reactivation of latent CMV in humans.

2 Results

2.1 Baseline characteristics of patients

Table 1 shows details on data of age, sex, type 2 diabetes (T2D), hypertension, body mass index (BMI), glucose, glycated hemoglobin (HbA1c), C-reactive protein (CRP), cholesterol, triglycerides, high-density lipoprotein (HDL), low-density lipoprotein (LDL), CMV and EBV (Epstein-Barr virus) seropositivity. Women were predominant, around 64% of patients, due to social constraints in our geographic environment.

2.2 TCR repertoire analysis

In order to study the immune receptor landscape in different tissue compartments, we assessed TCRβ repertoire diversity and overlap in obese patients from blood, oWAT, sWAT, and liver. It must be noted that liver samples were exclusively used for TCRβ analyses due to the small size of hepatic biopsies. We obtained a total of 5 million reads covering full V-D-J regions (400-600 bp long). After identifying the V and J alleles and the complementary determining region 3 (CDR3) sequence, we found 86,005 unique TCRs among our samples.

Chao index was calculated to measure repertoire richness, understood as the number of different clonotypes in a sample. Blood repertoires showed a significantly higher richness compared to solid tissue repertoires (4201 ± 2556 clonotypes in blood, 343 ± 166 in oWAT, 441 ± 181 in sWAT and 296 ± 173 in liver, Wilcoxon test, $p < 0.0001$) (Figure 1A). Clonality was calculated to measure the degree of clonal expansion in a TCR repertoire. We found that solid tissue samples are significantly more clonal than blood repertoires (0.11 ± 0.09 in blood, 0.23 ± 0.10 in oWAT, 0.24 ± 0.11 in sWAT and 0.26 ± 0.11 in liver, Wilcoxon test, $p < 0.05$) (Figure 1B). No significant differences in richness and clonality were observed between solid tissues. Additionally, we studied clonality by assessing the clonal space homeostasis, i.e., the proportion of the repertoire that is occupied by clonotypes of a given frequency. Four different groups were established: small (clonotype frequency ≤ 0.0001), medium (0.0001-0.001), large (0.001-0.01) and hyperexpanded (>0.01). Blood repertoires were mainly composed of medium clones, whereas solid tissues were dominated by hyperexpanded lymphocytes (Figure 1C). Altogether, these findings indicate that tissue infiltrating TCR repertoires were less diverse and more expanded compared to the set of circulating blood lymphocytes.

Overlap between blood and tissue repertoires was assessed with the Morisita index, where 0 meant that the samples do not have any clonotypes in common and 1 meant that all the TCRs occur in the same proportion in the two repertoires compared. Low overlap with blood was observed for all the solid tissues since the maximum overlap value observed was 0.13 in the blood-liver comparison of patient #1 (Figure 1D). No significant differences were observed

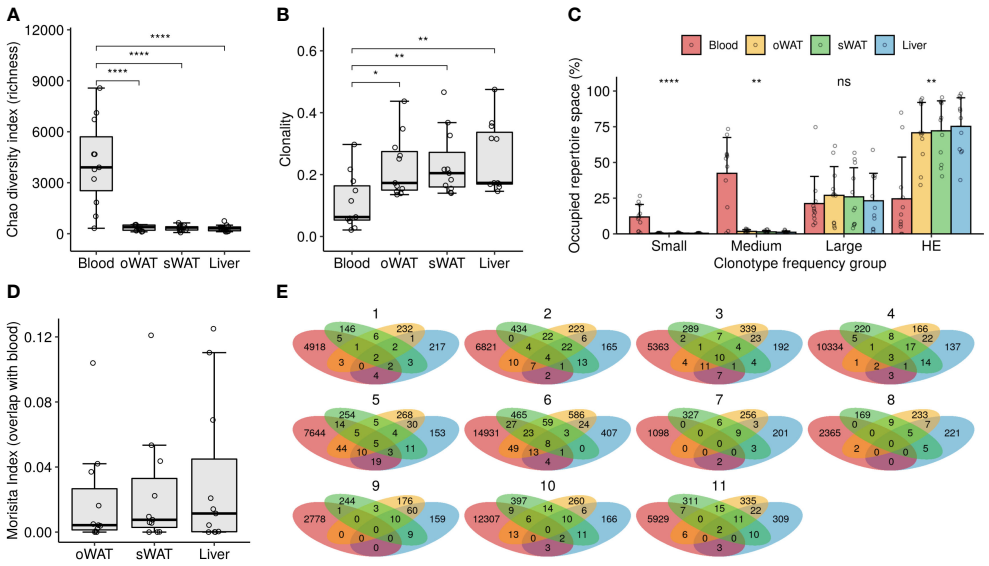

FIGURE 1
TCR repertoire diversity measurements. **(A)** Richness analysis (estimation of the number of different TCRs in a sample). **(B)** Clonality degree of the repertoires. **(C)** Percentage of occupied repertoire space by clones of a given size (i.e., relative frequency in the repertoire): small (≤ 0.0001), medium (0.0001 – 0.001), large (0.001 – 0.01) and hyperexpanded (HE, > 0.01). Statistical differences among tissues within each group were assessed with Kruskal-Wallis test. **(D)** Degree of overlap of the solid tissue repertoires with their respective blood repertoires. **(E)** Venn diagrams depicting the number of shared clonotypes among repertoires from the same patient. ns: non-significant, *: $p \leq 0.05$, **: $p \leq 0.01$, ****: $p \leq 0.0001$.

between solid tissues in the degree of overlap with blood repertoires (Kruskal-Wallis test, $p > 0.05$). The number of shared clonotypes between tissues of the same patient is shown in Figure 1E. Again, little to no overlap is observed among different TCR repertoires from the same patient, indicating that the subsets of tissue-infiltrated clonotypes are very distinct and that some of them are even undetectable in blood.

2.3 Antigen specificity prediction

To predict the antigen specificity of TCR repertoires we accessed the VDJdb database, which contains curated TCR sequences with *in vitro* determined antigen specificity that were used to annotate our repertoires by sequence similarity clustering. Of the 86,005 TCRs discovered in our repertoires, only 363 clustered with any CDR3 sequence of VDJdb, leaving 99.58% of our data unannotated for antigen specificity. This highlights the need to perform more *in vitro* antigen specificity assays to enlarge these databases.

Specificity to 30 epitopes from 19 antigens was found in our repertoires, both in blood and in solid tissues, including several viral epitopes from CMV, EBV and Influenza virus A (Figure 2, Supplementary Dataset 1). It must be noted that 24 of the 30 epitopes are presented by HLA class I and 6 by HLA class II. Moreover, none of the latter epitopes were present in oWAT. For each TCR/epitope pair, the VDJdb database provides information about the HLA allele that was used in the antigen specificity assay. However, due to the known promiscuity of HLA alleles in antigen presentation (20, 21), we showed all the antigen specificities discovered, even when the HLA allele reported in the database is not carried by our patients.

TCRs specific to 8 CMV epitopes were present exclusively in blood samples, while specificity to 4 epitopes was found both in blood and WAT in 5 out of 11 patients (45.5%). A*03/IE1$_{KLG}$ was predicted to be the most widely recognized CMV epitope in our cohort, with specific TCRs present in oWAT from patient #6 and sWAT from patients #6, #7, #9 and #10. It should be mentioned that it is the epitope with the largest number of known TCRs in the VDJdb database, which may bias the results. A*02/pp65$_{NLV}$ had cognate TCRs in all the patients but patient #9, which was consistent with them being the only patient who tested negative in CMV serology. Specificity against this antigen was predicted in oWAT from patients #6 (carrier of the HLA-A*02 allele, Supplementary Table 1), #10 and #11, and sWAT from patients #7 and #11. TCRs against another epitope from the CMV protein pp65, B*07/pp65$_{TPR}$, were found in oWAT from patient #2, which also carries the HLA-B*07 allele, occupying around 16.8% of the sequenced repertoire. Specificity to EBV epitopes was found to a lesser extent in blood and solid tissues. Particularly, TCRs specific to B*35/BZLF1$_{EPL}$ and A*11/EBNA4$_{AVF}$ epitopes were found in oWAT and sWAT from patient #6, which showed the broadest specificity against EBV epitopes of the entire cohort. Epitopes from Influenza A were predicted to be recognized mostly by TCRs from circulating T lymphocytes. Only patient #7 showed specificity against epitopes B*07/NP$_{LPR}$ and DRA*01-DRB1*01/M1$_{SGP}$ in oWAT and sWAT, respectively. Specificity to self-antigens was also predicted in our cohort. Especially to A*02/MLANA$_{ELA}$, derived from the melanoma antigen recognized by T cells 1 (known as MART1 or MLANA) in patients #2 and #6, which

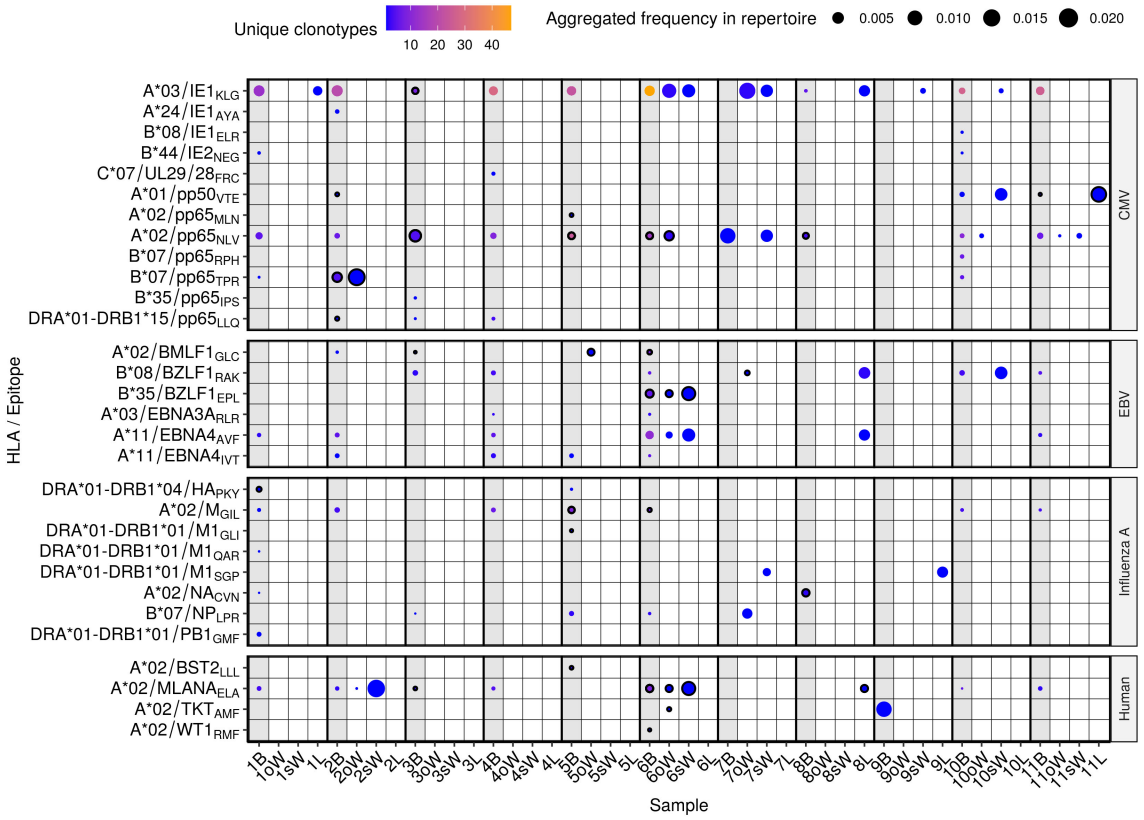

FIGURE 2
Predicted antigen specificity of the 44 TCR repertoires analyzed. Epitopes (y axis) are identified by the HLA allele presenting them, the protein of origin and their first three amino acids. Each circle represents the specificity of TCRs to each epitope in a given repertoire. Color scale stands for the number of different clonotypes recognizing that epitope, while size represents the relative frequency of those clonotypes in the repertoire. Blood samples from each donor are highlighted in light grey and outlined circles indicate that the patient carries the HLA allele presenting the epitope according to the VDJdb database. B, blood; oW, omental white adipose tissue; sW, subcutaneous white adipose tissue; L, liver tissue.

showed specific TCRs in blood, oWAT, but especially in sWAT, occupying 21.1% and 10.7% of the sequenced sWAT repertoire, respectively. Reactive T cells against MLANA appear in some pathological contexts, such as vitiligo and melanoma (22). Interestingly, patient #6 has been diagnosed with basal cell carcinoma afterwards.

2.4 ELISpot assay

One of the most notable results of the *in silico* antigen-specificity prediction was the relative abundance of CMV-specific TCRs in oWAT. To validate this result, we performed a functionality test with isolated T lymphocytes. ELISpot assays were carried out on every patient and results are shown in Figure 3A and Supplementary Figure 1.

The mean number of CMV reactive cells in oWAT was one order of magnitude more elevated than in peripheral blood mononuclear cells (PBMCs) (1174.45 ± 207.86 in oWAT *versus* 255.09 ± 194.37 in PBMCs, $p<0.001$, Figure 3B). In contrast, sWAT showed a reduced number of spots (45.36 ± 15.94). We must remark that the same number of mononuclear cells, either from blood or adipose tissue, was seeded in each well to perform the ELISpot assay. According to a previous article published by our group (9), the mononuclear set of stromal vascular fraction (SVF) is composed of 40-50% of T lymphocytes (in both, oWAT and sWAT). The mononuclear fraction of total blood is usually composed of 40-70% of T cells. In case of the study cohort, according to our cytometric data, these percentages are limited to 45-55% in all types of samples. Another remarkable difference was in the size of spots, which can be used as a measure of the amount of interferon-γ (IFN-γ) that is secreted by cells after TCR stimulation. In oWAT, a noticeable fraction of cells (around 16%) showed a high-secretion (spot area >2000μm^2) level of IFN-γ, while this fraction is marginal in blood (around 2%) and absent in sWAT. In addition, as shown in Figure 3C, the first decile of oWAT had spot sizes significantly larger than sWAT and blood.

2.5 Phenotypic analyses of T cells by flow cytometry

In order to analyze the phenotype of T lymphocytes in blood, oWAT and sWAT, two different cytometric panels were used. Panel 1 included markers to identify the naïve phenotype (CCR7 +/CD45RA+) and three memory populations: T central memory

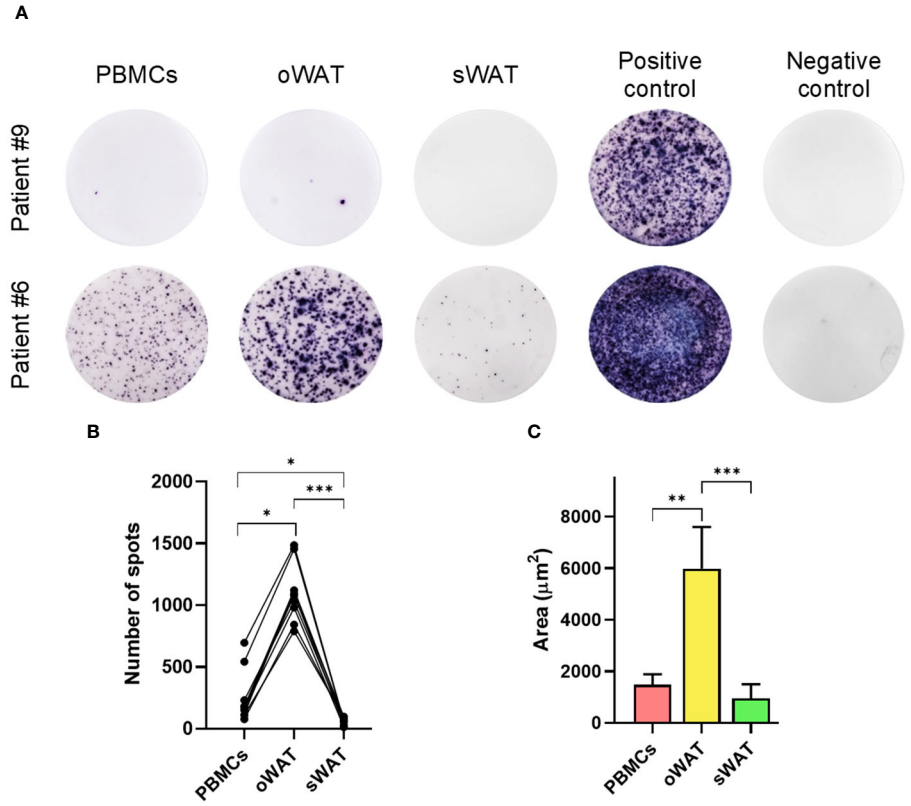

FIGURE 3
Cytomegalovirus ELISpot assays measurements. **(A)** Patient #9, negative for CMV and patient #6, positive for CMV in PBMCs and both tissues (oWAT and sWAT). **(B)** Total number of spots for all the different tissues in all CMV-positive patients. **(C)** First decile of the biggest spots for all the different tissues in all CMV-positive patients. *: $p \leq 0.05$, **: $p \leq 0.01$, ***: $p \leq 0.001$.

(Tcm: CCR7+/CD45RA-), T effector memory (Tem: CCR7-/CD45RA-) and T effector memory re-expressing CD45RA (Temra: CCR7-/CD45RA+). Panel 2 included several tissue-residence markers: CD69, CD49a and CD103.

Supplementary Figure 2A shows the SSC *versus* FSC plot of oWAT SVF and the gating strategy to identify CD4+ and CD8+ populations by Panel 2. Noteworthy, blood and tissue samples displayed different flow cytometry profiles (Supplementary Figures 2B, C). Such indicated that contamination with peripheral blood in tissue samples was negligible. One of the main differences shown by panel 1 was in the naïve population, which was abundant in blood but marginal in tissue (22.2% blood, 1.9% oWAT, 1.7% sWAT, $p<0.001$, Figure 4). Furthermore, the proportion of T cells positive for tissue-resident markers was different in blood and WAT, highlighting the fact that almost all T cells in tissue have a memory phenotype. As expected, CD103 and CD49a were nearly absent in blood (Supplementary Figures 2C, D, 3) and only a small fraction of T cells was positive for CD69 (CD4: 2.7%, CD8: 4.4%, Supplementary Figure 2C). In contrast, most adipose tissue T lymphocytes were positive for CD69 (CD4-oWAT: 86.8%, CD8-oWAT: 93.3%, CD4-sWAT: 72.5%, CD8-sWAT: 81.7%, Supplementary Figure 2C).

There were significantly more CD4+ and CD8+ T lymphocytes in oWAT than in sWAT (Figure 5A). This agrees with previous reports showing that FALCs are more abundant in oWAT than in sWAT (14, 15). Moreover, the CD4+:CD8+ ratio differed significantly between both types of adipose tissue (Figure 5B). In oWAT CD8+ cells dominated the T cell pool, while in sWAT CD4+ cells did so. Therefore, the increase of CD8+ T cells in oWAT was the main driving force behind the differences in the number of T cells between oWAT and sWAT.

In adipose tissue samples, naïve T cells were almost absent, which agrees with previous reports (23) (Figures 4B, C, E, F). In both adipose tissues, the most abundant CD4+ subset was Tem, followed by Tcm and Temra (Figures 4B, C). In the CD8+ subpopulation Tem was the larger subset in both tissues as well, followed by Temra and Tcm (Figures 4E, F). Furthermore, in blood samples, there were around 22% of naïve T cells in both CD4+ and CD8+ subpopulations (Figures 4A, D). It is worth noting that the number of naïve T cells can vary within individual's age since their production by the thymus decreases with senescence (24). Remarkably, in the CD8+ subpopulation of blood, Temra was the most abundant subset (Figure 4D) whereas it was almost absent in the CD4+ subset (Figure 4A). This was consistent with previous results, which described circulant Temra CD8+ as a major subset that increases with age (25).

In Trm cells, CD69 is usually co-expressed with CD49a and/or CD103. The percentage of CD103-positive T cells was minimal in adipose tissue (Supplementary Figures 2D, 3) whereas CD49a showed high levels, especially in oWAT (Supplementary

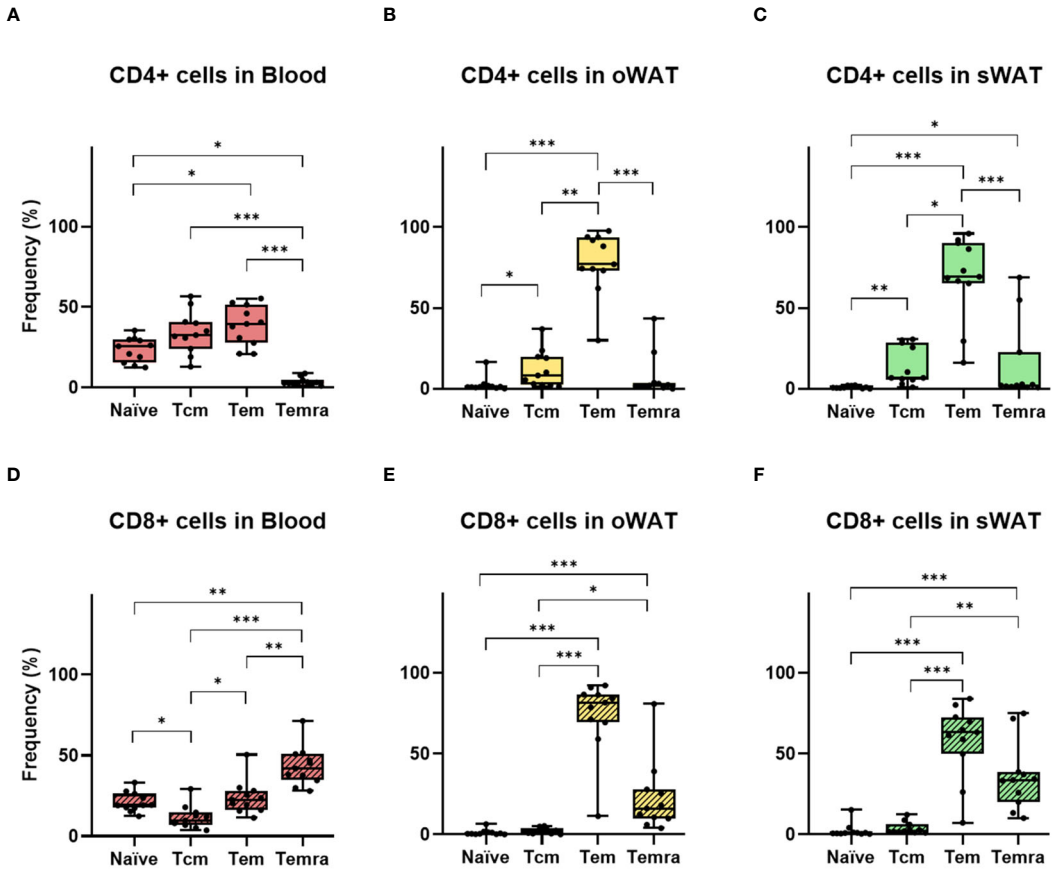

FIGURE 4
Differences between the number of naïve and memory T cells in $CD4^+$ and $CD8^+$ independently. **(A)** CD4+ subsets (T central memory, T effector memory, T effector memory re-expressing CD45RA) in blood. **(B)** CD4+ subsets in oWAT. **(C)** CD4+ subsets in subcutaneous sWAT. **(D)** CD8+ subsets in blood. **(E)** CD8+ subsets in oWAT. **(F)** CD8+ subsets in sWAT. *: $p \leq 0.05$, **: $p \leq 0.01$, ***: $p \leq 0.001$.

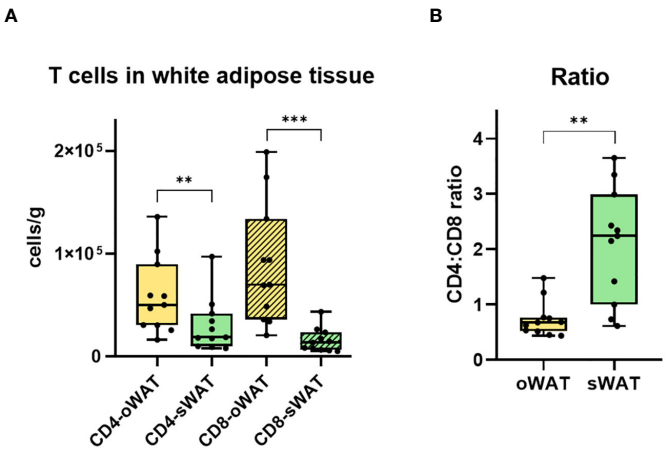

FIGURE 5
Differences in CD4+ and CD8+ T cells in adipose tissue. **(A)** Total number of CD4+ and CD8+ T lymphocytes per gram of oWAT and sWAT. **(B)** Ratio CD4:CD8 in omental and subcutaneous adipose tissue. **: $p \leq 0.01$, ***: $p \leq 0.001$.

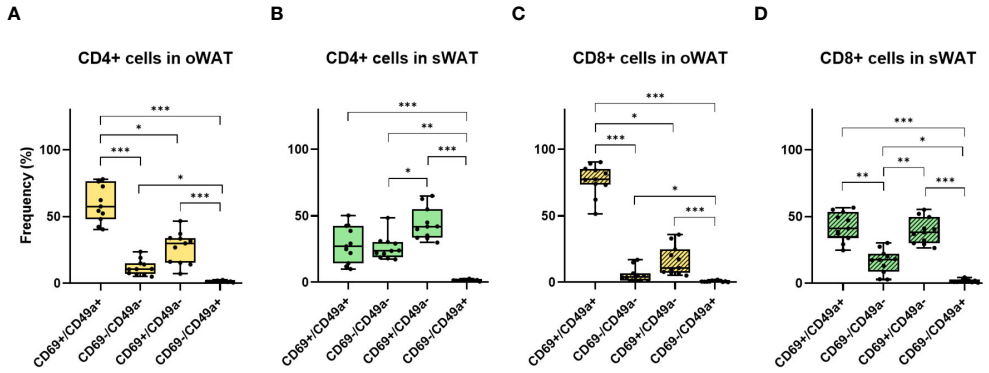

FIGURE 6
Differences between CD69 and CD49a profile for CD4+ and CD8+ in oWAT and sWAT. **(A)** CD4+ subsets in oWAT. **(B)** CD4+ subsets in sWAT. **(C)** CD8+ subsets in oWAT. **(D)** CD8+ subsets in sWAT. *: $p \leq 0.05$, **: $p \leq 0.01$, ***: $p \leq 0.001$.

Figure 2C). From CD69 and CD49a expression patterns, we extract two conclusions. Firstly, virtually all CD49a-positive T cells co-expressed CD69. Secondly, the double positive population (CD69+/CD49a+) was the most abundant in oWAT (particularly in the CD8+ subpopulation) (Figures 6A, C) while there was not a predominant population in sWAT (Figures 6B, D).

3 Discussion

3.1 Differences in human and mice adipose tissue

A growing body of evidence supports the immunological function of WAT (8). Nevertheless, most of the data are derived from murine models and they significantly differ from humans in their anatomy and physiopathology of adipose tissue (26). Humans have two main visceral fat depots in the intraperitoneal cavity (omental and mesenteric). Conversely, mice have a mesenteric and a well-developed gonadal depot but lack the omental depot, only visible in obese animals (27). The principal fat depots with the ability of expansion are subcutaneous and certain visceral depots. Concerning visceral expansion, rodents expand their gonadal depot, whereas humans mainly expand the omental fat depots, and both tissues differ notably. While murine gonadal fat drains to the systemic circulation, human omental adipose tissue drains to the portal circulation. Moreover, the presence of immune cells and FALCs is higher in human oWAT (14). This strategic location gives oWAT the opportunity of filtering a more diverse antigen repertoire. In both species an excessive expansion of intraperitoneal fat depots is associated with obesity-related pathologies (28). On the other hand, mesenteric depots have been much less studied, unlike omental and gonadal depots, due to the small quantity of this tissue in mice and the difficulty of taking biopsies in humans.

Our work is pioneering in studying the immunological component of oWAT in humans. Nevertheless, our data must be interpreted in the context of morbid obesity, where the excessive expansion of body fat depots changes the composition and phenotype of adipose tissue leukocytes. Obesity increases the infiltration of neutrophils and reduces the number of resident mast cells (9, 10). Furthermore, obesity induces a pro-inflammatory phenotypic switching in macrophages and disrupts the function of mast cells (11, 29). This state of low-level chronic inflammation, together with other factors (such as adipocyte hypertrophy, fibrosis, or tissue hypoxia) impairs the normal function of adipose tissue, promoting obesity-associated pathologies.

3.2 TCR-antigen prediction

Due to the low accuracy of current TCR antigen specificity prediction algorithms (30), the best TCR annotation strategy is cross-referencing with a database such as VDJdb. At the time of analysis, VDJdb listed 34685 TCR-antigen-HLA trios, which allowed us to annotate only 0.42% of our TCRs. The main limitation of these databases is that they contain antigen-specificity information for a negligible fraction of the possible TCRs that can be generated by the somatic recombination process. Furthermore, viral antigens are currently overrepresented, which leaves many non-viral epitopes without experimentally validated cognate TCR (30).

Although we have performed high-resolution HLA genotyping of our cohort, we did not set HLA matching as a strict filter to rule out antigen specificity annotations. The genetics of HLA is an intricate system (20, 21): hyper-polymorphic, multigenic and codominant. Moreover, it has been shown a proinflammatory environment may change the collection of peptides presented by HLA class I and II molecules (31, 32). Furthermore, the interaction between TCR and the antigen-HLA complex shows a wide spectrum of engagement, from high-affinity and high-specific interactions to low-affinity and promiscuous interactions.

Despite all the aforementioned limitations, our *in silico* antigen specificity analysis predicted the presence of CMV-specific T lymphocytes infiltrating adipose tissue and this was successfully validated in subsequent functional assays. This analysis would greatly benefit from future updates of VDJdb, providing a more

comprehensive TCR annotation to decipher the full landscape of antigen specificity of adipose tissue-infiltrating T lymphocytes.

3.3 Reactivity against CMV antigens by ELIspot assay

The ELIspot assay reveals certain particularities in oWAT, concerning the composition of the T cells reservoir. Firstly, the number of spots was significantly more elevated in oWAT than in blood and sWAT, showing a clear enrichment in CMV-reactive T cells. One previous study performed in human samples found relevant frequencies of T cells against CMV-antigens in blood, bone marrow, and lymphoid nodes but negligible in intestinal mucosa (19). Nevertheless, this study did not analyze adipose tissue samples. Secondly, although we lack specific experiments to confirm that T cells reacting in the ELISpot assay are Trm-like, there is a significant observation to consider. More than 95% of oWAT T cells show characteristics of memory T cells by flow cytometry. Additionally, there is negligible contamination with peripheral blood in tissues, so very few naïve T cells appear in tissue. Thirdly, the spot size was significantly larger in oWAT, which can be conditioned by cell phenotype and/or the TCR binding affinity.

In our cohort, some patients showed discrepancies between the antigen-specificity prediction and the ELISpot assays. Bioinformatics analyses predicted the presence of CMV-specific TCRs in blood but not in WAT (considering a 0.0001 frequency threshold). However, all of them were positive in the ELISpot assay in both blood and WAT. There could be several reasons (methodological and biological) for this discrepancy. On the one hand, we could have lost some TCR clonotypes due to sampling bias and/or quality controls and filters of subsequent data processing. On the other hand, the clonotype composition significantly differs between blood and oWAT. This phenomenon, together with the fact that most of VDJdb database annotations come from experiments with PBMCs, may cause the loss of relevant information.

3.4 Characteristics of T resident memory cells in adipose tissue

In a previous article, we reported that significant weight loss in subjects with morbid obesity did not alter either the proportion of adipose tissue T lymphocytes (into the ensemble of non-adipose cells) or the CD4+:CD8+ ratio (9). We do not have any data about the status of the adipose-tissue Trm reservoir in human lean subjects. Nevertheless, it is reasonable to think that the visceral fat depots of lean individuals act as a relevant reservoir of T cell memory as well. Further studies are needed to elucidate how obesity impacts the normal function of the adipose-tissue Trm reservoir. Additionally, Trm population may affect the development of obesity-related pathologies. In this way, a study in a murine model suggested that the infection of mCMV in its acute phase might impair the glucose metabolism (4). Moreover, other relevant issues remain unsolved, such as the immunological differences between human intraperitoneal fat depots (especially, omental and mesenteric depots), or their relationship with mucosa-associated immunity. What is established, and important to highlight, about the intraperitoneal fat depots examined in this study is that oWAT contains a higher abundance of FALCs and immune cells in comparison with sWAT.

One remarkable finding is the elevated proportion of CD8+ T cells in oWAT. The relative abundance of CD4+ and CD8+ T lymphocytes is controlled by different factors and is biologically relevant. The thymus produces more CD4+ than CD8+ lymphocytes (33) but the ratio between CD4+ and CD8+ T lymphocytes greatly varies between peripheral tissues (34). In general, CD4+ dominate the T cell pool in almost the entire body except in the intestine, where CD4+ and CD8+ T lymphocytes are in similar amounts (34). Nevertheless, both subpopulations expand with important differences under immunological stimulation (like a viral infection). In the case of CD4+ T cells, expansion is coupled with IFN-γ-mediated apoptosis. Thus, the number of CD4+ T cells does not significantly change after the stimulation. Oppositely, CD8+ T cells do not have an apoptosis mechanism coupled with expansion. Therefore, CD8+ T cells significantly increase after stimulation (35). When the immunological stimulation is low, the expansion of CD8+ T cells is mainly driven by the TCR recognition of the cognate epitope in an HLA class I molecule. When the immunological stimulation is high, CD8+ T cells can proliferate in a bystander way (TCR independent). This type of activation is characteristic of Tem and is quite infrequent in other subsets. In short, the CD8+ domination of the T cell pool in peripheral tissues is a marker of immunological stimulation.

CD69, a type II C-lectin receptor, is a classical early marker of lymphocyte activation, and also a marker of tissue retention (36). CD69 is widely expressed in Trm lymphocytes (37, 38) whereas the expression in circulant T cells, which is undetectable at steady-state, may be increased in diverse pathological contexts (36). CD69 is usually co-expressed in skin and mucosal tissues with other Trm markers, such as integrins CD49a and CD103. The expression pattern of Trm markers determines different phenotypes. For instance, CD49a seems to be essential for long-term persistence of Trm lymphocytes, in part by generating survival signals through the interaction with collagen IV (39, 40). Moreover, CD49a expression is associated with increased T-cells motility (41). Importantly, the recurrence of viral infections increases the proportion of CD49a+ cells in Trm lymphocytes (42–44). These data are in coherence with the prominence of the CD49a+ subset in adipose tissue T lymphocytes, particularly in oWAT CD8+ cells (42). In contrast, the expression of CD103 is almost absent in adipose tissue. This marker, which is important for epithelial retention of memory T cells (38, 45), does not appear relevant in the adipose tissue context. In our study, the expression pattern of CD69 and CD49a defined three main populations (CD69+/CD49a+, CD69+/CD49a- and CD69-/CD49a+) with presumably different roles. These results open an interesting research field. Future studies should include new Trm markers and characterize the role of different T cell populations in adipose tissue depots.

3.5 Adaptive immune response in the context of viral infection

The adaptive immune response against pathogens always begins with a rapid expansion of the clones reactive to pathogen antigens. Once the infection is controlled, this T cell population is contracted to avoid the deleterious effects of excessive activation of these cells. At this point, three different scenarios can occur: 1) if the pathogen is completely controlled and cleared, a memory population will remain stable over time to protect against reinfection; 2) if the pathogen is not completely controlled, it establishes a chronic infection, like HIV or hepatitis C virus (HCV), where the pathogen antigens are always present and T cells are continuously challenged. This causes the accumulation of memory cells over time that become exhausted. However, this term is being revised lately as phenotypical adaptation in the context of chronic inflammation by some authors (46); 3) if the pathogen is controlled (so it is undetectable) but it is not completely cleared, it establishes a latent infection. These latent pathogens are dormant during the lysogenic part of their cycle and thus are not detected by the immune system. However, they can periodically be activated and enter the lytic part of their cycle to reactivate the infection (47).

Oppositely to chronic viruses, the presence of antigens from latent viruses is not constant. Thus, there is no accumulation of exhausted T cells. However, the persistent reactivation of the infection triggers the accumulation of CD8+ Tem cells in a process called memory inflation. Besides, this memory T cell population behaves differently than normal memory T cell populations. Under normal conditions, Tem cells have a limited expansion capacity, and this pool relies on the proliferation and differentiation of Tcm cells (long-lived classical memory). Nevertheless, in latent infections Tem cells substantially increase their proliferation rate and maintain their pool without the support of Tcm cells (48). Such generates a new long-lived non-classical memory population in the Tem pool (49). Interestingly, the latent infection promotes changes not only in the phenotype and dynamics of the memory T cell population but also in the TCR repertoire.

Unlike antibodies, TCRs lack a mechanism for affinity maturation. Therefore, under normal conditions, very few T cells would be able to bind the HLA-peptide complex with enough affinity to generate a response and a memory population. Consequently, few mutations in the virus would be enough to escape the T cell response. Fortunately, the coreceptor molecules CD4 and CD8 solve this problem by increasing the stability of the TCR-peptide-HLA complex by binding conserved regions in the HLA. Such allows TCRs with moderate affinity to enter the memory compartment increasing its diversity and preventing immune escape through antigen mutation (50). This mechanism works very efficiently when the antigen load is high, like during the acute phase of the infection: TCRs with high affinity are saturated and low-affinity TCRs are able to bind the remaining antigens. However, in the latent phase, the antigen load is small, and the high-affinity TCRs outcompete the low-affinity TCRs. Therefore, after several lytic cycles, the response becomes very oligoclonal and directed to the most immunodominant antigens. For instance, the phosphoprotein pp65 and the immediate-early protein 1 (IE1) of CMV (49). This phenomenon may increase its relevance with age. This progressively more skewed response allows the reinfection with a genetically different variant of the latent virus in a process called superinfection (51). Importantly, this phenomenon has hampered the efforts to develop a vaccine against CMV or EBV (52). On top of that, CMV and EBV have a vast arsenal of immunoevasins to escape the immune response.

In conclusion, our results showed that adipose tissue, mainly oWAT, hosts a complete immune response against latent CMV infection, and presumable to other viruses (including EBV and influenza) or other pathogens. Thus, our study suggests that the immunological function is more robust in oWAT than sWAT. We found CMV-reactive T lymphocytes, inflation of the CD8+ population, and the skewed TCR repertoire against immunodominant antigens presented by HLA class I alleles. This strongly suggests that oWAT is a relevant immunological organ for antiviral responses in humans. Although our study has specifically examined oWAT and sWAT, other types of adipose tissue (even beyond the intraperitoneal cavity) may also play a relevant immunological role.

4 Materials and methods

4.1 Patient cohort

This study includes 11 morbidly obese patients who underwent laparoscopic bariatric surgery (gastric bypass or gastric sleeve) at San Cecilio University Hospital (Granada, Spain). The ethics committee of the hospital (Andalucia's Biomedical Research Ethics Committee of Granada) approved the study, and all participants signed written informed consent. Patients were excluded from the cohort if they presented any autoimmune disorder. All biochemical analyses were carried out within 24 hours by routine methods at the Clinical Analysis Laboratory of San Cecilio University Hospital (Granada, Spain). HLA genotyping, CMV and EBV serology were carried out at the Clinical Analyses and Immunology Unit of Virgen de las Nieves University Hospital (Granada, Spain). HLA genotyping was performed through PCR-SSO (Specific Sequence Oligonucleotides) with LABType kits from One Lambda (Los Angeles, CA, USA). PCR-SSO uses probes that hybridize to the most polymorphic regions of each *locus*. On the other hand, CMV and EBV serology were performed through CLIA (ChemiLuminescent ImmunoAssay), an ultrasensitive ELISA, with Alinity i CMV IgG and IgM, and EBV VCA IgM and EBNA-1 IgG kits by Abbott (Chicago, IL, USA). In the case of CMV, no specific antigen is used, but a total lysate of CMV from AD169 strain.

4.2 Sample processing

Blood samples were collected before surgery and after 10 h fasting. Liver (around 10 mg) and adipose tissue biopsies (around 3 g) were obtained at the moment of surgery and kept in PBS at 4 °C until they arrived at the laboratory. oWAT biopsies were obtained

from the greater omentum close to the stomach. sWAT tissue biopsies were obtained near the surgical incision.

Liver biopsies were entirely devoted to TCR analysis. Therefore, liver biopsies were preserved in 500 µl of lysis buffer (Qiagen, Hilden, Germany) at -20°C until total RNA extraction. Around 300 mg of the biopsies from each adipose tissue were preserved in 500 µl of lysis buffer (Qiagen) at -20°C for RNA extraction. The rest of each adipose tissue biopsy (around 2 g) was examined to remove small lymph nodes and blood vessels that were eventually present in the tissue. After that, they were digested in 10 ml of RPMI 1640 medium supplemented with 2 mg/ml type I collagenase (Sigma, St Louis, MO, USA), 1 mg/ml hyaluronidase (Sigma) and 5 mM CaCl2, for 2h, at 37°C.

The digestion was diluted with PBS and filtered through a 1 mm sieve. Later, it was centrifuged at 900 x g for 10 minutes and the pellet was resuspended in PBS, then filtered through a 100 µm filter, and centrifuged again at 900 x g for 10 minutes. The resulting pellet contained the SVF, and it was split for flow cytometry and ELISpot.

For flow cytometry, a quarter of the SVF was resuspended in 200µl of antibody staining buffer (PBS, 2% fetal bovine serum, 0.09% albumin, and 0.05% sodium azide) and mixed with an internal standard (CountBright Absolute Counting Beads). The internal standard is a suspension of a known number of autofluorescent beads with wide emission spectra. The internal control has different size and complexity values from any cell population, which enables the differentiation between them. For ELISpot, the rest of the SVF was resuspended in 1 ml of RPMI 1640 medium to isolate the mononuclear fraction from the SVF by ficoll gradient.

Likewise, PBMCs from 6 ml of blood samples diluted 1:1 with PBS were also isolated by ficoll gradient. The interphase obtained was washed with PBS and pellet was later preserved in 500 µl of lysis buffer at -20°C for RNA extraction.

4.3 RNA extraction and retrotranscription

Total RNA extraction from isolated peripheral blood lymphocytes and tissues (oWAT, sWAT, and liver) was carried out using standard silica-membrane columns from RNeasy Mini Kit by Qiagen. A minimum of 20ng/µl of RNA was retrotranscribed to cDNA using the iScript™ cDNA Synthesis Kit by BioRad (Hercules, CA, USA).

4.4 TCRβ library preparation and next-generation sequencing (NGS)

TCRβ repertoire sequencing was performed in the Ion S5 platform using Ion-530 chips and its extended modality, which can obtain reads up to 600pb. The coverage was around 140000 sequences per sample. During the preparation of NGS libraries, one of the main sources of bias is the ligation reaction, which is usually employed to join adaptors (53). For that reason, our innovative methodology prepared long-read TCRβ barcoded libraries without any ligation step. Moreover, as opposed to most current strategies based on short reads centered in the CDR3 (sequencing only the V segment end region), our long-read method covered the entire V segment. This improved the identification within highly conserved V families, particularly in V5 and V6 families. Reads also included D and J segments, a small part of C segment, the CDR-3 loop (functional part of the hypervariable region) and, CDR-1 and CDR-2 loops (provided by each V segment).

The methodology for TCRβ library preparation is fully detailed Supplementary Protocol 1. It involved an enrichment multiplex PCR where all TCRs were amplified simultaneously with a collection of primers capable of hybridizing with every V segment. It was followed by the "fishing" of the molecules of interest by magnetic particles. After that, the sequences of the adaptors for Ion S5 (A and P1) were added through the extension on the DNA strands covalently bound to the magnetic particles. This step was critical since it avoided ligation bias. Lastly, there was a final PCR to release the DNA from the microparticles and the purification of its product.

4.5 TCR repertoire analysis

Read length distribution and sequencing quality were assessed with FastQC and MultiQC (54) software. BAM files were filtered with SAMtools (55) to select reads between 400-500 nucleotides long, as it was the expected length range of our TCRβ amplification method. Demultiplexing by sample barcode identification, tetramer (CGAT) and C primer sequence integrity were ascertained with R package Biostrings (v2.50.2) (56). Reads that did not meet any of these criteria were discarded from the analysis. Identification of V and J gene segments and CDR3 sequence was performed with RTCR v0.5.1 (57) with default parameters.

Immune repertoire analyses were performed with the immunarch R package (v0.6.5). A unique clonotype was defined by its V and J gene segments and its CDR3 amino acid sequence. Proportional downsampling and bootstrapping with 100 replicates were performed in the diversity and overlap analyses (except for Venn diagrams) to account for differences in read counts between samples. Productive clonality was calculated as the square root of Simpson's diversity index of productive clonotypes.

4.6 Antigen specificity prediction

Antigen specificity prediction was performed following the guidelines by Pogorelyy and Shugay (2019) (58). First, the VDJdb database (59) was downloaded in June 2021 and all the TCRβ CDR3 sequences were clustered with our repertoires with GIANA (Geometric Isometry-based TCR AligNment Algorithm) (60) in query mode, considering V gene segment and CDR3 amino acid sequence. All query TCRs that clustered with a TCR present in the VDJdb database were annotated with the antigen specificity

information provided in the database. Only antigens whose cognate TCRs represented an aggregated frequency in the repertoire higher than 0.0001 (medium-sized, large-sized and hyperexpanded clones) were included in the analysis to control for unspecific annotations lower in frequency that may not reflect a true T-cell response.

4.7 ELISpot assays

ELISpot was performed with ELISpot Path PRO: Human IFN-γ (CMV) (Mabtech, Nacka Strand, Sweden). The CMV peptide included in the ELISpot assay consists of 42 peptides from CMV that induces the secretion of IFN-γ, from human CD4 and CD8 T cells. The antigens presented in the pool are pp50, pp65, IE1, IE2 and envelope glycoprotein B. Of the 42 peptides, 28 are HLA-I restricted (covering HLA-A1, HLA-A2, HLA-A3, HLA-A11, HLA-A23, HLA-A24, HLA-A26, HLA-A30, HLA-B7, HLA-B8, HLA-B18, HLA-B27, HLA-B35, HLA-B40/60, HLA-B41, HLA-B44, HLA-B57/58, HLA-C7) and 14 are HLA-II restricted (covering HLA-DRB1*01, 03, 04, 05, 07, 08, 11, 15, 20, 24, 53, HLA-DPw2, HLA-DQB, HLA-DP3*14, 20). Beforehand, we ensured that every donor in our cohort carry at least one HLA restriction allele, so that the pool covers all the donors.

The ELISpot plate, precoated with 1-D1K monoclonal antibody, was washed 4 times with sterile PBS and incubated with RPMI + 10% FBS medium for 2 hours. According to the manufacturer's instructions, duplicates (when possible) of 250000 cells from the mononuclear fraction of SVF and PBMCs were seeded in each well. Cells were resuspended in 100 µl of RPMI + 10% FBS medium with 2µg/ml of CMV peptide pool for human CD4 and CD8 T cells. Positive control cells were resuspended in media with 1:1000 anti-CD3. One negative control was also included. Positive and negative controls were performed only with PBMCs due to a lack of cells in oWAT and sWAT. Plates were incubated for 16 - 24 hours at 37°C in a 5% CO2 incubator. After 5 PBS washing steps, 100µl diluted 7-B6-1-ALP conjugate (1µg/ml) was added per well and incubated for 2 hours at room temperature. After another 5 times of PBS washes, 100µl of filtered BCIP/NBT- plus solution was added per well and left until spots emerged. To stop the color reaction, plates were washed with tap water. After letting the plate dry, photographs were taken with a FujiFilm X-T4 camera and a Canon macro lens of 100 mm. Spots were then counted, and their area was measured with ImageJ.

4.8 Flow cytometry

The SVF or fresh blood of the 11 donors was labelled with 2 ml of controls or fluorophore-conjugated antibodies at room temperature for 20 minutes. Later, cells were fixed, and the erythrocytes were lysed with 1 ml of BD FACS Lysing Solution for 30 minutes. After that, samples were centrifuged for 10 minutes at 3500 x g, and pellets were resuspended in 200 µl of PBS. Then, samples were stored at 4°C until the next day.

Flow cytometry was performed using BD FACS ARIA IIIu equipment, and data were generated with a logarithmic scale acquisition. The internal standard was used to calculate the number of cells per mg of tissue. Two panels with different fluorescent-conjugated antibodies were used. Panel 1: anti-CD3 BB515 (clone HIT3A, BD Biosciences), anti-CD4 APC (clone RPA-T4, BD Biosciences), anti-CD8 BV711 (clone SK1, BioLegend), anti-CCR7 PE-Cy7 (clone G043H7, BioLegend) and anti-CD45RA BV421 (clone HI100, BioLegend). Panel 2: anti-CD3 BV510 (clone OKT3, BioLegend), anti-CD4 FITC (clone RPA-T4, BD Biosciences), anti-CD8 BV711 (clone SK1, BioLegend), anti-CD69 PE-Cy7 (clone FN50, BD Biosciences), anti-CD49a APC (clone TS2/7, BioLegend) and anti-CD103 PE (clone Ber-ACT8, BioLegend).

4.9 Statistical tests

Unless otherwise specified, all statistical analyses were performed in R (v3.6.1). The normality of the data was assessed with the Shapiro-Wilk test and from there it was decided to conduct non-parametric tests. Kruskal-Wallis test was chosen to compare groups and *post-hoc* pairwise comparisons were performed with the two-sided Wilcoxon test. Graphics on Figures 3–6 were performed with GraphPad 8 (La Jolla, CA, USA).

Data availability statement

The datasets presented in this study can be found in online repositories. The names of the repository/repositories and accession number(s) can be found below: BioProject accession: PRJNA980167.

Ethics statement

The studies involving humans were approved by Andalucia's Biomedical Research Ethics Committee of Granada. The studies were conducted in accordance with the local legislation and institutional requirements. The participants provided their written informed consent to participate in this study.

Author contributions

AR: Conceptualization, Formal Analysis, Investigation, Methodology, Validation, Visualization, Writing – original draft, Writing – review & editing. MB: Conceptualization, Data curation, Formal Analysis, Methodology, Validation, Visualization, Writing – original draft, Writing – review & editing. DL: Investigation, Writing – original draft, Writing – review & editing. JG: Resources, Writing – review & editing. FT: Resources, Writing – review & editing. DP: Investigation, Software, Writing – review &

editing. SM: Software, Visualization, Writing – review & editing. IR: Resources, Visualization, Writing – review & editing. JP: Investigation, Writing – review & editing. JV: Investigation, Writing – review & editing. ML: Investigation, Writing – review & editing. FG: Supervision, Writing – review & editing. CC: Funding acquisition, Supervision, Writing – review & editing. JL: Conceptualization, Funding acquisition, Project administration, Supervision, Writing – review & editing. ÁC: Conceptualization, Funding acquisition, Project administration, Supervision, Writing – original draft, Writing – review & editing.

Funding

The author(s) declare financial support was received for the research, authorship, and/or publication of this article. This work was supported by Instituto de Salud Carlos III (grant PI15/01361 and DTS22/00151), FEDER/Junta de Andalucía (grant P18-RT-4930 and A-BIO-470-UGR20) and MCIN/AEI/10.13039/501100011033/FEDER (grant PID2021-128970OA-I00). AR-R was supported by European Social Fund (PEJ2018-003016-A). MB-C was supported by an FPU19/00576 predoctoral fellowship funded by the Spanish Ministry of Science, Innovation, and Universities.

Conflict of interest

The authors declare that the research was conducted in the absence of any commercial or financial relationships that could be construed as a potential conflict of interest.

The author(s) declared that they were an editorial board member of Frontiers, at the time of submission. This had no impact on the peer review process and the final decision.

Publisher's note

Supplementary material

The Supplementary Material for this article can be found online at: https://www.frontiersin.org/articles/10.3389/fimmu.2023.1303724/full#supplementary-material

References

1. Fowler K, Mucha J, Neumann M, Lewandowski W, Kaczanowska M, Grys M, et al. A systematic literature review of the global seroprevalence of cytomegalovirus: possible implications for treatment, screening, and vaccine development. *BMC Public Health* (2022) 22(1):1659. doi: 10.1186/s12889-022-13971-7

2. Holtappels R, Pahl-Seibert MF, Thomas D, Reddehase MJ. Enrichment of immediate-early 1 (m123/pp89) peptide-specific CD8 T cells in a pulmonary CD62L (lo) memory-effector cell pool during latent murine cytomegalovirus infection of the lungs. *J Virol* (2000) 74(24):11495–503. doi: 10.1128/JVI.74.24.11495-11503.2000

3. Emery VC. Investigation of CMV disease in immunocompromised patients. *J Clin Pathol* (2001) 54(2):84–8. doi: 10.1136/jcp.54.2.84

4. Contreras NA, Sitnik KM, Jeftic I, Coplen CP, Čičin-Šain L, Nikolich-Žugich J. Life-long control of cytomegalovirus (CMV) by T resident memory cells in the adipose tissue results in inflammation and hyperglycemia. *PLoS Pathogens* (2019) 15(6): e1007890. doi: 10.1371/journal.ppat.1007890

5. Wanjalla CN, McDonnell WJ, Ram R, Chopra A, Gangula R, Leary S, et al. Single-cell analysis shows that adipose tissue of persons with both HIV and diabetes is enriched for clonal, cytotoxic, and CMV-specific CD4+ T cells. *Cell Rep Med* (2021) 2 (2):100205. doi: 10.1016/j.xcrm.2021.100205

6. Scheja L, Heeren J. The endocrine function of adipose tissues in health and cardiometabolic disease. *Nat Rev Endocrinol* (2019) 15(9):507–24. doi: 10.1038/s41574-019-0230-6

7. Wu J, Cohen P, Spiegelman BM. Adaptive thermogenesis in adipocytes: Is beige the new brown? *Genes Dev* (2013) 27(3):234–50. doi: 10.1101/gad.211649.112

8. Trim WV, Lynch L. Immune and non-immune functions of adipose tissue leukocytes. *Nat Rev Immunol* (2022) 22(6):371–86. doi: 10.1038/s41577-021-00635-7

9. García-Rubio J, León J, Redruello-Romero A, Pavón E, Cozar A, Tamayo F, et al. Cytometric analysis of adipose tissue reveals increments of adipocyte progenitor cells after weight loss induced by bariatric surgery. *Sci Rep* (2018) 8(1):15203. doi: 10.1038/s41598-018-33488-7

10. Lopez-Perez D, Redruello-Romero A, Garcia-Rubio J, Arana C, Garcia-Escudero LA, Tamayo F, et al. In patients with obesity, the number of adipose tissue mast cells is significantly lower in subjects with type 2 diabetes. *Front Immunol* (2021) 12:664576. doi: 10.3389/fimmu.2021.664576

11. Lopez-Perez D, Redruello-Romero A, Garcia-Rubio J, Arana C, Garcia-Escudero LA, Tamayo F, et al. In obese patients with type 2 diabetes, mast cells in Omental adipose tissue decrease the surface expression of CD45, CD117, CD203c, and fcεRI. *Front Endocrinol (Lausanne)* (2022) 13:818388. doi: 10.3389/fendo.2022.818388

12. Unamuno X, Gómez-Ambrosi J, Rodríguez A, Becerril S, Frühbeck G, Catalán V. Adipokine dysregulation and adipose tissue inflammation in human obesity. *Eur J Clin Invest* (2018) 48(9):e12997. doi: 10.1111/eci.12997

13. Zhang Lj, Guerrero-Juarez CF, Hata T, Bapat SP, Ramos R, Plikus MV, et al. Dermal adipocytes protect against invasive Staphylococcus aureus skin infection. *Science* (2015) 347(6217):67–71. doi: 10.1126/science.1260972

14. Bénézech C, Luu NT, Walker JA, Kruglov AA, Loo Y, Nakamura K, et al. Inflammation-induced formation of fat-associated lymphoid clusters. *Nat Immunol* (2015) 16(8):819–28. doi: 10.1038/ni.3215

15. Moro K, Yamada T, Tanabe M, Takeuchi T, Ikawa T, Kawamoto H, et al. Innate production of TH2 cytokines by adipose tissue-associated c-Kit+Sca-1+ lymphoid cells. *Nature* (2010) 463(7280):540–4. doi: 10.1038/nature08636

16. Meza-Perez S, Randall TD. Immunological functions of the omentum. *Trends Immunol* (2017) 38(7):526–36. doi: 10.1016/j.it.2017.03.002

17. Han SJ, Zaretsky AG, Andrade-Oliveira V, Collins N, Dzutsev A, Shaik J, et al. The white adipose tissue is a reservoir for memory T cells that promotes protective memory responses to infection. *Immunity* (2017) 47(6):1154–68. doi: 10.1016/j.immuni.2017.11.009

18. Damouche A, Lazure T, Avettand-Fènoël V, Huot N, Dejucq-Rainsford N, Satie AP, et al. Adipose tissue is a neglected viral reservoir and an inflammatory site during chronic HIV and SIV infection. *PLoS Pathogens* (2015) 11(9):e1005153. doi: 10.1371/journal.ppat.1005153

19. Gordon CL, Miron M, Thome JJC, Matsuoka N, Weiner J, Rak MA, et al. Tissue reservoirs of antiviral T cell immunity in persistent human CMV infection. *J Exp Med* (2017) 214(3):651–67. doi: 10.1084/jem.20160758

20. Meyer D C, Aguiar VR, Bitarello BD, C. Brandt DY, Nunes K. A genomic perspective on HLA evolution. *Immunogenetics* (2018) 70(1):5–27. doi: 10.1007/s00251-017-1017-3

21. Rao X, Hoof I, Fontaine Costa AICA, van Baarle D, Keşmir C. HLA class I allele promiscuity revisited. *Immunogenetics* (2011) 63(11):691–701. doi: 10.1007/s00251-011-0552-6

22. Mandelcorn-Monson RL, Shear NH, Yau E, Sambhara S, Barber BH, Spaner D, et al. Cytotoxic T lymphocyte reactivity to gp100, melanA/MART-1, and tyrosinase, in HLA-A2-positive vitiligo patients. *J Invest Dermatol* (2003) 121(3):550–6. doi: 10.1046/j.1523-1747.2003.12413.x

23. Farber DL, Yudanin NA, Restifo NP. Human memory T cells: generation, compartmentalization and homeostasis. *Nat Rev Immunol* (2014) 14(1):24–35. doi: 10.1038/nri3567

24. Palmer D. The effect of age on thymic function. *Front Immunol* (2013) 4:316. doi: 10.3389/fimmu.2013.00316

25. Koch S, Larbi A, Derhovanessian E, Özcelik D, Naumova E, Pawelec G. Multiparameter flow cytometric analysis of CD4 and CD8 T cell subsets in young and old people. *Immun Ageing* (2008) 5:6. doi: 10.1186/1742-4933-5-6

26. Luong Q, Huang J, Lee KY. Deciphering white adipose tissue heterogeneity. *Biol (Basel)* (2019) 8(2):23. doi: 10.3390/biology8020023

27. Bagchi DP, MacDougald OA. Identification and dissection of diverse mouse adipose depots. *J Vis Exp* (2019) 149). doi: 10.3791/59499

28. Virtue S, Vidal-Puig A. It's not how fat you are, it's what you do with it that counts. *PLoS Biol* (2008) 6(9):e237. doi: 10.1371/journal.pbio.0060237

29. Lumeng CN, DelProposto JB, Westcott DJ, Saltiel AR. Phenotypic switching of adipose tissue macrophages with obesity is generated by spatiotemporal differences in macrophage subtypes. *Diabetes* (2008) 57(12):3239–46. doi: 10.2337/db08-0872

30. Hudson D, Fernandes RA, Basham M, Ogg G, Koohy H. Can we predict T cell specificity with digital biology and machine learning? *Nat Rev Immunol* (2023), 8:511–21. doi: 10.1038/s41577-023-00835-3

31. Jurewicz MM, Stern LJ. Class II MHC antigen processing in immune tolerance and inflammation. *Immunogenetics* (2019) 71(3):171–87. doi: 10.1007/s00251-018-1095-x

32. Prasad S, Starck SR, Shastri N. Presentation of cryptic peptides by MHC I is enhanced by inflammatory stimuli. *J Immunol* (2016) 197(8):2981–91. doi: 10.4049/jimmunol.1502045

33. Sinclair C, Bains I, Yates AJ, Seddon B. Asymmetric thymocyte death underlies the CD4:CD8 T-cell ratio in the adaptive immune system. *Proc Natl Acad Sci U S A* (2013) 110(31):E2905–14. doi: 10.1073/pnas.1304859110

34. Sathaliyawala T, Kubota M, Yudanin N, Turner D, Camp P, Thome JJC, et al. Distribution and compartmentalization of human circulating and tissue-resident memory T cell subsets. *Immunity* (2013) 38(1):187–97. doi: 10.1016/j.immuni.2012.09.020

35. Sckisel GD, Mirsoian A, Minnar CM, Crittenden M, Curti B, Chen JQ, et al. Differential phenotypes of memory CD4 and CD8 T cells in the spleen and peripheral tissues following immunostimulatory therapy. *J Immunother Cancer* (2017) 5:33. doi: 10.1186/s40425-017-0235-4

36. Cibrián D, Sánchez-Madrid F. CD69: from activation marker to metabolic gatekeeper. *Eur J Immunol* (2017) 47(6):946–53. doi: 10.1002/eji.201646837

37. Kumar BV, Ma W, Miron M, Granot T, Guyer RS, Carpenter DJ, et al. Human tissue-resident memory T cells are defined by core transcriptional and functional signatures in lymphoid and mucosal sites. *Cell Rep* (2017) 20(12):2921–34. doi: 10.1016/j.celrep.2017.08.078

38. Walsh DA, da Silva HB, Beura LK, Peng C, Hamilton SE, Masopust D, et al. The functional requirement for CD69 in establishment of resident memory CD8+ T cells varies with tissue location. *J Immunol* (2019) 203(4):946–55. doi: 10.4049/jimmunol.1900052

39. Bromley SK, Akbaba H, Mani V, Mora-Buch R, Chasse AY, Sama A, et al. CD49a regulates cutaneous resident memory CD8+ T cell persistence and response. *Cell Rep* (2020) 32(9):108085. doi: 10.1016/j.celrep.2020.108085

40. Richter MV, Topham DJ. The α1β1 integrin and TNF receptor II protect airway CD8+ Effector T cells from apoptosis during influenza infection1. *J Immunol* (2007) 179(8):5054–63. doi: 10.4049/jimmunol.179.8.5054

41. Reilly EC, Lambert Emo K, Buckley PM, Reilly NS, Smith I, Chaves FA, et al. TRM integrins CD103 and CD49a differentially support adherence and motility after resolution of influenza virus infection. *Proc Natl Acad Sci U S A* (2020) 117(22):12306–14. doi: 10.1073/pnas.1915681117

42. Chapman TJ, Topham DJ. Identification of a Unique Population of Tissue-Memory CD4+ T cells in the Airways after Influenza Infection that is Dependent on the Integrin VLA-1. *J Immunol* (2010) 184(7):3841–9. doi: 10.4049/jimmunol.0902281

43. Cheuk S, Schlums H, Gallais Sérézal I, Martini E, Chiang SC, Marquardt N, et al. CD49a expression defines tissue-resident CD8+ T cells poised for cytotoxic function in human skin. *Immunity* (2017) 46(2):287–300. doi: 10.1016/j.immuni.2017.01.009

44. Reilly EC, Sportiello M, Emo KL, Amitrano AM, Jha R, Kumar ABR, et al. CD49a identifies polyfunctional memory CD8 T cell subsets that persist in the lungs after influenza infection. *Front Immunol* (2021) 12:728669. doi: 10.3389/fimmu.2021.728669

45. Mackay LK, Stock AT, Ma JZ, Jones CM, Kent SJ, Mueller SN, et al. Long-lived epithelial immunity by tissue-resident memory T (TRM) cells in the absence of persisting local antigen presentation. *Proc Natl Acad Sci U S A* (2012) 109(18):7037–42. doi: 10.1073/pnas.1202288109

46. Speiser DE, Utzschneider DT, Oberle SG, Münz C, Romero P, Zehn D. T cell differentiation in chronic infection and cancer: functional adaptation or exhaustion? *Nat Rev Immunol* (2014) 14(11):768–74. doi: 10.1038/nri3740

47. Nikolich-Žugich J. Ageing and life-long maintenance of T-cell subsets in the face of latent persistent infections. *Nat Rev Immunol* (2008) 8(7):512–22. doi: 10.1038/nri2318

48. Muschaweckh A, Buchholz VR, Fellenzer A, Hessel C, König PA, Tao S, et al. Antigen-dependent competition shapes the local repertoire of tissue-resident memory CD8+ T cells. *J Exp Med* (2016) 213(13):3075–86. doi: 10.1084/jem.2016088

49. Klenerman P, Oxenius A. T cell responses to cytomegalovirus. *Nat Rev Immunol* (2016) 16(6):367–77. doi: 10.1038/nri.2016.38

50. Turner SJ, Doherty PC, McCluskey J, Rossjohn J. Structural determinants of T-cell receptor bias in immunity. *Nat Rev Immunol* (2006) 6(12):883–94. doi: 10.1038/nri1977

51. Hansen SG, Powers CJ, Richards R, Ventura AB, Ford JC, Siess D, et al. Evasion of CD8+ T cells is critical for super-infection by cytomegalovirus. *Science* (2010) 328 (5974):102–6. doi: 10.1126/science.1185350

52. Berry R, Watson GM, Jonjic S, Degli-Esposti MA, Rossjohn J. Modulation of innate and adaptive immunity by cytomegaloviruses. *Nat Rev Immunol* (2020) 20 (2):113–27. doi: 10.1038/s41577-019-0225-5

53. Potapov V, Ong JL, Langhorst BW, Bilotti K, Cahoon D, Canton B, et al. A single-molecule sequencing assay for the comprehensive profiling of T4 DNA ligase fidelity and bias during DNA end-joining. *Nucleic Acids Res* (2018) 46(13):e79. doi: 10.1093/nar/gky303

54. Ewels P, Magnusson M, Lundin S, Käller M. MultiQC: summarize analysis results for multiple tools and samples in a single report. *Bioinformatics* (2016) 32 (19):3047–8. doi: 10.1093/bioinformatics/btw354

55. Danecek P, Bonfield JK, Liddle J, Marshall J, Ohan V, Pollard MO, et al. Twelve years of SAMtools and BCFtools. *GigaScience* (2021) 10(2):giab008. doi: 10.1093/gigascience/giab008

56. Pagès H, Aboyoun P, Gentleman R, DebRoy S. *Biostrings: Efficient manipulation of biological strings*. (2023), Biostrings, R package version 2.70.1, Available at: https://bioconductor.org/packages/Biostrings

57. Gerritsen B, Pandit A, Andeweg AC, de Boer RJ. RTCR: a pipeline for complete and accurate recovery of T cell repertoires from high throughput sequencing data. *Bioinformatics* (2016) 32(20):3098–106. doi: 10.1093/bioinformatics/btw339

58. Pogorelyy MV, Shugay M. A framework for annotation of antigen specificities in high-throughput T-cell repertoire sequencing studies. *Front Immunol* (2019) 10:2159. doi: 10.3389/fimmu.2019.02159

59. Goncharov M, Bagaev D, Shcherbinin D, Zvyagin I, Bolotin D, Thomas PG, et al. VDJdb in the pandemic era: a compendium of T cell receptors specific for SARS-CoV-2. *Nat Methods* (2022) 19(9):1017–9. doi: 10.1038/s41592-022-01578-0

60. Zhang H, Zhan X, Li B. GIANA allows computationally-efficient TCR clustering and multi-disease repertoire classification by isometric transformation. *Nat Commun* (2021) 12(1):4699. doi: 10.1038/s41467-021-25006-7

frontiers | Frontiers in Immunology

TYPE Original Research
PUBLISHED 18 December 2023
DOI 10.3389/fimmu.2023.1322536

OPEN ACCESS

EDITED BY
Nick P. Goplen,
Mayo Clinic, United States

REVIEWED BY
Li Yuhua,
National Institutes for Food and Drug Control, China
Larry Ellingsworth,
Novavax Inc., United States

*CORRESPONDENCE
Jan Pravsgaard Christensen
jpc@sund.ku.dk
Allan Randrup Thomsen
athomsen@sund.ku.dk

†These authors have contributed equally to this work and share senior authorship

RECEIVED 17 October 2023
ACCEPTED 15 November 2023
PUBLISHED 18 December 2023

CITATION
Zhou J, Uddback I, Kohlmeier JE, Christensen JP and Thomsen AR (2023) Vaccine induced memory CD8+ T cells efficiently prevent viral transmission from the respiratory tract.
Front. Immunol. 14:1322536.
doi: 10.3389/fimmu.2023.1322536

Vaccine induced memory CD8$^+$ T cells efficiently prevent viral transmission from the respiratory tract

Jinglin Zhou[1], Ida Uddback[1], Jacob E. Kohlmeier[2], Jan Pravsgaard Christensen[1*†] and Allan Randrup Thomsen[1*†]

[1]Department of Immunology and Microbiology, University of Copenhagen, Copenhagen, Denmark, [2]Department of Microbiology and Immunology, Emory University, Atlanta, GA, United States

Introduction: Mucosal immunization eliciting local T-cell memory has been suggested for improved protection against respiratory infections caused by viral variants evading pre-existing antibodies. However, it remains unclear whether T-cell targeted vaccines suffice for prevention of viral transmission and to which extent local immunity is important in this context.

Methods: To study the impact of T-cell vaccination on the course of viral respiratory infection and in particular the capacity to inhibit viral transmission, we used a mouse model involving natural murine parainfluenza infection with a luciferase encoding virus and an adenovirus based nucleoprotein targeting vaccine.

Results and discussion: Prior intranasal immunization inducing strong mucosal CD8+ T cell immunity provided an almost immediate shut-down of the incipient infection and completely inhibited contact based viral spreading. If this first line of defense did not operate, as in parentally immunized mice, recirculating T cells participated in accelerated viral control that reduced the intensity of inter-individual transmission. These observations underscore the importance of pursuing the development of mucosal T-cell inducing vaccines for optimal protection of the individual and inhibition of inter-individual transmission (herd immunity), while at the same time explain why induction of a strong systemic T-cell response may still impact viral transmission.

KEYWORDS

vaccines, resident memory T cells (Trm), virus', mucosal surface, CD8 T cell, herd immunity

Introduction

Being in close and continual contact with the external environment, the respiratory tract is a major portal of entry for a variety of pathogens. Respiratory viruses, such as influenza virus, coronavirus, respiratory syncytial virus (RSV), and parainfluenza virus (PIV), cause mild upper respiratory infections and cold-like symptoms but may also cause bronchitis, pneumonia, and even death, as a result of increased lower respiratory tract involvement. With limited effective prevention or therapy currently, these infections are highly contagious to young children, the elderly and immunocompromised patients, leading to hospitalization and mortality. SARS-CoV-2, the cause of the COVID-19 pandemic, has resulted in over 620 million cases and over 6.5 million deaths worldwide (WHO, 2022). Seasonal influenza epidemics usually occur during winter and can infect up to 20% of the population, depending on which viruses are circulating, and they can cause substantial mortality - up to 650 000 deaths worldwide annually (WHO). Similarly, RSV circulates seasonally and is being increasingly recognized with morbidity and mortality among children and the elderly approaching what is seen with influenza (1). PIV also commonly infects infants and children, and it is still in the absence of effective prevention or therapy for human PIVs illness (CDC).

Given the global burden of viral respiratory infections, there is an urgent need for vaccination to boost protective immune responses. Most current vaccine strategies focus on the induction of neutralizing antibodies which primarily target conformational epitopes on surface proteins and rarely provide substantial cross-protection against viral escape variants (2, 3). In contrast, T cell epitopes consist of short linear amino acid sequences (4) which are widely distributed across proteins, including internal viral components, e.g. viral nucleoprotein, which are much more conserved across variants. Therefore invoking T cell immunity potentially could bring huge advantages to vaccines by offering broad and durable protection. Several studies have shown that specific T cell responses inversely correlate with disease risk and severity (5–10). There are three major subsets of memory T cells as defined by recent studies, which are termed central memory T cells (Tcm), effector memory T cells (Tem), and tissue resident memory T cells (Trm) (11, 12). Trm cells are sessile antigen-primed cells positioned in various non-lymphoid organs, particularly the barrier tissues skin and mucosa, but also in certain internal organs like brain and liver. In the upper and lower respiratory tract, Trm cells have been shown to play a critical role in the early local defense against respiratory infections, such as influenza (13, 14), RSV (15–17), and SARS-CoV-2 (18). The development of a stable population of respiratory tract Trm generally requires local antigen recognition (19–21), whereas conventional parenteral immunization do not suffice to drive substantial local accumulation of these cells. Induction of protective mucosal immunity is more likely to reduce transmission, because viral respiratory infections primarily initiate in the upper respiratory tract, which is also an important source for production of virus and virus containing droplets and aerosol particles to subsequently spread to other individuals.

Adenoviral (Ad) vectors have been extensively investigated and applied for vaccine research (22), and Ad vectors has recently been implemented as platforms for real life vaccines against Ebola (23) and corona viruses (24, 25). These vectors stimulate potent CD8+ T cell responses toward inserted transgene antigen with persistent expression leading to long-lasting immunity (21, 26). Using an Ad encoding influenza virus nucleoprotein, we have previously found that intranasal (i.n.) vaccination elicits a more prolonged protection than systemic vaccination through the footpad (s.c.). However, vaccination by the former route was relatively inefficient in inducing potent systemic T-cell memory as evident by fewer circulating antigen specific memory T cells. In contrast, combined vaccination provided very most robust and durable protection, which highlighted not only the role of resident memory T cells as a critical first line of defense, but also the important back-up role for circulating memory T cells that can expand and migrate to the infected tissue (21, 27).

Despite that a clear association between cell mediated immunity and host protection against severe disease has been demonstrated (5–9), the impact of a rapid T-cell response on transmissibility has only recently been studied, and the potential of using T-cell targeted vaccination to interrupt virus transmission has not been evaluated in detail. Since T cells need to detect and eliminate infected cells, a key question is whether vaccine-induced T-cell immunity may lower viral loads and infectiousness in immunized hosts fast and efficiently enough to prevent inter-individual transmission. Information on this issue is clearly of great significance if the goal is to elicit herd immunity through T-cell targeted vaccination.

Since human influenza viruses and coronaviruses are poorly infectious in mice without adaptation, attempts to establish relevant mouse models for studies of viral transmission have been relatively unsuccessful (28, 29). Related to human PIV, Sendai virus is a natural mouse pathogen that readily transmits between co-housed individuals (30, 31). Furthermore, by using luciferase-expressing challenge virus (rSeV) and a non-invasive *in vivo* imaging system (IVIS), we could - based on earlier observations showing that the intensity of bioluminescence correlates with the extent of viral infection (31) - perform a detailed mapping of the kinetics of the virus infection on an individual basis,. Using this model system we compared the durable protection afforded by systemic vs systemic plus local immunization with an Ad vector encoding Sendai virus nucleoprotein. We found that compared to s.c. vaccination – inducing systemic immunity only -, the combined local and systemic immunity induced by i.n.+s.c. vaccination elicited highly effective and immediate T-cell dependent virus control, which through the release of IFNγ could completely prevent virus transmission and lasted for at least five months. Of substantial interest, we also found that while parenteral vaccination alone failed to provide immediate virus control in the respiratory tract, systemic immunity still significantly reduced onward transmission, albeit not with the same efficiency as that associated with airway immunization.

Materials and methods

Mice

Female C57BL/6 mice aged 6-8 weeks were purchased from Taconic Biosciences. Upon arrival, all mice were rested for ≥ 1 week before use. Interferon-gamma deficient (IFNγ -/-), interferon-

gamma receptor deficient (IFNγR -/-) and perforin deficient (perforin -/-) mice on the C57BL/6 background were originally obtained from Jackson Laboratory and bred locally in the animal facility at the Faculty of Health and Medical Sciences at the University of Copenhagen. All experiments were conducted in accordance with national Danish guidelines regarding animal experiments as approved by the Danish Animal Experiments Inspectorate, Ministry of Justice (protocol code 2020-15-0201-00585, start date 20200101). The mice were housed in an AAALAC accredited facility in accordance with good animal practice as defined by FELASA.

Vaccination

Mice were first anesthetized with inhaled isoflurane (Baxter Healthcare Corporation) and immunized intranasally (i.n.) and/or subcutaneously (s.c.) in the right footpad. A replication-deficient adenovirus (Ad) type 5 with deleted E1 and a non-functional E3 gene was used at a dose of 2×10^7 plaque-forming units (PFU) in 30 µl of PBS. Ad expressing Sendai virus nucleoprotein (Ad-SenNP) was administrated i.n.+s.c. or s.c. only. Ad carrying the nucleoprotein from influenza virus strain A/Puerto Rico/8/1934 (Ad-fluNP) was used as sham control and given i.n. and s.c. These adeno vectors were produced and stored as described previously (27).

Virus challenge and transmission

A luciferase-expressing recombinant Sendai virus (rSeV) was kindly provided by Charlie J. Russell, St. Jude Children's Research Hospital (31, 32). For Sendai virus challenge, rSeV was used at a dose of 1500 PFU in 30 µl PBS and administrated i.n. after isoflurane anesthesia. For transmission studies, index mice were i.n. infected with 1500 PFU rSeV and one day later each of these were transferred to a cage with four naïve mice; mice were co-housed until the experiment was terminated.

Quantification of Sendai virus

Mice were anesthetized by intraperitoneal (i.p.) injection with avertin (2,2,2 tribromoethanol in 2-methyl-2-butanol, 250 mg/kg, Alfa Aesar) and exsanguinated. For nasal flush, a catheter was gently inserted into the trachea, 0.5 ml 1% BSA in PBS was flushed from the trachea to the nasopharynx, and the liquid coming out from the nares was collected. Lungs were homogenized in 1% FBS in PBS using sterile sand, mortar, and pestle to obtain a 10% weight/volume suspension. Homogenates were then clarified by centrifugation at 600 × g, for 15 minutes at 4°C. The nasal flush and lung sample supernatants were stored at -80°C until use.

Vero cells grown in DMEM 1965 with $NaHCO_3$ supplemented with 10% FBS, 200 IU/ml Penicillin, 50 µg/ml Streptomycin, 2 mM L-glutamine, 1% Sodium Pyruvate at 37°C, 5% CO_2 were used for Sendai plaque assay. 1×10^5 cells were seeded in 24-well plates and the following day, cells were washed with PBS and then incubated with 200 µl of tenfold diluted virus samples in serum free media with 5 units/ml TPCK Trypsin (Sigma-Aldrich) for 1 hour at 37 °C and 5% CO_2. Virus samples were then gently removed, and an overlay media prepared with 50% 2 × eagle's minimal essential medium (MEM) with $NaHCO_3$, 0.2% BSA, 200 IU/ml Penicillin, 50 µg/ml Streptomycin, 2 mM L-glutamine, 1% Sodium Pyruvate, 50% methylcellulose (1.8% 400cp), 5 units/ml TPCK Trypsin was added to the cells. After incubation for 4 days at 37 °C, 5% CO_2, overlay was removed and cells were fixed with 4% formaldehyde in PBS for 15 minutes, washed with PBS, and stained with 0.1% crystal violet (Sigma-Aldrich) in PBS for 15 minutes at room temperature. PFU/ml nasal flush and PFU/g lung tissue were calculated accordingly:

$$\text{dilution factor} \times \text{average number of plaque/well} \times 5 = \text{PFU/ml}$$

$$\text{dilution factor} \times \text{average number of plaque/well} \times 50 = \text{PFU}/g$$

In vivo imaging system

The rSeV infection of challenged or co-housed mice was quantified by bioluminescence measurement. Every 24 hours mice were injected i.p. with 3 mg luciferin substrate (PerkinElmer) in PBS. After 15 minutes, mice were anesthetized using inhaled isoflurane through a 5-port manifold, placed in supine positions, scanned for bioluminescence by the IVIS CCD camera (Caliper LifeSciences) using auto-exposure and a 23 cm imaging field of view (FOV). Images were analyzed with Living Image 4.3.1 software (PerkinElmer). To quantify bioluminescence, square regions of interest (ROI) were defined manually including the upper and lower respiratory tract (nasopharynx, trachea and lungs) of each animal, quantified and expressed as "Avg Radiance" - numbers of photons emitted per unit time from a defined area (photons per second per square centimeter per steradian, p/s/cm²/sr). Bioluminescence curves were graphed over time, and the area under the curve (AUC) was calculated using GraphPad Prism with one as the baseline.

T cell effector functions depletion and blockade

For local CD8 T cells depletion, mice were treated with monoclonal α-CD8a antibody (clone YTS 169.4, BioXcell) 1 day before challenge using 5 µg i.n. For systemic CD8 T cell depletion, mice were treated 1 day before challenge with 200 µg i.p., followed by 100 µg i.p. on day 1 and day 4 post challenge. Fingolimod (FTY720, Sigma-Aldrich) was dissolved to 2.5 mg/L in drinking water and given from day 3 prior to challenge, this strategy has previously been found to prevent CD8+ T cell recirculation (33).

Single cell preparation and flow cytometry

To isolate tissue-positioned lymphocytes, mice were intravenously injected with 1.5 µg PE-CF594-conjugated α-CD3e (clone 145-2C11) fluorophore-conjugated antibody in 200 µl PBS in the tail vein. Five minutes later, mice were anesthetized using avertin and exsanguated. For bronchoalveolar lavage (BAL) sampling, the trachea was exposed and a small incision was made for inserting a catheter. The lungs were flushed 5 times with 1 ml cold Hanks BSS medium, and the lavage fluid was collected. For single cell preparation of mediastinal lymph node (MLN) and spleen, these organs were aseptically removed, mechanically dissociated and mashed through a 70 µm nylon cell-strainer (BD falcon). Lungs were harvested and digested with 5 g/L Collagenase D (Roche) and 2×10^6 units/L DNAse (Sigma) for 30 minutes, 37° C, and lymphocytes were enriched by 40%/80% Percoll gradient centrifugation. Cell counts were done by an automated cell counter Countess (Invitrogen).

Cells were stained with NP324-332/Kb (FAPGNYPAL) tetramers conjugated to allophycocyanin (APC) for 1 hour, dark at room temperature. Subsequently cells were washed twice with PBS and stained with ZombieNIR (Biolegend) and fluorochrome conjugated antibodies: BV785 conjugated α-CD8a (clone 53-6.7), FITC conjugated α-CD44 (clone IM7), PE conjugated α-CD69 (clone H1.2F3), and BV605 conjugated α-CD103 (clone 2E7) in PBS for 20 minutes, dark on ice. Samples were analyzed by LSRFortessa analyzer (BD Biosciences) with data analysis conducted using FlowJo software version 10 (TreeStar); representative plots detailing the gating strategy are depicted in Supplementary Figure 1. All antibodies were purchased from Biolegend and tetramers were kindly provided by Søren Buus of this institute.

Statistical analysis

Statistical analysis was carried out using Excel and GraphPad Prism. For comparisons of more than two groups, one-way ANOVA followed by Tukey's multiple comparisons test, or Kruskal-Wallis test followed by Dunn's multiple comparisons test. Only if groups were found to differ significantly, statistical comparison between two groups was assessed using the Mann-Whitney rank sum test (two-tailed). Levels of statistical significance is represented as: ns (not significant), *($P < 0.05$), **($P < 0.01$), ***($P < 0.001$), ****($P < 0.0001$).

Results

Combined intranasal and systemic immunization with Ad5 encoding Sendai nucleoprotein induces long standing antigen-specific CD8+ T cell memory in the airways

First, we evaluated the immunogenicity of the chosen vector system, and how the route of immunization influenced the magnitude and localization of the elicited CD8+ T cell response. To this end, C57BL/6 mice were immunized with an adenovector vaccine expressing the Sendai virus nucleoprotein (Ad-SenNP) either in the footpad (s.c.) only or by application of the vaccine s.c. as well as intranasally. Thirty and 150 days later (d30, d150), antigen-specific CD8+ T cells was quantified in bronchoalveolar lavage (BAL), lungs, mediastinal lymph nodes (MLN), and spleens using flow cytometry. Intravascular staining with flourochrome labelled anti-CD3 was used to differentiate circulating (anti-CD3+) and tissue-positioned (anti-CD3-) T cells in the respiratory system. Antigen-specific memory CD8+ T cells were determined by tetramer staining of CD8+ T cells targeting a dominant Kb-restricted peptide epitope of the Sendai nucleoprotein (SenNP), together with T cell activation marker CD44 (Figure 1A).

Robust numbers of SenNP-specific CD8+ memory T cells emerged in the spleen following either systemic or combined routes of Ad-SenNP vaccination (Figure 1B). In addition to a systemic response, high numbers of these cells were more efficiently induced in the MLN, BAL, and lungs by combined (s.c.+i.n.) compared to s.c. vaccination. Notably, these BAL and lung located antigen specific CD8+ memory T cells co-expressed CD69 and CD103 to a substantially higher degree in s.c.+i.n. animals, suggesting tissue resident properties, whereas s.c. immunization established mainly a systemic pool of memory CD8+ T cells (Figure 1C). The pronounced SenNP-specific CD8+ memory T cell response was seen locally and systemically at day 30 and lasted for at least 150 days (Figures 1B, C).

Protective capacity of local versus systemic immunity against viral challenge

To evaluate the protection afforded by having an expanded local CD8+ T cell population versus systemic immunity only, mice were immunized with the Ad-SenNP vaccine via s.c.+ i.n. or s.c. To control for a possible impact of trained immunity, a similar Ad5 vector encoding an unrelated nucleoprotein from influenza virus was used as a sham vaccine and this was also given s.c.+i.n.; age-matched unvaccinated mice served as negative controls. Thirty or 150 days after vaccination mice were challenged with 1500 PFU of rSeV encoding the gene for firefly luciferase and differences in the dynamics of infection in vaccinated versus control mice as revealed in the pattern of bioluminescence was followed for 10 days.

Regardless of time after vaccination, mice previously subjected to combined local and systemic immunization with Ad-SenNP (s.c.+i.n.) had an absolute advantage in controlling the degree of viral infection, and this effect was obvious from the very beginning (Figures 2A, D). There was no detectable replication in the lung, and very little if any replication in the upper airways (see Figure 2C for results in mice challenged 150 days after vaccination). In contrast, systemic immunity (induced by s.c. immunization only) did not play a significant role in the first 2 days but began to impact viral replication around day 3 post challenge, and an accelerated decline in bioluminescence was observed. Lacking specific immunity prior to challenge, sham vaccinated and unvaccinated controls continued to support an increasing bioluminescence that peaked at 1.0E6 p/s/cm2/

10.3389/fimmu.2023.1322536

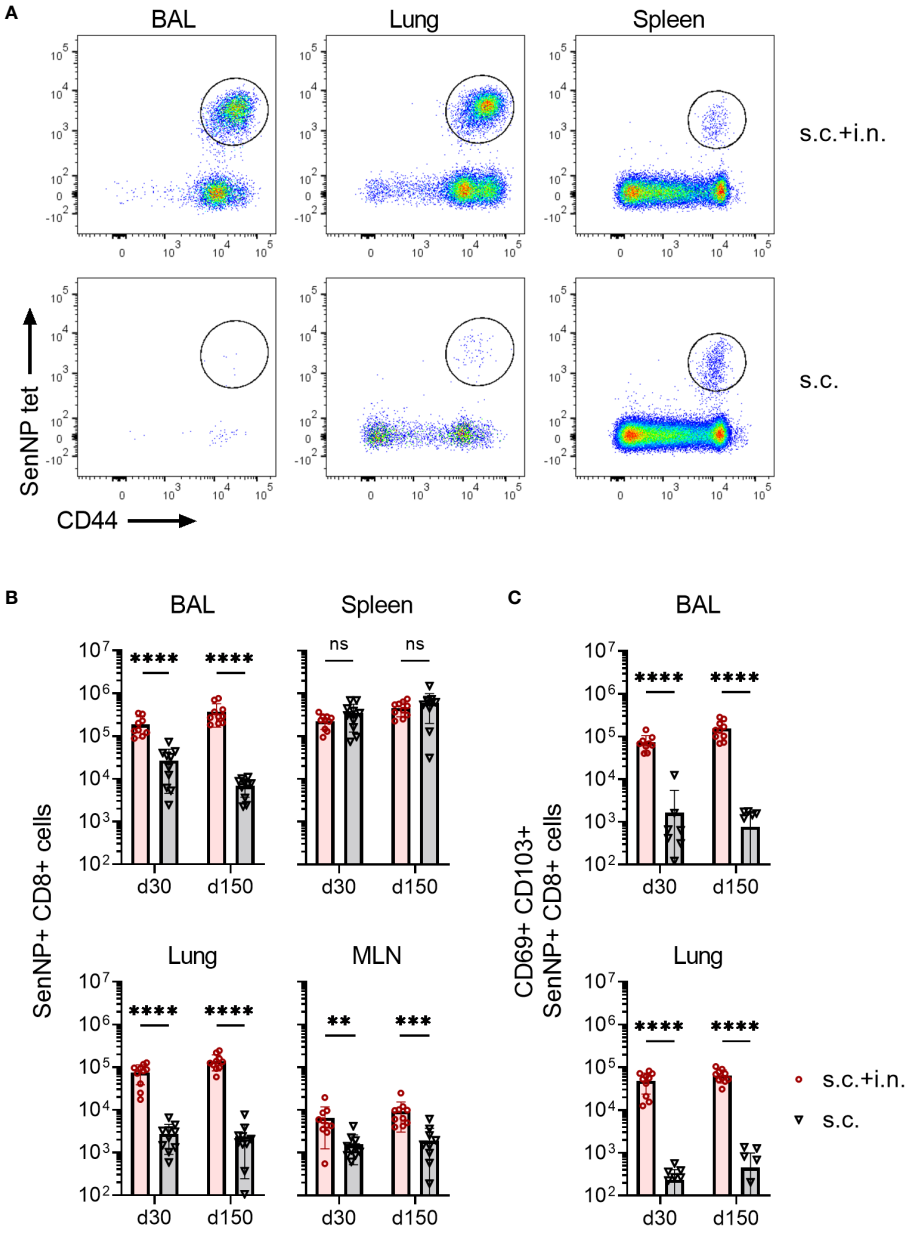

FIGURE 1
Magnitude and localization of antigen-specific memory CD8+ T cells elicited by Ad5 encoding Sendai nucleoprotein. C57BL/6 mice were immunized with Ad-SenNP s.c.+i.n. or s.c. Thirty and 150 days later (labeled as d30, d150), mice were given flourochrome labelled anti CD3 i.v. and spleen, MLN, lungs, and BAL were isolated for tetramer analysis. **(A)** Representative plots at d150 and **(B)** absolute numbers of SenNP+CD8+ T cells. **(C)** Absolute numbers of SenNP+CD8+ T cells that co-expressed CD69 and CD103. In B and C, each dot represents one animal and bars represent means with SD, based on groups of 10 animals. Statistical significance was determined using Mann-Whitney test; ns (not significant), **($P < 0.01$), ***($P < 0.001$), ****($P < 0.0001$).

sr. This was higher than that following s.c. vaccination, and unlike the situation in mice with pre-established systemic immunity, the level of infection remained high for a week (Figures 2A, C, D).

The remarkable protection induced by combined local or systemic immunization with the Ad-SenNP vaccine had a durability of at least 5 months. However, while there was no significant difference in the pattern of bioluminescence between 30 and 150 days post vaccination in any other group, the protection afforded by combined vaccination seemed to wane slightly over time, resulting in a slightly higher peak bioluminescence as well as a higher AUC at d150 compared to d30 post vaccination (Figures 2A, B). Nevertheless, very efficient protection was still observed at this time point.

Role of CD8+ T cells in vaccine induced protection against viral infection

The protective mechanisms elicited by Ad-SenNP were further assessed using CD8 depletion with monoclonal antibodies and Fingolimod (FTY720) treatment. Animals were either combined

10.3389/fimmu.2023.1322536

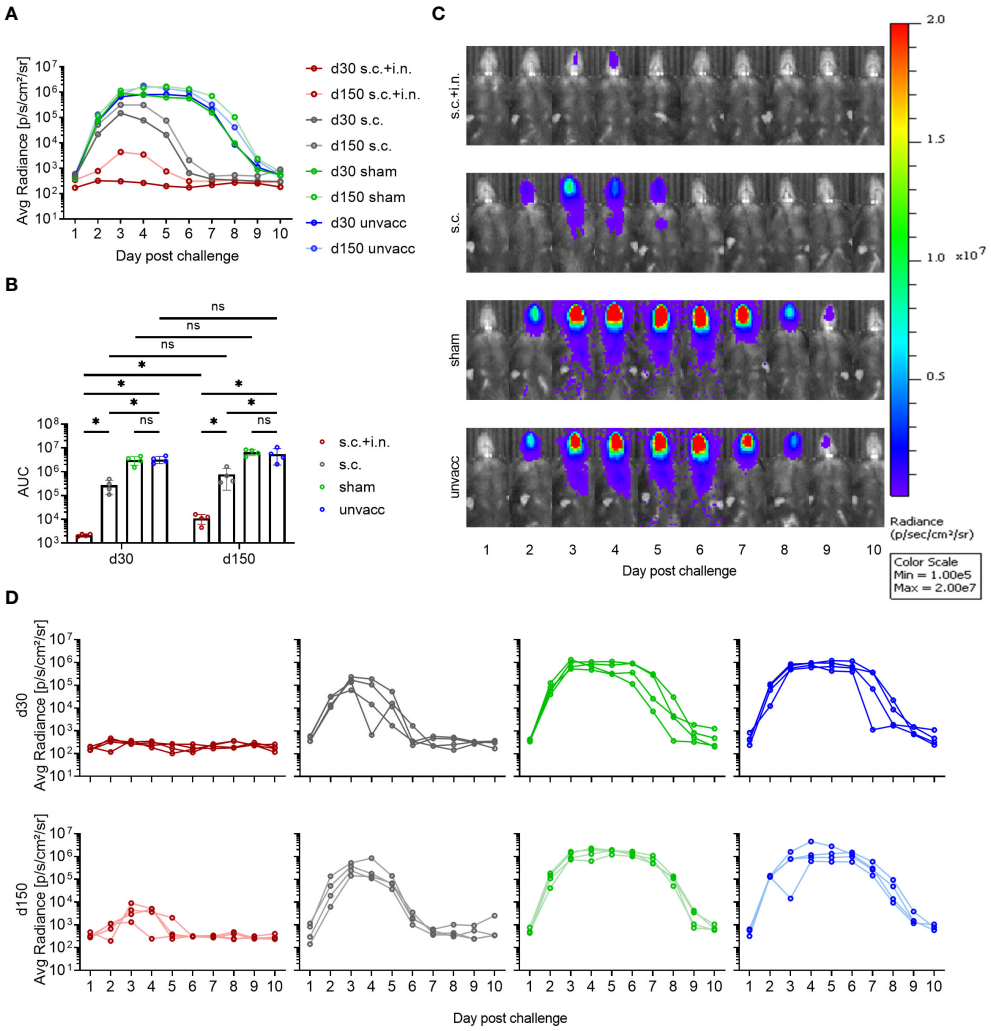

FIGURE 2
Protective capacity of local versus systemic immunity against viral challenge. C57BL/6 mice were immunized with Ad-SenNP s.c.+i.n., Ad-SenNP s.c., or Ad-fluNP s.c.+i.n. (sham control), with unvaccinated mice as controls (unvacc). Thirty and 150 days later (d30, d150), all mice were challenged i.n. with 1500 PFU rSeV expressing luciferase. Each curve represents **(A)** the average or **(D)** the individual bioluminescence of 4 mice per group. **(B)** Bars represent the mean AUC of bioluminescence with SD error bars and individual data points. Statistical significance was determined using Mann-Whitney test; ns (not significant), *($P < 0.05$). **(C)** Representative images of a single mouse from each group at d150 were displayed as radiance on a colorimetric scale ranging from 1.0E5 (blue) to 2.0E7 (red) photons/s/cm2/steradian.

or s.c. vaccinated, challenged at day 30, and infection induced bioluminescence was measured as described previously.

The infection in s.c.+ i.n., s.c., and unvaccinated mice repeatedly showed distinct dynamics and significantly different AUC regarding bioluminescence, correlating to the level of induced local or systemic immunity. When CD8+ T cells were depleted, similar lack of immunity was seen in both groups of vaccinated mice. The robust protection resulting from added local immunization was fully abrogated, and the impact of systemic immunity seen from day 3 and onwards was also greatly affected, leading to delayed virus clearance and markedly higher AUC in depleted mice (Figure 3). Thus, a central role of CD8+ T cells was evident in both the local and systemic immunity against rSeV infection.

To gauge the relevance of recirculating cells, FTY720 was used to prevent lymphocyte egress from secondary lymphoid tissues. We found that FTY720 treatment delayed the protective response in s.c. vaccinated mice, with slightly higher bioluminescence levels at early times post infection, which became more pronounced during days 3-6 post challenge, resulting in a higher average AUC than that observed in s.c. vaccinated mice without treatment. On the other hand, FTY720 had little, if any effect on virus control and marginally increased the AUC of bioluminescence in combined vaccinated mice, consistent with the idea that tissue resident cells played the major role in these mice and that secondary recruitment of circulating effector T cells played little if any role in this case (Figure 4).

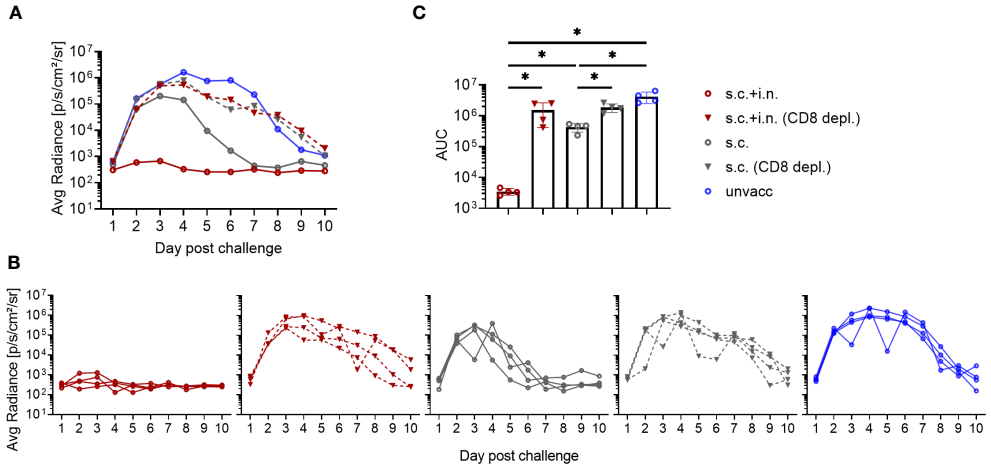

FIGURE 3
Role of CD8+ T cells in vaccine induced protection against viral infection. C57BL/6 mice were immunized with Ad-SenNP s.c.+i.n. or s.c. Thirty days later these mice, together with unvaccinated controls (unvacc) received an i.n. challenge of 1500 PFU rSeV. Part of the vaccinated mice were subjected to *in vivo* CD8+ T cell depletion as described in Materials and Methods. Each curve represents **(A)** the average or **(B)** the individual bioluminescence of 4 mice per group. **(C)** Bars represent the mean AUC of bioluminescence with SD error bars and individual data points. Statistical significance was determined using Mann-Whitney test; ns (not significant), *($P < 0.05$).

CD8+ T cells mediate early resistance to viral challenge primarily through release of IFNγ

To determine the immunological effector mechanisms of the immediate protection against reinfection, IFNγ -/-, or perforin -/- mice were included. In this case mice subjected to combined vaccination were challenged 30 days later, and bioluminescence was measured for the first 3 days after challenge.

Both the lack of IFNγ or perforin molecule impacted the early virus control elicited by combined vaccination, but to a quite different extent. Thus, the effect of perforin was rather limited, while the infection in IFNγ -/- and CD8+ T-cell depleted mice continued to develop, indicating substantially reduced immunity from the combined vaccination in these mice (Figures 5A–C). Matching results were obtained in IFNγR -/- mice (data not shown).

Interestingly, in a follow-up analysis where we studied mechanisms of virus control at latter stages (Supplementary

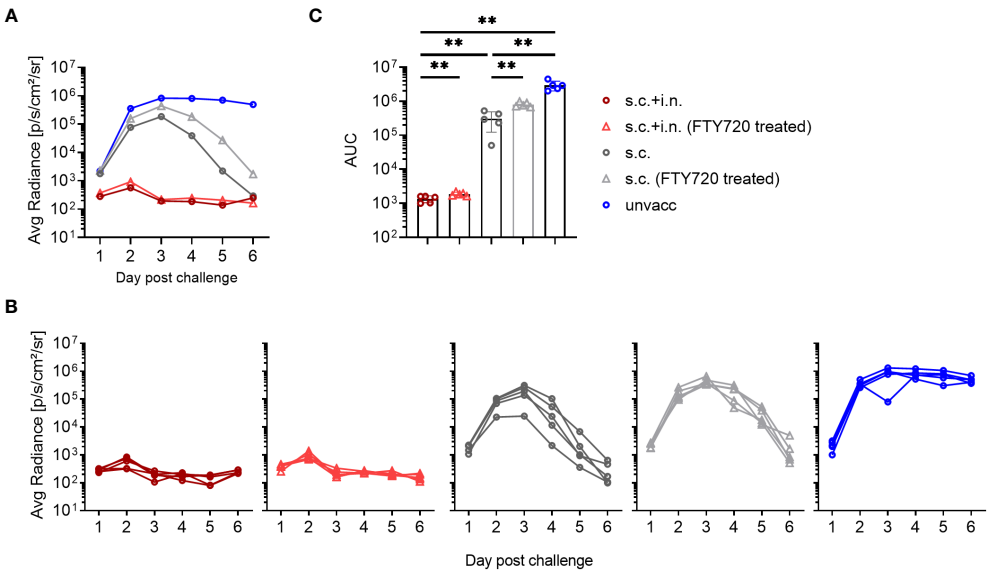

FIGURE 4
Role of recirculating lymphocytes. C57BL/6 were immunized with Ad-SenNP s.c.+i.n. or s.c. Thirty days later, these mice together with unvaccinated controls (unvacc), were challenged i.n. with 1500 PFU rSeV. Part of the vaccinated mice were given Fingolimod (FTY720) as described in Materials and Methods. Each curve represents **(A)** the average or **(B)** the individual bioluminescence of 5 mice per group. **(C)** Bars represent the mean AUC of bioluminescence with SD error bars and individual data points. Statistical significance was determined using Mann-Whitney test; ns (not significant), **($P < 0.01$).

Figure 3), we saw that although virus control was markedly delayed in IFNγ -/- mice, virus replication was eventually shut down also in these mice. In the light of the prolonged impact of CD8 depletion revealed in Figures 3, 5, this observation points to the relevance of additional vaccine-induced CD8+ T-cell dependent effector mechanism in the later phases of infection. Which these are is not presently clear, at no point did we see a marked impact of lacking perforin.

To ascertain that the observed reduction in protection did not reflect differences in the number or localization of primed SenNP-specific CD8+ T cells in vaccinated gene targeted mice, we compared the magnitude and distribution of memory CD8+ T cells in these mice to that in similarly vaccinated wild type mice. Importantly, similar numbers of SenNP-specific CD8+ memory T cells were recovered from the circulation and local tissues of all types of vaccinated mice, indicating that the observed reduction in protection directly reflected reduced effector capacity of primed CD8+ T cells in the gene targeted mice (Figures 5D, E).

Transmission capacity and local viral titers are differentially impacted by local and systemic immunity

Since prior vaccination clearly reduced viral replication following challenge, the next step was to assess whether the subsequent transmission was impacted by local and systemic immunity. Therefore, co-housing experiments were set up, with the four groups of differentially treated mice (referred to as index mice): vaccinated with Ad-SenNP s.c.+i.n. or s.c. only, Ad-fluNP s.c.+i.n (sham control), and unvaccinated. Each of the index mice were infected with rSeV 30 or 150 days after vaccination, and 1 day later co-housed with 4 unvaccinated naïve mice, referred to as contact mice (Figure 6A). The viral spreading, which was manifested by transmission to the contact mice, was followed by bioluminescence measurements for 10 days post contact.

No bioluminescence was detected in the contact mice co-housed with s.c.+i.n vaccinated index mouse, neither early nor late after vaccination. Evidence of limited early transmission was observed in cages with s.c. vaccinated index mice, particularly when challenged 150 days after vaccination. In this case detectable bioluminescence in contact mice tended to decline by day 3-4 and mostly became absent thereafter, while full blown infection was noted only in a few of the contact mice. This pattern is indicative of transmission, but at low-level intensity. Following co-housing with challenged sham vaccinated and unvaccinated index mice, early transmission was noted in the majority of cases, and in a high proportion of these mice evidence of prolonged infection was observed. The sham and unvaccinated index mice transmitted the virus to a similar extent, while the AUCs of bioluminescence in the contact mice co-housed with s.c.+i.n. and s.c. index mice was significantly decreased. All index mice seemed to retain a similar transmission capacity at days 30 and 150 post vaccination, based on infection of contact mice (Figures 6B, C).

Considering that it was a great surprise that prior local immunization with a CD8+ T cell targeting vaccine caused

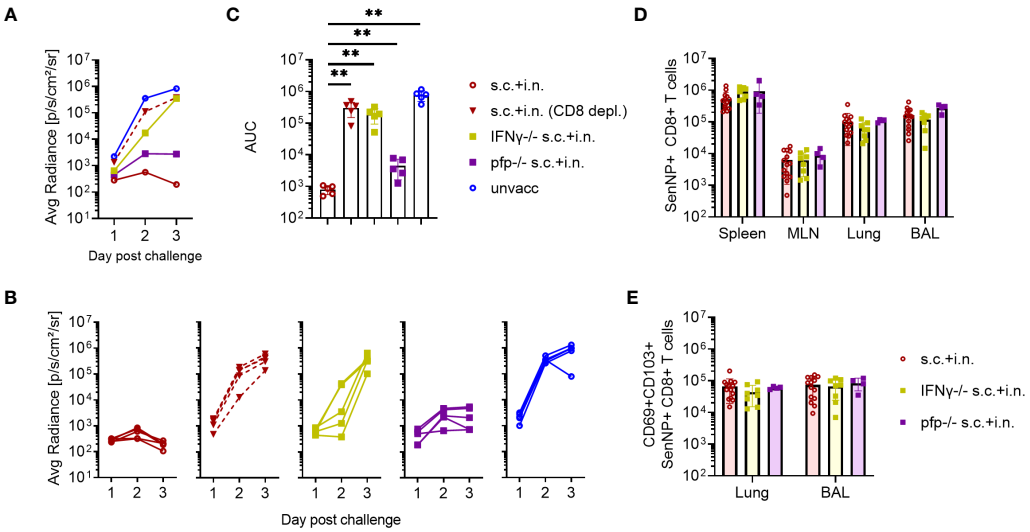

FIGURE 5
CD8+ T cells and effector molecules mediate resistance to viral challenge. C57BL/6 wild type, IFNγ -/-, and perforin (pfp) -/- mice were immunized with Ad-SenNP s.c.+i.n. Thirty days later these mice, together with unvaccinated controls (unvacc, the same as in Figure 4)), were i.n. challenge with 1500 PFU rSeV. A group of vaccinated (s.c.+i.n.) C57BL/6 mice depleted of CD8+ T cells as previously described were included for comparison. Each curve represents **(A)** the average or **(B)** the individual bioluminescence of 5 mice per group. **(C)** Bars represent the mean AUC of bioluminescence with SD error bars and individual data points. Statistical significance was determined using Mann-Whitney test; ns (not significant), **($P < 0.01$). C57BL/6 wild type, IFNγ -/-, pfp -/- mice were immunized s.c.+i.n. and thirty days later, spleen, MLN, lungs, and BAL were isolated for tetramer analysis of **(D)** absolute number of SenNP+CD8+ T cells and **(E)** absolute numbers of SenNP+CD8+ T cells in the airways that co-expressed CD69 and CD103. Each dot represents one animal and bars represent means with SD, based on a group of 4-14 animals. Statistical significance was determined using Mann-Whitney test, and no significant difference was observed in **(D, E)**.

10.3389/fimmu.2023.1322536

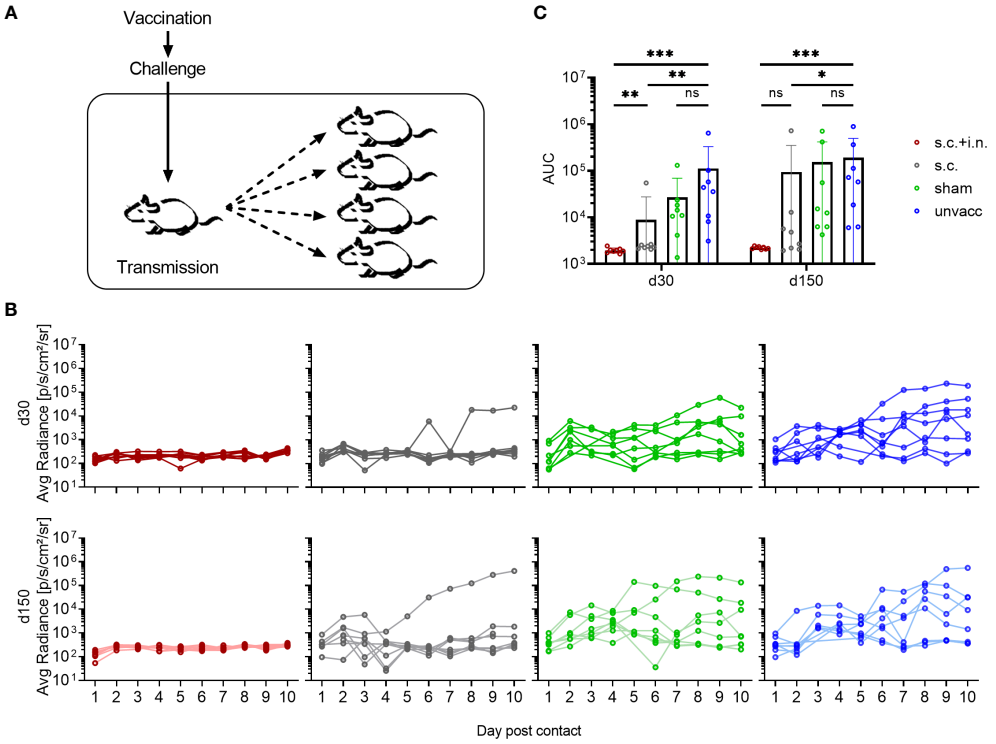

FIGURE 6
Transmission capacity is impacted by local and systemic immunity. **(A)** C57BL/6 mice immunized with Ad-SenNP s.c.+i.n., Ad-SenNP s.c., or Ad-fluNP s.c.+i.n. (sham control), and unvaccinated controls were used as index mice. Thirty and 150 days later (d30, d150), each of these animals was challenged i.n. with 1500 PFU rSeV and one day later co-housed with four naïve mice. **(B)** Curves represent bioluminescence of 8 contact mice per group. **(C)** Bars represent the mean AUC of bioluminescence with SD error bars and individual data points. Statistical significance was determined using Mann-Whitney test; ns (not significant), *($P < 0.05$), **($P < 0.01$), ***($P < 0.001$).

almost sterile immunity – for a comparison with the natural immunity following Sendai infection inducing both humoral and cell mediated immunity, see Supplementary Figure 2 - and zero transmission, we wanted to validate our methodology and directly measure the local viral replication. In naïve mice lacking pre-existing immunity, both bioluminescence and viral titers peaked 3 days after infection. By day 7, the nasal flush samples contained much less virus. The bioluminescence signal was also substantially reduced at this time-point, albeit not to quite the same degree, probably reflecting that luciferase was eliminated more slowly than the viral infection per se. Viral titers in the lungs were mostly below the level of detectability (Figure 7A). Following this validation of our experimental approach, mice were vaccinated either s.c. +i.n. or s.c. For control, other groups of mice were subjected to combined vaccination with an irrelevant vaccine or left untreated. Thirty days later all mice were challenged i.n., and viral titers in nasal flush was determined on day 3 post challenge. Similar to what had been observed previously, combined vaccination was able to significantly restrain viral replication, as both bioluminescence and viral titers were greatly reduced, and in fact, in three out of five mice we could not detect infectious virus in the nasal flush. The s.c. vaccinated mice showed comparable bioluminescence but slightly lower viral titers, compared to the unvaccinated controls. And the sham and unvaccinated mice did not significantly differ from each other in terms of neither bioluminescence nor viral titers (Figure 7B).

Role of CD8+ T cells in the immunological control of inter-individual virus transmission

Finally, to investigate the role of CD8+ T cells in controlling virus transmission after vaccination, mice immunized with Ad-SenNP s.c.+i.n. or s.c. as well as unvaccinated controls were used as index mice in co-housing experiments. Thirty days post vaccination, part of the vaccinated mice were depleted of their CD8+ T cells and all the mice were challenged i.n. and co-housed with naïve animals as described previously (Figure 8A).

Again the transmission capacity of s.c.+i.n., s.c., and unvaccinated index mice were significantly different from one another, correlating with the route of immunization. Compared to the absence of detectable transmission from combined vaccinated mice with an intact CD8 population, clear transmission from such immunized mice occurred following CD8+ T cell depletion. Already in the early phase - day 1-2 of cohousing - the lack of control of transmission by resident CD8+ T cells was noteworthy, with elevated bioluminescence in contact mice co-housed with s.c.+i.n. (CD8 depleted) index mice. Again, s.c. vaccinated mice transmitted more than matched s.c.+i.n. index mice. Co-housing with s.c. immunized index mice depleted of CD8+ T cells lead to a further increase in the bioluminescence, distinguishing these contact mice from those co-housed with s.c. immunized index

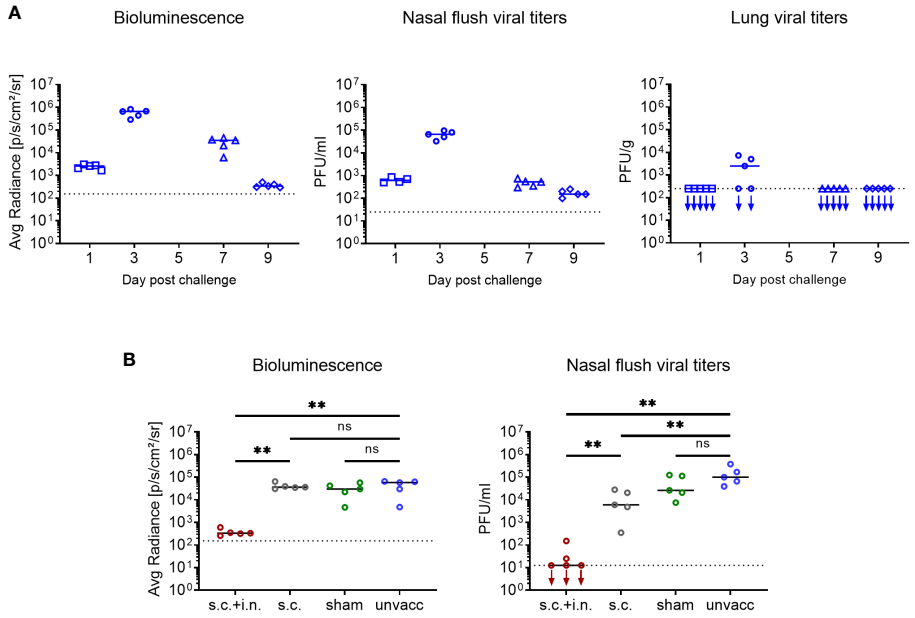

FIGURE 7
Correlation between bioluminescence and organ virus titers. **(A)** C57BL/6 mice were infected i.n. with 1500 PFU rSeV, and on days 1, 3, 7, 9 post challenge measured for bioluminescence and viral titers in nasal flush and lungs. **(B)** C57BL/6 mice were immunized with Ad-SenNP s.c.+i.n., Ad-SenNP s.c., or Ad-fluNP s.c.+i.n. (sham control). Thirty days later these mice and unvaccinated controls were infected i.n. with 1500 PFU rSeV, on day 3 post challenge measured for bioluminescence and viral titers in nasal flush. Each dot represents one animal and lines represent group medians, with 4 or 5 mice per group. The dotted line indicates the mean bioluminescence measured on 2 animals for several days without rSeV infection, or the detection limit of viral titers. Statistical significance was determined using Mann-Whitney test; ns (not significant), **($P < 0.01$).

mice without depletion as early as day 3 post contact. Moreover, when we looked at the bioluminescence in contact mice at a later stage during day 5-10 post co-housing, we observed evidence of more frequent, prior substantial viral transmission as well as a higher AUC of bioluminescence in the mice co-housed with s.c. (CD8+ T-cell depleted) mice (Figures 8B, C).

Discussion

The current SARS-CoV-2 pandemic has highlighted some key unknowns regarding vaccine induced prevention of respiratory tract infections. One relevant question is, how efficiently does parenteral immunization, eliciting a potent systemic T-cell response, impact the capacity of the immunized host to transmit the infection? Or to phrase it differently, can we rely on systemic vaccination at all for induction of herd immunity? Results from animal studies have clearly emphasized the importance of local immunization in order to obtain optimal immune mediated protection in the airways, whereas systemic immunity fails to provide a similar first line of defense (13, 27). When the new corona vaccines were introduced, authorities recommended vaccination arguing that you should get vaccinated not only for your own sake, but also to protect risk groups such as the elderly. This communication strategy implied a significant effect on viral transmission in addition to protection of the individual by systemic vaccinations. While epidemiological studies suggest that this may have been partly true with the earliest SARS-CoV-2 variants of relatively low infectiousness, this view point is more difficult to uphold with circulation of highly infectious variants of the omicron lineage (34–37). Given that T cells primarily target internal proteins, which are not subject to ongoing selection by neutralizing antibodies, it would be logical to target e.g. viral nucleoprotein in a new generation of more robust vaccines with increased breadth of antiviral protection against antibody selected escape variants. However, introducing such vaccines requires prior knowledge about the efficiency of the elicited T cell responses not only in protecting the vaccinated individual, but similar to preformed antibodies also to significantly reduce inter-individual transmission. This perhaps represent the most important uncertainty as T cells unlike antibodies are only effective once an infection is already established.

To address these issues, we chose to use murine infection with Sendai virus as our model system. Unlike SARS-CoV-2 and influenza, this is a natural mouse pathogen that easily transmits in mouse colonies. By comparing systemic immunization with combined local and systemic immunization, we could confirm that local immunization in the airways very significantly improved the capacity to resist subsequent challenge with live virus. Our vaccine expressed only the NP gene from the Sendai challenge virus, and thus the response was strongly biased towards a T-cell response (38, 39), as confirmed by the observed impact of CD8 depletion. Quite surprisingly and somewhat counterintuitively, we could conclude that CD8+ T-cell immunity under the right conditions could provide nearly sterile immunity. Obviously, incipient infection must take place in the vaccinated

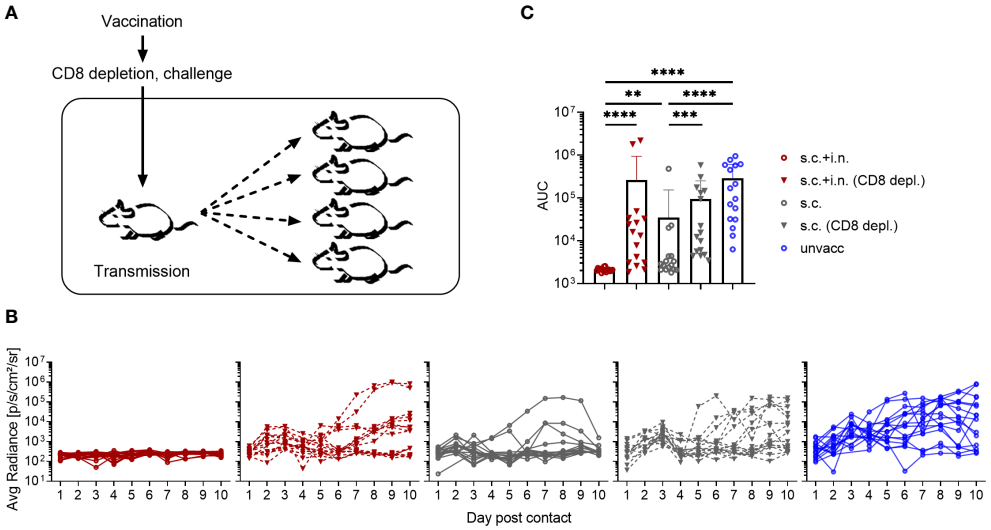

FIGURE 8
Role of CD8+ T cells in preventing virus transmission. **(A)** C57BL/6 mice were immunized with Ad-SenNP s.c.+i.n. or s.c. Thirty days later, each of these and unvaccinated index mice were infected i.n. with 1500 PFU rSeV and one day later co-housed with four naïve animals. Part of the vaccinated index animals were depleted of CD8+T cells as previously described. **(B)** Curves represent bioluminescence of 16 contact mice per group. **(C)** Bars represent the mean AUC of bioluminescence with SD error bars and individual data points. Statistical significance was determined using Mann-Whitney test; ns (not significant), **($P < 0.01$), ***($P < 0.001$), ****($P < 0.0001$).

mice, but it borders on the level of detection, and most importantly, no inter-individual transmission is seen from mice with local immunization. Our results also support the importance of local residency as a critical first line of protection, since blocking of T cell circulation using FTY720 does not reduce early protection. The speed and efficiency with which local T cells appear to shut-down the incipient infection even in mice challenged with a relatively high dose, point to a primary role of an antiviral activity based on a diffusible factor. Consistent with this assumption, analysis of relevant gene knock-out mice demonstrates that the early virus control relies heavily on the production of IFNγ, while the importance of perforin, requiring a one-on-one interaction with each infected cell, is very limited at this early stage. Regarding the interpretation of these findings, it should be emphasized that the initial course of infection was identical in unvaccinated knock-out and wild type mice (Supplementary Figure 3). Moreover, analysis of the number and distribution of NP-specific CD8+ T cells in the vaccinated knock-out mice revealed no differences in immune cell numbers or recruitment to the airways compared to wild type mice prior to challenge. Thus it is most likely the impairment of the targeted effector function that explains the differences in the observed early virus control. Notably, for the s.c. immunized mice treatment with FTY720 tended to delay virus clearance, suggesting that recruitment of circulating cells play a role, in case the first line of virus control is insufficient. This is in complete accordance with the model for the secondary anti-flu response previously proposed by D. Woodland et al (40).

Regarding the capacity of CD8+ T cells to inhibit viral transmission, we made two important observations. While the importance of local immunization for optimal T-cell mediated control of a viral challenge in itself is unsurprising, the magnitude of the impact resulting from local priming is remarkable: viral replication was hardly detectable. Thus, our results highlight the potential of a strong forward CD8+ T-cell defense to control early viral replication to a degree which almost matches that of preexisting antibodies. Under these conditions it is hardly surprising that subsequent viral transmission is prevented. Thus, co-housing of naïve contact mice with challenged index mice previously subjected to mucosal immunization revealed no detectable infection of the former. However, even in the case of mice vaccinated only s.c., and with no reduction of early viral replication following viral challenge, we still found substantially reduced transmission. Thus, for most of naïve cage mates co-housed with s.c. vaccinated, virus challenged index mice, we saw evidence of limited viral take and only a few developed a full-blown infection. This is unlike the situation in cage mates of virus-challenged sham or unvaccinated index mice. This difference in transmission capacity suggests that the amount of infectious virus released from the challenged parenterally immunized index mice is substantially reduced, despite an almost unimpaired viral replication in the respiratory tract during the first few days of infection. We find this observation to be important as it could suggest that it is perhaps not so much the peak viral load as the longevity of productive infection or a combination of both, which matters most for viral transmission. In this context it should be noted that mice immunized only parentally, still have a distinct population of memory T-cells present in their lungs, which could modify the course of infection. If our findings can be generalized, this holds clear implications for how we should look upon the potential of Covid-19 vaccines to induce effective herd immunity. Evaluation of viral loads in vaccinated human patients with SARS-CoV-2 break-through infections have revealed a pattern strikingly similar to that in parentally immunized mice, with evidence pointing to almost full-blown viral replication in the first few

days of infection followed by an accelerated clearance over the next days (41). If therefore, our findings can be directly translated to respiratory tract infections in humans, there is still reason to assume that strong systemic immunity may reduce transmission of viral respiratory tract infections to some degree, although there is clearly a substantial advantage to be gained, if local immunization could be implemented for the next generation of Covid-19 vaccines.

In conclusion, our results have revealed an almost immediate and highly efficient capacity of local antiviral T cells to abort viral infection of the respiratory tract. This supports the feasibility of using T-cell targeted vaccines not only to efficiently control severe viral infection of the respiratory tract, but also as a means to prevent transmission/induce herd immunity. However, for this defense to be most efficient, local immunization leading to elicitation of airway Trm cells is important. Thus our findings emphasizes the need for mucosal vaccines. Nevertheless, even in the absence of local immunization, strong systemic T cell immunity may suffice to accelerate virus clearance and cause some reduction in inter-individual transmission.

Data availability statement

The raw data supporting the conclusions of this article will be made available by the authors, without undue reservation.

Ethics statement

The animal study was approved by Danish Animal Experiments Inspectorate, Ministry of Justice (protocol code 2020-15-0201-00585, start date 20200101). The study was conducted in accordance with the local legislation and institutional requirements.

Author contributions

JZ: Data curation, Formal Analysis, Investigation, Writing – original draft, Writing – review & editing. IU: Conceptualization, Data curation, Formal Analysis, Investigation, Writing – review & editing. JK: Conceptualization, Writing – review & editing. JC: Conceptualization, Supervision, Writing – review & editing. AT: Conceptualization, Investigation, Supervision, Writing – original draft, Writing – review & editing.

Funding

The author(s) declare financial support was received for the research, authorship, and/or publication of this article. This work was supported by Jens Ove Jacobsens Almene Fond, Læge Sophus Carl Emil Friis og hustru Olga Doris Friis Legat and a project grant to IU from the Lundbeck Foundation.

Conflict of interest

The authors declare that the research was conducted in the absence of any commercial or financial relationships that could be construed as a potential conflict of interest.

The author(s) declared that they were an editorial board member of Frontiers, at the time of submission. This had no impact on the peer review process and the final decision.

Publisher's note

Supplementary material

The Supplementary Material for this article can be found online at: https://www.frontiersin.org/articles/10.3389/fimmu.2023.1322536/full#supplementary-material

SUPPLEMENTARY FIGURE 1
Gating strategy. Lymphocytes were first gated on a forward area and side area plot. After gating single cells on a forward area and height plot and a side area and height plot, live cells were identified with ZombieNIR. Intravascular staining was used to discriminate circulating (i.v. CD3+) and resident (i.v. CD3-) cells in the lungs, BAL and MLN. SenNP+CD44+CD8+ cells were defined as antigen-specific (tetramer+) memory T cells and were then gated into a new plot with CD69 and CD103.

SUPPLEMENTARY FIGURE 2
Ad-SenNP vaccine efficacy compared to natural immunity. C57BL/6 mice were immunized with Ad-SenNP s.c.+i.n., or rSeV i.n. 30 days ago, together with unvaccinated controls, followed by 1500 PFU rSeV i.n. challenge. Each curve represents **(A)** the average or **(B)** the individual bioluminescence of 8 mice per group. **(C)** Bars represent the mean AUC of bioluminescence with SD error bars and individual data points. Statistical significance was determined using Mann-Whitney test; ns (not significant), ***($P < 0.001$).

SUPPLEMENTARY FIGURE 3
Role of CD8 effector molecules in virus control. C57BL/6 wild type, IFNγ -/-, and perforin (pfp) -/- mice were immunized with Ad-SenNP s.c.+i.n. Thirty days later these mice, together with unvaccinated (unvacc) C57BL/6 wild type, IFNγ -/-, and pfp -/- mice, were i.n. challenge with 1500 PFU rSeV. Each curve represents **(A)** the average or **(B)** the individual bioluminescence of 4-5 mice per group. **(C)** Bars represent the mean AUC of bioluminescence with SD error bars and individual data points. Statistical significance was determined using Mann-Whitney test; ns (not significant), *($P < 0.05$), **($P < 0.01$).

References

1. Jansen AGSC, Sanders EAM, Hoes AW, van Loon AM, Hak E. Influenza- and respiratory syncytial virus-associated mortality and hospitalisations. *Eur Respir J* (2007) 30(6):1158–66. doi: 10.1183/09031936.00034407

2. Lipsitch M, Grad YH, Sette A, Crotty S. Cross-reactive memory T cells and herd immunity to SARS-CoV-2. *Nat Rev Immunol* (2020) 20(11):709–13. doi: 10.1038/s41577-020-00460-4

3. Thomson EC, Rosen LE, Shepherd JG, Spreafico R, Filipe A da S, Wojcechowskyj JA, et al. Circulating SARS-CoV-2 spike N439K variants maintain fitness while evading antibody-mediated immunity. *Cell* (2021) 184(5):1171–1187.e20. doi: 10.1016/j.cell.2021.01.037

4. Noh JY, Jeong HW, Kim JH, Shin EC. T cell-oriented strategies for controlling the COVID-19 pandemic. *Nat Rev Immunol* (2021) 21(11):687–8. doi: 10.1038/s41577-021-00625-9

5. Sridhar S, Begom S, Bermingham A, Hoschler K, Adamson W, Carman W, et al. Cellular immune correlates of protection against symptomatic pandemic influenza. *Nat Med* (2013) 19(10):1305–12. doi: 10.1038/nm.3350

6. Hayward AC, Wang L, Goonetilleke N, Fragaszy EB, Bermingham A, Copas A, et al. Natural T cell–mediated protection against seasonal and pandemic influenza. Results of the flu watch cohort study. *Am J Respir Crit Care Med* (2015) 191(12):1422–31. doi: 10.1164/rccm.201411-1988OC

7. Wilkinson TM, Li CKF, Chui CSC, Huang AKY, Perkins M, Liebner JC, et al. Preexisting influenza-specific CD4+ T cells correlate with disease protection against influenza challenge in humans. *Nat Med* (2012) 18(2):274–80. doi: 10.1038/nm.2612

8. Wang Z, Wan Y, Qiu C, Quiñones-Parra S, Zhu Z, Loh L, et al. Recovery from severe H7N9 disease is associated with diverse response mechanisms dominated by CD8+ T cells. *Nat Commun* (2015) 6(1):6833. doi: 10.1038/ncomms7833

9. McMichael AJ, Gotch FM, Noble GR, Beare PAS. Cytotoxic T-cell immunity to influenza. *N Engl J Med* (1983) 309(1):13–7. doi: 10.1056/NEJM198307073090103

10. Eser TM, Baranov O, Huth M, Ahmed MIM, Deák F, Held K, et al. Nucleocapsid-specific T cell responses associate with control of SARS-CoV-2 in the upper airways before seroconversion. *Nat Commun* (2023) 14(1):2952. doi: 10.1038/s41467-023-38020-8

11. Rosato PC, Beura LK, Masopust D. Tissue resident memory T cells and viral immunity. *Curr Opin Virol* (2017) 22:44–50. doi: 10.1016/j.coviro.2016.11.011

12. Schenkel JM, Masopust D. Tissue-resident memory T cells. *Immunity* (2014) 41(6):886–97. doi: 10.1016/j.immuni.2014.12.007

13. Wu T, Hu Y, Lee YT, Bouchard KR, Benechet A, Khanna K, et al. Lung-resident memory CD8 T cells (T_{RM}) are indispensable for optimal cross-protection against pulmonary virus infection. *J Leukoc Biol* (2014) 95(2):215–24. doi: 10.1189/jlb.0313180

14. Zens KD, Chen JK, Farber DL. Vaccine-generated lung tissue–resident memory T cells provide heterosubtypic protection to influenza infection. *JCI Insight* (2016) 1(10). doi: 10.1172/jci.insight.85832

15. Kinnear E, Lambert L, McDonald JU, Cheeseman HM, Caproni LJ, Tregoning JS. Airway T cells protect against RSV infection in the absence of antibody. *Mucosal Immunol* (2018) 11(1):249–56. doi: 10.1038/mi.2017.46

16. Luangrath MA, Schmidt ME, Hartwig SM, Varga SM. Tissue-resident memory T cells in the lungs protect against acute respiratory syncytial virus infection. *ImmunoHorizons* (2021) 5(2):59–69. doi: 10.4049/immunohorizons.2000067

17. Jozwik A, Habibi MS, Paras A, Zhu J, Guvenel A, Dhariwal J, et al. RSV-specific airway resident memory CD8+ T cells and differential disease severity after experimental human infection. *Nat Commun* (2015) 6(1):10224. doi: 10.1038/ncomms10224

18. Hassan AO, Kafai NM, Dmitriev IP, Fox JM, Smith BK, Harvey IB, et al. A single-dose intranasal chAd vaccine protects upper and lower respiratory tracts against SARS-coV-2. *Cell* (2020) 183(1):169–84. doi: 10.1016/j.cell.2020.08.026

19. Lee YT, Suarez-Ramirez JE, Wu T, Redman JM, Bouchard K, Hadley GA, et al. Environmental and antigen receptor-derived signals support sustained surveillance of the lungs by pathogen-specific cytotoxic T lymphocytes. *J Virol* (2011) 85(9):4085–94. doi: 10.1128/JVI.02493-10

20. McMaster SR, Wein AN, Dunbar PR, Hayward SL, Cartwright EK, Denning TL, et al. Pulmonary antigen encounter regulates the establishment of tissue-resident CD8 memory T cells in the lung airways and parenchyma. *Mucosal Immunol* (2018) 11(4):1071–8. doi: 10.1038/s41385-018-0003-x

21. Uddbäck I, Cartwright EK, Schøller AS, Wein AN, Hayward SL, Lobby J, et al. Long-term maintenance of lung resident memory T cells is mediated by persistent antigen. *Mucosal Immunol* (2021) 14(1):92–9. doi: 10.1038/s41385-020-0309-3

22. Singh S, Kumar R, Agrawal B. Adenoviral vector-based vaccines and gene therapies: current status and future prospects. In: Desheva Y, editor. *Adenoviruses*. Rijeka: IntechOpen (2018). doi: 10.5772/intechopen.79697

23. Tapia MD, Sow SO, Ndiaye BP, Mbaye KD, Thiongane A, Ndour CT, et al. Safety, reactogenicity, and immunogenicity of a chimpanzee adenovirus vectored Ebola vaccine in adults in Africa: a randomised, observer-blind, placebo-controlled, phase 2 trial. *Lancet Infect Dis* (2020) 20(6):707–18. doi: 10.1016/S1473-3099(20)30016-5

24. Voysey M, Costa Clemens SA, Madhi SA, Weckx LY, Folegatti PM, Aley PK, et al. Single-dose administration and the influence of the timing of the booster dose on immunogenicity and efficacy of ChAdOx1 nCoV-19 (AZD1222) vaccine: a pooled analysis of four randomised trials. *Lancet* (2021) 397(10277):881–91. doi: 10.1016/S0140-6736(21)00432-3

25. Rearte A, Castelli JM, Rearte R, Fuentes N, Pennini V, Pesce M, et al. Effectiveness of rAd26-rAd5, ChAdOx1 nCoV-19, and BBIBP-CorV vaccines for risk of infection with SARS-CoV-2 and death due to COVID-19 in people older than 60 years in Argentina: a test-negative, case-control, and retrospective longitudinal study. *Lancet* (2022) 10331):1254–64. doi: 10.1016/S0140-6736(22)00011-3

26. Tatsis N, Fitzgerald JC, Reyes-Sandoval A, Harris-McCoy KC, Hensley SE, Zhou D, et al. Adenoviral vectors persist in *vivo* and maintain activated CD8+ T cells: implications for their use as vaccines. *Blood* (2007) 110(6):1916–23. doi: 10.1182/blood-2007-02-062117

27. Uddback IEM, Pedersen LMI, Pedersen SR, Steffensen MA, Holst PJ, Thomsen AR, et al. Combined local and systemic immunization is essential for durable T-cell mediated heterosubtypic immunity against influenza A virus. *Sci Rep* (2016) 6(1):20137. doi: 10.1038/srep20137

28. Bouvier NM, Lowen AC. Animal models for influenza virus pathogenesis and transmission. *Viruses* (2010) 2(8):1530–63. doi: 10.3390/v20801530

29. Lowen AC, Mubareka S, Tumpey TM, García-Sastre A, Palese P. The Guinea pig as a transmission model for human influenza viruses. *Proc Natl Acad Sci* (2006) 103(26):9988–92. doi: 10.1073/pnas.0604157103

30. Faísca P, Desmecht D. Sendai virus, the mouse parainfluenza type 1: A longstanding pathogen that remains up-to-date. *Res Vet Sci* (2007) 82(1):115–25. doi: 10.1016/j.rvsc.2006.03.009

31. Burke CW, Mason JN, Surman SL, Jones BG, Dalloneau E, Hurwitz JL, et al. Illumination of parainfluenza virus infection and transmission in living animals reveals a tissue-specific dichotomy. *PloS Pathog* (2011) 7(7):1–13. doi: 10.1371/journal.ppat.1002134

32. Burke CW, Bridges O, Brown S, Rahija R, Russell CJ. Mode of parainfluenza virus transmission determines the dynamics of primary infection and protection from reinfection. *PloS Pathog* (2013) 9(11):e1003786. doi: 10.1371/journal.ppat.1003786

33. Nazerai L, Schøller AS, Bassi MR, Buus S, Stryhn A, Christensen JP, et al. Effector CD8 T cell-dependent zika virus control in the CNS: A matter of time and numbers. *Front Immunol* (2020) 11:1977. doi: 10.3389/fimmu.2020.01977

34. Harris RJ, Hall JA, Zaidi A, Andrews NJ, Dunbar JK, Dabrera G. Effect of vaccination on household transmission of SARS-coV-2 in England. *N Engl J Med* (2021) 385(8):759–60. doi: 10.1056/NEJMc2107717

35. Shah ASV, Gribben C, Bishop J, Hanlon P, Caldwell D, Wood R, et al. Effect of vaccination on transmission of SARS-cov-2. *N Engl J Med* (2021) 385(18):1718–20. doi: 10.1056/NEJMc2106757

36. Willett BJ, Grove J, MacLean OA, Wilkie C, De Lorenzo G, Furnon W, et al. SARS-CoV-2 Omicron is an immune escape variant with an altered cell entry pathway. *Nat Microbiol* (2022) 7(8):1161–79.

37. Lyngse FP, Mortensen LH, Denwood MJ, Christiansen LE, Møller CH, Skov RL, et al. Household transmission of the SARS-CoV-2 Omicron variant in Denmark. *Nat Commun* (2022) 13(1):5573. doi: 10.1038/s41467-022-33328-3

38. Cole GA, Katz JM, Hogg TL, Ryan KW, Portner A, Woodland DL. Analysis of the primary T-cell response to Sendai virus infection in C57BL/6 mice: CD4+ T-cell recognition is directed predominantly to the hemagglutinin-neuraminidase glycoprotein. *J Virol* (1994) 68(11):6863–70. doi: 10.1128/jvi.68.11.6863-6870.1994

39. Cole GA, Hogg TL, Woodland DL. The MHC class l-restricted T cell response to Sendai virus infection in C57BL/6 mice: a single immunodominant epitope elicits an extremely diverse repertoire of T cells. *Int Immunol* (1994) 6(11):1767–75. doi: 10.1093/intimm/6.11.1767

40. Hikono H, Kohlmeier JE, Ely KH, Scott I, Roberts AD, Blackman MA, et al. T-cell memory and recall responses to respiratory virus infections. *Immunol Rev* (2006) 211:119–32. doi: 10.1111/j.0105-2896.2006.00385.x

41. Chia PY, Ong SWX, Chiew CJ, Ang LW, Chavatte JM, Mak TM, et al. Virological and serological kinetics of SARS-CoV-2 Delta variant vaccine breakthrough infections: a multicentre cohort study. *Clin Microbiol Infect* (2022) 28(4):612.e1–7. doi: 10.1016/j.cmi.2021.11.010

frontiers | Frontiers in Immunology

TYPE Perspective
PUBLISHED 05 February 2024
DOI 10.3389/fimmu.2024.1355910

OPEN ACCESS

EDITED BY
Lalit K. Beura,
Brown University, United States

REVIEWED BY
Kyra Zens,
University of Zurich, Switzerland

*CORRESPONDENCE
Henrique Borges da Silva
borgesdasilva.henrique@mayo.edu

RECEIVED 14 December 2023
ACCEPTED 16 January 2024
PUBLISHED 05 February 2024

CITATION
Macedo BG, Masuda MY and Borges da Silva H (2024) Location versus ID: what matters to lung-resident memory T cells? *Front. Immunol.* 15:1355910. doi: 10.3389/fimmu.2024.1355910

Location versus ID: what matters to lung-resident memory T cells?

Bruna Gois Macedo, Mia Y. Masuda and Henrique Borges da Silva*

Department of Immunology, Mayo Clinic, Scottsdale, AZ, United States

Tissue-resident memory T cells (T_{RM} cells) are vital for the promotion of barrier immunity. The lung, a tissue constantly exposed to foreign pathogenic or non-pathogenic antigens, is not devoid of these cells. Lung T_{RM} cells have been considered major players in either the protection against respiratory viral infections or the pathogenesis of lung allergies. Establishment of lung T_{RM} cells rely on intrinsic and extrinsic factors. Among the extrinsic regulators of lung T_{RM} cells, the magnitude of the impact of factors such as the route of antigen entry or the antigen natural tropism for the lung is not entirely clear. In this perspective, we provide a summary of the literature covering this subject and present some preliminary results on this potential dichotomy between antigen location versus antigen type. Finally, we propose a hypothesis to synthesize the potential contributions of these two variables for lung T_{RM} cell development.

KEYWORDS

lung, tissue-resident memory CD8(+) T cells, tissue-resident memory CD4(+) T cells, T cells, route of immunization, antigen tropism

Introduction

The lung is a respiratory organ specialized in gas exchange: within its alveoli, oxygen is extracted from the air and exchanged by carbon dioxide. A consequence of this fundamental role is the constant exposure to airborne antigens, innocuous or pathogenic. Many of these antigens elicit strong T cell responses, and understanding how those responses form is crucial to define how these immune responses can either eliminate pathogenic threats or promote unwanted responses to innocuous agents. $CD4^+$ and $CD8^+$ T cells are primed by antigen-presenting cells in secondary lymphoid organs, and effector cells migrate towards antigen-rich sites to perform their function (1, 2). After antigen clearance, a portion of T cells survive long-term, forming memory populations which are important to mount quick, efficient responses against secondary antigen exposure (3). Memory T cells can be divided by their migratory characteristics. Circulating memory T cells (T_{CIRCM}) recirculate between blood, secondary lymphoid organs, and tissues, without taking up residency; these cells can be further subdivided into central memory (T_{CM}), effector memory (T_{EM}) and, in the case of $CD8^+$ T cells, long-lived effector cells (LLEC) (3, 4). In contrast, resident memory T cells (T_{RM}) establish long-term residency in tissues, mostly barrier tissues (5). The lung is, naturally, one

of these tissues. Prior evidence strongly suggests that lung T_{RM} cells are pivotal in promoting local immune responses which can either be protective against pathogens (6, 7) or deleterious – for example, in response to allergens (8).

Since their discovery (9, 10), several studies aimed to define how T_{RM} cells form in the lung, as well as their specific function. From these studies, a few notions are relatively well-established. First, both $CD4^+$ and $CD8^+$ T cells can form lung T_{RM} or T_{RM}-like populations, and this is true in response to infections (11, 12) and to allergens (8). Second, while $CD4^+$ lung T_{RM} cells are somewhat stable over time (7, 8), $CD8^+$ lung T_{RM} cells are notoriously short-lived, with a faster rate of decay if compared to $CD8^+$ T_{RM} cells in other tissues (13, 14). Finally, both $CD8^+$ and $CD4^+$ T cells form heterogeneous lung T_{RM} populations, with distinct transcriptional and functional characteristics (7, 14, 15). There are, however, several unanswered questions. One of the most important unsolved puzzles in the biology of lung T_{RM} cells lies on the nature of the signals that educate T cells to acquire a resident memory phenotype. While much evidence points out that the routes of infection (or sensitization) are paramount in defining the magnitude of the lung T_{RM} response, other works suggest that, at least partially, the type of antigen can dictate the homeostasis of lung T_{RM} cells. In this perspective article, we will briefly review previous research, provide preliminary data, and propose a hypothesis for this outstanding question.

Where am I from? How the route of antigen priming can affect lung T_{RM} cell establishment

T_{RM} cell development occurs through a series of processes where initial priming, T cell sensing of peripheral tissue-derived signals, and tissue microenvironmental factors play a role in the acquisition of a T_{RM} signature (16, 17). Because of their residency establishment inside the lung parenchyma, lung T_{RM} cells must acquire certain transcriptional and protein expression characteristics. Among these characteristics, T cells (a) downregulate molecules associated with tissue egress (e.g., CCR7, S1PR1 and S1PR5), as well as upregulate molecules associated with tissue retention (e.g., TGF-βRII, CD69 and/or CD103) (17–19), and (b) express chemokine receptors such as CXCR3, which sense CCL9 and/or CCL10 released in the lung parenchyma during local immune responses (12, 20). The need for sensing of lung-derived chemokines means that optimal alterations in the lung microenvironment are paramount for the formation of lung T_{RM} cells. These changes, such as production of CCL9 or CCL10 or of IL-33, a danger signal associated with heightened lung inflammation (21), are associated with local tissue antigen recognition. Indeed, airway infections or immunizations are very effective in the generation of lung T_{RM} cells, and persistent antigen in the lungs promote long-term survival of lung T_{RM} cells (22–26). The notion that lung initial antigen encounter is necessary for optimal lung-resident T cell responses is relatively well-established (27). In response to murine influenza, local antigen encounter is needed for $CD8^+$ T_{RM} cell establishment (28), and the same is true for T_{RM} cells forming in response to Bacillus Calmette-Guerin (BCG) vaccination (23, 29).

Lung mucosal sites are often the first barrier encountered by pathogens or allergens. These sites are composed of a complex network of heterogeneous epithelial cells, peripheral nervous cells, innate and adaptive immune cells, covered by a mucous layer. Each one of these components can harness the tissue inflammation following local infections or allergen sensitization. IL-33 production by epithelial cells (21), nervous system regulation of immune responses (30), and the capture of antigens by local dendritic cells (31, 32) all play a role in the initiation and sustenance of lung T cell responses. The lung, due to its physiological role, must balance the induction of such responses with maintenance of its function of gas exchange. During viral infections, for example, the balance between pathogen clearance and immune modulation is tightly regulated by the epithelial cell-immune cell axis, and dysregulation of this balance can lead to severe tissue damage (33). Consequently, the production and release of effector molecules is likely regulated even within the lung tissue.

Due to the highly controlled immune environment in the lung, the presence of adjuvants to elucidate immune responses is widely used to enhance immunogenicity in the lung. Adjuvants (which are common components of vaccines) can increase the magnitude and durability of antiviral immunity, impacting the phenotype of recruited innate cells (34). In response to infections or airway allergen sensitization, natural adjuvants are pathogen-associated molecular patterns (PAMPs) present on viruses, bacteria, fungi, protozoans, recognized by pattern recognition receptors (PRRs) expressed by epithelial and resident immune cells. The establishment of an appropriate resistant or tolerant environment, the engagement of distinct PRR combinations, results in recruitment of immune cell types and cytokines produced (35). This, associated with a combination of cytokines, chemokines, and danger signals, offer evidence that the lung microenvironment is critical to promote lung T_{RM} cell establishment.

Studies on T_{RM} cells have focused on identification of tissue-derived signals, while understanding how priming of committed precursors in distinct secondary lymphoid organs has been less explored (36). Dendritic cells, for instance, are responsible for the imprinting of specific migratory patterns in the T cells during activation. DCs in skin-draining lymph nodes induce the preferential expression of homing molecules for entry into skin, whereas DCs in mesenteric lymph nodes elicit tropism for the small intestine (37). This indicates that T_{RM} cell preconditioning in an organ-dependent way already occurs during homeostasis, whereas imprinting for tissue-selective homing occurs during T cell priming. In addition, migratory DCs from different tissues might have varying capacities for TGF-β activation in draining lymph nodes, since preconditioning was less pronounced in mediastinal lymph nodes, even though these tissues had comparable induction of CD103 in naïve T cells at both sites (38). This adds another layer on how the route of antigen priming can regulate the quality and/or magnitude of lung T_{RM} cell establishment.

Other routes of antigen entry, such as intramuscular immunizations, can also induce lung T_{RM} cells, but the phenotype of these cells seems to be heterogenic, with lower proportion of cells located in the lung parenchyma (39). Thus, intramuscular immunizations have traditionally been considered poor inducers of mucosal T_{RM} cell responses (40, 41). Intranasal vaccination strategies

can induce strong protection, as evidenced by past studies on RSV, Mtb and influenza (23, 26, 27, 42–44). However, this route has potential issues in antigen delivery to dendritic cells in the respiratory tract, perhaps due to physical barriers such as nasal clearing or mucus (45–47). A combination of intramuscular (i.e., distal antigen priming) and intranasal immunization approaches has been suggested as a candidate to enhance lung T_{RM} cell development in response to vaccines (41, 48, 49). Another evidence from vaccination also challenges the notion that lung antigen priming is the sole factor inducing optimal lung T_{RM} cells: the recent revolution in mRNA vaccines to combat SARS-CoV-2 (50) and, more recently, influenza (51). These immunizations, which are intramuscular, lead to robust lung $CD4^+$ and $CD8^+$ T_{RM}-like cell responses, as studies in mice suggest (48, 51). Future studies will be necessary to identify how mRNA vaccines promote lung T_{RM} cells even without intranasal priming, and whether long-lived lung T_{RM} cells are generated in humans. It is important to note that, although these studies suggest that intranasal immunization is not strictly necessary for lung T_{RM} cell responses, intranasal priming is still sufficient to improve lung T_{RM} cell establishment in these cases (23, 26, 27).

Who am I? How antigen nature and tropism can influence lung T_{RM} cell establishment

In contrast with evidence for route of antigen priming, other factors may also dictate the generation of lung T_{RM} cells, for example antigen (pathogen) load, pathogen life cycle characteristics, or the strength of TCR-MHC interaction. In mouse models of viral infection, $CD8^+$ T_{RM} cells in brain and kidney express higher affinity to MHC class I tetramers (> 20x) than T_{CIRCM} cells (52). We observed a similar trend in preliminary experiments comparing influenza-specific lung T_{RM} cells with T_{CIRCM} cells (Figure 1A), suggesting that a selection of high-affinity clones may also happen for lung $CD8^+$ T_{RM} cells.

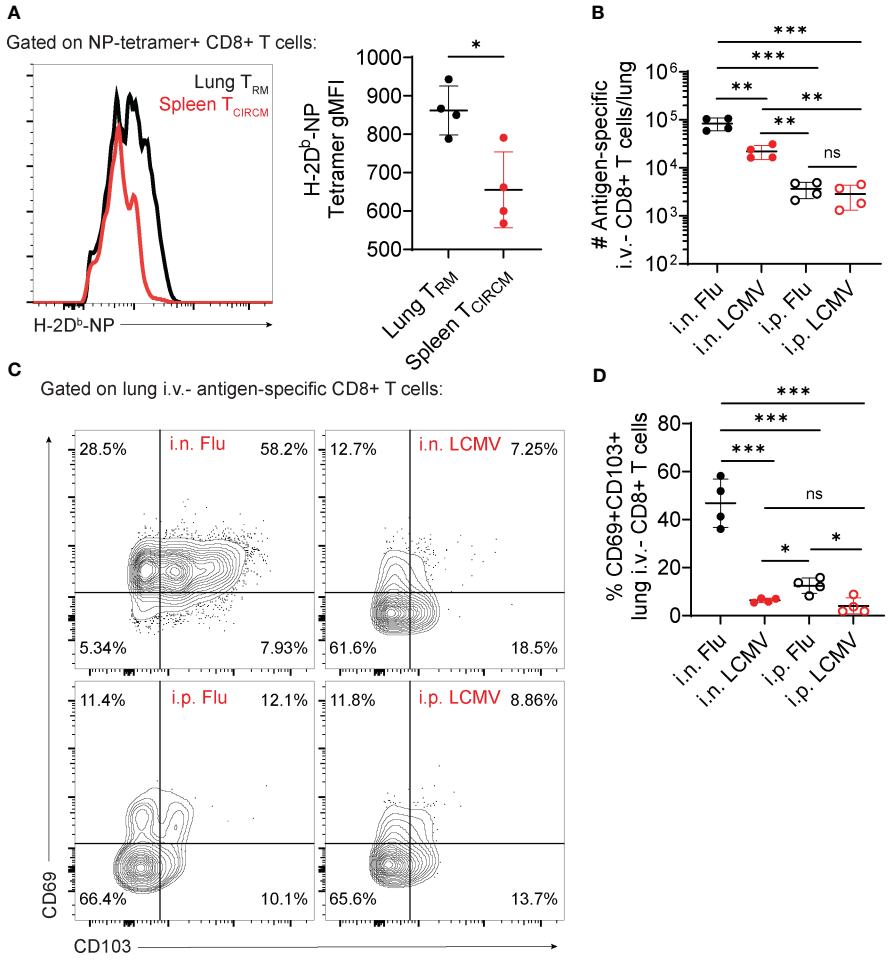

FIGURE 1
Contribution of antigen nature versus route of priming for lung $CD8^+$ T_{RM} cell establishment. **(A–D)** C57BL/6 mice were infected with influenza, PR8 strain (Flu) or LCMV-Armstrong (LCMV) through the indicated infection routes (intranasal – i.n; intraperitoneal – i.p.). At day 28 post-infection, the number and phenotype of antigen-specific $CD8^+$ T cells were assessed. **(A)** Representative histogram (left) and average gMFI values (right) of H-$2D^b$-NP tetramer staining in NP tetramer+ lung versus spleen $CD8^+$ T cells. **(B)** Average numbers of antigen-specific lung i.v.$^-$ $CD8^+$ T cells ($CD44^+$ H-$2D^b$-tetramer$^+$). **(C)** Representative flow cytometry plots showing expression of CD69 and CD103 in antigen-specific lung i.v.- $CD8^+$ T cells. **(D)** Average percentages of $CD69^+CD103^+$ antigen-specific lung i.v.- $CD8^+$ T cells. Data from two independent experiments, n=4. **(A)** Unpaired t-test **(B, D)** One-way ANOVA with Tukey's post-test, *p<0.05, **p<0.01, ***p<0.001. ns, not significant.

A preferential selection of lung T_{RM} cells with high TCR affinity for antigen could either occur at the effector stage, after T cells migrated to the lung tissue, or at the priming and activation stage, in secondary lymphoid organs. Although these two hypothetical scenarios would suggest a major effect of the route of priming as a selector of lung T_{RM} cells, different lung viral infections induce distinct magnitudes of a lung T_{RM} cell response. In mice, while in response to influenza >50% of lung memory $CD8^+$ T cells express the T_{RM} markers CD69 and CD103 (14), in response to RSV or BCG these numbers are much lower (23, 53). These differences may suggest that distinct antigen types or differences in TCR affinity regulate the establishment and phenotype of lung T_{RM} cells. Alternatively, they could also be explained by differences in how distinct pathogens interact with the lung immune system, for example differences in induction of cytokine production.

To test the potential contributions of route of priming versus antigen type, we infected mice with LCMV, Armstrong strain (a systemic virus with no tropism for the mouse lung) or influenza, using intraperitoneal versus intranasal infection routes. Intranasal infection with LCMV or influenza led to significantly increased numbers of lung parenchymal antigen-specific $CD8^+$ T cell accumulation (Figure 1B). Per se, these results are indicative of the importance of airway antigen entry in the formation of lung T_{RM} cells. However, the magnitude of lung T_{RM} cell accumulation is higher in response to intranasal influenza if compared to intranasal LCMV (Figure 1B). A more detailed characterization of these lung T_{RM} cells also show that intranasal influenza is unique in promoting upregulation of CD69 and CD103, in comparison to intranasal LCMV (Figures 1C, D). Confirming previous findings (27, 54), intraperitoneal influenza, despite failing to promote the numerical accumulation of lung T_{RM} cells (Figure 1B), was sufficient to induce a consistent upregulation of CD69 and CD103 in a small proportion of lung T_{RM} cells (Figures 1C, D). These preliminary findings suggest that, despite an important role for the intranasal route of immunization, the acquisition of a classic lung T_{RM} phenotype may strongly rely on the antigen type, more specifically their natural lung tropism.

Conclusions and a proposed hypothesis

Most past studies strongly suggest that airway exposure to antigens is an important factor in the establishment of lung T_{RM} cells, but additional evidence from us and others also point to the antigen type, more specifically its natural lung tropism, as another regulating factor. We believe that optimal lung T_{RM} cell generation will take advantage of these two variables, and the magnitude of lung T_{RM} cell responses obeys a continuum (Figure 2). In response to airway exposure to lung allergens or to respiratory infections, both lung antigen tropism and airway route of exposure are present, and consequently a strong lung T_{RM} cell response is mounted. On the

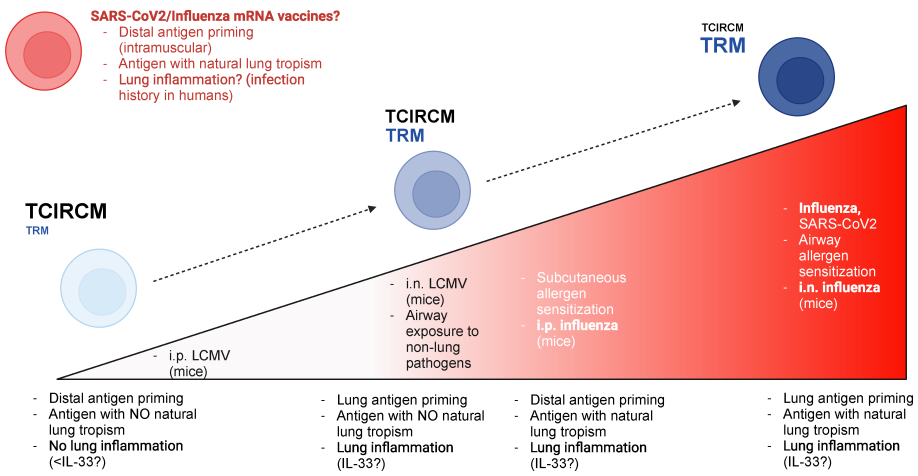

FIGURE 2
Hypothetical model for the relative contributions of antigen priming location versus antigen nature for lung T_{RM} generation. Based on past research and on our preliminary results, we postulate that the T_{RM} education of lung T cells relies on both local antigen priming and the lung tropism of relevant antigens. The magnitude of lung T_{RM} responses is at its peak when lung-tropic antigens are recognized locally (i.e., in the lung); this is the case, for example, in response to respiratory infections such as influenza or SARS-CoV-2 or to intranasal allergen sensitization. On the other hand, recruitment of lung T_{RM} cells is minimal when antigens with no lung tropism are recognized distally (e.g., systemic, or subcutaneous). When antigens with lung tropism are introduced through non-airway routes, the magnitude of lung T_{RM} cell accumulation is greatly reduced, but some accumulation may still occur; lung inflammatory responses may play an essential role in this scenario, by creating chemotactic signals for lung T cell infiltration. An example of this situation in real life is subcutaneous exposure to lung allergens. Finally, local recognition of antigens with no lung tropism, at least in experimental models, can induce a relevant accumulation of lung parenchymal T cells; however, these cells still fail to acquire a bona-fide T_{RM} phenotype, perhaps due to diminished lung inflammation – since the lack of lung tropism hinders the ability of such antigens to establish in the lung tissue. A possible exception to this rule is the product of mRNA vaccines to SARS-CoV-2 or influenza (which are in clinical trials). These immunizations, which are distal (i.e., intramuscular), would theoretically lead to intermediate lung T_{RM} responses based on our model; however, current evidence suggests a strong lung T cell accumulation upon immunization. It is possible that a heightened state of basal lung inflammation (due to past infection history in humans) could tip the balance in favor of stronger lung T_{RM} cell responses, even in the absence of local priming. This figure was generated using BioRender.

other end of the spectrum, systemic infections with pathogens lacking lung tropism do not elicit lung T_{RM} cell responses. In "hybrid" scenarios, such as intraperitoneal exposure to influenza or intranasal exposure to LCMV, lung T_{RM} cell generation will be partial, with the magnitude of the response relying on other factors induced by either lung inflammatory responses or antigen persistence.

Some questions, however, are still unanswered. First, what is the exact influence of lung inflammatory responses (such as the ones induced by innate immune cells or epithelial cells) in this "T_{RM} continuum"? When considering our intranasal LCMV system, for example, the lack of a CD69/CD103 phenotype can be due to changes during T cell priming, but the lack of lung tropism of LCMV possibly also translates in decreased infectivity in the lungs. Consequently, inflammatory responses during the acute phase are expected to be lower in lungs, which could influence the local release of signals such as TGF-β, which are necessary to educate nascent T_{RM} cells for CD103 expression (55). $CD8^+$ T_{RM} cells can be generated in tissues without antigen if sterile inflammation is administered to such tissues simultaneously to systemic antigen immunization. This is true for skin T_{RM} cells (56, 57) and female reproductive tract T_{RM} cells (58). Future systematic investigations on whether such "prime and pull" strategies are sufficient for lung T_{RM} cell generation will be important.

Another important point to consider is the fact that $CD4^+$ and $CD8^+$ T_{RM} cells, despite sharing common pathways and molecular requirements, are not the same. $CD4^+$ T_{RM} cells typically locate outside of epithelial sites, partly due to their inability to respond to TGF-β – which is controlled by their downregulation of Runx3 (59). This is also true in the lungs, where $CD4^+$ T_{RM} cells are mostly concentrated within the lung parenchyma, with some of them in close contact with B cells and other immune cells (7, 15). Our model heavily takes into consideration our findings with lung $CD8^+$ T_{RM} cells, as well as the abundant literature on these cells (6, 13, 14, 28). It will be interesting to assess the relative contributions of the route of priming versus antigen tropism (versus local inflammation) for lung $CD4^+$ T_{RM} cell establishment. In conclusion, in this perspective we provided a short review of the known literature on how lung T_{RM} cells form, and how lung tissue versus antigen type can influence their formation. Understanding the relative roles of each one of these variables will lead, in our opinion, to the discovery of more efficient approaches to boost the generation of lung T_{RM} cells that can provide protection against infections – or to block undesirable lung T_{RM} cell formation in response to lung allergens.

Materials and methods

Mice

Male and female 6- to 8-week-old adult C57BL/6 (B6) mice were purchased from Jackson and were allowed to acclimate to our housing facilities for at least one week. Animals were maintained under specific-pathogen-free conditions at Mayo Clinic Arizona. In all experiments, mice were randomly assigned to experimental groups. All experimental procedures were approved by the institutional animal care and use committee at Mayo Clinic Arizona (IACUC A00005542-20).

Viral strains

LCMV (Armstrong strain) was maintained at −80°C until infection and diluted to $2x10^6$ PFU/ml in PBS. Influenza (PR8 strain) was maintained at −80°C and diluted to $7x10^4$ PFU/ml in PBS (intranasal infection) or $7x10^7$ PFU/ml in PBS (intraperitoneal infection) at the time of infection studies.

Infection studies

Mice were infected with LCMV-Armstrong ($2x10^5$ PFU, intraperitoneally or intranasally). Other mice were infected with Influenza-PR8 (100 PFU, intranasally or $1x10^6$ PFU, intraperitoneally).

Flow cytometry

Lymphocytes were isolated from spleen or lungs as previously described (60, 61). Lungs were removed and cut in small pieces into Erlenmeyer flasks containing 30 mL of 0.5 mg/ml Collagenase type IV. During isolation of lymphocytes from lungs, in all experiments, 50 µg of Treg-Protector (anti-ARTC2.2) nanobodies (BioLegend) were injected i.v. 30 minutes prior to mouse sacrifice (62). Direct *ex vivo* staining was performed as described (60). To identify LCMV-specific or Flu-specific $CD8^+$ T cells, tetramers were obtained from the Yerkes NIH Tetramer Core: D^b-gp33 and D^b-NP-flu tetramers conjugated with APC- or PE-Streptavidin were used. For detection of vascular-associated lymphocytes in non-lymphoid organs, *in vivo* i.v. injection of PerCP-Cy5.5-conjugated CD8α antibody was performed (63). Among LCMV- or Flu-specific $CD8^+$ T cells, the following markers were used to distinguish lung T_{RM} cells: i.v.$CD8\alpha^-CD69^{+/-}CD103^{hi/int/lo}$. In all flow cytometry experiments, Live/Dead Near-IR was used to distinguish between live and dead cells. Flow cytometric analyses were performed on FACS Symphony (BD Biosciences) and data was analyzed using FlowJo software (Treestar).

Statistical analyses

Data were subjected to the Kolmogorov-Smirnov test to assess normality of samples. Statistical differences were calculated by using unpaired two-tailed Student's t-test (or one-way ANOVA with Tukey post-test, where indicated). All experiments were analyzed using Prism 9 (GraphPad Software). Graphical data was shown as mean values with error bars indicating the SD. P values of < 0.05 (*), < 0.01 (**), < 0.001 (***) indicated significant differences between groups.

Data availability statement

The raw data supporting the conclusions of this article will be made available by the authors, without undue reservation.

Ethics statement

The animal study was approved by IACUC, project number A00005542-20. The study was conducted in accordance with the local legislation and institutional requirements.

Author contributions

BM: Conceptualization, Writing – original draft, Writing – review & editing. MM: Data curation, Formal analysis, Investigation, Writing – original draft, Writing – review & editing. HB: Conceptualization, Data curation, Formal analysis, Funding acquisition, Project administration, Resources, Supervision, Writing – original draft, Writing – review & editing.

Funding

The author(s) declare financial support was received for the research, authorship, and/or publication of this article. HB was supported by the National Institutes of Health, National Institute of Allergy and Infectious Diseases (R01AI170649).

Acknowledgments

We thank the Borges da Silva lab for intellectual support.

Conflict of interest

The authors declare that the research was conducted in the absence of any commercial or financial relationships that could be construed as a potential conflict of interest.

Publisher's note

References

1. Ruterbusch M, Pruner KB, Shehata L, Pepper M. *In Vivo* CD4(+) T cell differentiation and function: Revisiting the Th1/Th2 Paradigm. *Annu Rev Immunol* (2020) 38:705–25. doi: 10.1146/annurev-immunol-103019-085803

2. Williams MA, Bevan MJ. Effector and memory CTL differentiation. *Annu Rev Immunol* (2007) 25:171–92. doi: 10.1146/annurev.immunol.25.022106.141548

3. Mueller SN, Gebhardt T, Carbone FR, Heath WR. Memory T cell subsets, migration patterns, and tissue residence. *Annu Rev Immunol* (2013) 31:137–61. doi: 10.1146/annurev-immunol-032712-095954

4. Omilusik KD, Nadjsombati MS, Shaw LA, Yu B, Milner JJ, Goldrath AW. Sustained Id2 regulation of E proteins is required for terminal differentiation of effector CD8(+) T cells. *J Exp Med* (2018) 215:773–83. doi: 10.1084/jem.20171584

5. Schenkel JM, Masopust D. Tissue-resident memory T cells. *Immunity* (2014) 41:886–97. doi: 10.1016/j.immuni.2014.12.007

6. Laidlaw BJ, Zhang N, Marshall HD, Staron MM, Guan T, Hu Y, et al. CD4+ T cell help guides formation of CD103+ lung-resident memory CD8+ T cells during influenza viral infection. *Immunity* (2014) 41:633–45. doi: 10.1016/j.immuni.2014.09.007

7. Swarnalekha N, Schreiner D, Litzler LC, Iftikhar S, Kirchmeier D, Kunzli M, et al. T resident helper cells promote humoral responses in the lung. *Sci Immunol* (2021) 6 (55):eabb6808. doi: 10.1126/sciimmunol.abb6808

8. Hondowicz BD, An D, Schenkel JM, Kim KS, Steach HR, Krishnamurty AT, et al. Interleukin-2-dependent allergen-specific tissue-resident memory cells drive asthma. *Immunity* (2016) 44:155–66. doi: 10.1016/j.immuni.2015.11.004

9. Masopust D, Vezys V, Marzo AL, Lefrancois L. Preferential localization of effector memory cells in nonlymphoid tissue. *Science* (2001) 291:2413–7. doi: 10.1126/science.1058867

10. Gebhardt T, Wakim LM, Eidsmo L, Reading PC, Heath WR, Carbone FR. Memory T cells in nonlymphoid tissue that provide enhanced local immunity during infection with herpes simplex virus. *Nat Immunol* (2009) 10:524–30. doi: 10.1038/ni.1718

11. Wein AN, McMaster SR, Takamura S, Dunbar PR, Cartwright EK, Hayward SL, et al. CXCR6 regulates localization of tissue-resident memory CD8 T cells to the airways. *J Exp Med* (2019) 216:2748–62. doi: 10.1084/jem.20181308

12. Sakai S, Kauffman KD, Schenkel JM, McBerry CC, Mayer-Barber KD, Masopust D, et al. Cutting edge: control of Mycobacterium tuberculosis infection by a subset of lung parenchyma-homing CD4 T cells. *J Immunol* (2014) 192:2965–9. doi: 10.4049/jimmunol.1400019

13. Slutter B, Van Braeckel-Budimir N, Abboud G, Varga SM, Salek-Ardakani S, Harty JT. Dynamics of influenza-induced lung-resident memory T cells underlie waning heterosubtypic immunity. *Sci Immunol* (2017) 2(7):eaag2031. doi: 10.1126/sciimmunol.aag2031

14. Takamura S, Yagi H, Hakata Y, Motozono C, McMaster SR, Masumoto T, et al. Specific niches for lung-resident memory CD8+ T cells at the site of tissue regeneration enable CD69-independent maintenance. *J Exp Med* (2016) 213:3057–73. doi: 10.1084/jem.20160938

15. Son YM, Cheon IS, Wu Y, Li C, Wang Z, Gao X, et al. Tissue-resident CD4(+) T helper cells assist the development of protective respiratory B and CD8(+) T cell memory responses. *Sci Immunol* (2021) 6(55):eabb6852. doi: 10.1126/sciimmunol.abb6852

16. Kok L, Masopust D, Schumacher TN. The precursors of CD8(+) tissue resident memory T cells: From lymphoid organs to infected tissues. *Nat Rev Immunol* (2022) 22:283–93. doi: 10.1038/s41577-021-00590-3

17. Mueller SN, Mackay LK. Tissue-resident memory T cells: local specialists in immune defence. *Nat Rev Immunol* (2016) 16:79–89. doi: 10.1038/nri.2015.3

18. Evrard M, Wynne-Jones E, Peng C, Kato Y, Christo SN, Fonseca R, et al. Sphingosine 1-phosphate receptor 5 (S1PR5) regulates the peripheral retention of tissue-resident lymphocytes. *J Exp Med* (2022) 219(1):e20210116. doi: 10.1084/jem.20210116

19. Skon CN, Lee JY, Anderson KG, Masopust D, Hogquist KA, Jameson SC. Transcriptional downregulation of S1pr1 is required for the establishment of resident memory CD8+ T cells. *Nat Immunol* (2013) 14:1285–93. doi: 10.1038/ni.2745

20. Seung E, Cho JL, Sparwasser T, Medoff BD, Luster AD. Inhibiting CXCR3-dependent CD8+ T cell trafficking enhances tolerance induction in a mouse model of lung rejection. *J Immunol* (2011) 186:6830–8. doi: 10.4049/jimmunol.1001049

21. Thwaites RS, Uruchurtu ASS, Negri VA, Cole ME, Singh N, Poshai N, et al. Early mucosal events promote distinct mucosal and systemic antibody responses to live attenuated influenza vaccine. *Nat Commun* (2023) 14:8053. doi: 10.1038/s41467-023-43842-7

22. Uddback I, Cartwright EK, Scholler AS, Wein AN, Hayward SL, Lobby J, et al. Long-term maintenance of lung resident memory T cells is mediated by persistent antigen. *Mucosal Immunol* (2021) 14:92–9. doi: 10.1038/s41385-020-0309-3

23. Perdomo C, Zedler U, Kuhl AA, Lozza L, Saikali P, Sander LE, et al. Mucosal BCG vaccination induces protective lung-resident memory T cell populations against tuberculosis. *mBio* (2016) 7(6):e01686-16. doi: 10.1128/mBio.01686-16

24. Armitage E, Quan D, Florido M, Palendira U, Triccas JA, Britton WJ. CXCR3 provides a competitive advantage for retention of mycobacterium tuberculosis-specific tissue-resident memory T cells following a mucosal tuberculosis vaccine. *Vaccines (Basel)* (2023) 11(10):1549. doi: 10.3390/vaccines11101549

25. Ogongo P, Tezera LB, Ardain A, Nhamoyebonde S, Ramsuran D, Singh A, et al. Tissue-resident-like CD4+ T cells secreting IL-17 control Mycobacterium tuberculosis in the human lung. *J Clin Invest* (2021) 131(10):e142014. doi: 10.1172/JCI142014

26. Ogongo P, Porterfield JZ, Leslie A. Lung tissue resident memory T-cells in the immune response to mycobacterium tuberculosis. *Front Immunol* (2019) 10:992. doi: 10.3389/fimmu.2019.00992

27. Zens KD, Chen JK, Farber DL. Vaccine-generated lung tissue-resident memory T cells provide heterosubtypic protection to influenza infection. *JCI Insight* (2016) 1 (10):e85832. doi: 10.1172/jci.insight.85832

28. McMaster SR, Wein AN, Dunbar PR, Hayward SL, Cartwright EK, Denning TL, et al. Pulmonary antigen encounter regulates the establishment of tissue-resident CD8 memory T cells in the lung airways and parenchyma. *Mucosal Immunol* (2018) 11:1071–8. doi: 10.1038/s41385-018-0003-x

29. Basile JI, Liu R, Mou W, Gao Y, Carow B, Rottenberg ME. Mycobacteria-specific T cells are generated in the lung during mucosal BCG immunization or infection with mycobacterium tuberculosis. *Front Immunol* (2020) 11:566319. doi: 10.3389/fimmu.2020.566319

30. Wang W, Cohen JA, Wallrapp A, Trieu KG, Barrios J, Shao F, et al. Age-related dopaminergic innervation augments T helper 2-type allergic inflammation in the postnatal lung. *Immunity* (2019) 51:1102–1118.e7. doi: 10.1016/j.immuni.2019.10.002

31. Si Y, Wang Y, Tian Q, Wang Q, Pollard JM, Srivastava PK, et al. Lung cDC1 and cDC2 dendritic cells priming naive CD8(+) T cells *in situ* prior to migration to draining lymph nodes. *Cell Rep* (2023) 42:113299. doi: 10.1016/j.celrep.2023.113299

32. Jenkins MM, Bachus H, Botta D, Schultz MD, Rosenberg AF, Leon B, et al. Lung dendritic cells migrate to the spleen to prime long-lived TCF1(hi) memory CD8(+) T cell precursors after influenza infection. *Sci Immunol* (2021) 6:eabg6895. doi: 10.1126/sciimmunol.abg6895

33. Mettelman RC, Allen EK, Thomas PG. Mucosal immune responses to infection and vaccination in the respiratory tract. *Immunity* (2022) 55:749–80. doi: 10.1016/j.immuni.2022.04.013

34. Li Z, Jackson RJ, Ranasinghe C. Vaccination route can significantly alter the innate lymphoid cell subsets: a feedback between IL-13 and IFN-gamma. *NPJ Vaccines* (2018) 3:10. doi: 10.1038/s41541-018-0048-6

35. Moldoveanu B, Otmishi P, Jani P, Walker J, Sarmiento X, Guardiola J, et al. Inflammatory mechanisms in the lung. *J Inflammation Res* (2009) 2:1–11.

36. Enamorado M, Khouili SC, Iborra S, Sancho D. Genealogy, dendritic cell priming, and differentiation of tissue-resident memory CD8(+) T cells. *Front Immunol* (2018) 9:1751. doi: 10.3389/fimmu.2018.01751

37. Dudda JC, Martin SF. Tissue targeting of T cells by DCs and microenvironments. *Trends Immunol* (2004) 25:417–21. doi: 10.1016/j.it.2004.05.008

38. Mani V, Bromley SK, Aijo T, Mora-Buch R, Carrizosa E, Warner RD, et al. Migratory DCs activate TGF-beta to precondition naive CD8(+) T cells for tissue-resident memory fate. *Science* (2019) 366(6462):eaav5728. doi: 10.1126/science.aav5728

39. Thompson EA, Darrah PA, Foulds KE, Hoffer E, Caffrey-Carr A, Norenstedt S, et al. Monocytes acquire the ability to prime tissue-resident T cells via IL-10-mediated TGF-beta release. *Cell Rep* (2019) 28:1127–1135.e4. doi: 10.1016/j.celrep.2019.06.087

40. Knight FC, Wilson JT. Engineering vaccines for tissue-resident memory T cells. *Adv Ther (Weinh)* (2021) 4(4):2000230. doi: 10.1002/adtp.202000230

41. Hassan AO, Kafai NM, Dmitriev IP, Fox JM, Smith BK, Harvey IB, et al. and lower respiratory tracts against SARS-CoV-2. *Cell* (2020) 183:169–184.e13. doi: 10.1016/j.cell.2020.08.026

42. Nelson SA, Dileepan T, Rasley A, Jenkins MK, Fischer NO, Sant AJ. Intranasal nanoparticle vaccination elicits a persistent, polyfunctional CD4 T cell response in the murine lung specific for a highly conserved influenza virus antigen that is sufficient to mediate protection from influenza virus challenge. *J Virol* (2021) 95:e0084121. doi: 10.1128/JVI.00841-21

43. Hartwell BL, Melo MB, Xiao P, Lemnios AA, Li N, Chang JYH, et al. Intranasal vaccination with lipid-conjugated immunogens promotes antigen transmucosal uptake to drive mucosal and systemic immunity. *Sci Transl Med* (2022) 14:eabn1413. doi: 10.1126/scitranslmed.abn1413

44. Spearman P, Jin H, Knopp K, Xiao P, Gingerich MC, Kidd J, et al. Intranasal parainfluenza virus type 5 (PIV5)-vectored RSV vaccine is safe and immunogenic in healthy adults in a phase 1 clinical study. *Sci Adv* (2023) 9:eadj7611. doi: 10.1126/sciadv.adj7611

45. Lycke N. Recent progress in mucosal vaccine development: potential and limitations. *Nat Rev Immunol* (2012) 12:592–605. doi: 10.1038/nri3251

46. Li M, Wang Y, Sun Y, Cui H, Zhu SJ, Qiu HJ. Mucosal vaccines: Strategies and challenges. *Immunol Lett* (2020) 217:116–25. doi: 10.1016/j.imlet.2019.10.013

47. Lobaina Mato Y. Nasal route for vaccine and drug delivery: Features and current opportunities. *Int J Pharm* (2019) 572:118813. doi: 10.1016/j.ijpharm.2019.118813

48. Kunzli M, O'Flanagan SD, LaRue M, Talukder P, Dileepan T, Stolley JM, et al. Route of self-amplifying mRNA vaccination modulates the establishment of pulmonary resident memory CD8 and CD4 T cells. *Sci Immunol* (2022) 7:eadd3075. doi: 10.1126/sciimmunol.add3075

49. Kong HJ, Choi Y, Kim EA, Chang J. Vaccine strategy that enhances the protective efficacy of systemic immunization by establishing lung-resident memory CD8 T cells against influenza infection. *Immune Netw* (2023) 23:e32. doi: 10.4110/in.2023.23.e32

50. Corbett KS, Edwards DK, Leist SR, Abiona OM, Boyoglu-Barnum S, Gillespie RA, et al. SARS-CoV-2 mRNA vaccine design enabled by prototype pathogen preparedness. *Nature* (2020) 586:567–71. doi: 10.1038/s41586-020-2622-0

51. McMahon M, O'Dell G, Tan J, Sarkozy A, Vadovics M, Carreno JM, et al. Assessment of a quadrivalent nucleoside-modified mRNA vaccine that protects against group 2 influenza viruses. *Proc Natl Acad Sci U.S.A.* (2022) 119:e2206333119. doi: 10.1073/pnas.2206333119

52. Frost EL, Kersh AE, Evavold BD, Lukacher AE. Cutting edge: Resident memory CD8 T cells express high-affinity TCRs. *J Immunol* (2015) 195:3520–4. doi: 10.4049/jimmunol.1501521

53. Malloy AMW, Lu Z, Kehl M, Pena DaMata J, Lau-Kilby AW, Turfkruyer M. Increased innate immune activation induces protective RSV-specific lung-resident memory T cells in neonatal mice. *Mucosal Immunol* (2023) 16:593–605. doi: 10.1016/j.mucimm.2023.05.012

54. Wu T, Hu Y, Lee YT, Bouchard KR, Benechet A, Khanna K, et al. Lung-resident memory CD8 T cells (TRM) are indispensable for optimal cross-protection against pulmonary virus infection. *J Leukoc Biol* (2014) 95:215–24. doi: 10.1189/jlb.0313180

55. Zhang N, Bevan MJ. Transforming growth factor-beta signaling controls the formation and maintenance of gut-resident memory T cells by regulating migration and retention. *Immunity* (2013) 39:687–96. doi: 10.1016/j.immuni.2013.08.019

56. Mohammed J, Beura LK, Bobr A, Astry B, Chicoine B, Kashem SW, et al. Stromal cells control the epithelial residence of DCs and memory T cells by regulated activation of TGF-beta. *Nat Immunol* (2016) 17:414–21. doi: 10.1038/ni.3396

57. Davies B, Prier JE, Jones CM, Gebhardt T, Carbone FR, Mackay LK. Cutting edge: Tissue-resident memory T cells generated by multiple immunizations or localized deposition provide enhanced immunity. *J Immunol* (2017) 198:2233–7. doi: 10.4049/jimmunol.1601367

58. Shin H, Iwasaki A. A vaccine strategy that protects against genital herpes by establishing local memory T cells. *Nature* (2012) 491:463–7. doi: 10.1038/nature11522

59. Fonseca R, Burn TN, Gandolfo LC, Devi S, Park SL, Obers A, et al. Runx3 drives a CD8(+) T cell tissue residency program that is absent in CD4(+) T cells. *Nat Immunol* (2022) 23:1236–45. doi: 10.1038/s41590-022-01273-4

60. Borges da Silva H, Beura LK, Wang H, Hanse EA, Gore R, Scott MC, et al. The purinergic receptor P2RX7 directs metabolic fitness of long-lived memory CD8(+) T cells. *Nature* (2018) 559:264–8. doi: 10.1038/s41586-018-0282-0

61. Santiago-Carvalho I, Almeida-Santos G, Macedo BG, Barbosa-Bomfim CC, Almeida FM, Pinheiro Cione MV, et al. T cell-specific P2RX7 favors lung parenchymal CD4(+) T cell accumulation in response to severe lung infections. *Cell Rep* (2023) 42:113448. doi: 10.1016/j.celrep.2023.113448

62. Borges da Silva H, Wang H, Qian LJ, Hogquist KA, Jameson SC. ARTC2.2/P2RX7 signaling during cell isolation distorts function and quantification of tissue-resident CD8(+) T cell and invariant NKT subsets. *J Immunol* (2019) 202:2153–63. doi: 10.4049/jimmunol.1801613

63. Anderson KG, Mayer-Barber K, Sung H, Beura L, James BR, Taylor JJ, et al. Intravascular staining for discrimination of vascular and tissue leukocytes. *Nat Protoc* (2014) 9:209–22. doi: 10.1038/nprot.2014.005

Frontiers in Immunology

Explores novel approaches and diagnoses to treat immune disorders.

The official journal of the International Union of Immunological Societies (IUIS) and the most cited in its field, leading the way for research across basic, translational and clinical immunology.

Discover the latest Research Topics

See more →

Frontiers

Avenue du Tribunal-Fédéral 34
1005 Lausanne, Switzerland
frontiersin.org

Contact us

+41 (0)21 510 17 00
frontiersin.org/about/contact